Neuroimaging biomarkers associated with clinical dysfunction in Parkinson disease

Conor Owens-Walton

July 2019

A thesis submitted for the degree of Doctor of Philosophy of

The Australian National University

ANU Medical School

College of Health and Medicine

The Australian National University

Candidate statement

I certify that, to the best of my knowledge, the content of this thesis is my own work, unless otherwise specified, and that this thesis complies with The Australian National University Research Award Rules and has not been previously accepted for award of a degree or diploma to any other institution of higher learning. The research presented in this thesis was supported by an ANU University Research Scholarship.

Word count: 38,803

Signed: 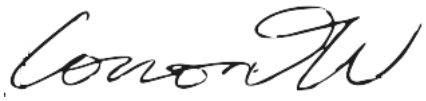

Date: 23/07/2019

Acknowledgements

First of all I must first thank my PhD supervisors at the ANU, Jeff Looi and Marnie Shaw. Jeff, thank you for being my primary supervisor and mentor. It has been such a privilege having your guidance. You have shown me what it is to act with scientific and also personal integrity. Thank you Marnie for being such an incredible support since joining my panel. Your effortless ability to dismantle difficult concepts, and help me navigate through them, was so integral to getting my project to where it is.

Thank you also to Mark Walterfang, Brian Power, Danielle van Westen and Oskar Hansson for your supervision and support from afar. Your willingness to read drafts and provide feedback and advice was always deeply appreciated. You have all shown me what true dedication to health and medical research looks like, and the way you balance clinical commitments with research is truly inspiring.

To my family, Mum, Dad and Lilli. Thank you for your unwavering support. There is nothing else I could have asked for in a family, and I hope I can repay you.

Finally to Julia. You are my inspiration. I would never have made it this far without you. Thank you for everything.

"*The things that frighten us the most*

are usually the ones that deserve our greatest attention."

John Kaag

Abstract

Parkinson disease (PD) is the second most common neurodegenerative disorder in the world, directly affecting 2-3% of the population over the age of 65. People diagnosed with the disorder can experience motor, autonomic, cognitive, sensory and neuropsychiatric symptoms that can significantly impact quality of life. Uncertainty still exists about the pathophysiological mechanisms that underlie a range of clinical features of the disorder, linked to structural as well as functional brain changes.

This thesis thus aimed to uncover neuroimaging biomarkers associated with clinical dysfunction in PD. A 'hubs-and-spokes' neural circuit-based approach can contribute to this aim, by analysing the component elements and also the interconnections of important brain networks. This thesis focusses on structures within basal ganglia-thalamocortical neuronal circuits that are linked to a range functions impacted in the disorder, and that are vulnerable to the consequences of PD pathology. This thesis investigated neuronal 'hubs' by studying the morphology of the caudate nucleus, putamen, thalamus and neocortex. The caudate nucleus, putamen and thalamus are all vital subcortical 'hubs' that play important roles in a number of functional domains that are compromised in PD. The neocortex, on the other hand, has a range of 'hubs' spread across it, regions of the brain that are crucial for neuronal signalling and communication. The interconnections, or 'spokes', between these hubs and other brain regions were investigated using seed-based resting-state functional connectivity analyses. Finally, a morphological analysis was used to investigate possible structural changes to the corpus callosum, the major inter-hemispheric white matter tract of the brain, crucial to effective higher-order brain processes.

This thesis demonstrates that the caudate nucleus, putamen, thalamus, corpus callosum and neocortex are all atrophied in PD participants with dementia. PD participants also demonstrated a significant correlation between volumes of the caudate nuclei and general cognitive functioning and speed, while putamina volumes were correlated with general motor function. Cognitively unimpaired PD participants demonstrated minimal morphological alterations compared to control participants, however they demonstrated significant increases in functional connectivity of the caudate nucleus, putamen and thalamus with areas across the frontal lobe, and decreases in functional connectivity with parietal and cerebellar regions. PD participants with mild cognitive impairment and dementia show decreased functional connectivity of the thalamus with paracingulate and posterior cingulate cortices, respectively.

This thesis contributes a deeper understanding of the relationship between structures of basal ganglia-thalamocortical neuronal circuits, corpus callosal and neocortical morphology, and the clinical dysfunction associated with PD. This thesis suggests that functional connectivity changes are more common in early stages of the disorder, while morphological alterations are more pronounced in advanced disease stages.

Table of Contents

List of Manuscripts

The following manuscripts were published during my PhD candidature, derived from research project material presented in this thesis.

Project one: Owens-Walton, C., Jakabek, D., Li, X., Wilkes, F. A., Walterfang, M., Velakoulis, D., Van Westen, D., Looi, J. C. L. & Hansson, O. 2018. Striatal changes in

Parkinson disease: An investigation of morphology, functional connectivity and their relationship to clinical symptoms. *Psychiatry Research: Neuroimaging*, 275, 5-13.

Project two: Owens-Walton, C., Jakabek, D., Power, B. D., Walterfang, M., Velakoulis, D., Van Westen, D., Looi, J. C. L., Shaw, M. & Hansson, O. 2019. Increased functional connectivity of thalamic subdivisions in patients with Parkinson's disease. *PLOS ONE*, 14, e0222002.

List of Figures

List of Tables

List of Abbreviations

Abbreviation	Explanation
A	Anterior
α-synuclein	Alpha synuclein
AF	Animal fluency test
AG	Angular gyrus
AQT	A quick test of cognitive speed test
BA	Brodmann area

BOLD	Blood oxygen-level-dependent
BCV	Bilateral caudate nucleus volume
BPV	Bilateral putamen volume
CN	Caudate nucleus
DD	Disease duration
DMN	Default mode network
DTI	Diffusion tensor imaging
DWI	Diffusion weighted imaging
DVARS	Average image intensity of each frame *n* in relation to *n*+1
eTIV	Estimated total intracranial volume
ECN	Executive control network
FA	Fractional anistropy
FC	Functional connectivity
Functional MRI	T_2^*-weighted echo planar functional MRI
FDR	False-discovery rate
FP	Frontal pole
FPM	Frontal pole (medial)
GLM	General linear model
GP	Globus pallidus
GPe	Globus pallidus externa
GPi	Globus pallidus interna
H&Y	Hoehn and Yahr Scale
ICA	Independent component analysis
ICV	Intracranial volume
IFG	Inferior frontal gyrus
L-DOPA	Levodopa
LEDD	Levodopa equivalent daily dosage
LCV	Left caudate nucleus volume
LH	Left hemisphere
LOC	Lateral occipital cortex
LPV	Left putamen volume
LSF	Letter s fluency test
MANCOVA	Multivariate analysis of covariance
MCI	Mild cognitive impairment
MD	Mean diffusivity
MFG	Middle frontal gyrus
MMSE	Mini mental state examination
MD/A	Mediodorsal/anterior
MSP	Mid-sagittal plane
MNI	Montreal Neurological Institute
P	Putamen
PCC	Posterior cingulate cortex
PCG	Paracingulate gyrus
PET	Positron-emission tomography
PD	Parkinson disease
PD-CU	Parkinson disease cognitively unimpaired
PD-MCI	Parkinson disease with mild cognitive impairment
PDD	Parkinson disease dementia
PostCG	Postcentral gyrus
PreCG	Precentral gyrus
R	Right hemisphere
RCV	Right caudate nucleus volume
RH	Right hemisphere
ROI	Region/s-of-interest
rs-fMRI	Resting-state functional magnetic resonance image/ing

RPV	Right putamen volume
SFP	Superior frontal gyrus
SN	Substantia nigra
SNR	Signal-to-noise ratio
SPECT	Single-photon emission computed tomography
STN	Subthalamic nucleus
Structural MRI	Structural T_1-weighted MRI
Th	Thalamus
TUG	Timed up and go test
UPDRS-III	Unified Parkinson disease rating scale-III
VA	Ventral anterior
VL	Ventrolateral

1. Introduction

1.1. Overview

This thesis asks whether we can find neuroimaging biomarkers associated with clinical dysfunction in PD. If so, what do these putative biomarkers tell us about the pathophysiology of the disorder? The introduction to this thesis begins with a presentation of the research rationale as well as the approach used to address these main research questions. The introduction then provides a background on the epidemiology, aetiology, neuropathology and symptomology of PD. This introduction then provides background on neuroimaging biomarkers in PD and the theoretical framework used in this thesis to explore this field of research. The introduction finishes by presenting the main aims and hypotheses of the thesis, investigated with each of the project chapters.

1.2. Research Rationale

PD is a complex multi-system neurodegenerative disorder that causes significant motor, autonomic, cognitive and neuropsychiatric symptoms. Some of the core motor features can be effectively managed with therapeutic interventions, however a number of symptoms persist despite treatment, significantly impacting quality of life. There is a lack of reliable biomarkers that can detect brain changes related to the disorder (Strafella et al., 2018), which in turn make staging of disease and thus monitoring treatment response difficult. The lack of such staging/prognosis measures may thus contribute to difficulties in developing effective disease-modifying or neuroprotective therapies available for PD. It follows that development of reliable biomarkers is necessary to advance therapeutics. The development of effective therapeutic interventions for neurodegenerative disorders like PD requires a complete

understanding of the *in vivo* neurobiology associated with each disorder, and accordingly the neural circuit basis of clinical dysfunction (Looi et al., 2014). Neuroimaging can be used to investigate neural circuits in PD, with the complete investigation of a neural circuit requiring an analysis of brain structures and also their interconnections (Sporns et al., 2005). This is particularly pertinent in PD, as a number of clinical features are linked to structural changes to the brain, while others are thought to arise from aberrant brain activity (Mcgregor and Nelson, 2019). Accordingly, this thesis uses a neural circuit-based approach to study structural and functional brain changes associated with clinical dysfunction in PD. The investigation of structural brain changes was performed via an analysis of the morphology of important brain 'hubs' while the investigation of functional brain changes was performed via an analysis of the functional connectivity of 'spokes' connecting brain regions.

1.3. Approach

This thesis seeks to answer the key research questions using four projects, presented graphically in Figure 1.1. Project one focusses on morphological and functional connectivity changes to the striatum, considered an important input hub within basal ganglia-thalamocortical circuits that are impacted in PD. Project two investigates morphological and functional connectivity changes to the thalamus, an output hub within these circuits. Project three investigates morphological and functional connectivity changes to the striatum and thalamus, but distinguishes between PD participants based on levels of cognitive impairment. And finally, Project four investigates how the structure of the corpus callosum is impacted in PD, due to the crucial role played by the structure in facilitating inter-hemispheric cortical activity.

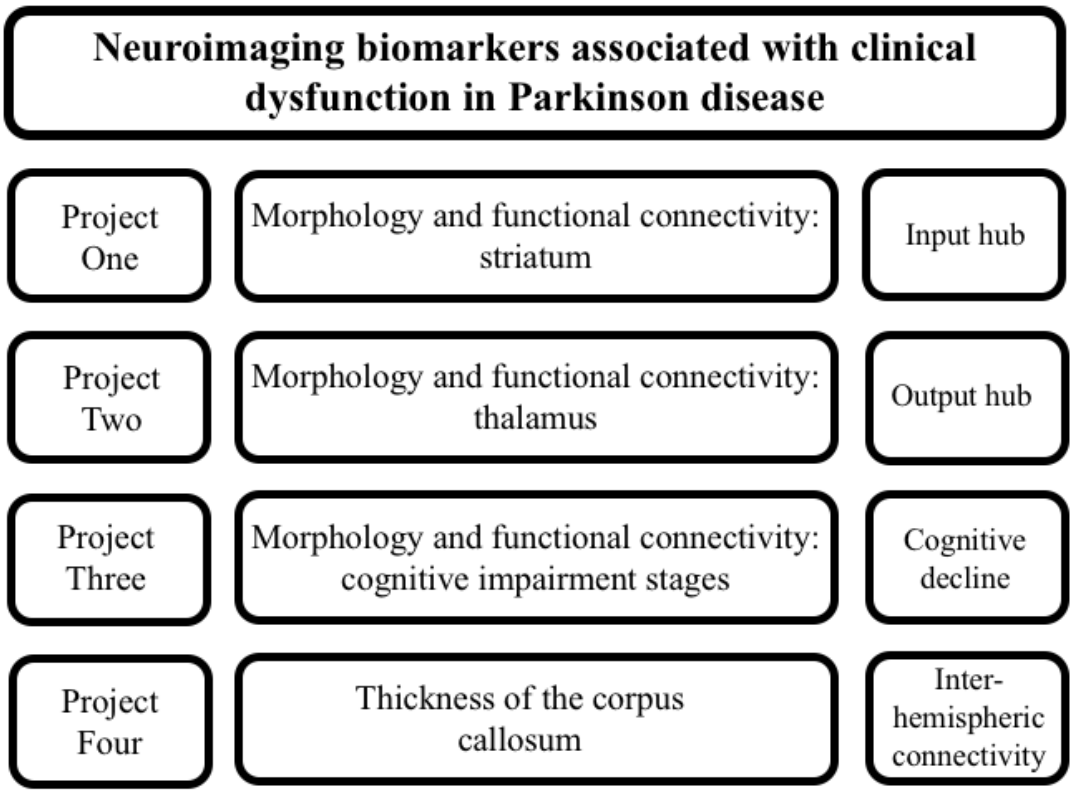

Figure 1.1: Thesis projects. This figure shows the four projects undertaken in this thesis, the main focus for each one, and a brief reason for their analysis.

1.4. Background

The first formal neurological description of PD was written by the eponymous James Parkinson in the monograph '*An essay on the shaking palsy*' (1817). In this work, Parkinson described a cohort of patients with '*involuntary tremulous motion*', a propensity to '*bend the trunk forward*,' and '*extreme slowness*' (Parkinson, 1817). These core motor features, diagnosed in a modern clinical context as resting tremor, postural instability and bradykinesia, are now known to be accompanied by a myriad of other manifestations including alterations in gait and balance, eye control, speech, swallowing and bladder function (Mcgregor and Nelson, 2019). Some of the core motor symptoms respond well to the typical dopamine replacement therapy using the dopamine precursor levodopa (L-DOPA) or a dopamine agonist, and a positive

response to the medication is an important criteria for the clinical diagnosis (Gray et al., 2014). People with PD also face significant non-motor symptoms including cognitive impairment, psychiatric disturbances, autonomic dysfunction, pain and fatigue (Aarsland et al., 2017). These clinical features can arise before or after the onset of the classic motor symptoms, and many of these features do not respond fully to standard pharmacological treatment (Mcgregor and Nelson, 2019). The neurobiology and pathophysiological mechanisms that might underlie these clinical manifestations require further investigation. This task is becoming more urgent as the number of people diagnosed with the disorder continues to rise due to aging populations around the world (Dorsey et al., 2018).

1.5. Epidemiology

PD is the second most common neurodegenerative disorder in the world, impacting 0.3% of the global population and 2-3% of people over the age of 65 (Pringsheim et al., 2014). The disorder is age- and gender-related, with an incident rate in females of 3.26 per 100,000 person-years within the 40-49 age-bracket, increasing to 103.48 at 80 years and over. The rate is higher in males, rising from 3.57 per 100,000 person-years within the 40-49 age-bracket, to 258.47 at age 80 years and over (Hirsch et al., 2016). Significant variation in incidence rates exists in the epidemiological data (Dorsey et al., 2018), highlighting the importance of genetic contributions to the aetiology, neuropathology and molecular mechanisms underlying PD.

1.6. Aetiology, neuropathology and molecular mechanisms

1.6.1. Aetiology

The number of genes found to be associated with PD and its various phenotypes continues to increase. A small proportion of cases result from direct gene mutations, with leucine-rich repeat kinase 2 genes the most common cause of autosomal dominant forms of the disorder, followed by mutations in the alpha-synuclein gene (Singleton et al., 2013). Autosomal recessive forms of PD are associated with mutations to PRKN, PINK1 and DJ-1 genes, while rare forms of recessive parkinsonism are tied to mutations in ATP13A2, PLA2G6 and FBX07 genes (Singleton et al., 2013). Several genes have been linked to an increased risk for sporadic PD, where the most important are heterozygous mutations in the GBA and LRRK2 genes (Poewe et al., 2017). Genome-wide association studies have identified over 35 risk loci for PD (Chang et al., 2017), while meta-analyses have identified numerous low-risk susceptibility variants that account for additional heritability, each variant potentially acting in a small but none-the-less additive manner (Lill, 2016). While more is yet to be uncovered in terms of the contribution of genes to the aetiology of PD, the neuropathological signature of the disorder is well characterised.

1.6.2. Neuropathology

PD research has made significant advances in identifying and characterising the neuropathology associated with the disorder. Early reports on the neurobiological underpinnings of PD argued that the brains of people with the disorder showed no observable or consistent abnormalities (Przedborski, 2017). PD is now associated with a clear neuropathological signature, with a definitive diagnosis requiring the loss of neuromelanin laden cells of the ventrolateral substantia nigra (pars compacta), as

well as the abnormal build-up of intraneuronal alpha-synuclein (α-synuclein) in the cytoplasm within particular cells in the brain (known as a Lewy pathology) (Hughes et al., 1992). Lewy pathology is the neurotoxic outcome of a process whereby the once soluble α-synuclein converts from monomers to oligomers, then progressively into insoluble α-synuclein fibrils (Kim and Lee, 2008). Lewy pathology presents at neuroanatomical sites along an ascending trajectory in the brain, codified in a series of stages by Braak et al. (2003). The earliest signs of Lewy pathology are said to be the glossopharyngeal-vagus complex and anterior olfactory nucleus (Stage 1). From there Lewy pathology can be found at sites in the medulla oblangata and pontine tegmentum (Stage 2), the ventrolateral substantia nigra pars compacta of the midbrain (Stage 3), the basal prosencephalon including meso- and allocortices (Stage 4), the higher association and prefrontal cortices (Stage 5) and finally the motor and primary sensory cortices (Stage 6) (Braak et al., 2003). When a patient is diagnosed with PD, Stage 3 of the Braak model, it is estimated that between 30-50% of substantia nigra pars compacta cells have already been lost (Politis, 2014).

1.6.3. Molecular mechanisms

PD Lewy pathology and the death of vulnerable cells associated with the disorder has been tied to a number of interrelated molecular mechanisms, including mitochondrial dysfunction, oxidative stress and neuroinflammation. Mitochondrial dysfunction has been proposed to be central to the pathogenesis of both familial and sporadic PD (Rocha et al., 2018). Two of the most important functions in cells are performed by mitochondria, including the production of ATP by oxidative phosphorylation and the mediation of signals for apoptotic cell death. α-synuclein is found in low levels in mitochondria, and the oligomerisation and accumulation of the protein within

mitochondria has been linked to neuronal degeneration (Schapira, 2007), while the clearance of defective mitochondria has been shown to be affected by the presence of α-synuclein (Rocha et al., 2018). Oxidative stress is also a consequence of mitochondrial dysfunction, and is often increased in the brain tissue of patients with PD (Dias et al., 2013). Neurons of the substantia nigra are particularly vulnerable to oxidative damage as they possess long, unmyelinated axons with large synapse numbers, requiring large amounts of energy to be sustained (Bolam and Pissadaki, 2012). A complex interplay also takes place between mitochondria and other cellular machinery, including impacting the production of free radicals, calcium homeostasis, and in the regulation and instigation of the cell-death pathway (Henchcliffe and Beal, 2008). Further support for this crucial role played by the mitochondria in PD can be seen by the fact that a number of PD-associated genes are involved in these pathways, and mutations have been linked to the maintenance of dynamic networks of mitochondrial structures (Henchcliffe and Beal, 2008). The outcome of these changes to mitochondria and other cellular components may be the activation of the neuroimmune response in PD, causing further damage to the brain. Neuroinflammation has been demonstrated in post-mortem, neuroimaging and cerebrospinal fluid biomarker studies, indicating that this is a salient feature of the disorder (Moehle and West, 2015). As stated, the oligomerized α-synuclein can be present in mitochondria, and there is substantial evidence that this can cause the generation of reactive oxygen species causing oxidative stress (Wang et al., 2016). One pathway for the generation of oxidative stress due to the build-up of oligomerized α-synuclein relates to the activation of microglia in the brain, which are highly sensitive to cellular damage signals (Rocha et al., 2018). This activation of microglia is tied to important brain homeostasis mechanisms, but research has shown

that α-synuclein-induced activation of microglia leads to a number of proinflammatory changes that are ultimately neurotoxic (Hoenen et al., 2016). Support for the important role of neuroinflammation also comes from genome studies that indicate close links between a number of genes, α-synuclein protein aggregates and neuroinflammation (Gao et al., 2008). Regardless of the mechanism linked to the pathogenesis of PD, all of these molecular mechanisms contribute to a disorder that manifests in observable motor dysfunction once midbrain cells of the substantia nigra pars compacta are lost.

1.7. Clinical dysfunction

1.7.1. Motor dysfunction

The clinical diagnosis of probable PD requires the presence of bradykinesia in combination with one of either rigidity or resting tremor. Clinical diagnosis also requires two or more supportive criteria including a responsiveness to L-DOPA, the presence of L-DOPA-induced dyskinesias or olfactory loss (Postuma et al., 2015). Bradykinesia can manifest in reductions in the amplitude of movement, velocity or initiation, and can impact a range of muscle groups. Tremor is a variable motor symptom, presenting at ~5Hz in most patients, is likely to be present at rest, diminishes with voluntary movement and responds well to therapy with L-DOPA or dopamine agonists (Mcgregor and Nelson, 2019). With disease progression additional motor symptoms can develop that do not respond well to dopaminergic treatment. These include impairments of gait, balance and postural reflexes. Speech becomes impaired, while swallowing is typically impacted in advanced disease stages, leading to significant increases in mortality due to dysphagia and aspiration pneumonia (Martinez-Ramirez et al., 2015). While these motor features of PD are crucial to

quality of life, there is increasing awareness of the extensive and damaging impact non-motor features have on people with PD, many of which show variable responses to standard pharmacological treatment.

1.7.2. Non-motor dysfunction

Some of the earliest non-motor features of PD include autonomic disturbances relating to sleep and wakefulness (Fénelon et al., 2010) or constipation (Pedrosa Carrasco et al., 2018). Patients can experience depressive symptoms (Starkstein et al., 1998, Tandberg et al., 1996) as well as disorders of affect, including anxiety and apathy (Dissanayaka et al., 2010, Pontone et al., 2009). Impulse control disorders are common in PD, and can include compulsive gambling, purchasing, sexual behaviour and eating (Voon and Fox, 2007). Recognition of the high prevalence and significant impact of cognitive dysfunction in PD has drawn attention to disease-related mild cognitive impairment (MCI) (Goldman et al., 2018) which is associated with a significantly increased likelihood of developing dementia (Broeders et al., 2013, Emre et al., 2007). People diagnosed with PD-related dementia face significantly higher mortality and reduced quality of life (Kehagia et al., 2010, Williams-Gray et al., 2007), underscoring the importance of studying cognitive impairment in the disorder.

1.7.3. Cognitive impairment and dementia in PD

Cognitive impairment in PD was traditionally thought to impact only a small subset of patients, however it is now recognised that it can present at any point during the disease course (Goldman et al., 2018) and is one of the most common and important non-motor symptoms (Aarsland et al., 2017). In the earliest stages of the disorder, 24 to 36% of PD patients show cognitive impairments (Foltynie et al., 2004). Three years

after diagnosis this prevalence rate can be as high as 50% (Aarsland et al., 2009, Broeders et al., 2013). Cognitive dysfunction in PD occurs in a broad range of cognitive areas, including executive, (Williams-Gray et al., 2007), visuospatial (Cronin-Golomb and Braun, 1997), working memory (Lewis et al., 2003), attentional and language domains (Dujardin et al., 1999). The high prevalence and heterogeneity of cognitive impairment, and the lack of standardised protocol for its definition, led to the development of a formal diagnostic criteria of MCI in PD which identifies patients at greater risk of developing dementia (Litvan et al., 2012). The Litvan criteria (2012) will be used in this thesis to categorise participants as having MCI, aligning this work with other research studies in this field. However, it should be acknowledged that cognitive impairment in PD is a complex issue. Dementia in PD is a multifaceted co-morbidity, impacting a high percentage of people with the disorder, and causing disruption to a range of functional domains. Longitudinal work has demonstrated that over a four year period 62% of patients with PD-related MCI will develop dementia, while only 20% of cognitively unimpaired patients will be diagnosed with dementia during the same period (Janvin et al., 2006, Williams-Gray et al., 2007). A diagnosis of dementia in PD identifies patients with a symptom profile that may involve impairment in memory, visuospatial, constructional and executive functions, impaired and fluctuating attention and apathy. Core language functions are generally preserved, however verbal fluency and anomia are common (Emre, 2014). Unlike a diagnosis of Alzheimer disease, people with a diagnosis of dementia in PD do not necessarily have to present with memory impairment. Non-memory related clinical features of PD-dementia relate to clinical and behavioural features including apathy, excessive sleepiness (Goldman et al., 2018), motor and autonomic disturbances (Emre et al., 2007) and visual hallucinations, all of which are often dysphoric and fear provoking

(Gomperts, 2016). PD-related dementia has been linked to diffuse cortical Lewy body disease pathology (Hurtig et al., 2000), amyloid-β plaque deposition (Emre et al., 2007) and cerebrovascular disease (Halliday et al., 2014) while a substantial proportion of patients also meet the diagnostic criteria for Alzheimer disease-type pathology (Compta et al., 2011). Dementia in PD is associated with a range of neurotransmitter systems including acetylcholine (Bohnen and Albin, 2009), dopamine (Rinne et al., 2000) and norepinephrine circuits (Zweig et al., 1993).

The profile of cognitive deficits in PD is heterogeneous, in terms of which domains of function are affected, but also due to the temporal nature of the symptoms. For instance, a dual-profile of cognitive impairment in PD has been suggested that might be able to differentiate between two broad syndromes. The first is a profile of neuropsychological deficit in non-demented people with PD who have MCI and also tremor-dominant motor phenotypes on tests of working memory and executive function and are more responsive to dopaminergic amelioration of symptoms (Kehagia et al., 2013). The second subtype, an akinetic subtype with pronounced gait disturbance, demonstrate deficits in visuospatial function and semantic fluency and have a more rapid decline to dementia and in whom cholinergic treatment can be effective (Kehagia et al., 2013). Further, it has been shown that the age of onset can also be an important factor. Studies have shown that older patients at diagnosis experience a more severe phenotype (Pagano et al., 2016). As these symptomatic and pathological profiles suggest, the clinical features of PD are multifaceted and likely the result of dysfunction in multiple systems in the brain (Postuma and Berg, 2019). A neural circuit-based approach involving basal ganglia-thalamocortical circuits offers an opportunity investigate such a multifaceted system, which may uncover

pathophysiological changes that underlie clinical dysfunction associated with the disorder. This thesis will now introduce basal ganglia-thalamocortical circuits and how they relate to symptoms in PD. It will then be shown how a search for neuroimaging biomarkers associated with clinical dysfunction can benefit from analyses within these brain circuits.

1.8. Basal ganglia-thalamocortical circuits

1.8.1. Circuit structure

The basal ganglia are a set of highly organised subcortical nuclei that are crucial to effective movement, learning, working memory, emotion and behaviour (Obeso et al., 2008). Component nuclei include the striatum, globus pallidus (pars externa and interna), the subthalamic nucleus and the substantia nigra (pars compacta and reticulata) (the thalamus is included for reference) (Figure 1.2).

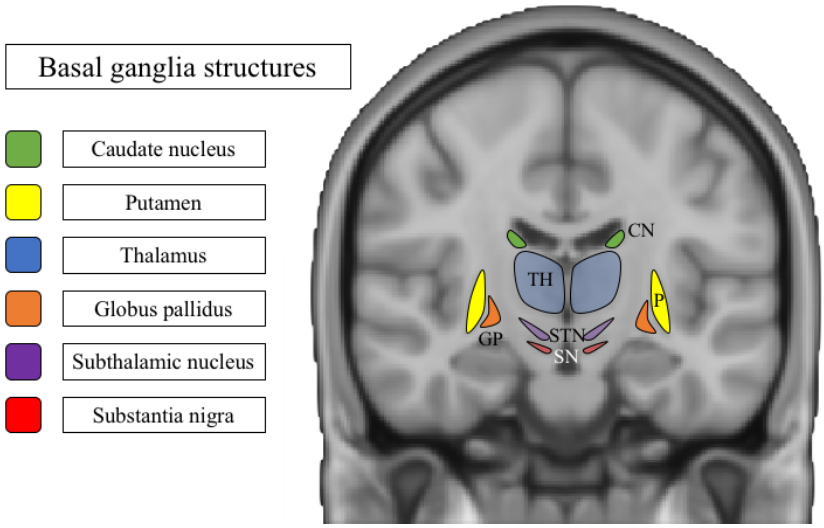

Figure 1.2: Structures of the basal ganglia. This figure displays the component structures of the basal ganglia overlaid on a Montreal Neurological Institute 152 standard T_1-weighted structural MRI scan in the coronal plane. **Abbreviations:** CN, caudate nucleus; TH, thalamus; P, putamen; SN, substantia nigra; STN, subthalamic nucleus; GP, globus pallidus.

Nuclei of the basal ganglia connect with the bilateral thalami and cortical regions to form re-entrant basal ganglia-thalamocortical circuits. Originally thought to only subserve motor functions (Delong and Georgopoulos, 1981), Alexander et al. (1986) expanded this view to describe motor, dorsolateral prefrontal (associative), anterior cingulate (limbic), oculomotor and lateral orbitofrontal basal ganglia-thalamocortical circuits. The different behavioural associated with each of these circuits is linked to the functions performed by the site of origin of each circuit in the cortex (Delong and Wichmann, 2009). The basic architecture of each circuit is the same, with cortical areas connecting with the nuclei of the striatum (caudate nucleus and putamen), which then connect with the globus pallidus interna/substantia nigra complex, projecting to the thalamus and back to the site of origin in the cortex (Alexander et al., 1986).

The three most commonly studied circuits are the motor, limbic and associative circuits. The motor circuit, involved in mediating the overall amount of movement, originates in the supplementary motor area, premotor and motor cortex and somatosensory cortex, projecting to the putamen in a topographic manner (Tekin and Cummings, 2002). The circuit then sends afferent input to the central and dorsal globus pallidus and also to the ventral substantia nigra (Haber and Calzavara, 2009). The circuit then connects with the ventrolateral and ventral anterior thalamic nuclei, reconnecting back with the somatomotor cortices (Tekin and Cummins, 2002).

The limbic circuit mediates processes involved reward-based behaviour and learning. This circuit begins in the anterior cingulate and ventromedial prefrontal cortical regions, projects to the rostral and ventro-medial striatum, then projects to the ventral palladium and to the medial substantia nigra. From there, the circuit projects to

ventral anterior nucleus of the thalamus, which then closes the loop by reconnecting back with their site of origin in medial prefrontal cortical regions (Haber and Calzavara, 2009).

The associative circuit mediates a range of processes involved in cognitive function, including strategic planning, working memory, and executive functioning. This circuit begins in the dorsolateral prefrontal cortex which projects to the rostral and dorsal caudate nucleus. The circuit then connects with the central part of the globus pallidus and substantia nigra, which projects to the ventral anterior and mediodorsal thalamus. The circuit closes by reconnecting back with the dorsolateral prefrontal cortex (Haber and Calzavara, 2009). While each of the motor, limbic and associative circuits follow a broadly similar structure, within each circuit there is a direct and indirect pathway that perform opposing functional roles based on their connectivity and neurotransmitter architectures.

1.8.2. Direct and indirect pathways

Both the direct and indirect pathways begin in the same cortical regions and connect with the caudate nucleus and putamen via excitatory glutamatergic transmission. The direct pathway, which bears D1 dopaminergic neurons, has inhibitory γ-amino-butyric acid connections from the striatum to the globus pallidus interna/substantia nigra complex. The indirect pathway, which bears D2 dopaminergic neurons, has inhibitory γ-amino-butyric acid connections from the striatum to the globus pallidus externa which then projects inhibitory γ-amino-butyric acid connections to the subthalamic nucleus (Delong and Wichmann, 2009). The important connective distinction between these two pathways is the output from the subthalamic nucleus, which projects back

to the globus pallidus interna/substantia nigra complex via excitatory glutaminergic connections. Both circuits output from the globus pallidus interna to the thalamus via inhibitory γ-amino-butyric acid fibres, with the final connection from the thalamus to the cortex being an excitatory glutaminergic connection (Figure 1.3) (Mega and Cummings, 1994).

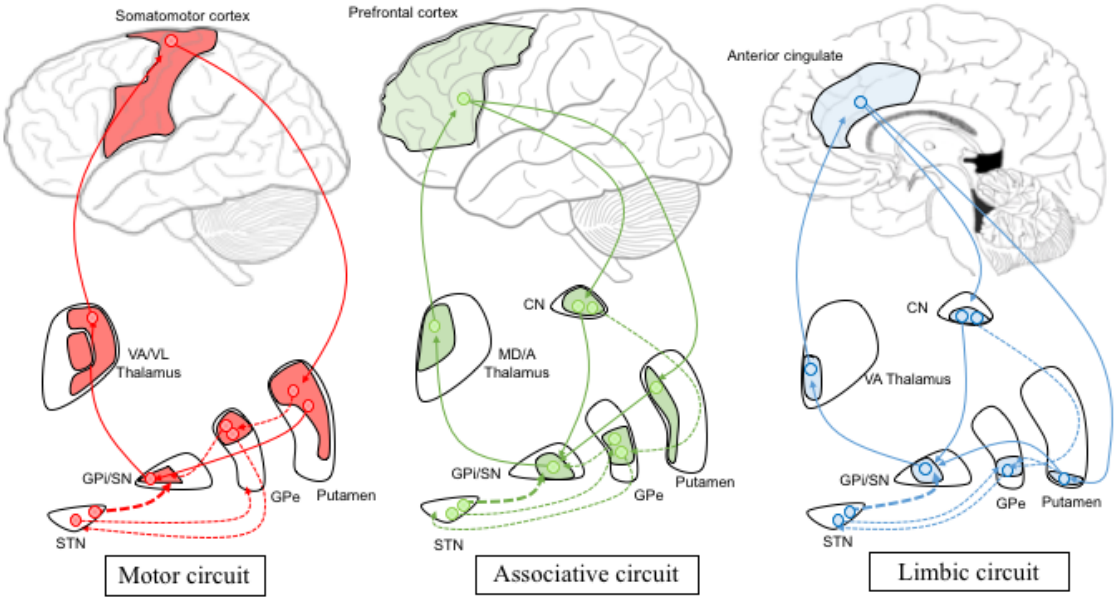

Figure 1.3: Basic organisation of basal ganglia-thalamocortical circuits. Solid lines indicate connectivity via direct circuits which input to the striatum, connect with the globus pallidus interna/substantia nigra complex, then to the thalamus, projecting back to their sites of origin in the cortex. Indirect pathways are represented by broken lines, connecting the striatal nuclei to the globus pallidus interna, the subthalamic nucleus, then connecting with the globus pallidus intern/substantia nigra complex. **Abbreviations:** CN, caudate nucleus; GPe, globus pallidus externa; GPi/SN, globus pallidus interna/substantia nigra complex; STN, subthalamic nucleus; VA, ventral anterior thalamic nuclei; VL, ventrolateral thalamic nuclei; MD/A, mediodorsal and anterior thalamic nuclei. This figure is adapted from Obseo et al. (2008).

The direct and indirect pathways modulate circuit activity depending on the input they receive. Dysfunction of the direct pathway can cause abnormal thalamic inhibition, while dysfunction of the indirect circuit can cause disinhibition and thalamic

overactivity. This dual effect is due to the influence of dopamine over D1 and D2 receptors, exciting D1 neurons in the direct pathway and inhibiting D2 neurons in the indirect pathway (Obeso et al., 2008). A clear example of how the breakdown of basal ganglia-thalamocortical circuitry can explain clinical dysfunction in PD relates to the cardinal motor symptoms of hypokinesia.

1.8.3. Circuit dysfunction

Loss of dopaminergic input to the striatum causes an imbalance between the direct pathway and the indirect pathway. The net effect of this imbalance is hypothesised to be disinhibition of the subthalamic nucleus that leads, in turn, to excessive inhibition of thalamo-cortical activity and the clinical symptoms of hypokinesia (Albin et al., 1989, Braak and Del Tredici, 2008, Delong, 1990). There is a wealth of experimental and clinical evidence to support this framework (Alvarez et al., 2005, Aziz et al., 1991, Bergman et al., 1990, Fine et al., 2000), which has resulted in the widespread use of dopaminergic medication and more recently deep brain stimulation (temporary lesioning of neuroanatomical sites in the indirect pathway) as evidence-based therapeutic options (Volkmann et al., 2010). However, the effects of restoring the balance between the two pathways within basal ganglia-thalamocortical circuits does not fully account for a number of clinical symptoms in the disorder. The role played by medication in mediating circuit activity in PD is crucial from a diagnostic and also treatment perspective, and warrants further discussion as it can reveal important information about the link between basal ganglia-thalamocortical circuits and clinical dysfunction.

1.8.4. Basal ganglia-thalamocortical circuits, treatments and clinical dysfunction

The effects of dopaminergic medication and deep brain stimulation on non-motor symptoms in PD have traditionally been mixed (Volkmann et al., 2010). Clinical accounts in PD suggest that certain cognitive symptoms can improve (Kulisevsky, 2000) and also worsen with dopaminergic therapy in PD (Frank, 2005). This is supported by research in primate models, where L-DOPA treatments that greatly improved motor symptoms were associated with minimal or worsening cognitive performance (Schneider et al., 2013). The use of dopaminergic medication to restore the balance of these circuits is also associated with dyskinesias (Connolly and Lang, 2014) and impulse control disorders (Moustafa and Poletti, 2013), both which significantly increase disability in PD (Poewe, 2009). Recent research using probabilistic tractography on PD participants after deep brain stimulation surgery has been able to uncover distinct neural circuits associated with elements of impulse control disorders in PD, including faulty reward perception and impatience (Mosley et al., 2019). The first network, a 'reward evaluation network', was associated with *stronger* connectivity between the ventral striatum and the ventromedial prefrontal cortex in PD participants who demonstrated riskier behaviour, while a second network, a 'response inhibition network', was associated with *weaker* connectivity between the subthalamic nucleus and the pre-supplementary motor area in patients who demonstrated greater impulsivity (Mosley et al., 2019). As these studies show, there is strong evidence for a neural-circuit basis to some of the symptoms in PD, however due to the variability in findings, more investigation is required to fully understand the mechanisms associated with clinical dysfunction in the disorder. To investigate these potential pathophysiological mechanisms, a network-based approach

is thus important as it may reveal neuroimaging biomarkers associated with clinical dysfunction in the disorder.

1.9. Network-based approaches to neuroimaging biomarkers

1.9.1. Neuroimaging biomarkers in PD

A number of methodologies have been used to investigate neuroimaging biomarkers associated with PD. These methodologies can provide insight to possible structural, functional and perfusion pattern changes in the disorder, and can be used for differential diagnosis as well as for more accurately understanding disease pathophysiology. Neuroimaging methodologies that have been used to search for biomarkers in PD include transcranial sonography (TCS), MR approaches utilising structural, functional and diffusion weighted MR imaging (DWI) sequences, and molecular techniques like positron-emission technology (PET) and single-photon emission computed tomography (SPECT). This thesis will now provide an overview of these neuroimaging methodologies and show how the work of the current thesis aims to build on this field of research.

TCS is a technique that has been used mainly to search for biomarkers of dysfunction to the substantia nigra (Bouwmans et al., 2013). Changes found at the substantia nigra using TCS are evidenced by hyperechoic signals that are likely associated with increased iron deposition, leading to oxidative stress and associated cell loss (Hwang, 2013). Increased echogenicity has been shown to be found in 90% of people with PD, however it is less effective in differentiating between different subgroups of PD participants, meaning that the biomarker can serve as a good measure for disease

detection (Postuma et al., 2015) but it has less utility in helping understand symptoms of the disorder.

DWI enables the investigation of changes to white matter in the brain by measuring the random Brownian motion of water molecules within tissue (Baliyan et al., 2016). When used to search for biomarkers in neurodegenerative disorders like PD, tensor-based approaches can reveal important information about the microstructural integrity of white matter tracts in the brain and how these changes relate to disease (Atkinson-Clement et al., 2017). Two crucial measures of tensor-based diffusion imaging (DTI) are mean diffusivity (MD) and fractional anistrophy (FA) (Basser and Pierpaoli, 1996). These metrics provide information about the movement and orientation of water molecules in the brain, which are considered reflective of white matter damage associated with disorders like PD. In the field of neuroimaging biomarkers in PD, DTI has primarily focussed on the differential diagnosis between PD and atypical Parkinsonian conditions (Meijer et al., 2013), as well as investigating the anatomical connectivity of important brain regions (Mishra et al., 2019). These studies have demonstrated that PD is associated with changes in white-matter structural integrity in a range of cortical and subcortical brain regions (Atkinson-Clement et al., 2017) and that white-matter structural changes are correlated with disease duration and clinical symptoms (Mishra et al., 2019).

The role of structural and functional imaging will be expanded upon in more detail in Section 2.1.1 and 2.1.2, but it is important to note briefly some of the progress that has been made in the search for neuroimaging biomarkers in PD using these methods. Possible changes to the SN have been proposed as potential diagnostic neuroimaging

biomarkers for PD, with dorsolateral areas showing characteristic low signals on high field strength MRI with T2-weighted sequences compared to controls (Blazejewska et al., 2013). Possible improvements in structural biomarkers in PD are showing more promise due to important development in high-field imaging, improved spatial resolution and improved methods for analysing this brain imaging data (He et al., 2018). Imaging of brain activity is performed with functional MRI, and using this technique it is possible to search for biomarkers of PD. The field has developed from investigating task-related activity changes to isolated brain regions, to searching for changes in and between intrinsic, large-scale networks associated with the disorder and its symptoms (Helmich et al., 2018). As explored in this thesis, the focus of analysis has mainly centred on changes within structures of the basal ganglia (He et al., 2018). Functional MRI analysis methods has shown promise from a diagnostic standpoint, able to find networks of interconnected brain regions can differentiate PD patients from control participants with high sensitivity and specificity (Szewczyk-Krolikowski et al., 2014). However, how these network changes are related to clinical symptoms, coupled with the lack of few clear patterns between research studies (Khan et al., 2018), make this an area of research requiring further investigation.

Another important methodology used to investigate neuroimaging biomarkers in PD centres around the imaging of dopamine. Due to the loss of dopaminergic cells of the SN and subsequent denervation of the striatum, various methods have been used to assess the altered function of nigrostriatal dopaminergic terminals. The most common approach is to use PET, or SPECT, which can be used to monitor the uptake of certain radiotracers that are linked to dopaminergic transmission. Uptake of 6-[18F]-fluoro-L-3,4-dihydroxyphenylalanine has been shown to be reduced in the striatum in early

stages of PD, as well as in anterior thalamic regions as the disease progresses (Pavese et al., 2011). Due to success in this area, *normal* functional imaging of the presynaptic dopaminergic system is an exclusion criteria for the Movement Disorder Society diagnosis of PD (Postuma et al., 2015). Recent research using dopamine transporter imaging in people with non-manifest LRRK2 and GBA mutation carriers has shown that clinical symptoms may predate dopaminergic changes (Simuni et al., 2020), paving the way for improved understanding of the relationship between the pathophysiology of the disorder and its manifestation.

As shown, clinical dysfunction in PD may be tied to changes in the structure of the brain as well as changes in the activity of brain regions. A neural circuit 'hubs-and-spokes' approach can be used to investigate structure and function of brain regions (Mesulam, 1990), which has the potential to reveal neuroimaging biomarkers associated with the disorder.

1.9.2. Hubs

Networks in the brain rely on the function of important structures called 'hubs,' which occupy positions of topological centrality within brain networks and make strong contributions to their functioning (Van Den Heuvel and Sporns, 2013, Crossley et al., 2014). While hubs within brain networks are crucial to functioning, they are uniquely vulnerable to the neuropathological processes underlying a range of brain disorders (Zhou et al., 2012). A key step in relating clinical dysfunction to the structure of the brain in neurodegenerative disorders like PD is to quantify disease related effects on brain morphology (Looi et al., 2014), which can be performed using T_1-weighted structural MRI.

This thesis thus investigates the morphology of two crucial hubs within basal ganglia-thalamocortical circuits, the striatum (Project one) and thalamus (Project two) in a search for neuroimaging biomarkers associated with clinical dysfunction in PD. Although analysing the structure of hubs within brain networks helps us understand the fundamental architecture of brain regions, and how this relates to clinical dysfunction, it is also necessary to consider the neural circuitry that connects brain regions.

1.9.3. Spokes

White matter tracts, which support functional dynamics of the brain (Bullmore and Sporns, 2009) can be considered 'spokes' along which neurodegenerative changes may take place (Looi et al., 2014). This thesis studies the spokes that interconnect brain regions using two approaches.

The first approach involves the use of resting-state functional MRI (rs-fMRI) in Projects one through three. This method allows for the investigation of the activity of intrinsic connectivity networks in the brain while a participants are 'at rest', producing a measure of 'functional connectivity' between brain regions (Biswal et al., 1995). A discussion of functional connectivity relative to 'structural connectivity' is presented in section 2.1.2 of this thesis.

The second way that spokes are investigated in this thesis is via an analysis of the structure of the corpus callosum, the largest white matter tract in the brain (Project four). The corpus callosum is the major inter-hemispheric connection in the brain

enabling the efficient transfer of information for a number of sensory, motor and cognitive functions (Looi et al., 2014).

Using this hubs-and-spokes framework, this thesis incorporates four projects to investigate neuroimaging biomarkers associated with clinical dysfunction in PD. Individual rationales, aims and hypotheses of each project are now presented.

1.10. Aims and hypotheses

1.10.1. Project one - Striatum

1.10.1.1. Rationale

Project one focusses on the striatum due to its position as a hub within basal ganglia-thalamocortical circuits (Looi and Walterfang, 2013), and due to the functional consequences of the loss of nigrostriatal dopaminergic input associated with the disorder (Kish et al., 1988).

1.10.1.2. Aims

Project one of this thesis aimed to investigate how the volume and surface shape of striatal structures were impacted in PD, and how changes in morphology related to clinical dysfunction. Project one then aimed to investigate whether there were any functional connectivity changes to these structures in the disorder.

1.10.1.3. Hypotheses

We hypothesised that there would be (1) significant reductions in striatal volumes in the PD cohort relative to the control subjects and that these reductions would be more pronounced in advanced disease stages, as measured by disease duration. It was also

hypothesised that (2) the PD group would display localised shape changes to the dorsal caudate nucleus and the posterior putamen, due to disease-related dopaminergic depletion at these sites (Kish et al., 1988). In the PD cohort, it was hypothesised that (3) atrophy of striatal nuclei would be correlated with poorer performance on measures of clinical function. Finally, it was hypothesised that (4) PD patients would display altered functional connectivity that would relate to the clinical symptoms observed in the disease.

1.10.2. Project two - Thalamus

1.10.2.1. Rationale

Project two of this thesis investigated the bilateral thalami due to their position as output hubs within basal ganglia-thalamocortical circuits (Power and Looi, 2014, Hwang et al., 2017), and due to the increased inhibition of thalamocortical projections consequent to dopaminergic depletion of the striatum. The thalami are also vulnerable to the underlying pathology of PD, with the presence of Lewy pathology and associated cell loss found in medial nuclear regions (Halliday, 2009).

1.10.2.2. Aims

Project two of this thesis therefore aimed to investigate the volume and the surface shape of the thalami, how these elements are impacted in PD, and how these variables are associated with clinical dysfunction. Project two then aimed to investigate whether the thalami undergo functional connectivity changes in PD.

1.10.2.3 Hypotheses

Based on the location of Lewy pathology within the thalami in PD and associated cell loss found postmortem, we hypothesised that (1) there would be reductions in volumes of the thalamus in PD patients compared to controls, based on the presence of PD neuropathology and the associated cell loss found post-mortem (Halliday, 2009). We also hypothesised that (2) there would be localised surface changes to medial regions of thalamus in PD, compared to controls. We hypothesised that (3) there would be a correlation between smaller overall volumes of the thalamus and poorer performance on measures of clinical function. Finally, we hypothesised that (4) there would be functional connectivity changes in our PD group due to the integral position the thalamus occupies within basal ganglia-thalamocortical circuits.

1.10.3. Project three - Cognitive impairment stages

1.10.3.1. Rationale

Project three of this thesis investigated the morphology and functional connectivity of the striatum and thalamus using MCI and dementia as disease progression stages. The presence of cognitive impairment in PD is tied to an increased likelihood of developing dementia, which is associated with increased mortality and significant reductions in quality of life (Goldman et al., 2018), making an understanding of the pathophysiology behind cognitive impairment of crucial importance.

1.10.3.2. Aims

Project three of this thesis thus aimed to uncover any volumetric and surface shape changes to the caudate nucleus, putamen and thalamus, and how they were impacted in PD relative to the presence of MCI and dementia. Project three then aimed to

investigate possible changes in the functional connectivity of these structures. Finally, Project three aimed to better understand what may be driving changes in functional connectivity by performing a correlation analysis between functional connectivity of the caudate nucleus, putamen and thalamus and clinical variables.

1.10.3.3. Hypotheses

Functional MRI research in PD patients has revealed areas of both *over*- and *under*-activity during the performance of cognitive tasks, suggesting a combined presence of decreased brain function and compensatory mechanisms (Ray and Strafella, 2012). Research has argued that such a compensatory response may rely on sufficient neuronal resources. Accordingly, we present novel hypotheses whereby (1) cognitively unimpaired participants with PD would have sufficient neural resources to support functional compensation, and display increased functional connectivity, concomitant with no volumetric or surface-based shape alterations to the caudate, putamen and thalamus. However, we hypothesise that (2) morphological alterations to these structures would take place in PD-MCI, representing a 'critical threshold,' where functional connectivity begins to decrease along with reductions in morphology, evidenced by reduced volumes and surface deflation when compared to cognitively unimpaired PD participants, and controls. Finally, we hypothesised that (3) PDD participants would demonstrate significant and profound reductions in volumes and surface shape, along with significant decreases in functional connectivity of the caudate nuclei, putamina and thalami compared to all experimental groups.

1.10.4. Project four - Corpus callosum and cortex

1.10.4.1. Rationale

Projects one, two and three focussed on intra-hemispheric neural circuits that mediate a range of behaviours linked to the clinical manifestations associated with PD. To extend this analysis and gain a fuller understanding of the neural circuit basis of clinical dysfunction, Project four investigates the morphology of the corpus callosum, the largest white matter structure in the brain. The corpus callosum is integral for the integration of inter-hemispheric cortical activity via its connectivity of homotopic cortical regions.

1.10.4.2. Aims

Project four aimed to uncover possible alterations to the morphology of the corpus callosum. An analysis of the cerebral cortex, which is the site of origin for basal ganglia-thalamocortical circuits, was also performed as this has the potential to yield neuroimaging biomarkers of clinical dysfunction, due to its link to both cognitive impairment and PD-related dementia (Halliday et al., 2008, Zarei et al., 2013), coupled with the fact that the cortex is the site of origin and termination of basal ganglia-thalamocortical circuits.

1.10.4.3. Hypotheses

Evidence suggests that white matter integrity of the corpus callosum is impacted in PD (Agosta et al., 2014a), while the thickness of the cortex decreases with disease progression (Wilson et al., 2019). It was thus hypothesised that (1) PD participants would demonstrate reduced thickness of the corpus callosum and cortex compared to controls. Research has shown that greater thickness of the callosum is linked to

measures of general cognitive ability (Luders et al., 2007) and as there are increased structural changes to both grey and white matter structures in the brain with increasing levels of cognitive impairment, we hypothesised that (2) changes in thickness of the corpus callosum would be more pronounced in MCI participants compared to cognitively unimpaired PD, and controls, while PD participants with dementia would have significant and widespread reductions in callosal thickness compared to PD with MCI and cognitively unimpaired PD participants. Due to the structural connectivity between the corpus callosum and cortex, we present the novel hypothesis that (3) the thickness of the corpus callosum would correlate with thickness at particular cortical regions, highlighting a potential usefulness for corpus callosal thickness as a proxy measure of cortical degeneration in PD.

Before presenting the four project chapters, this thesis will now provide background to the main methodological approaches that were employed in these projects.

2. Methodology

This chapter begins with a description of the Swedish BioFinder Study, the data of which forms the material for this PhD thesis. This chapter then presents the general methodology used, outlining concepts that are important to the understanding of neuroimaging biomarkers in PD. This chapter then outlines the use of structural and functional MRI data, followed by the presentation of the methods used to extract data from each modality. The chapter finishes by outlining the core data processing and analysis techniques used to investigate the structural and functional neuroimaging data.

2.1. Swedish BioFinder Study Details

2.1.1. Recruitment and participants

The data for this PhD thesis derives from the Swedish BioFinder study, which is a prospective and longitudinal program aiming to learn more about the pathological mechanisms underlying important neurodegenerative disorders as well as in normal aging. According to my interest in neuroimaging biomarkers for PD, this thesis is a secondary analysis of existing data, and comprising the clinical and neuroimaging data of the parent BioFinder Parkinsonian cohort. The current thesis focusses on patients within the Parkinsonian cohort with a diagnosis of PD (n = 101) based on the National Institute of Neurological and Stroke Diagnostic Criteria (Gelb et al., 1999) who are treated at the Skåne University Hospital, in the Skåne region of Sweden. Participants received their clinical assessments between 23/05/2012 and 13/03/2014. The study also focuses on control participants who were also recruited from the Skåne region. Exclusion criteria for this study included refusing MRI, the presence of

significant alcohol or substance misuse and/or a significant systematic illness or organ failure.

2.1.2. MRI Acquisition

T_1-weighted MRI was performed on a 3T scanner (Trio Magnetom, Siemens, Erlangen, Germany) equipped with a 20-channel head-coil. High-resolution three-dimensional anatomical brain images were acquired using a magnetisation-prepared rapid acquisition technique with gradient-echo sequence (repetition time = 7 ms; echo time = 3 ms; flip angle = 90 degrees; voxel size = isotropic 1mm^3). Image matrix size was 356 voxels in the coronal and sagittal planes and 176 voxels in the axial plane, with no interslice gap.

Functional imaging was also performed on participants in the BioFinder Study. This consisted of 256 T_2*-weighted echo planar imaging volumes (repetition time = 1850 ms; echo time 30 ms; flip angle = 90 degrees; matrix 64 × 64; voxel size 3 × 3 × 3.75 mm^3). Image matrix size was 64 voxels in the coronal and sagittal planes and 36 voxels in the axial plane. Participants were instructed to lie still with their eyes closed, not to fall asleep and not to think of anything in particular during the scan.

2.1.3. Clinical Assessment

All participants underwent a cognitive and neurological examination by a medical doctor with extensive experience with movement disorders, while PD participants remained on their usual medication regimes. Clinical functioning was quantified using the Hoehn and Yahr staging, assessing the progression of the disorder; the Unified Parkinson's Disease Rating Scale Part-III test (UPDRS-III), assessing the motor signs

of PD (Fahn and Elton, 1987); the Mini Mental State Examination (MMSE), assessing cognitive mental state (Folstein et al., 1975); the Animal Fluency and Letter S Fluency tests, assessing verbal fluency and executive function (Tombaugh et al., 1999) and the A Quick Test of cognitive speed assessing perceptual and cognitive speed (Palmqvist et al., 2010).

2.2. Neuroimaging data and analysis methods

2.2.1. Structural MRI data

Structural T_1-weighted MRI (structural MRI) is used in this thesis to investigate neuroimaging biomarkers via the analysis of changes in brain morphology. To do this, regions-of-interest (ROI) are segmented within participant's structural MRI using observable boundaries between anatomical structures or brain tissue types. Different segmentation methods are used depending on the research aims, and once performed, elements of morphology can be calculated and analysed. This thesis models elements of morphology using volumes, surface shape and structure thickness.

2.2.2. Functional MRI data

T_2^*-weighted echo planar functional MRI (functional MRI) is a commonly used tool for mapping brain activity, as well as a means of investigating the dynamics of neuronal circuits (Logothetis et al., 2001). Functional MRI provides information about haemodynamic changes after increased neural activity, producing observable changes in the blood-oxygen-level-dependent (BOLD) signal. Functional MRI works on the premise that increases in the BOLD signal relate to neural activation which induces a localised increase in blood flow producing hyperoxygenation and a relative decrease in the concentration of deoxyhaemoglobin (Logothetis, 2008). BOLD

functional MRI images are obtained sequentially over a series of timepoints, with each image made up of small volume elements (voxels). Each voxel within these three-dimensional images, once stacked sequentially, can be considered a vector of signal intensities over time, and are thus referred to as timeseries data (Bandettini et al., 1993).

After its inception into neuroimaging research, functional MRI was primarily used with stimuli or task-based paradigms to investigate BOLD timeseries data in different brain regions (Shen, 2015). Biswal et al. (1995) first investigated spontaneous timeseries data in participants who lay in fMRI scanner and performed no tasks. This pioneering resting-state fMRI research showed that during 'rest', brain activity is both structured and organised, and that the activity of brain regions that are known to function together demonstrate 'functional connectivity' (Biswal et al., 1995). Functional connectivity indicates areas of the brain with a temporal dependence between neuronal activity patterns (Friston et al., 1993). Significant research has since corroborated this theory, showing that areas in the brain that share similar temporal BOLD timeseries form functional networks (Murphy et al., 2013).

It is important to note, though, that functional connectivity does not measure direct structural connectivity of white matter tracts as afforded using diffusion weighted imaging. Despite this, there are a number of important factors that make the use functional connectivity a valuable approach for this thesis. Firstly, research has shown that the method is able to successfully probe brain networks, evidenced by the high correspondence between resting-state networks and the underlying white matter architecture of the brain (Van Den Heuvel et al., 2009). There is also a strong

correspondence between the brain's functional architecture during task activation and at rest (Smith et al., 2009). This correspondence enables researchers to use rs-fMRI functional connectivity as a valid measure to study brain networks that are tied to behavioural processes (i.e. sensorimotor, visual, auditory and executive control), indicating that the networks utilised by the brain during action are continuously and dynamically active in the brain during the resting state. Finally, this approach has a number of methodological benefits, including being low-cost, non-invasive, it has high spatial resolution and it does not require participants to engage in difficult behavioural programs which can be difficult with certain experimental cohorts (Gao and Wu, 2016).

2.3. Structural MRI: ROI segmentation

This thesis investigates the morphology of structural ROIs using volume, surface-based shape analysis and thickness measures. Investigating volumes of ROIs in the brain can inform on atrophy/hypertrophy, while surface-based shape analyses can reveal subtle localised morphological changes that may not be discoverable using volumetry. The third metric used to investigate morphology in this thesis is thickness, which is used to model changes in the morphology of the corpus callosum and neocortex.

The two main ways that brain morphology can be quantified in structural MRI data are manual and semi-automated segmentation approaches. When aiming to quantify volume or surface-based shape changes of brain ROIs, manual segmentation is considered the gold-standard, especially when dealing with patient cohorts (Morey et al., 2009, Power and Looi, 2015). However as brain imaging datasets have increased

in size, semi-automated segmentation approaches have become a necessity. Further, to have a potential for clinical application, semi-automated segmentation techniques hold more promise given that time-consuming manual segmentation approaches by clinicians are likely not a feasible option (Guenette et al., 2018). As striatal and thalamic structures were segmented on a cohort of 101 (Projects one and two), manual segmentation methods were used for these projects. The statistics on the reliability and reproducibility this tracing approach is presented in Appendix 1: Manual ROI segmentation tracing reliability. Due to the complex nature of quantifying morphology of the corpus callosum and cortex, semi-automated software pipelines were used for Project four.

2.3.1. ROI segmentation: caudate nucleus

Segmentation of the bilateral caudate nuclei and putamina from participant's structural MRI data was performed using validated manual tracing protocols (Looi et al., 2009, Looi et al., 2008) with the aid of a neuroanatomical atlas (Duvernoy, 2012). These tracing methods produce 3-D object maps of the structures that can be analysed at the group-level for any experimental effects on volume and surface shape. The protocol for manually segmenting the caudate nucleus (Looi et al., 2008) begins with the most inferior MRI slice where the head of the caudate is distinct from the putamen, separated by the internal capsule. The medial border of the caudate is the lateral wall of the lateral ventricle, while the lateral surface of the caudate is the medial border of the internal capsule. Tracing of the caudate is performed in each axial 2D slice moving in the superior direction until the caudate is no longer visible next to the wall of the lateral ventricle in its most superior slice (Figure 2.1).

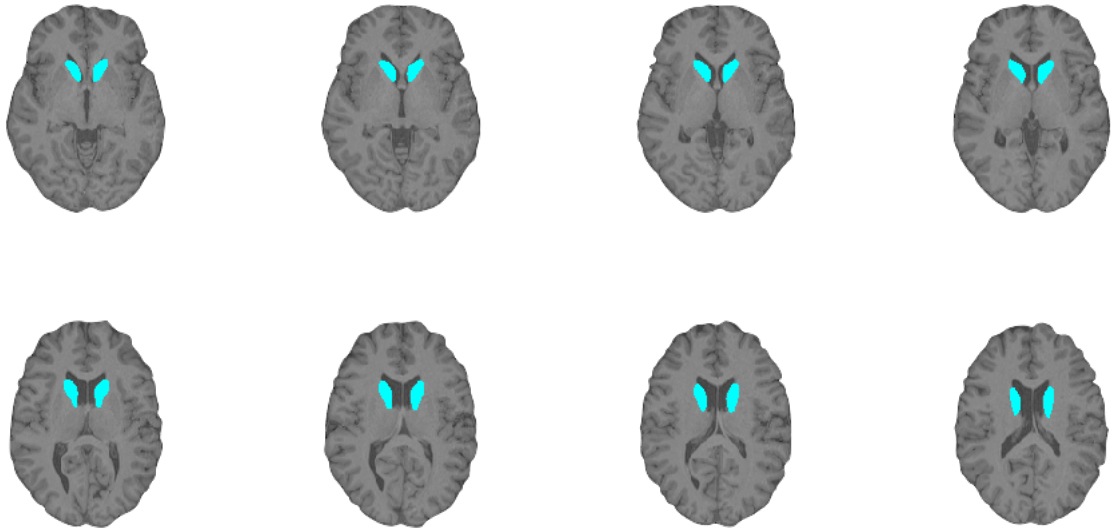

Figure 2.1: Segmentation of the caudate nucleus. An example tracing of the bilateral caudate nuclei on a participant's structural MRI in the axial plane. The caudate nuclei are highlighted in light blue.

2.3.2. ROI segmentation: putamen

The protocol for manually segmenting the putamen (Looi et al., 2009) begins in the same axial slice as the caudate nucleus, where the two structures are separated by the anterior limb of the internal capsule. The medial border of the putamen is traced along the lamina of white matter of the internal capsule separating the structure from the globus pallidus while the lateral border of the structure follows the white matter of the external capsule running between the putamen and the claustrum. The superior boundary of the putamen is selected as the slice prior to the structure no longer being visible (Figure 2.2).

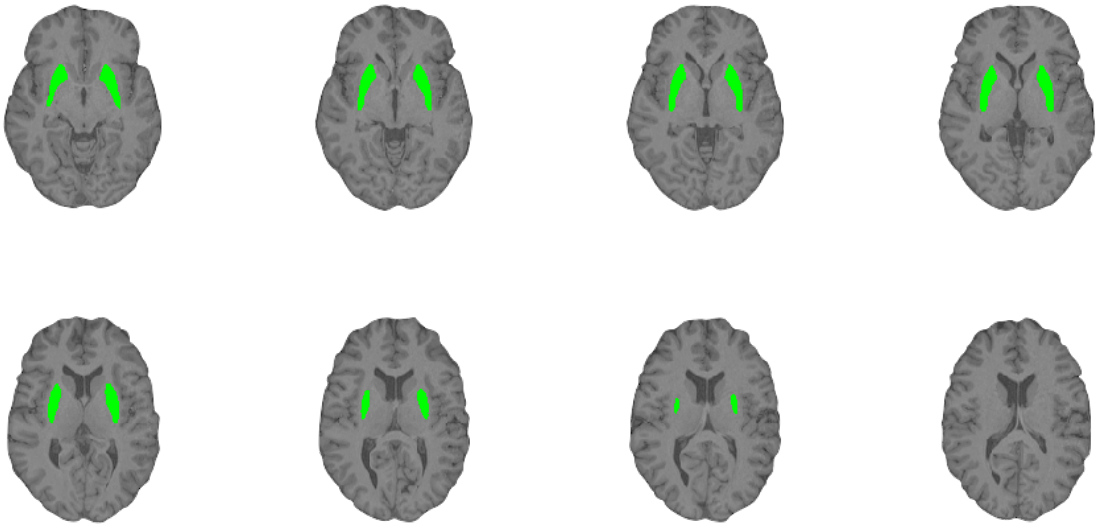

Figure 2.2: Segmentation of the putamen. An example tracing of the bilateral putamina on a participant's structural MRI in the axial plane. The putamina are highlighted in green.

2.3.3. ROI segmentation: thalamus

Segmentation of the bilateral thalami from participant's structural MRI data was also performed using a validated manual tracing protocol (Power et al., 2015) with the aid of two neuroanatomical atlases (Duvernoy, 2012, Morel, 2007). Segmentation was performed in the coronal plane and proceeded in a caudal-rostral direction, starting by tracing the most caudal part of the thalamus (pulvinar) as it emerges under the crux fornix. ROIs in subsequent slices are traced in the rostral direction until the crus cerebri is seen to separate from the body of the pons. The medial border of the structure is clearly defined by the third ventricle, and the superior cistern in more caudal sections. The lateral border of the structure is defined by the reticular nucleus, while the inferior border is defined by characteristic white matter tracts proximal to prominent neuroanatomical landmarks including those adjacent to the red nucleus and subthalamic nucleus, and in more rostral slices, the hypothalamic sulcus. The superior border was defined by the floor of the lateral ventricle. The rostral aspect of the thalamus is characterized by the emergence of the mamillary bodies and

hypothalamus, with the most rostral slice visualised at the inferior pole of the head of the caudate (Figure 2.3).

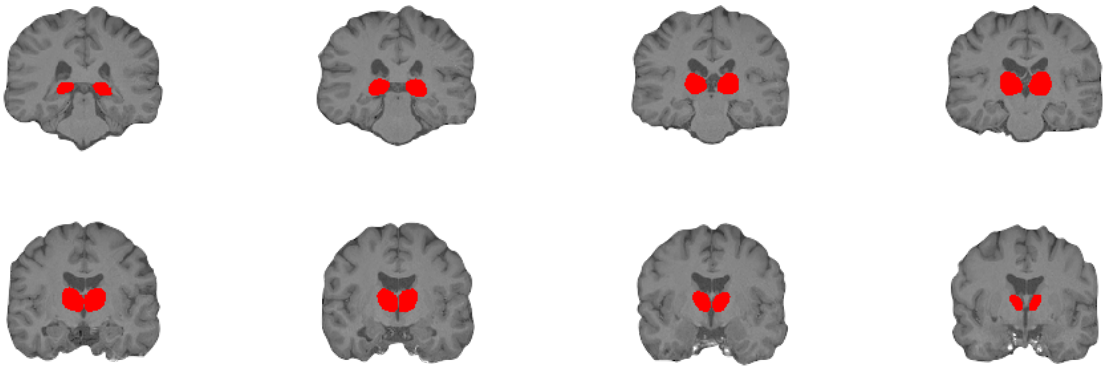

Figure 2.3: Segmentation of the thalamus. An example tracing of the bilateral thalami on a participant's structural MRI in the coronal plane. The thalami are highlighted in red.

2.3.4. ROI segmentation: corpus callosum

Morphology of the corpus callosum was modelled using midsagittal corpus callosal thicknesses, segmented using an automated pipeline described in published works (Adamson et al., 2014, Adamson et al., 2011) (Figure 2.4).

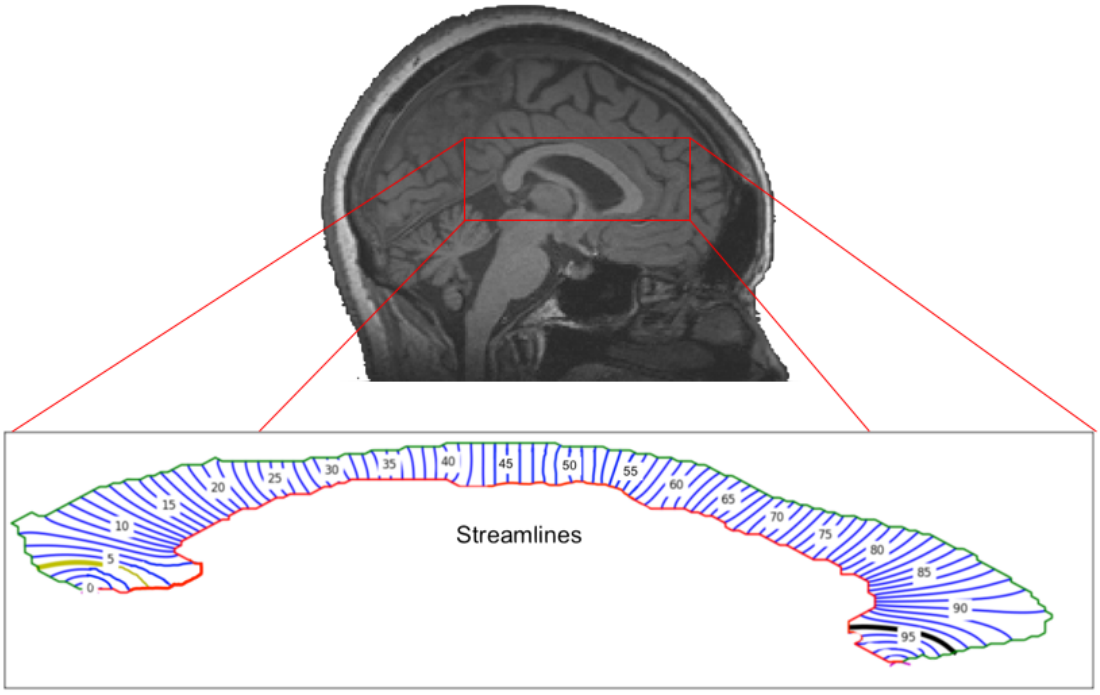

Figure 2.4: Midsagittal corpus callosum and thickness streamlines. This figure displays an example of a corpus callosum midsagittal plane that has been segmented from a structural MRI. Thickness streamlines are drawn at the 100 nodes along the structure, represent evenly spaced non-overlapping thickness profiles that connect perpendicularly with the upper (green) and lower (red) boundaries of the structure.

The production of these thickness streamlines involves three key steps: the identification of the midsagittal plane within a participant's structural image; segmentation of the structure; and the generation of a thickness profile. Extracting the midsagittal plane from the original structural MRI is performed by finding the plane that intersects the falx cerebri, the cerebral aqueduct, the pineal stalk and the peaked roof of the fourth ventricle (Mitchell et al., 2003). Once the midsagittal plane has been identified, the corpus callosum is segmented using a template guided method that corrects for topological errors and removes any anterior and posterior pericallosal vessels. After segmentation, the software generates the thickness profile of each participant's corpus callosum using the following steps: the corpus callosum is split into left (posterior) and right (anterior) halves; endpoints are defined as the bottom-

right and bottom-left extrema of the structure, which form the start and end of a midline contour. This midline contour runs equipotentially (at an even distance from top and bottom boundaries), subdividing the outside of the corpus callosum into superior and inferior contours. 100 streamlines are then generated at evenly spaced intervals along the centre contour, which are non-overlapping nominally parallel lines intersecting the superior and inferior contours orthogonally along the anterior-posterior trajectory. The length of each streamline is then saved for each participant and used as a dependent variable during subsequent statistical analyses.

2.3.5. ROI segmentation: cerebral cortex

The quantification of cortical thickness in the current thesis was performed using semi-automated FreeSurfer analyses, described in published works (Dale et al., 1999, Fischl and Dale, 2000). This process involves motion correction and averaging of multiple volumetric structural MRI images (if working on multiple participants) (Reuter et al., 2010), removal of non-brain tissue using a deformation procedure (Segonne et al., 2004), automated Talairach transformation, intensity normalisation (Sled et al., 1998), tessellation of the grey matter-white matter boundary, automated topology correction (Fischl et al., 2001, Segonne et al., 2007), surface deformation along intensity gradients to optimally define cortical surface borders, registration to a spherical atlas using individual cortical folding patterns to align cortical anatomy between participants (Fischl et al., 1999), and finally, the parcellation of the cerebral cortex into units with respect to gyral and sulcal structure based on the Desikan-Killiany atlas (Desikan et al., 2006, Fischl et al., 2004). Once this processing has been performed, an average thickness of each cortical ROI in the Desikan-Killainy atlas is

saved for each participant and used as a dependent variable during subsequent statistical analyses.

2.4. Structural ROI analysis techniques

2.4.1. Volumetrics

Quantitative morphological assessment of brain structures is commonly performed using volumetric measurements. First suggested by Lande (1979) as a way to investigate morphology of brain regions, volumetry can inform on atrophic or hypertrophic changes that take place in response to healthy aging or disease processes. Studies have revealed atrophy of several brain regions in disorders including Alzheimer disease (Apostolova et al., 2006), Huntington disease (Aylward et al., 1997) and schizophrenia (Vita et al., 2006), while innovative work by Maguire et al. (2000) showed that hypertrophy of the hippocampus was associated with navigational experience in London taxi drivers. Assessment of volumes are performed by summing the voxels within a ROI mask or segmentation, adjusting for partial volume effects (due to the effect of dealing with MRI voxels containing multiple tissue types), and multiplying this number by the size of an individual voxel.

2.4.2. Shape analyses

Shape analysis has become a significant neuroimaging tool used in the analysis of brain morphology due to its potential to locate precise changes between pathological and non-pathological brain structures. This is due to the fact that structural shape changes at specific neuroanatomical locations are not sufficiently reflected in volumetric measurements (Styner et al., 2006). Shape analysis can thus be used as a complementary technique to measure morphological changes that might be missed at

by analysis at the volumetric level. Early work by Wang et al. (2001) was able to demonstrate the usefulness of localised shape analysis methods, as they found that shape of the hippocampus could differentiate between control participants and participants with schizophrenia, whereas volumetry of the hippocampus could not. Research such as this spurred the development of techniques that can fully characterise biological and pathological-based shape variability in neuroanatomical ROIs (Gerig et al., 2001). The shape of an object provides information on quantities that do not vary when the object is moved, rotated, enlarged or reduced (Bookstein, 1997). Shape analysis can be performed using a number of methods, such as tensor-based morphology (Chiang et al., 2007), radial distance mapping (Thompson et al., 2004), voxel based morphometry (Wright et al., 1995) or spherical harmonic point distribution models (SPHARM-PDM) (Cootes et al., 1995, Gerig et al., 2001, Styner et al., 2006). The approach chosen to analyse possible localised morphological changes to brain structures in the current thesis is surface analysis, performed using SPHARM-PDM. This approach maps nodes on the surface of a ROI to the surface of sphere, with every node being associated with a voxel vertex. The resulting arrangement of vertex nodes on the sphere accurately reflects the geometry of the original ROI (Brechbühler et al., 1995). This parametrisation of the ROI surface onto a sphere produces one-to-one mapping of surface vertices and makes possible a comparison of object average surfaces between experimental groups or in relation to clinical variables (Figure 2.5).

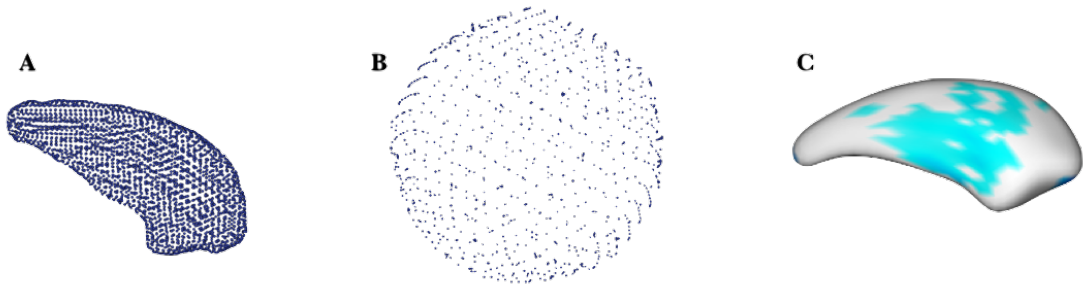

Figure 2.5: SPHARM-PDM Example. This figure demonstrates A) how points are distributed over the surface of a ROI segmentation. These then get parametrised onto the surface of a sphere B) which enables the comparison of surface shape between experimental groups, producing inflation and deflation maps C) indicating regions with significant surface change in one group compared to another.

2.4.3. Thickness of corpus callosum

To model the morphology of the corpus callosum, this thesis used a midsagittal thickness metric. As cortico-cortical connections through the corpus callosum are primarily arranged topographically, an investigation of the thickness of the corpus callosum serves two purposes. The first is that it may reveal information about the impact of primary white matter pathology on the corpus callosum (i.e myelin injury). The second purpose is that it may be able to inform on changes to the structure that are the result of neurodegenerative changes to connected cortical ROIs (Goldman et al., 2017). MRI studies investigating callosal morphology have found midsagittal thickness of the corpus callosum is associated with levels of clinical function (Luders et al., 2007), while morphological changes to the structure have been found in a number of disorders including frontotemporal lobar degeneration (Walterfang et al., 2014), Huntington (Di Paola et al., 2012) and Alzheimer disease (Ardekani et al., 2014). A number of schemes have been used to describe the morphology of the corpus callosum, including subdivision based on arithmetic fractions of the maximum anterior-posterior extent (Witelson, 1989), cortical endpoint (Hofer and Frahm, 2006)

and boundary tangent models (Joshi et al., 2013). The current thesis employed a cross-sectional midsagittal thickness approach. This approach can be easily quantified using an automated pipeline and shows a high segmentation accuracy when compared to manual segmentation. Further, the macroscopic properties of the wider corpus callosum can be extracted from the analysis of the midsagittal plane alone (Adamson et al., 2014).

2.4.4. Thickness of the cerebral cortex

To model the morphology of the cortex, this thesis uses an average cortical thickness metric. The cerebral cortex is the outermost layer of the brain, comprised of a highly folded sheet of neurons varying greatly in thickness, from 1 to 4.5 mm (Kandel et al., 2000). Cortical thinning is regionally specific, and the progress and positioning of atrophy can reveal important information about brain disorders (Fischl and Dale, 2000). Investigating cortical thickness relies on the fact that the cerebral cortex is organised into ontogenetic columns that run perpendicular to the surface of the brain (Kandel et al., 2000, Rakic, 1988). This means that cortical thickness is likely driven by the number of cells within each of the cortical columns, suggesting that cortical thickness reflects the arrangement of neurons in a biologically and topologically meaningful way (Hanganu and Monchi, 2016).

Cortical thickness has also shown to be effective in matching of neuronally homologous cortical regions between participants giving it an advantage over other cortical morphology approaches such as cortical volumes or surface areas (Zarei et al., 2013). Cortical thickness has been investigated in a wide variety of disorders including mild cognitive impairment and Alzheimer disease (Dickerson et al., 2008),

frontotemporal dementia (Du et al., 2007), amyotrophic lateral sclerosis (Schuster et al., 2014) as well as in PD (Pereira et al., 2012, Wilson et al., 2019).

2.5. Resting-state functional MRI: preprocessing

In order to investigate the connectivity of spokes between brain hubs, this thesis analysed functional MRI using a resting-state (rs-fMRI) functional connectivity approach. This form of analysis involves two major stages: preprocessing and data analysis. Significant preprocessing is necessary in rs-fMRI functional connectivity analyses as the neuronal BOLD signals-of-interest comprise around 3% of the total fMRI signal, with the rest considered noise (Bianciardi et al., 2009). If implemented correctly, preprocessing and data analysis can accurately and reliably detect BOLD activation in the resting brain, despite this noisy structure of the data. In what follows, an overview of preprocessing and data analysis methodologies are presented, with any deviations from the approach for a particular project stipulated in the relevant chapter.

2.5.1. Registration

One of the first steps in rs-fMRI preprocessing is functional image registration. Movement of research participants during the acquisition of a functional image can lead to specific brain tissue shifting from one voxel location to another over time. This can produce both false positives (voxels being incorrectly labelled as “active”) and false negatives (voxels being incorrectly labelled as “inactive”) during the analysis of data. This potential confound can be addressed by aligning each scan 3D fMRI scan within a 4D timeseries dataset to a reference scan, in a process called registration. Registration also serves the dual purpose of spatially aligning images with each other so that subsequent analysis steps can extract MRI data from consistent

anatomical locations across different scans or modalities (structural and functional MRI) for the same subject, or from the same location in different participants (Figure 2.6).

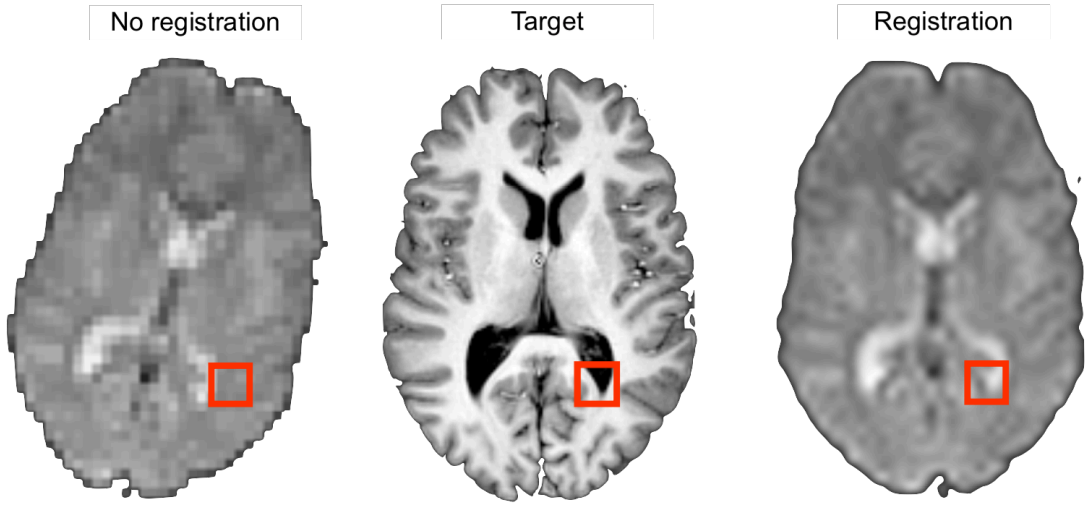

Figure 2.6: Image registration. An example of two BOLD images, one on the left that has not been registered to the target, and one on the right that has. The red squares indicate where a consistent neuroanatomical region should exist, the posterior horn of the left lateral ventricle, which aligns in the registered image but not the unregistered image.

2.5.2. Temporal and spatial filtering

Temporal and spatial filtering can be used to improve the signal-to-noise ratio (SNR) of functional MRI data. Temporal filtering is a process of identifying noise components by their frequencies. These noise components can be related to non-neuronal sources due to scanner-related drifts or physiological effects. Scanner-related drifts are slowly changing signals produced by imperfections of the MRI hardware, such as the heating of components within the scanner. Physiological effects are mainly induced by cardiac and respiratory processes (e.g. pulsatile motion of brain due to cardiac cycles). These effects are typically low frequency and their presence can be minimised within the data using temporal filtering (Woolrich et al., 2001). To

remove low frequency components, high-pass filtering is performed via the convolution of timeseries with the hemodynamic response function. The underlying idea is that the rate at which BOLD signal can change in the brain occurs at frequencies that are relatively well-defined, as they are constrained by blood flow around the brain. Therefore it is possible to choose a 'smoothing kernel' that maximises of the signal-of-interest relative to other frequencies. Assuming that the fMRI timeseries has a set of linearly separable components, including for instance high-frequency noise, low-frequency noise and low-frequency signal, using temporal filtering in this way can highlight the haemodynamics contributing to a functional MRI timeseries and reduce the noise.

Spatial filtering (often referred to as spatial smoothing) involves using a smoothing kernel to blur data by calculating a locally weighted average of the intensities around each voxel at each point in time (Jenkinson and Chappell, 2018). Spatial filtering is able to increase SNR because averaging noise within the data will reduce the amplitude, whereas averaging signal has the effect of maintaining the same value. This is possible as long as neighbouring voxels contain signal of interest. The amount of smoothing that is chosen, specified as the full width at half maximum in millimetres, sets the size of the Gaussian kernel that is used to calculate the weights for local averaging. Performing spatial smoothing also enables the use of Gaussian random field theory which is used to correct for the issue of multiple testing (multiple comparisons) that assumes a level of smoothness to the data. An example of the effect of spatial smoothing on functional MRI data is shown in Figure 2.7. Implications of smoothing functional MRI data are discussed in Discussion section 7.3.3.

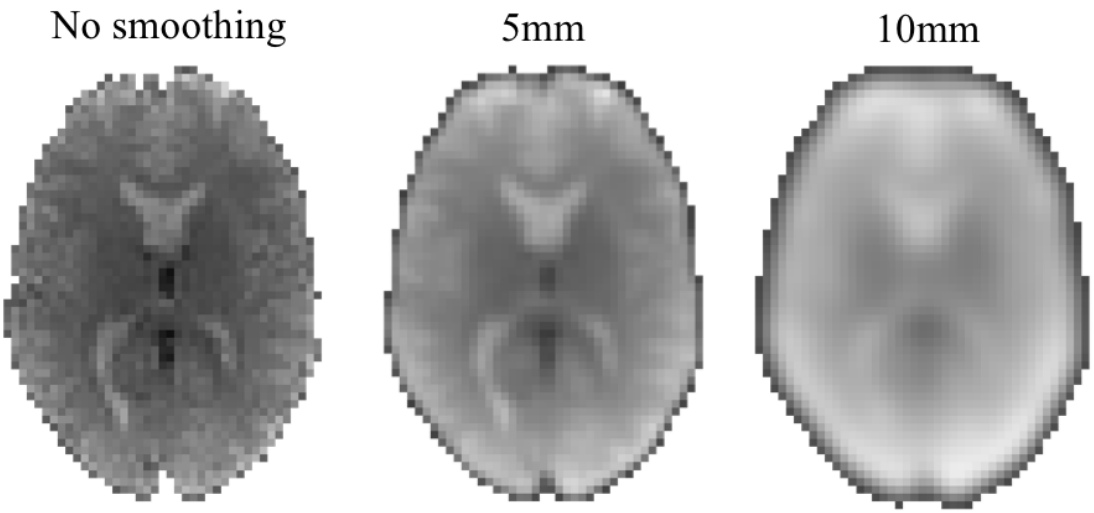

Figure 2.7: Spatial filtering. Spatial filtering enables an image to be smoothed to increase SNR, however it has the effect of blurring the image, as can be seen in this figure demonstrating the appearance of the same functional MRI image with no smoothing, smoothing with a 5mm and with a 10mm full width half maximum Gaussian kernel.

2.5.3. Intensity normalisation

Intensity normalisation (or grand mean scaling) is an important process applied in all fMRI analysis pipelines. The process provides a way of compensating for a variety of changes that exist between subject fMRI data. The mean intensity of an fMRI image is taken over all voxels and all points in time, and is then scaled to some fixed value. The effect is then consistent across all participants, and allows for a reduction in between-subject variance, improving statistical power at the group level (Jenkinson and Chappell, 2018).

2.5.4. Independent component analysis denoising

This thesis also used independent component analysis (ICA)-based denoising procedure to further increase the SNR. This process involves the decomposition of 4D fMRI data into sets of spatially-structured components (Beckmann and Smith, 2004). These vectors describe signal variation across the temporal domain (time-courses) and

across the spatial domain (maps) by optimising for non-Gaussian spatial source distributions using a fixed-point iteration technique (Hyvarinen, 1999). Component maps are also divided by the standard deviation of the residual noise and thresholded by fitting a mixture model to the histogram of intensity values. The value of each component in the spatial map represents the amount of that particular component's timecourse that exists in the functional MRI data at each location (Jenkinson and Chappell, 2018). This process identifies voxels in a statistic image that share a large proportion of the same timecourse and therefore show areas of the brain that share a common signal and are likely part of the same network. This process produces a set of neuronal network components, however it can also be used to identify structured noise within the 4D image. Components labelled as signal can be left in the data, while the variance associated with noise components can be removed from the data using linear regression.

2.6. Resting-state functional MRI: data analysis

2.6.1. Resting-state fMRI data analysis: seed-based correlation analysis

Seed-based correlation mapping is one of the most widely used approaches to study functional connectivity of brain regions (Zhang and Raichle, 2010). In a seed-based correlation analysis, a seed-ROI is chosen that forms the basis for the resulting functional connectivity map. This seed-ROI can be a single voxel, a whole structure or a functional region that is made up of a group of voxels. The aim of a seed-based correlation analysis is to create a 'statistic image' that describes the strength of functional connectivity of all voxels in the brain with the chosen seed-ROI. While seed-based analysis is not the only option for functional connectivity analyses, they are appropriate for hypothesis-driven experimentation with *a priori* ROIs (Zhang and

Raichle, 2010), as is undertaken in this thesis. To create this functional connectivity statistic image, average BOLD timeseries data is extracted from within the seed-ROI and correlated with all voxels in the brain at the individual-level general linear model (GLM) stage in a mass univariate approach (Figure 2.8).

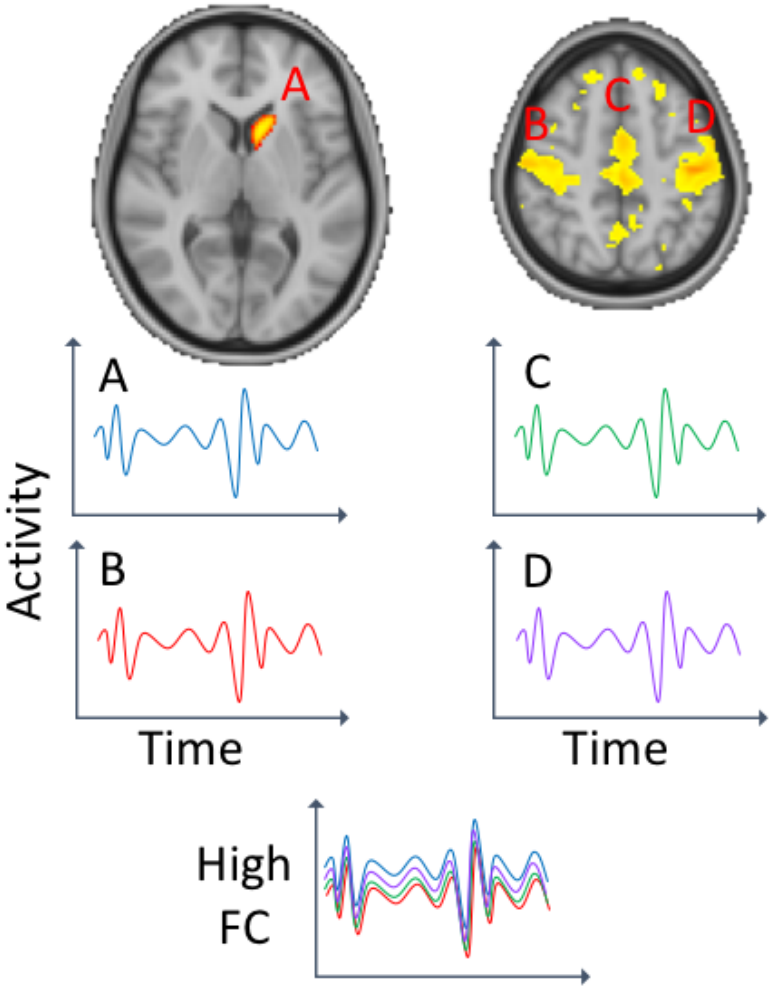

Figure 2.8: rs-fMRI seed-based correlation analyses. This figure shows how the average BOLD signal (activity) can be taken from a seed-ROI (A) and correlated with activity all around the brain using a general linear model framework. Areas of the brain that share a high temporal dependency in their timeseries (B, C, D) are said to show high functional connectivity with the seed region and are thus potentially part of the same functional network. **Abbreviation:** FC, functional connectivity.

2.6.2. General linear modelling: mass univariate approach

Statistical analysis of functional MRI data begins at the voxel level, involving the analysis of the statistic image to assess possible experimental effects. This requires the use of a method that accounts for the inherent multiplicity of testing thousands of voxels simultaneously. This is performed using general linear modelling, first at the individual-level and secondly at the group-level.

2.6.2.1. Individual-level GLM

Individual-level GLMs are used to probe the relationship between the BOLD signal within seed-ROIs and the rest of the brain, in a voxelwise mass univariate manner. The goal of this process is to separate signal from noise, while maximising the true positive rate and minimising the false positive rate. To perform these individual-level GLMs, BOLD timeseries data extracted from within a seed-ROI act as explanatory variable, while timeseries data from nuisance variables serves as covariates that are regressed from the data. Nuisance regression involves extracting data from sources that may contribute noise to the functional MRI signal. Potential sources of noise include white matter, ventricles and whole brain activity (global signal) as well as head motion. Timeseries data for white matter, ventricles and whole brain regions area are created by using masks of these regions and extracting average activity at each point in the timeseries which can be regressed from the data. Head motion parameters can be quantified by calculating values for the rigid-body transformations used during image registration, which are then saved as a set of parameters that are regressed from the data. The output from the individual-level GLM approach is a whole-brain functional connectivity statistic image which is used in subsequent group-level analyses.

2.6.1.2. Group-level GLM

In this thesis, comparing statistic images between experimental groups was performed using a group-level mass univariate GLM framework. This framework relates a dependent variable, which is each voxel within a statistic image, to an independent variable (an experimental condition), after removing the effects of group-level covariates (i.e. age, sex, years of education or medication data). The resulting statistic image is then assessed for statistical significance using random field theory which identifies voxels in the image where there is significant evidence to reject the null hypothesis (Friston et al., 1994, Poline et al., 1997, Worsley, 1995). This analysis is performed at each voxel within the brain, resulting in tens of thousands of voxels being analysed. Because of this, the problem of multiple comparisons is significant and a correction needs to be applied to the *p*-values to ensure the statistics are valid.

Among the many approaches available, cluster-extent based thresholding is the most popular when analysing functional MRI data at the group level. This approach detects statistically significant clusters within a statistic image based on the number of contiguous voxels where the test statistic is above a pre-determined cluster-forming threshold (Woo et al., 2014). Rather than controlling the false positive probability of every voxel in the contiguous region, cluster-extent thresholding enables researchers to control the false positive probability of the region as a unified whole. A *p*-value is then calculated for each cluster based on its size and mass using the principles of Gaussian random field theory or permutation testing (Smith and Nichols, 2009). Benefits of cluster-extent thresholding include its high sensitivity when compared to other approaches such the Bonferroni method, and it accounts for the fact that

activation of voxels does not occur in isolation, but rather is dependent on the activity of neighbouring voxels, particularly in spatially smoothed data (Wager et al., 2007). There are other alternatives to cluster-based thresholding, addressed in Discussion section 7.3.3.

2.7. Methodology summary

This chapter has presented the key methodological components used for each project of this thesis. As all four projects were performed sequentially, there are a number of adaptations that were made between each one, based on feedback from both co-authors and journal peer-reviewers. These iterations are stipulated within each project chapter, along with some necessary duplicity of methodological components as described above. Each subsequent chapter also contains the detailed literature as it is relevant to each project. This thesis will now present the body of research that comprises this PhD study, beginning with Project one, the analysis of the striatum.

3. Project one: Striatum

This thesis begins by investigating the morphology and functional connectivity of the input structures to basal ganglia-thalamocortical circuits, the caudate nucleus and the putamen.

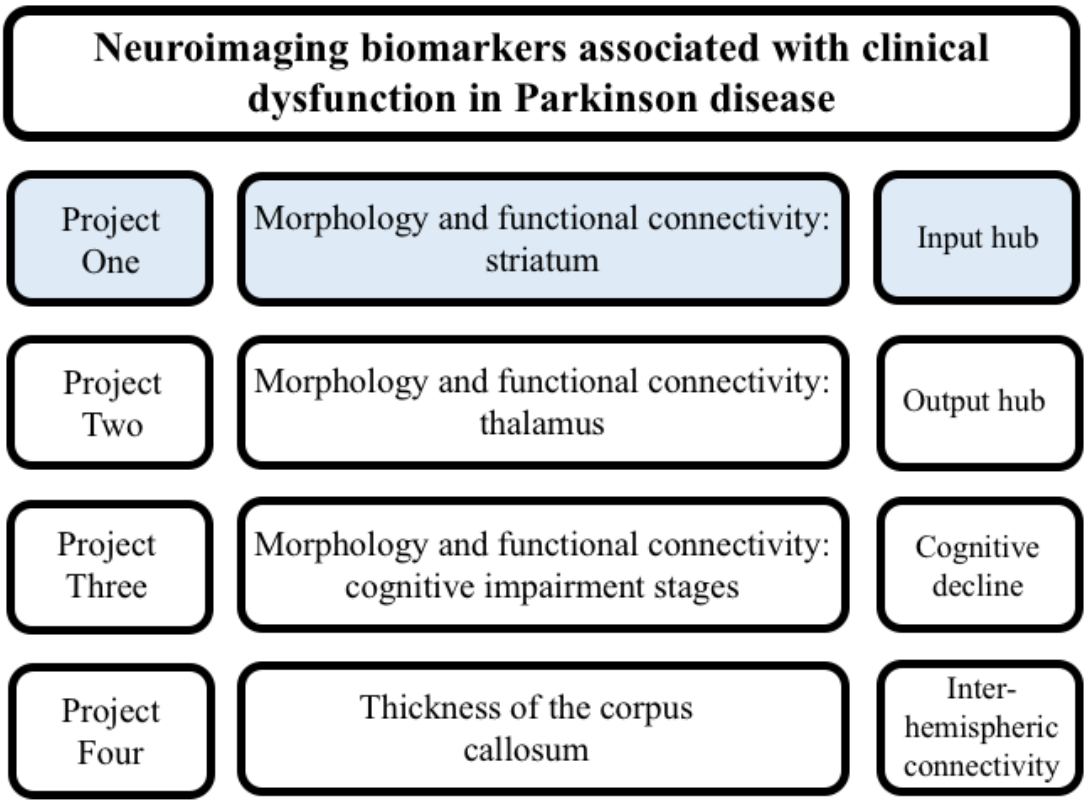

Figure 3.1: Project One. The current project focusses on the morphology and functional connectivity of the striatum, as the key input hub to basal ganglia-thalamocortical circuitry.

Research for this chapter is based on the following publication (https://doi.org/10.1016/j.pscychresns.2018.03.004): Striatal changes in Parkinson disease: An investigation of morphology, functional connectivity and their relationship to clinical symptoms. *Psychiatry Research: Neuroimaging*, 275, 5-13.

This work can be presented in this thesis as the publisher Elsevier allow authors the right to distribute the article for Scholarly Sharing purposes (confirmed with the

publisher). The chapter appears in its published form, excluding page and section numbering, acronyms, small amendments and supplementary information which are changed to match the overall format of this thesis. Edits were also made based on feedback from thesis reviewers.

Title:

Striatal changes in Parkinson disease: an investigation of morphology, functional connectivity and their relationship to clinical symptoms

Authors:

Conor Owens-Walton[a, *], David Jakabek[b], Xiaozhen Li[c, d], Fiona A Wilkes[a], Mark Walterfang[e, f], Dennis Velakoulis[e], Danielle van Westen[g, h], Jeffrey CL Looi[a, e] and Oskar Hansson[d, i]

Affiliations:

[a] Research Centre for the Neurosciences of Ageing, Academic Unit of Psychiatry and Addiction Medicine, School of Clinical Medicine, Australian National University Medical School, Canberra, Australia
[b] Graduate School of Medicine, University of Wollongong, Wollongong, Australia
[c] Division of Clinical Geriatrics, Centre for Alzheimer Disease Research, Department of Neurobiology, Care Sciences and Society (NVS), Karolinska Institute, Huddinge, Sweden
[d] Department of Clinical Sciences, Lund University, Malmö, Sweden
[e] Neuropsychiatry Unit, Royal Melbourne Hospital, Melbourne Neuropsychiatry Centre, University of Melbourne & Northwestern Mental Health, Melbourne, Australia
[f] Florey Institute of Neurosciences and Mental Health, University of Melbourne, Melbourne, Australia
[g] Center for Medical Imaging and Physiology, Skåne University Hospital, Lund, Sweden
[h] Diagnostic Radiology, Department of Clinical Sciences, Lund University, Lund, Sweden
[i] Memory Clinic, Skåne University Hospital, Malmö, Sweden

* Corresponding author: Conor Owens-Walton: Academic Unit of Psychiatry and Addiction Medicine, School of Clinical Medicine, ANU Medical School, Canberra Hospital, Woden, A.C.T, 2605, Australia. Email: conor.owens-walton@anu.edu.au

Author Contributions:

CO-W selected the statistical approach, performed the volumetric analyses and prepared the manuscript (> 80% of total work). DJ performed the SPHARM-PDM analysis and contributed to drafts of the manuscript. FW was involved in the training of CO-W and contributed to drafts of the manuscript. XL performed the rs-fMRI analysis and contributed to drafts of the manuscript. MW and DV provided crucial computational infrastructure and contributed to drafts of the manuscript. DvW contributed to project design, organised the clinical/imaging elements of the study and contributed to drafts of the manuscript. JCLL contributed to project design, acted as supervisor for CO-W and contributed to drafts of the manuscript. OH contributed to project design, organised the clinical/imaging elements of the study and contributed to drafts of the manuscript.

3.1. Abstract

We sought to investigate morphological and resting state functional connectivity changes to the striatal nuclei in PD and examine whether changes were associated with measures of clinical function. Striatal nuclei were manually segmented on 3T-T1 weighted MRI scans of 74 PD participants and 27 control subjects, quantitatively analysed for volume, shape and also functional connectivity using functional MRI data. Bilateral caudate nuclei and putamen volumes were significantly reduced in the PD cohort compared to controls. When looking at left and right hemispheres, the PD cohort had significantly smaller left caudate nucleus and right putamen volumes compared to controls. A significant correlation was found between greater atrophy of

the caudate nucleus and poorer cognitive function, and between greater atrophy of the putamen and more severe motor symptoms. Resting-state functional MRI analysis revealed altered functional connectivity of the striatal structures in the PD group. This research demonstrates that PD involves atrophic changes to the caudate nucleus and putamen that are linked to clinical dysfunction. Our work reveals important information about a key structure-function relationship in the brain and provides support for caudate nucleus and putamen atrophy as neuroimaging biomeasures in PD.

3.2. Introduction

PD is the second most common neurodegenerative disorder in the world, affecting 2-3% of the population over the age of 65. Cardinal manifestations of PD include bradykinesia, postural instability, resting tremor and rigidity (Poewe et al., 2017). These motor symptoms are accompanied and often preceded by non-motor symptoms including executive dysfunction, impulse control disorders, obsessive compulsive disorders, psychotic symptoms, disorders of mood, autonomic dysfunction as well as sensory dysfunction and pain (Weintraub and Burn, 2011). Widespread neuropathological changes are found at autopsy in PD, relating to the presence of α-synuclein-immunopositive Lewy bodies and neurites. This neuropathology is associated with a loss of dopaminergic neurons in the substantia nigra pars compacta, resulting in depletion of dopamine in the connected nuclei of the striatum (Obeso et al., 2008).

Significant efforts have been made to better understand the neural basis of PD, with mounting evidence supporting the notion that clinical symptoms of the disease arise

from system-level dysfunctions in neuronal networks (Caligiore et al., 2016). To understand how neuronal network dysfunction in PD may produce clinical symptoms, both the component elements and also the interconnections within these networks require further examination (Looi et al., 2014). Investigating the component elements can be achieved by measuring morphological changes to neuroanatomical loci or 'hubs' which are central nodes within neuronal networks (Buckner et al., 2009). The interconnections between hubs can be investigated by studying white matter tracts of the brain, or 'spokes', which potentially yield information about disease related connectivity changes (Looi et al., 2014). A growing number of resting-state functional MRI (rs-fMRI) studies are using activation in brain regions and the correlation of timeseries fluctuations between brain regions to infer information the connectivity of the brain. While these methods do not directly investigate white matter tracts in the brain, the hypothesis is that correlated fluctuations accurately reflect synchronised variations of neuronal activity in a network of regions (Birn et al., 2008). Studying functional connectivity in this way enables us to investigate possible connectivity changes to the nuclei of the striatum associated with PD.

Using the theoretical framework of hubs and spokes and how they are affected in PD may produce neuroimaging biomeasures that reveal information about the neural circuit basis of the clinical dysfunction observed in PD. If empirically validated, these biomeasures can be used as biomarkers that help clinicians monitor disease progression and aid surgical treatments that target the restoration of function to large-scale networks in neurodegenerative diseases such as PD (Looi et al., 2014).

Our study focuses on two subcortical nuclei within the basal ganglia, the bilateral caudate nucleus and bilateral putamen, which form the dorsal striatum (herein referred to as the striatum). The caudate nucleus is primarily involved with emotion regulation, reward processing, decision making and executive functioning, while the putamen is primarily associated with the planning and implementation of motor functions (Alexander et al., 1986). Neuroimaging research has supported these putative functional roles as being related to the connectivity of fronto-striato-palladio-thalamo-cortical re-entrant circuits (herein referred to as basal ganglia-thalamocortical circuits) that link specific areas of the cortex with the nuclei of the striatum, globus pallidus and the thalamus (Haber, 2003). Due to the to the strategic location and connectivity of the caudate nuclei and the putamen within basal ganglia-thalamocortical circuits, morphological changes to these nuclei may be linked to the clinical functioning of patients with the disease. Further, changes to the functional connectivity of basal ganglia-thalamocortical circuitry may uncover more information about the putative network breakdown that underpins clinical symptoms in PD.

The findings of research in this field are varied and thus necessitate further investigation. A number of research groups have demonstrated significant striatal volumetric differences in PD cohorts compared to control groups (Geng et al., 2006, Hopes et al., 2016, Pitcher et al., 2012, Sterling et al., 2013), while other studies have failed to detect these atrophic changes (Almeida et al., 2003, Apostolova et al., 2010, Garg et al., 2015, Menke et al., 2014, Messina et al., 2011). Research investigating localised shape changes to the striatum has demonstrated that the head of the caudate nucleus (Apostolova et al., 2010, Pitcher et al., 2012, Sterling et al., 2013) and the more caudal regions of the putamen (Nemmi et al., 2015, Sterling et al., 2013) are

structurally affected in PD, while other research groups have failed to find such changes (Garg et al., 2015, Menke et al., 2014, Messina et al., 2011). A number of research groups have demonstrated relationships between morphology of the striatum and the clinical functioning of PD patients (Apostolova et al., 2010, Geng et al., 2006, Nemmi et al., 2015, Pitcher et al., 2012, Sterling et al., 2013). Apostolova et al., (2010) demonstrated a trend-level correlation between atrophy of the head of the caudate and scores of general cognitive function in a PD cohort. Nemmi et al., (2015) demonstrated a correlation between atrophy of the putamen and general motor function as measured by the UPDRS-III, while Pitcher et al., (2012) demonstrated a correlation between striatal volumes and disease staging as measured by the H&Y test. Finally, Sterling et al., (2013) found that surface deflation of the ventrolateral putamen and body and dorsal surfaces of the caudate was correlated with cognitive function. Despite this, a number of other groups have failed to find associations between structural changes to the striatal nculei and measures of clinical function, necessitating further investigation (Almeida et al., 2003, Garg et al., 2015, Geevarghese et al., 2014, Lewis et al., 2016, Mak et al., 2015). Regarding intrinsic connectivity differences between PD cohorts and controls, rs-fMRI research using a comparable seed-based methodology has demonstrated altered connectivity of the putamen with the parietal lobe (Helmich et al., 2010) and reduced connectivity of the striatal nuclei with the extended brainstem region (Hacker et al., 2012).

We investigated striatal changes in PD by performing a region-of-interest manual segmentation of the caudate nucleus and putamen in participants MRI data, producing morphological information for subsequent analysis. The relationship between striatal morphology and clinical function was assessed using regression models, and further

investigated via the use of rs-fMRI analysis. Due to our use of a manual region-of-interest tracing of striatal structures, comprehensive clinical data set and adjunct resting-state functional connectivity analysis, our study is well positioned to help clarify areas of ambiguity and further develop this field of enquiry.

We hypothesised that there would be significant reductions in striatal volumes in the PD cohort relative to the control subjects and that these reductions would be more pronounced in advanced disease stages, as measured by disease duration. We hypothesised that the PD group would display localised shape changes to the anterior caudate nucleus and the posterior putamen, due to disease-related dopaminergic depletion at these sites. In the PD cohort, we hypothesised that atrophy of the caudate nucleus and putamen would be correlated with poorer performance on measures of cognitive and motor performance, respectively. We hypothesised that localised atrophy (represented by surface change) to the head of the caudate nucleus would be associated with poorer cognitive function, while atrophy of the posterior putamen would be associated with poorer motoric function. Finally, we hypothesised that PD patients would display altered frontostriatal functional connectivity that would relate to the clinical symptoms observed in the disease.

3.3. Methods

3.3.1. Subjects

Participants in this research (n = 101) were derived from the Lund University BioFinders Study. All participants gave informed written consent, the research was performed in accordance with the World Medical Association's Declaration of Helsinki, and ethical approval was obtained through the Ethical Review Board of

Lund, Sweden, and the Human Research Ethics Committee at the Australian National University, Canberra, Australia. Diagnosis of probable PD (Total PD cohort of n = 74) was based on the National Institute of Neurological and Stroke Diagnostic Criteria (Gelb et al., 1999). Categorisation of participants into PD disease subgroups was based on years since clinical diagnosis, with Early PD (n = 34) 5 years or less, Late PD (n = 23) longer than 5 years and advanced PD (PDD) (n = 17) comprising individuals with PD who also received a diagnoses of probable PD dementia (Emre et al., 2007). The demarcation of early and late PD based on a disease duration of 5 years has been experimentally chosen as a crucial disease progression milestone due to changes in medication response often found after this time period. This is shown by the fact that positive response to levodopa medication within 5 years of diagnosis is one of the supportive diagnostic criteria in the UK Parkinson's Disease Society Brain Bank for diagnosing Parkinson disease (Jankovic, 2008). A healthy control group (Control) (n = 27) was used for comparison. All participants underwent a thorough medical history, cognitive and neurological examination. Exclusion criteria included poor knowledge of the Swedish language, developmental disability, psychiatric disorder and a history of alcohol or substance abuse, as detailed in (Hall et al., 2012). A resting-state functional connectivity analysis was performed on 53 PD and 25 Control subjects, after meeting image quality assurance standards outlined in section '3.3.4 Resting-state functional connectivity of the striatum.'

Clinical functioning of participants was measured using the following tests; The Unified Parkinson's disease Rating Scale part-III (UPDRS-III) assessing the motor signs of PD (Fahn and Elton, 1987); the Timed Up and Go (TUG) test, assessing mobility (Podsiadlo and Richardson, 1991); the Animal Fluency and Letter S Fluency

tests, assessing verbal fluency and executive function (Tombaugh et al., 1999); the Mini Mental State Examination (MMSE), assessing cognitive mental state (Folstein et al., 1975) and the A Quick Test of Cognitive Speed (AQT) test, assessing perception and cognitive speed (Palmqvist et al., 2010).

3.3.2. MRI acquisition

Magnetic resonance imaging was performed on a 3T scanner (Trio, Siemens Magnetom, Erlangen, Germany) equipped with a 20-channel head-coil. High-resolution T1-weighted three-dimensional anatomical brain images were acquired using a magnetisation-prepared rapid acquisition technique with gradient-echo sequence (repetition time = 7 ms; echo time = 3 ms; flip angle = 90 degrees; voxel size = 1mm^3 isotropic). Parameters were 256 mm in the coronal and sagittal planes and 176 mm in the axial plane. The rs-fMRI protocol consisted of 256 T2*-weighted echo planar imaging volumes (repetition time = 1850 ms; echo time 30 ms; flip angle = 90 degrees; voxel size 3 × 3 × 3.75 mm^3). Parameters were 61 voxels in the sagittal and axial planes and 73 voxels in the coronal plane. Subjects were instructed to lie still with their eyes closed, not to think of anything in particular and not to fall asleep during the scan.

3.3.3. Manual segmentation of the striatum

Manual region-of-interest segmentations of the bilateral caudate nucleus and putamen were performed in a blinded fashion by C-OW, using ANALYZE 11.0 software (Mayo Clinic, Rochester, Minnesota, USA) on an Apple Mac computer (MacBook Pro, Apple Inc., Cupertino, California, USA) using previously validated protocols (Looi et al., 2009, Looi et al., 2008). For a detailed description, see Methodology

section 2.2.1 and 2.2.2. Test-retest reliability statistics of the manual segmentation process is provided in Appendix 1.

3.3.4. Resting-state functional connectivity of the striatum

The rs-fMRI analysis was performed using a pipeline involving AFNI and FSL software packages (Cox, 1996, Jenkinson et al., 2012). Quality assurance criteria excluded subjects who had more than 1.5mm maximum displacement in the x, y, or z plane or greater than 1.5° of angular rotation about any axis. As an extra precautionary step, the voxel-to-voxel BOLD-signal correlations across the whole brain (including GM, WM and CSF) were calculated and summed with outliers in this measure (4%) removed as they are likely to have originated in a motion-induced global signal capable of eluding conventional motion detection (He and Liu, 2012). Pre-processing of the fMRI data included deletion of the first 5 time frames in each dataset to ensure signals reached the steady state, spatial smoothing with a Gaussian filter (full width half maximum = 4mm) and temporal filtering with a band-pass filter (0.01–0.1Hz). Data was then corrected for slice-dependent time shifts and a head motion correction was performed using AFNI's 3dvolreg based on 6-parameter rigid body image registration. T1-weighted images were then skull-stripped and segmented in grey matter, white matter, and cerebrospinal fluid maps using FSL's automated Brain Extraction Tool (Smith, 2002). The fMRI data was first co-registered to the T1-weighted images acquired from the same subject and then normalised to the 152-brain Montreal Neurological Institute normalised space. The timeseries of regions-of-interest in the white matter and cerebrospinal fluid, as well as the 6 affine motion parameters, were used as nuisance variables and regressed out of the data using a general linear model.

Functional connectivity was examined using a seed voxel correlation approach. Two seed areas representing the caudate nucleus and putamen were based on the manual segmentation mask for each individual, resampled to 3 x 3 x 3 mm^3 standard space to enable extraction of timeseries from each subject's rs-fMRI data. Correlation functional analyses were performed by computing temporal correlation between each seed reference area and the rest of the brain in a voxel-wise manner. The correlation coefficients in each voxel were then transformed to z-value images using the Fisher r-to-z transformation to improve normality, creating an entire brain z-value map for each subject.

3.3.5. Statistical analysis

Statistical analyses were performed using SPSS 22.0 (IBM Corporation, Somers, New York, USA). Estimated total intracranial volumes (eTIV) were used to control for head size derived from FreeSurfer's recon-all analysis (Fischl, 2012). This research was conducted in an *a priori* planned-analysis style based on the hypotheses of the study. When comparing the morphology of striatal structures between the groups, significant volumetric findings were a prerequisite for further investigation of localised shape changes. Similarly, when investigating the relationship between striatal morphology and clinical functioning of PD patients, significant volumetric findings were a prerequisite for further investigation of localised shape change. Significant results at the Total PD level was also a prerequisite for further analysis at the PD disease subgroup level. Bonferroni family-wise error rate corrections were incorporated into our analyses to control for the problem of multiple comparisons/tests (Mcdonald, 2014).

3.3.6. Group comparisons: volume

Between-groups striatal volumetric differences were investigated via a multivariate analysis of covariance (MANCOVA) model with adjustments for age, eTIV and sex (covariates). Effect sizes are represented via partial eta squared values (η^2). Preliminary checks were conducted to ensure that there was no violation of the assumptions of normality, linearity, homogeneity of variances, homogeneity of regression slopes, and reliable measurement of the covariate (Pallant, 2013).

3.3.7. Group comparisons: shape

Shape analysis was performed using spherical harmonic parameterization and sampling in a three-dimensional point distribution model (SPHARM-PDM) (Styner et al., 2006), outlined in full in Methodology section 2.3.2. Generally speaking, SPHARM-PDM shape analysis uses the masks of participants right and left caudate nucleus and putamen created during the manual segmentation process, providing visualisations of the local surface changes to the structures via mean difference displacement maps. These maps display the magnitude of surface change (deflation or inflation) in millimeters between corresponding points on the mean surfaces of the caudate nuclei or putamen in patients with PD relative to the Control group, or between disease subgroups.

3.3.8. Correlations between morphology and clinical symptoms: volume

Correlational analyses between clinical function and striatal volume were investigated via the use of hierarchical multiple regression analyses controlling for covariates and also years of education (the latter only for measures of cognitive function). Effect sizes are represented by standardised beta values (β). Preliminary checks were

conducted to ensure that there were no violations of the assumptions of normality, linearity, multicollinearity and homoscedasticity (Pallant, 2013).

3.3.9. Correlations between morphology and clinical symptoms: shape

Shape analysis investigating the relationship between surface morphology and measures of clinical function followed a SPHARM-PDM method that produces local correlation coefficient maps that represent the relationship between inflation/deflation at surface regions and performance on clinical function tests.

3.3.10. Resting-state functional connectivity analysis

Individual z-value maps were entered into a 2-sample t-test to identify group differences in connectivity between the Total PD group and Control groups for the right and left caudate nucleus and putamen. Age and gender were used as nuisance covariates in all statistical analyses, as well as grey matter intensity maps as a voxel-level covariate. We employed a spatially connected minimum cluster size of 14 voxels ($p < 0.05$) and a t-value of > 2.90 ($p < 0.05$) with a false discovery rate correction at the cluster level. Multiple correction values were produced using an AFNI AlphaSim Monte Carlo inference tool which indicated that a minimum cluster size of 14 was significant at $p < 0.05$ (uncorrected voxel threshold p = 0.005, 1-sided t-test, FWHM = 4mm, 1000 iterations).

3.4. Results

Table 3.1: Demographic and clinical characteristics of participants

Items	Control	Early PD	Late PD	PDD	Total PD
N	27	34	23	17	74
Sex (m:f)	15:12	16:18	12:11	10:7	38:36
Age (years)	69.47 ± 6.09	69.65 ± 5.42	70.19 ± 6.57	73.70 ± 6.67	70.75 ± 6.22
eTIV (cm^3)	1550.68 ± 156.38	1539.17 ± 187.02	1584.01 ± 183.65	1562.33 ± 225.09	1558.43 ± 193.55
DD (years)	-	2.82 ± 1.38	10.43 ± 3.76	11.88 ± 5.48	7.27 ± 5.39
Edu (years)	12.54 ± 3.47	9.29 ± 5.79	13.05 ± 5.65	11.5 ± 4.52	11.02 ± 5.69
UPDRS-III[$]	-2.26 ± 2.82	-11.29 ± 5.76	-15.78 ± 12.61	-33.00 ± 12.21	-17.68 ± 12.67
TUG[$]	-8.59 ± 1.45	-10.33 ± 2.47	-15.78 ± 12.61	-12.73 ± 6.47	-10.48 ± 3.48
AF	23.56 ± 6.80	22.21 ± 5.75	21.09 ± 7.23	11.81 ± 4.18	19.58 ± 7.22
LSF	18.56 ± 6.26	13.41 ± 4.67	16.76 ± 6.66	9.31 ± 4.24	13.48 ± 5.83
MMSE	28.56 ± 1.34	28.26 ± 1.54	28.30 ± 1.36	22.88 ± 3.77	27.04 ± 3.16
AQT[$]	-60.41 ± 15.73	-71.09 ± 24.32	-66.26 ± 13.73	-132.93 ± 73.26	-81.72 ± 44.64

Key: Values are expressed as mean ± standard deviation excluding the variable of sex which denotes the male to female ratio; all data correct to 2 decimal places. **Abbreviations:** *N*, number of participants; eTIV, estimated total intracranial volume ; DD, disease duration; Edu, years of education; UPDRS-III, Unified Parkinson's Disease Rating Scale part III; TUG, Timed Up and Go; AF, Animal Fluency; LSF, Letter S Fluency; MMSE, Mini Mental-State Examination; [$] scores for these clinical measures were inverted so that increasing scores became representative of better performance; AQT, A Quick Test of Cognitive Speed;

3.4.1. Participant characteristics

Two chi-square tests for independence were used to investigate the relationship between sex and group membership between Total PD and Control groups as well as between the disease progression and Control groups (p = 0.88 and p = 0.086, respectively). Three independent samples t-tests were conducted to investigate the relationships between age, eTIV, years of education and group membership at the Total PD and Control group level (p = 0.36, 0.85 and 0.22, respectively). Three one-

way analyses of variance were conducted to investigate the relationships between these participant characteristics and group membership at the PD disease progression subgroup and Control group level (p = 0.11, p = 0.84 and p = 0.04, respectively). While a significance was found between years of education and group membership at the disease subgroup level, *post hoc* tests found no significant differences between any disease subgroups and or between subgroups and the Control group. Estimated mean volumes of striatal structures are presented in Table 3.2.

Table 3.2: **Estimated mean volumes of striatal structures**

Region of interest	Control (mm^3)	Total PD (mm^3)	Early PD (mm^3)	Late PD (mm^3)	PDD (mm^3)
Bilateral caudate nucleus	7571.33 ± 839.17	7138.32 ± 1105.11	7397.18 ± 1084.78	7325.22 ± 997.73	6367.76 ± 976.10
Right caudate nucleus	3796.89 ± 422.36	3600.28 ± 565.83	3746.00 ± 569.69	3662.22 ± 446.95	3225.06 ± 562.53
Left caudate nucleus	3774.44 ± 449.53	3538.04 ± 565.04	3651.18 ± 539.11	3663.00 ± 564.64	3142.71 ± 450.88
Bilateral putamen	6669.74 ± 1048.03	6233.69 ± 1019.62	6374.76 ± 965.83	6337.91 ± 937.811	5810.53 ± 1167.00
Right putamen	3263.22 ± 539.19	3047.62 ± 514.71	3125.06 ± 534.45	3065.74 ± 464.64	2868.24 ± 524.72
Left putamen	3406.52 ± 578.86	3186.07 ± 573.31	3249.71 ± 485.86	3272.17 ± 562.92	2942.29 ± 703.30

Key: Data presented as mean ± standard deviation; data correct to 2 decimal places.

3.4.2. Group comparisons: volume

Pairwise comparisons of the striatal structures are presented in Table 3.3. Bilateral caudate nuclei and bilateral putamina volumes were significantly reduced in the Total PD cohort compared to the Control group (p = 0.049 and p = 0.032 respectively). Left caudate nucleus and the right putamen volumes were significantly reduced in the Total PD cohort compared to the Control group (p = 0.041 and p = 0.038 respectively). Due to these significant results, following our *a priori* planned comparisons style, disease subgroup analysis (Table 3.4) only focussed on bilateral caudate nucleus and putamen volumes, left caudate nucleus and right putamen

volumes. This analysis revealed the bilateral caudate nuclei volumes in the PDD group to be significantly smaller than the Control and Early PD groups ($p = 0.001$ and $p = 0.004$ respectively). Volumes of the left caudate nucleus were found to be significantly smaller in the PDD group compared to the Control, Early PD and Late PD groups ($p = 0.001$, $p = 0.01$ and $p = 0.038$, respectively). The effect sizes for all significant results were all of a small magnitude as indicated by their η^2 values.

Table 3.3: MANCOVA comparisons of striatal structures - Total PD and Controls

Region of interest	[Group 1]	[Group 2]	Mean difference [1-2] (mm^3)	*p* value	η^2
Bilateral caudate nucleus	Control	Total PD	400.391	0.049*	0.040
Right caudate nucleus	Control	Total PD	181.024	0.081	0.031
Left caudate nucleus	Control	Total PD	219.367	0.041*	0.043
Bilateral putamen	Control	Total PD	397.185	0.032*	0.047
Right putamen	Control	Total PD	196.553	0.038*	0.044
Left putamen	Control	Total PD	200.632	0.070	0.034

Key: η^2, partial eta squared; * significant at $p < 0.05$; p-values adjusted for multiple comparisons in the model using a Bonferroni correction; data correct to 3 decimal places with mean differences in mm^3.

Table 3.4: MANCOVA comparisons of striatal structures - PD disease groups and Controls

Region of interest	[Group 1]	[Group 2]	Mean difference [1-2] (mm^3)	*p* value[$]	η^2
Bilateral caudate nucleus	Control	Early PD	150.817	1.000	0.154
	Control	Late PD	321.433	1.00	0.154
	Control	PDD	1054.166	0.001*	0.154
	Early PD	Late PD	170.617	1.000	0.154
	Early PD	PDD	903.349	0.004*	0.154
	Late PD	PDD	732.732	0.055	0.154
Left caudate nucleus	Control	Early PD	112.66	1.000	0.147
	Control	Late PD	146.923	1.000	0.147
	Control	PDD	553.770	0.001*	0.147
	Early PD	Late PD	34.263	1.000	0.147
	Early PD	PDD	441.111	0.01*	0.147
	Late PD	PDD	406.847	0.038*	0.147
Bilateral putamen	Control	Early PD	260.705	1.000	0.075
	Control	Late PD	410.964	0.463	0.075
	Control	PDD	673.908	0.058	0.075
	Early PD	Late PD	150.26	1.000	0.075
	Early PD	PDD	413.203	0.574	0.075
	Late PD	PDD	262.944	1.000	0.075
Right putamen	Control	Early PD	120.379	1.000	0.068
	Control	Late PD	237.956	0.275	0.068
	Control	PDD	303.18	0.134	0.068

Early PD	Late PD	117.577	1.000	0.068
Early PD	PDD	182.802	0.89	0.068
Late PD	PDD	65.225	1.000	0.068

Key: η^2, partial eta squared; * significant at $p < 0.05$; $ adjustment for multiple comparisons incorporated into the model: Bonferroni; data are correct to 3 decimal places. Note that duplicates of MANCOVA comparisons were removed from the table (i.e 1 – 2 and 2 – 1).

3.4.3. Group comparisons: shape

SPHARM-PDM shape analysis found no localised areas of shape change to the surface of the caudate nucleus or putamen in the Total PD group compared to the Control group, after accounting for the false-discovery rate (Figure 3.2). Following the *a priori* planned comparisons style, further between-group investigation at the disease subgroup level was not performed.

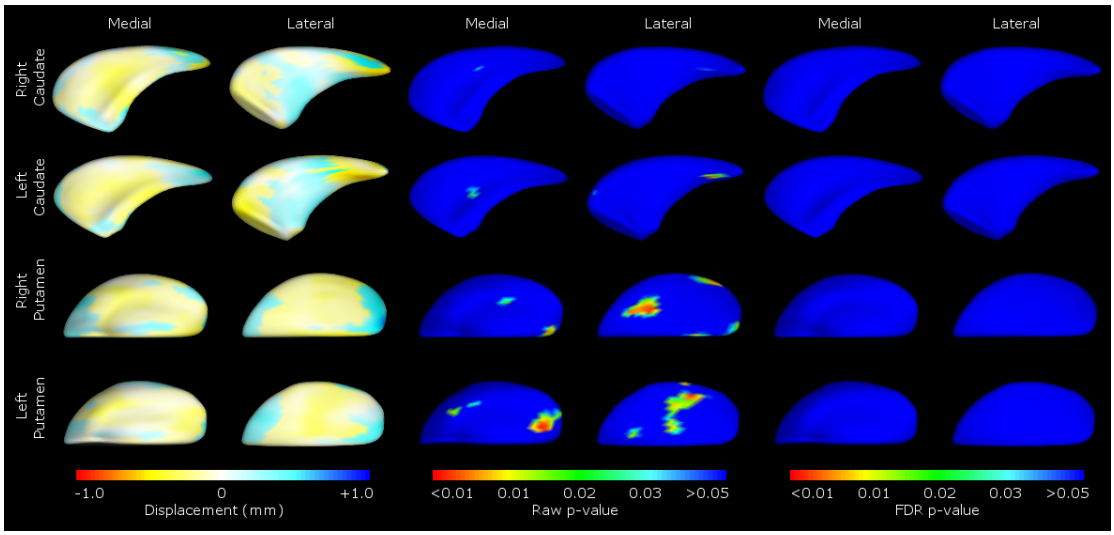

Figure 3.2: Group difference in localised shape of the caudate nucleus and putamen between Total PD and Control groups. For ease of reference we present the data by structure (caudate nucleus top, putamen bottom), with medial and lateral views of structure shown. Mean difference displacement maps occupy the left two columns, raw p-value significance maps occupy the middle two columns and false-discovery rate (FDR) corrected *p*-value significance maps the right two columns. Displacement colour scale corresponds to the millimetres of deflation/inflation of the surface in that region; warmer colours corresponding to greater degrees of deflation and cooler colours corresponding to greater degrees of inflation. For the raw and FDR *p*-value significance scale, warmer colours correspond to lower *p* values while cooler colours correspond to higher *p* values. Anterior

ends of the structures are to the left of the image.

3.4.4. Correlations between morphology and clinical symptoms: volume

The results from the hierarchical regression analyses of striatal volumes and performance on measures of clinical function are presented in Table 3.5 and Appendix Table 1 for PD disease subgroups. When investigating the relationship between volume and clinical function in the Total PD cohort, after controlling for family-wise error rate using the Bonferroni method, the amended p-value required to reach significance (based on performing 36 individual regression analyses) was $p < 0.0014$. Using this criteria, a significant positive correlation was found between volumes of the bilateral putamen and improved performance on the UPDRS-III test ($p = 0.001358$). Significant positive correlations were also found between volumes of the bilateral, right and left caudate nuclei and improved performance on the MMSE test ($p = 0.000563$, $p = 0.00132$ and $p = 0.000565$, respectively) and also on the 'A Quick Test of Cognitive Speed' test ($p = 0.000113$, $p = 0.000189$ and $p = 0.000193$, respectively) in the Total PD group. Based on standardised beta values, these relationships were all of medium and large effect size as shown in Table 3.3 (small effect, β: 0.01-0.29; medium effect, β: 0.30-0.49; large effect, β: 0.50-1.00) (Cohen, 1992). At the disease subgroup level of analysis, no significant results were found after controlling for multiple comparisons.

Table 3.5: Correlations between striatal volumes and clinical function - Total PD and Controls

Group	Nuclei	Clinical measure	R^2 change	β	*p* value
Control	BPV	UPDRS-III	0.002	-0.064	0.83
Total PD			0.118	0.438	0.001358**
Control	RPV		0.011	0.246	0.615
Total PD			0.105	0.410	0.0027
Control	LPV		0.026	-0.213	0.429
Total PD			0.091	0.360	0.005
Control	BPV	TUG	0.000	-0.02	0.946
Total PD			0.057	0.305	0.050
Control	RPV		0.013	0.161	0.584
Total PD			0.035	0.237	0.127
Control	LPV		0.014	-0.159	0.559
Total PD			0.056	0.284	0.052
Control	BCV	AF	0.010	0.085	0.593
Total PD			0.085	0.350	0.021
Control	RCV		0.005	-0.102	0.694
Total PD			0.081	0.341	0.024
Control	LCV		0.012	-0.134	0.545
Total PD			0.078	0.331	0.027
Control	BCV	LSF	0.134	-0.482	0.029
Total PD			0.069	0.315	0.037
Control	RCV		0.094	-0.432	0.075
Total PD			0.066	0.306	0.042
Control	LCV		0.149	-0.470	0.021
Total PD			0.064	0.300	0.045
Control	BCV	MMSE	<0.001	-0.009	0.963
Total PD			0.176	0.504	0.000563**
Control	RCV		<0.001	0.023	0.911
Total PD			0.154	0.47	0.00132**
Control	LCV		<0.001	-0.031	0.863
Total PD			0.176	0.497	0.000565**
Control	BCV	AQT	0.013	-0.152	0.531
Total PD			0.224	0.569	0.000113**
Control	RCV		0.017	-0.183	0.483
Total PD			0.211	0.550	0.000189**
Control	LCV		0.009	-0.116	0.606
PD			0.210	0.544	0.000193**

Key: β, standardised beta values; ** significant at the Bonferroni corrected $p < 0.0014$; Data correct to 3 decimal places, except where expanded to display statistical accuracy..
Abbreviations: BCV, bilateral caudate nucleus volume; RCV, right caudate nucleus volume; LCV, left caudate nucleus volume; BPV, bilateral putamen volume; RPV, right putamen volume; LPV, left putamen volume; UPDRS-III, Unified Parkinson's Disease Rating Scale part III; TUG, Timed Up and Go; AF, Animal Fluency; LSF, Letter S Fluency; MMSE, Mini Mental-State Examination; AQT, A Quick Test of Cognitive Speed.

3.4.5 Correlations between morphology and clinical symptoms: shape

SPHARM-PDM shape analysis found a significant positive correlation between surface volumes of the medial-anterior and dorsal areas of the right caudate nucleus and performance on the Animal Fluency test in the Total PD group (Figure 3.3).

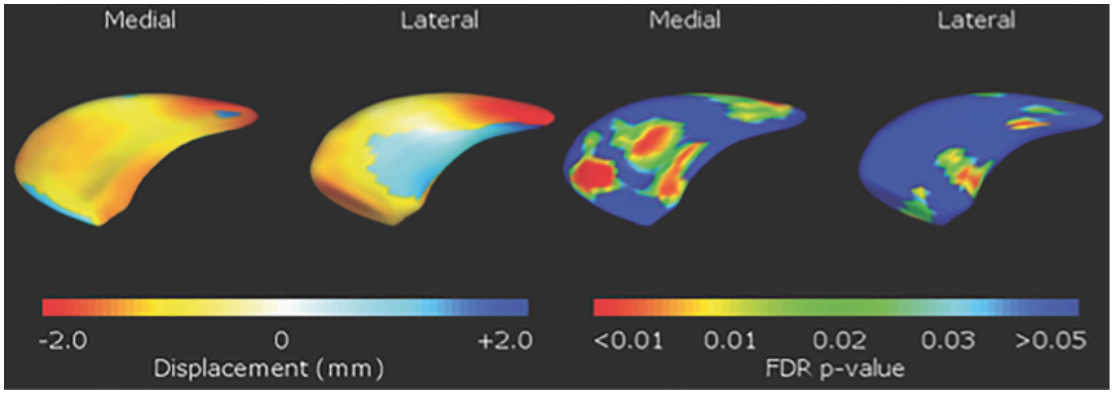

Figure 3.3: SPHARM-PDM within-group correlational analysis of the right caudate nuclei surfaces with performance on the Animal Fluency test in the Total PD group. Pearson correlation coefficient colour map (left) and false discovery rate corrected p-value (right). Pearson correlation coefficient colour maps visualise the degree of positive and negative correlation of the surface at that region. Warmer colours (red) correspond to negative correlation coefficients while cooler colours (blue) to positive correlation coefficients.

3.4.6. Resting state functional connectivity of striatal nuclei

The results of the investigation into the functional connectivity of the striatal nuclei are shown in Figure 3.4 and Figure 3.5 with the data displayed in Table 3.6 and 3.7. In the Total PD group, we found areas of increased functional connectivity of the caudate nucleus with medial frontal gyrus, anterior cingulate and superior frontal gyrus. Decreased functional connectivity was found between the caudate nucleus and the brainstem, thalamus, parahippocampal gyrus and precuneus. The PD group also showed decreased connectivity of the putamen with the cerebellum, inferior and superior parietal lobules.

Table 3.6: Group difference on functional connectivity with caudate between Total PD and Controls

	Brain regions	Hemisphere	Voxels	MNI coordinate x	y	z	*t*-
Increased	Medial Frontal Gyrus	R	63	-6	-57	4	4.05
	Anterior Cingulate	R	19	-3	1	-5	4.48
	Superior Frontal	L	17	26	-54	5	3.84
Decreased	Brainstem	-	20	-2	26	-45	-3.39
	Thalamus	R	18	0	3	4	-3.12
	Parahippocampus	L	14	14	4	-11	-3.24
	Precuneus	L	14	19	55	30	-3.34

Key: Coordinates were defined in the MNI space. **Abbreviations:** FC, functional connectivity; R, right; L, left.

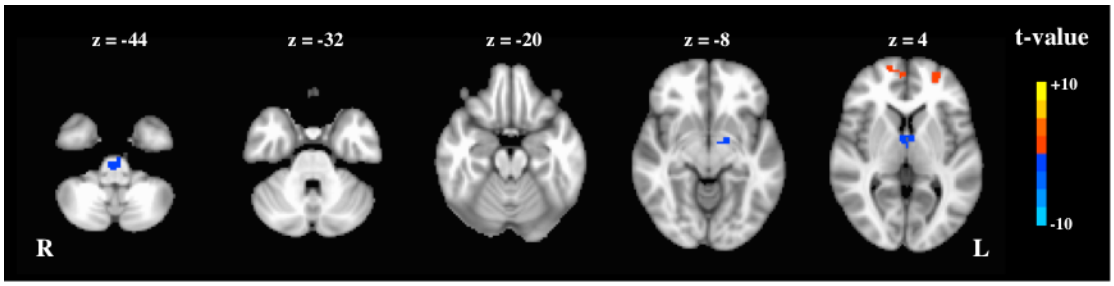

Figure 3.4: Group difference in functional connectivity of the caudate between Total PD and Controls. The statistical maps are overlayed on a T_1-weighted MNI template at the threshold of $p < 0.05$, corrected for multiple comparisons. Hot colours (red) represents increased functional connectivity whereas cold colours (blue) represents decreased functional connectivity in the Total PD group compared to the Control group. The colour bar displays the t-value. **Abbreviations:** R, right; L, left.

Table 3.7 Reduced putamen seed functional connectivity in Total PD group comparing with Controls.

	Brain regions	Hemisphere	Voxels	MNI coordinate x	y	z	*t*-
Decreased	Cerebellum	L	263	15	55	-58	-3.64
	Inferior Parietal	L	31	52	46	46	-4.25
	Superior Parietal	L	25	30	62	46	-3.22

Key: Coordinates were defined in the MNI space. **Abbreviations:** FC, functional connectivity; R, right; L, left.

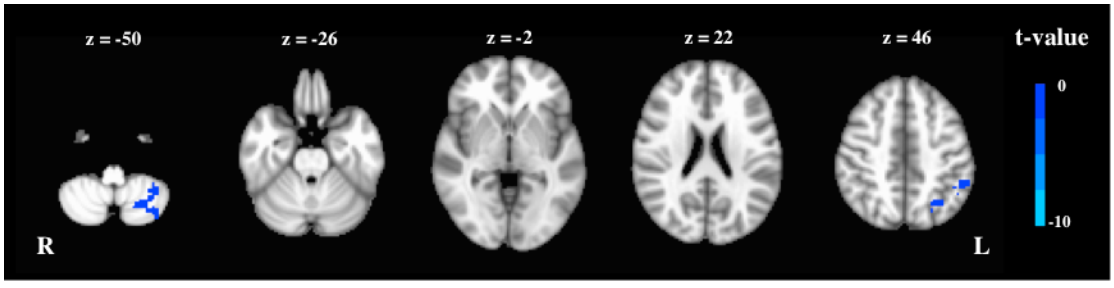

Figure 3.5: Reduced putamen seed functional connectivity in Total PD group compared with the Controls. The statistical maps are overlayed on a T_1-weighted MNI template at the threshold of $p < 0.05$, corrected for multiple comparisons. Cold colours (blue) represents decreased functional connectivity in the Total PD group compared to the Control group. The colour bar displays the t-value. **Abbreviations:** R, right; L, left.

3.5. Discussion

3.5.1. Discussion

We conducted a thorough morphological investigation of the striatum in PD, how morphological changes relate to clinical symptoms, and how the functional connectivity of the striatum is altered in the disease. We found that PD subjects had significantly smaller bilateral caudate nuclei and putamina volumes compared to the Control group, supporting the findings of similar research in this field (Pitcher et al., 2012, Sterling et al., 2013). As lateralised analysis only demonstrated volumetric reductions of the left caudate nucleus and the right putamen, our results only partially support our hypotheses. Regarding possible mechanisms that may explain these findings, research in this field often argues that atrophy of striatal nuclei is linked to the loss of nigrostriatal neurons, resulting in fluctuating or depleted levels of dopamine in the striatum (Pitcher et al., 2012, Sterling et al., 2013). Supporting this explanation, experimental research using MPTP-treated monkeys has demonstrated that striatal spine loss is dependent on the degree of dopamine depletion, even in the absence of observable motor symptoms (Villalba et al., 2009). Another possibility is that PD related Lewy pathology in striatal projection sites may cause structural changes to the striatum via a trans-synaptic spread of neurodegeneration. Researchers have argued that proteopathic agents may take seed in projection sites and spread along the neuraxis over time (Power and Looi, 2015) with the striatum particularly

vulnerable to this neurodegenerative process due to its position as a key hub within widescale neuronal networks (Looi and Walterfang, 2013).

Our findings contrast with a number of research groups who found no volumetric difference between a PD cohort and a control group (Garg et al., 2015, Menke et al., 2014, Messina et al., 2011, Nemmi et al., 2015). As these previous studies used semi-automated region-of-interest segmentation methods, our results are important because we employed a manual segmentation protocol which is considered the gold-standard approach (Morey et al., 2009). However, a methodological factor that should be raised when considering our findings is our inclusion of 17 participants in the Total PD group who had received a clinical diagnosis of PD with dementia. The inclusion of these participants raises the possibility that the pathophysiology underlying the dementia diagnosis may contribute to atrophic changes to the striatum in the Total PD group. Supporting this idea, when investigating striatal volumes at the disease subgroup level, we found considerable bilateral and left caudate nuclei atrophy when comparing Controls and the PDD group, but not when comparing Controls to PD patients without dementia (the Early PD and Late PD groups). The inclusion of PD patients with dementia is an important issue and warrants further discussion. Estimates of the point prevalence of PD patients who are also diagnosed with dementia is around 30-40% (Emre et al., 2007). Longitudinal research indicates that 5 years after initial diagnosis, 28% of PD patients will be diagnosed with dementia, while after 15 years this prevalence increases to 50% (Emre et al., 2007). These statistics indicate a strong temporal link between the progression of PD and patients developing dementia, and it was for this reason that participants who were diagnosed with dementia were not excluded from our study. Our research approach ensures that

the PD cohort analysed is a comprehensive one that closely resembles a clinical PD cohort, including participants from across the entire spectrum of the PD disease course.

A conceivable reason why we only found volumetric changes to the left caudate nucleus and the right putamen could relate to disease lateralisation. In PD the decline in dopamine capacity in the striatum has been shown to be pronounced in the contralateral hemisphere to the more clinically affected side (Politis, 2014). If the proposed mechanism linking fluctuating or depleted levels of dopamine with cellular and structural changes in the striatum is accepted, PD participants with motor symptom dominance to a particular hemisphere may have lateralised disease related structural changes that were not controlled for in this research.

Using an advanced shape analysis technique, we attempted to uncover the exact location of the atrophic changes that were found at the volumetric level by analysing surface changes between the Total PD and Control groups, however, no localised surface changes were found. Our results thus do not support our between-group comparison hypotheses and they contrast with previous research (Apostolova et al., 2010, Nemmi et al., 2015, Pitcher et al., 2012, Sterling et al., 2013) that has demonstrated localised striatal atrophy corresponding to areas of the greatest dopaminergic depletion. A possible explanation for the differences in findings across this field of research may relate to variability in symptom profiles of PD patients. It is widely recognised that PD is a complex heterogeneous neurodegenerative syndrome with a range of clinicopathologic phenotypes. For this reason, we should consider the possible effects of disease subtype variability across studies, as different subtypes

may have unique pathological footprints in the brain (Thenganatt and Jankovic, 2014) making the comparison between studies difficult.

When investigating the relationship between morphology and clinical function in the Total PD group, we found significant positive correlations between caudate nuclei volumes and higher levels of cognitive function, and also between putamen volumes and higher levels of motor function, supporting our hypotheses. Specifically, we demonstrated that higher caudate nuclei volumes were positively correlated with better performance on the MMSE and A Quick Test of Cognitive Speed tests. We also found that higher bilateral putamen volumes were correlated with better performance, or lower levels of motor dysfunction, as measured by the UPDRS-III test. After surviving a strict corrections for multiple comparisons, and with relationships of medium and large effect sizes, our findings clearly demonstrate that greater atrophy of the caudate nuclei is associated with poorer cognitive functioning, and that greater atrophy of the putamen is associated with greater motor dysfunction. Interestingly, the relationship between striatal volumes and clinical function was not found in Control subjects, highlighting the importance of the PD disease process in influencing the structure of the striatal nuclei and consequently clinical function in turn. Our results indicate that the striatum plays an important role in the cognitive and motor symptomology of PD and that atrophy of the caudate nucleus and putamen may be indicative of a breakdown to the frontostriatal circuits subserving cognitive and motor function.

Our findings for the caudate nucleus support previous research (Pitcher et al., 2012), however they contrast with recent studies that found no relationship between caudate

volumes and measures of executive or general cognitive function (Lewis et al., 2016, Mak et al., 2015). Our findings showing the relationship between putamen atrophy and UPDRS-III scores also contrast with recent research (Mak et al., 2014, Nemmi et al., 2015), and as discussed, possible differences in symptom and disease subtype profiles of participants between studies may contribute to these inconsistencies.

In the Total PD group, analyses of striatal shape found significant positive correlations between performance on the Animal Fluency test and surface volumes in general areas of the right caudate nucleus connected to the dorsolateral prefrontal cortex, the area of the brain that mediates executive function (Haber, 2003). This particular result makes intuitive sense as the Animal Fluency test is designed to measure aspects of executive function. However, there were a number of non-significant results in this section of analysis, meaning our findings only partially support our hypotheses.

Our results contrast with previous research that has demonstrated regionally pronounced trend-level correlations between MMSE scores and the head of the caudate nucleus (Apostolova et al., 2010) and significant correlations between the volumes of the head of the caudate nucleus and measures of cognitive performance (Sterling et al., 2013). Due to these inconsistencies, further work is still needed to precisely map how the morphology of these structures change in PD and how this relates to clinical functioning of patients with the disease.

Adding to the findings of volumetric changes to the striatal nuclei in PD, we also detected changes to the functional connectivity of both the caudate nucleus and the

putamen in PD. We found minor increases in functional connectivity between the caudate nucleus and the medial frontal and superior frontal gyri, as well as to the anterior cingulate. We found decreases in functional connectivity between the caudate nucleus and regions of the brainstem, thalamus, parahippocampal gyrus and precuneus, while the putamen showed decreases in functional connectivity with the cerebellum, inferior and superior parietal lobes.

Our findings of decreased connectivity with the brainstem concord with recent research (Hacker et al., 2012) and support the notion that certain clinical manifestations of PD such as sleep disturbances and dysautonomia may relate to brainstem dysfunction. Reduced connectivity of the caudate nuclei with the thalamus supports the notion that changes to the striatal nuclei in PD may indicate a breakdown in frontostriatal circuits that help execute and mediate planned, motivated behaviours (Haber, 2003). The findings of reduced connectivity of the putamen with the areas of the parietal lobule support previous research and may indicate a change in functional connectivity between the structure and components of the sensorimotor system (Helmich et al., 2010). While it may seem counter-intuitive to find both increases and decreases in intrinsic connectivity of the caudate nucleus in our PD group, similar results have been found in previous research, and may reflect functional compensation of the brain in response to disease related damage (Helmich et al., 2010). Our morphological results support this proposition, as while the PD group demonstrated atrophy of the caudate nucleus that correlated with poorer cognitive performance, our functional connectivity analysis revealed increases in functional connectivity of the structure with regions of frontal cortex that mediate aspects of cognitive function. It is possible that these increases of functional connectivity in PD

are a response to the atrophic damage that takes place in the caudate nucleus in the disease (Helmich et al., 2010).

While our findings of altered functional connectivity to both striatal nuclei conform with recent work, dealing with the caudate nucleus and putamen as unitary structures in functional connectivity analyses may obscure more precise changes that may be able to be demonstrated if functional subterritories were used (Hacker et al., 2012). Future research on how these modalities could be used in a more complimentary fashion will now be discussed along with possible limitations of this research.

3.5.2. Limitations and future research

Our methodological approach investigated possible localised shape change using SPHARM-PDM in an adjunct fashion, only when we had found significant volumetric results for a particular section of the analysis. Using this *a priori* planned analysis approach, it is possible that we may have missed a range of subtle disease related changes that were not found when investigating morphology at the volumetric level. We should also acknowledge the small number of control subjects in this research, which may have impacted our results. To bring more clarity to the relationship between morphology, functional connectivity and clinical symptoms, future research will use parcellations of striatal nuclei with targeted regions of interest in the cortex also incorporating clinical function data into the functional connectivity analyses. It is hoped that this will improve the concordance between the different neuroimaging processing modalities and may yield more precise information about the relationship between striatal morphology, functional connectivity and their relationship to specific clinical symptoms in PD.

3.5.3. Conclusion

This research serves as a comprehensive morphological, clinical and functional connectivity analysis of the striatum in PD. We have demonstrated that atrophic changes to the striatal nuclei take place in PD compared to controls. We found that atrophy of the caudate nucleus within the PD group is associated with slower processing and poorer overall cognitive performance, while atrophic changes to the putamen are associated with more significant motor symptoms. We also found altered resting-state connectivity of both striatal nuclei in PD compared to Controls. Our research indicates that both the 'hubs' and 'spokes' within neuronal networks are affected in PD, supporting a neural circuit basis for the clinical dysfunction observed in the disease. Our research highlights the importance of the striatum as a crucial neuroanatomical structure within frontostriatal networks and indicates a potential usefulness of striatal volumes as neuroimaging biomeasures in PD, reinforcing the importance of these nuclei to the clinical manifestations of the disease.

4. Project two: Thalamus

Project one of this thesis investigated the morphology and functional connectivity of the caudate nucleus and putamen, the main input structures of basal ganglia-thalamocortical circuits. Project two focusses on the output structures of these circuits, the bilateral thalami, to investigate possible neuroimaging biomarkers of clinical dysfunction in PD. This chapter is based on a published manuscript, however as with Project one, certain elements have been changed to streamline the project with the thesis.

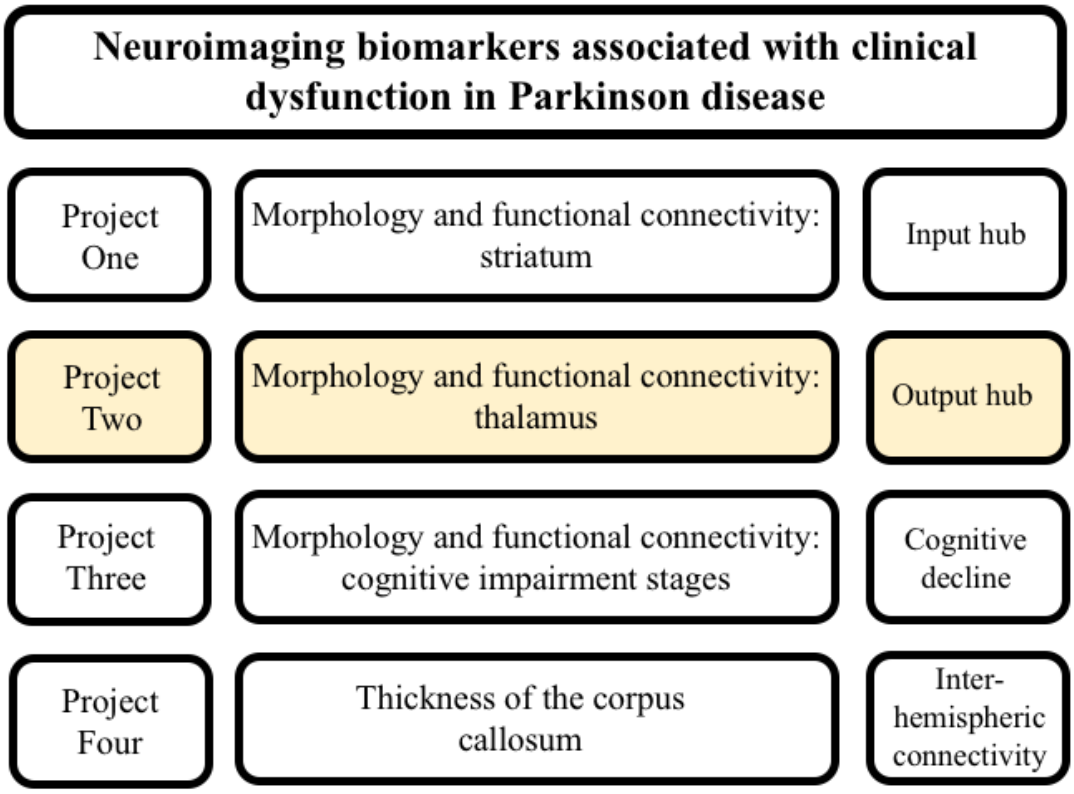

Figure 4.1: Project two. The current project focusses on the thalamus as the key output hub of basal ganglia-thalamocortical circuitry, coupled with the fact that the structure contributes to the abnormal neural activity in PD and is vulnerable to the Lewy pathology underlying the disorder (Halliday, 2009).

This chapter is based on the following publication; Owens-Walton, C., Jakabek, D., Power, B. D., Walterfang, M., Velakoulis, D., Van Westen, D., Looi, J. C. L., Shaw, M. & Hansson, O. 2019. Increased functional connectivity of thalamic subdivisions in patients with Parkinson's disease. PLOS ONE, 14, e0222002. However, it appears in here in a modified form to streamline it with the thesis as a whole.

Title:

Increased functional connectivity of the thalamus in patients with Parkinson disease

Author names:

Conor Owens-Walton[1,*], David Jakabek[2], Brian D. Power[3, 4], Mark Walterfang[5,6], Dennis Velakoulis[5], Danielle van Westen[7, 8, ¶], Jeffrey C.L. Looi[1, 5, ¶], Marnie Shaw[9, ¶] and Oskar Hansson[10, 11, ¶]

Affiliations:

[1] Research Centre for the Neurosciences of Ageing, Academic Unit of Psychiatry and Addiction Medicine, School of Clinical Medicine, Medical School, Australian National University, Canberra, Australia
[2] Graduate School of Medicine, University of Wollongong, Wollongong, Australia.
[3] School of Medicine, The University of Notre Dame, Fremantle, Australia
[4] Clinical Research Centre, North Metropolitan Health Service – Mental Health, Perth, Australia
[5] Neuropsychiatry Unit, Royal Melbourne Hospital, Melbourne Neuropsychiatry Centre, University of Melbourne & Northwestern Mental Health, Melbourne, Australia
[6] Florey Institute of Neurosciences and Mental Health, University of Melbourne, Melbourne, Australia
[7] Center for Medical Imaging and Physiology, Skåne University Hospital, Lund, Sweden
[8] Diagnostic Radiology, Department of Clinical Sciences, Lund University, Lund, Sweden
[9] College of Engineering and Computer Science, The Australian National University, Canberra, Australia
[10] Memory Clinic, Skåne University Hospital, Malmö, Sweden
[11] Department of Clinical Sciences, Lund University, Malmö, Sweden

* Corresponding author: conor.owens-walton@anu.edu.au (CO-W)
¶ Joint senior authors

Author contributions:

CO-W contributed to project design, selected the statistical approach, performed the volumetric and functional connectivity analyses and prepared the manuscript (> 80% of total work). BDP contributed to project design, provided supervision for CO-W, provided expert thalamic manual segmentation training for CO-W and contributed to drafts of the manuscript. DJ performed the SPHARM-PDM analysis and contributed to drafts of the manuscript. MW and DV provided crucial software/hardware infrastructure and contributed to drafts of the manuscript. DvW contributed to project design, organised the clinical/imaging aspects of the study and contributed to drafts of the manuscript. JCLL contributed to project design, acted as supervisor for CO-W and contributed to drafts of the manuscript. MS acted as supervisor for CO-W, helped with functional connectivity analyses and contributed to drafts of the manuscript. OH contributed to project design, organised the clinical/imaging aspects of the study and contributed to drafts of the manuscript.

4.1. Abstract

Parkinson's disease (PD) affects 2-3% of the population over the age of 65 with loss of dopaminergic neurons in the substantia nigra impacting the functioning of basal ganglia-thalamocortical circuits. The precise role played by the thalamus is unknown, despite its critical role in the functioning of the cerebral cortex, and the abnormal neuronal activity of the structure in PD. Our objective was to more clearly elucidate how functional connectivity and morphology of the thalamus are impacted in PD (n = 32) compared to Controls (n = 20). To investigate functional connectivity of the

thalamus we subdivided the structure into two important regions-of-interest, the first with putative connections to the motor cortices and the second with putative connections to prefrontal cortices. We then investigated potential differences in the size and shape of the thalamus in PD, and how morphology and functional connectivity relate to clinical variables. Our data demonstrate that PD is associated with increases in functional connectivity between motor subdivisions of the thalamus and the supplementary motor area, and between prefrontal thalamic subdivisions and nuclei of the basal ganglia, anterior and dorsolateral prefrontal cortices, as well as the anterior and paracingulate gyri. These results suggest that PD is associated with increased functional connectivity of subdivisions of the thalamus which may be indicative alterations to basal ganglia-thalamocortical circuitry.

4.2. Introduction

PD is the second most common neurodegenerative disorder in the world, affecting 2-3% of the population over the age of 65 (Poewe et al., 2017). Characteristic motor symptoms of the disorder include resting tremor, rigidity and postural instability. These are accompanied by non-motor symptoms including cognitive impairment (executive dysfunction, memory deficits, hallucinations and dementia), autonomic dysfunction (urogenital dysfunction, hypotension and constipation), disorders of sleep-wake cycle regulation, sensory disturbances (hyposmia) and pain (Schapira et al., 2017). The neuropathological hallmark of PD is the presence of α-synuclein-immunopositive Lewy bodies and neurites (Dickson et al., 2009). This neuropathology results in a degeneration of nigrostriatal dopaminergic neurons, depletion of dopamine across the striatum (Kish et al., 1988) and consequent dysfunction of basal ganglia-thalamocortical networks (Alexander et al., 1986).

Dysfunction of these circuits is critical as they work in concert with the cortex to orchestrate and mediate a range of cognitive, motor and limbic functions in the brain (Haber, 2003).

To understand the functioning of a network, it is necessary to study the elements of the network and also their interconnections (Sporns et al., 2005). Investigating elements of brain networks can be done via studying the morphology of key neuroanatomical nuclei acting as 'hubs' within these networks (Sporns et al., 2007). Hubs are nodes within brain networks that make strong contributions to global network function (Van Den Heuvel and Sporns, 2013) and the interconnections between these hubs can be investigated through the use of resting-state functional connectivity MRI methods that measure the functioning of intrinsic connectivity networks in the brain at rest (Biswal et al., 1995). Spontaneous fluctuations of the blood oxygen level-dependent (BOLD) signal that are temporally coherent indicate areas in the brain that may be functionally and anatomically related (Fox and Raichle, 2007).

As dopamine replacement therapies provide some relief of motor symptoms in PD, significant research effort has focused on the role played by dopaminergic-depleted nuclei of the striatum (Caligiore et al., 2016). However, there is now considerable evidence that the pathology underlying PD affects certain nuclei in the thalamus, and that the structure plays an important role in PD as loss of dopaminergic input to the striatum results in increased GABA-mediated inhibition of thalamocortical projections (Obeso et al., 2008). The thalamus, considered an integrative hub within functional brain networks (Hwang et al., 2017), is thus an important neuroanatomical

structure which we can use to investigate how basal ganglia-thalamocortical circuits are affected in PD, potentially revealing important information about the pathophysiology of the disease.

There is a clear lack of consensus in this field of research, necessitating further investigation. Functional connectivity studies implicating the thalamus have yielded inconsistent results with research demonstrating both increased coupling between the thalamus and sensorimotor regions in PD (Agosta et al., 2014b) and no significant differences in thalamic functional connectivity in PD (Bell et al., 2015). Studies have indicated that PD is associated with thalamic volumetric changes compared to control groups (Lee et al., 2011), while other work presents conflicting results showing no differences in thalamic volumes in a PD cohort compared to control participants (Lee et al., 2014, Mak et al., 2015, Mckeown et al., 2008, Menke et al., 2014, Messina et al., 2011, Nemmi et al., 2015, Tinaz et al., 2011). Research has demonstrated subtle changes to the surface of the thalamus in a PD cohort compared to controls (Garg et al., 2015, Mckeown et al., 2008). Garg et al., (2015) found atrophy primarily in the mediodorsal aspect of the thalamus in PD compared to controls, which has connectivity with limbic and cognitive areas of the brain. McKeown et al., (2008) found a small area of atrophy to midline areas of the thalamus, which they link to the centre-median parafasicular region of the thalamus. This area receives input from the cerebral cortex as well as subcortical structures like the globus pallidus, midbrain regions like the superior colliculus, and plays an important role in attention and arousal (Jones, 2012). Other research has found no significant localised shape changes to the thalamus in PD participants compared to controls (Lee et al., 2014, Menke et al., 2014, Nemmi et al., 2015). Although the thalamus plays a key modulatory role in

the brain, there is a lack of evidence for a relationship between thalamus volumes and clinical function (Lee et al., 2014, Mak et al., 2014, Mak et al., 2015, Tinaz et al., 2011).

We hypothesised that there would be reductions in volumes of the thalamus in PD patients compared to controls based on the presence of PD neuropathology and the associated cell loss found post-mortem (Halliday, 2009). We also hypothesised that there would be localised surface changes to medial regions of thalamus in PD, compared to controls. We hypothesised that there would be a correlation between smaller overall volumes of the thalamus and poorer performance on measures of clinical function. Finally, we hypothesised that there would be functional connectivity changes in our PD group due to the integral position the thalamus occupies within basal ganglia-thalamocortical circuits.

4.3. Methods

4.3.1. Participants

Participants in this research were members of the Swedish BioFINDER Study (www.biofinder.se). The study is based in Sweden and is affiliated with the Clinical Memory Research Unit and The Biomedical Centre, both at Lund University. Participants were recruited from the Memory and neurology clinics at Skåne University Hospital. Participants gave written informed consent and this research was performed in accordance with the World Medical Association's Declaration of Helsinki. Participants in the current study received their clinical assessments between 23/05/2012 and 13/03/2014. Ethical approval was obtained through the Ethical Review Board of Lund, Sweden, and the Human Research Ethics Committee at the

Australian National University, Canberra, Australia. Diagnosis of PD (n = 32) was made by a neurologist using the National Institute of Neurological and Stroke Diagnostic criteria (Gelb et al., 1999). A healthy control group (Controls) (n = 20) was used for comparison. Exclusion criteria for the Swedish BioFinder study included poor knowledge of the Swedish language, developmental disability, psychiatric disorder, alcohol or substance abuse or the presence of a metabolic disorder. This current study also had an exclusion criteria of a diagnosis of probable PD dementia (Emre et al., 2007). A healthy control group (Controls) (n = 26) was used for comparison. As new and more thorough preprocessing analyses were performed by the primary author, COW, relative to Project one, the numbers of participants in the current study were different to those outlined in the previous chapter, primarily relating to the use in this project of more stringent head motion exclusion criteria during functional MRI acquisition, which resulted in the exclusion of a number of participants. A preliminary investigation of functional MRI data indicated a significant difference in subject head motion during image acquisition. We therefore implemented a strict study-specific head motion exclusion criterion of > 0.26mm (defined as mean relative displacement) and used advanced denoising procedures (FSL-FIX) as nuisance regression can be insufficient in removing the spurious effects of movement artefacts in MRI data (Power et al., 2012).

All participants underwent a cognitive and neurological examination by a medical doctor with extensive experience in movement disorders. PD patients remained on medication as per their usual regime for both MRI acquisition and clinical assessment, with a levodopa equivalent daily dosage (LEDD) metric recorded for each participant. Functioning of participants was quantified using the Unified Parkinson's Disease

Rating Scale Part-III test (UPDRS-III), to assess the motor signs of PD (Fahn and Elton, 1987); the Mini Mental State Examination (MMSE), to assess cognitive mental state (Folstein et al., 1975); the Timed Up and Go (TUG) test, assessing mobility (Podsiadlo and Richardson, 1991), the Animal Fluency and Letter S Fluency tests, assessing verbal fluency and executive function (Tombaugh et al., 1999) and the A Quick Test of Cognitive Speed (AQT) test, assessing perception and cognitive speed (Palmqvist et al., 2010).

4.3.2. MRI acquisition

Magnetic resonance imaging was performed on a 3T scanner (Trio, Siemens Magnetom, Erlangen, Germany) equipped with a 20-channel head-coil. High-resolution T1-weighted three-dimensional anatomical brain images were acquired using a magnetization-prepared rapid acquisition technique with gradient-echo sequence (repetition time = 7 ms; echo time = 3 ms; flip angle = 90 degrees; voxel size = isotropic 1=mm3). Image matrix size was 356 voxels in the coronal and sagittal planes and 176 voxels in the axial plane.

Resting state functional magnetic resonance images (rs-fMRI) (256 volumes per subject) were acquired using T2*-weighted echo planar imaging volumes (repetition time = 1850 ms; echo time 30 ms; flip angle = 90 degrees; matrix 64 × 64; voxel size 3 × 3 × 3.75 mm3). Image matrix size was 64 voxels in the coronal and sagittal planes and 36 voxels in the axial plane. Subjects were instructed to lie still with their eyes closed, not to fall asleep and not to think of anything in particular during the scan, which lasted for approximately 8 minutes.

4.3.3. Manual segmentation of the thalamus

Manual ROI tracing was performed on participant's T_1-weighted structural MRI data using ANALYZE 12.0 software (Mayo Biomedical Imaging Resource, Rochester, Minnesota, USA) following a validated method (Power et al., 2015). See Methodology 2.2.3 for a full description. Associated reliability statistics are presented in Appendices Section 1: Tracing reliability of manual ROI segmentation. The tracing for each thalamus was saved as a binary image for rs-fMRI seed-based functional connectivity and shape-based morphological analyses.

4.3.4. Resting-state functional connectivity preprocessing

All rs-fMRI preprocessing used FMRIB Software Library (FSL) software package tools (FMRIB Software Library, Oxford, UK; FSL version 5.0.10, RRID:SCR_002823) (Jenkinson et al., 2012). FMRI Expert Analysis Tool (FEAT) (version 6.00) was used for the removal of the first 6 volumes, motion correction using FMRIB Motion Correction Linear Registration Tool (MCFLIRT) (Jenkinson et al., 2002); slice-timing correction using Fourier-space timeseries phase-shifting, removal of non-brain structures using FSL's Brain Extraction Tool (BET) (Smith, 2002); spatial smoothing using a full-width half-maximum gaussian kernel of 5 mm, grand mean intensity normalization and high-pass temporal filtering (gaussian-weighted least-squares straight line fitting, with sigma = 50.0s) (Woolrich et al., 2001). Registration of functional images to participant's high resolution T_1-weighted structural images used boundary-based registration (Greve and Fischl, 2009) within the FLIRT linear registration tool (Jenkinson et al., 2002, Jenkinson and Smith, 2001). Registration of functional images to Montreal Neurological Institute (MNI) 152 T_1 $2mm^3$ standard space was also performed using FLIRT with 12 degrees of freedom,

further refined using FNIRT nonlinear registration (Andersson et al., 2007a, Andersson et al., 2007b) with a warp resolution of 10mm and a resampling resolution of 4mm. Denoising of head motion, scanner and cerebrospinal fluid artefacts was performed using a probabilistic Multivariate Exploratory Linear Optimized Decomposition into Independent Components (MELODIC version 3.15) independent component analysis method (Beckmann and Smith, 2004). To do this, observations were decomposed into sets of vectors describing the variation of signal across both the temporal (time-courses) and spatial (maps) domains, optimising for non-Gaussian spatial source distributions using a fixed-point iteration technique (Hyvarinen, 1999). The FSL-FIX classifier (version 1.06) (Salimi-Khorshidi et al., 2014) was then trained on our particular dataset by first running the 'Standard.RData trained-weights' classifier over a sample of ICA maps for 10 Controls and 10 PD participants, with the classifier categorising maps as either 'signal' or 'noise'. We checked each classification against the validated guidelines of Griffanti et al. (2014), choosing the conservative approach to component reclassification as outlined in that work. Following this, the FIX classifier was re-trained using this new data and run over the ICA datasets for all participants, regressing out noise components while also cleaning up motion confounds (24 regressors: 6 motion parameters, 6 first derivatives and the squares of these 12 regressors). This process creates a de-noised filtered functional file which is used at the individual-level GLM stage.

The Oxford Thalamic Structural Connectivity Probability Atlas (Behrens et al., 2003) within FSL's visualization GUI FSLEyes was used to parcellate bilateral thalamic manual segmentation masks into two seed regions-of-interest masks (seed-ROIs) (Figure 4.2), representing important functional subdivisions of the thalamus. Due to

the cardinal motor symptoms in PD, our first seed-ROI incorporated voxels with the highest probability of connectivity with pre- and primary motor cortices and are intended to represent the ventral lateral posterior, ventral lateral and ventral anterior thalamic nuclei. Due to the significant cognitive dysfunction observed in PD, our second seed-ROI incorporated voxels with the highest probability of connectivity to the prefrontal cortex, intended to represent the mediodorsal and anterior thalamic nuclei (Behrens et al., 2003). For ease of reference we will refer to these seed-ROIs as the VLp/VA thalamus and MD/A thalamus, respectively. Generic VLp/VA and MD/A thalamic masks were thresholded to only include voxels that had a greater than 50% chance of inclusion, then registered to subject-specific functional MRI space, and finally eroded by zeroing non-zero voxels when found in kernel, to reduce partial volume effects. A visual inspection of a subset of VLp/VA and MD/A masks was then performed to check the alignment of masks within functional data. We then extracted the mean activation of the functional data within the two seed-ROI masks at each functional timepoint for use as explanatory variables at the individual-level general linear model (GLM) stage in a mass univariate voxelwise whole-brain analysis.

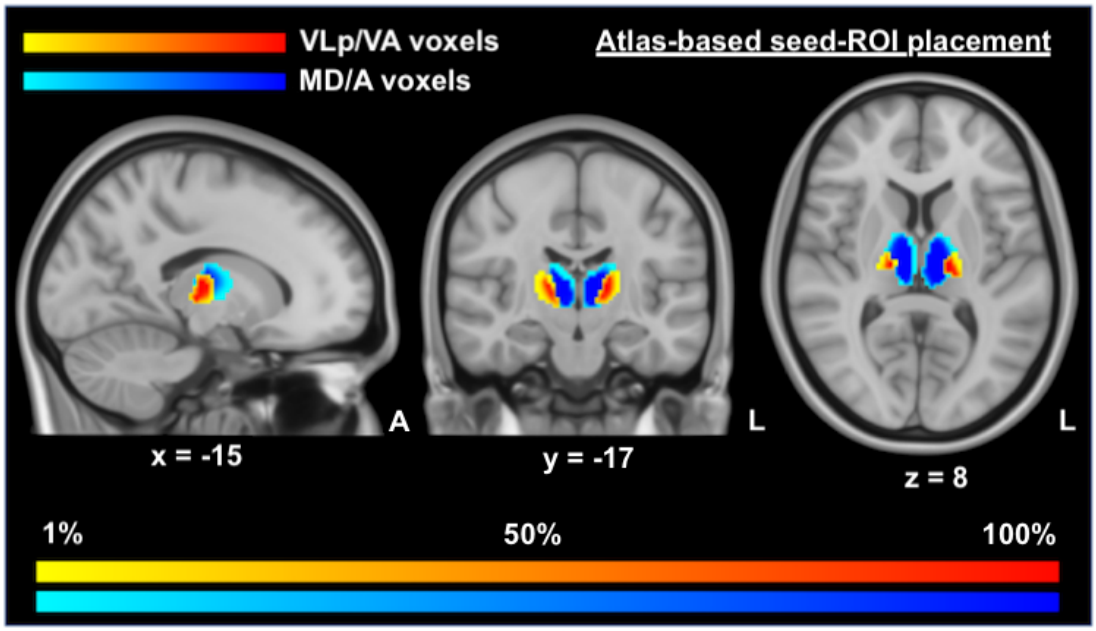

Figure 4.2. Positioning and likelihood-map of seed voxels for VLp/VA and MD/A thalamic masks. This figure displays the voxels used in seed-ROI masks for the functional connectivity analyses, overlaid on MNI T1 0.5mm images. **Key:** This image was produced by combining all of the binary masks of each participant into one unified mask, with warm (yellow - red) colors indicating the positioning of the VLp/VA voxels and cold colors (light blue - dark blue) indicating the positioning of the MD/A voxels. Darker tones are indicative of a greater proportion of voxels in that region being included in the relevant seed-ROI mask. VLp/VA, ventral lateral posterior and ventral anterior thalamic voxels; MD/A, mediodorsal and anterior thalamic voxels.

4.3.5. Resting-state fMRI statistical analyses

Two individual-level FC analyses were performed for each participant, using a GLM approach (Woolrich et al., 2004). BOLD timeseries data within the VLp/VA and MD/A thalamus were correlated with activity in the rest of the brain, shifting the model with a temporal derivative to account for lags in the onset of the hemodynamic response function, removing volumes corrupted by large motion and regressing out

average timeseries data from whole brain (global signal regression), white matter and ventricle masks. Higher-level analysis of FC differences between PD and Control subjects were investigated in standard space using FSL-FEAT. We chose a nonparametric permutation-based approach (n = 5000) (Nichols and Holmes, 2002) via FSL-randomise (Winkler et al., 2014) with a threshold-free cluster enhancement method controlling the family-wise error rate at $p < 0.05$. This approach avoids selecting arbitrary threshold values, while also potentially improving sensitivity to test signal shapes and SNR values (Smith and Nichols, 2009). Due to there being a significant difference in education between PD and Control groups, we included years of education as a covariate, along with age and sex.

4.3.6. Correlation between functional connectivity and clinical data

To investigate the relationship between FC and clinical variables we conducted a series of post-hoc partial correlational analyses. These focused on the average parameter estimate for VLp/VA and MD/A thalamus at the peak voxel locations derived from the between group analyses. Spherical ROIs (7mm radius) were generated around the voxel locations with the average parameter estimate extracted for each subject. Average FC for each ROI was then correlated against LED, disease duration, UPDRS-III, TUG, AQT and Animal Fluency scores.

4.3.7. Group comparisons: volume

Statistical analyses of volumetric data were performed with SPSS 22.0 (IBM Corporation, Somers, New York, USA) utilising multivariate analysis of covariance models controlling for head size (eTIV, derived from recon-all FreeSurfer processing

(Fischl, 2012), age and sex. *p*-values were adjusted for family-wise error rate using a Bonferroni correction. Effect sizes are represented by partial eta squared values (η^2).

4.3.8. Group comparisons: shape

Shape analysis was performed using spherical harmonic parameterisation and sampling in a three-dimensional point distribution model (SPHARM-PDM) (Styner et al., 2006) outlined in detail in Methodology section 2.4.2. Generally speaking, SPHARM-PDM shape analysis provides visualisations of the local surface changes to the thalamus between groups via mean difference displacement maps, mapping the magnitude of surface change (deflation or inflation) in millimetres between corresponding points on the mean surfaces of the PD participants compared to Controls. Significant surface change was displayed at $p < 0.05$ with a correction for multiple comparisons performed using a false-discovery rate (FDR) bound q of 5% (Genovese et al., 2002).

4.3.9. Correlations between morphology and clinical symptoms: volume

We used hierarchical multiple regression models to assess whether thalamic volumes can predict clinical symptoms. These models incorporated two levels, the first level controlled for eTIV, age, sex and years of education (the latter when dealing with measures of cognitive function), and the second level held the independent variable of interest (volume of right or left thalamus), measuring the unique contribution of that variable in predicting each measure of clinical function. Effect sizes are represented by standardized beta values (β).

4.3.10. Correlations between morphology and clinical symptoms: shape

Shape analyses investigating the relationship between surface morphology and measures of clinical function followed a SPHARM-PDM method that produces local correlation coefficient maps that represent the relationship between inflation/deflation at surface regions and performance on clinical function tests.

4.4. Results

4.4.1. Participant characteristics

There were no significant differences in age, head size (eTIV) or proportions of males and females in groups, between the PD cohort and Controls. Years of education, UPDRS-III and AQT performance was significantly reduced in PD compared to Controls (Table 4.1).

Table 4.1. Demographic and clinical characteristics of participants.

Item	Controls	PD	*p*-value
Number of participants	20	32	-
Female/Male	10/10	18/14	0.878
Age	69.06 ± 6.86	69.36 ± 5.82	0.868
LED	-	523.36 ± 295.31	-
Disease duration	-	5.16 ± 3.62	-
eTIV (cm^3)	156.81 ± 15.84	152.06 ± 17.71	0.333
Years of education	13.14 ± 3.68	9.78 ± 6.05	0.042
Relative displacement	0.13 ± 0.06	0.16 ± 0.06	0.066
H&Y	-	1.75 ± 0.55	-
UPDRS-III	2.40 ± 3.02	10.69 ± 7.06	<0.001
TUG	8.60 ± 1.54	9.68 ± 2.39	0.079
MMSE	28.8 ± 1.2	28.28 ± 1.42	0.18
AQT	57.25 ± 15.09	66.47 ±14.78	0.035
AF	24.80 ± 6.59	23.03 ± 5.67	0.309

Data presented as mean ± standard deviation; *p*-values, one-way independent samples *t*-test, excluding male/female numbers which was analyzed via a chi-square test for independence; LED, levodopa equivalent dosage (mg); eTIV, estimated total intracranial volume; Relative displacement, mean value derived from MCFLIRT FSL motion correction; H&Y, Hoehn and Yahr Scale; UPDRS-III, Unified Parkinson's Disease Rating Scale part III; TUG, Timed Up and Go test; MMSE, Mini Mental-state Examination; AQT, A quick test of cognitive speed; AF, Animal fluency test.

4.4.2. Functional connectivity of the VLp/VA thalamus in PD

Analysis of the VLp/VA thalamus in PD found significant clusters of increased FC with the right supplementary motor area (BA6) and the left paracingulate gyrus (BA32). Analysis of the VLp/VA thalamus also found a significant cluster of decreased FC with the left lateral occipital cortex (BA19) (Fig 4.3, Table 4.2).

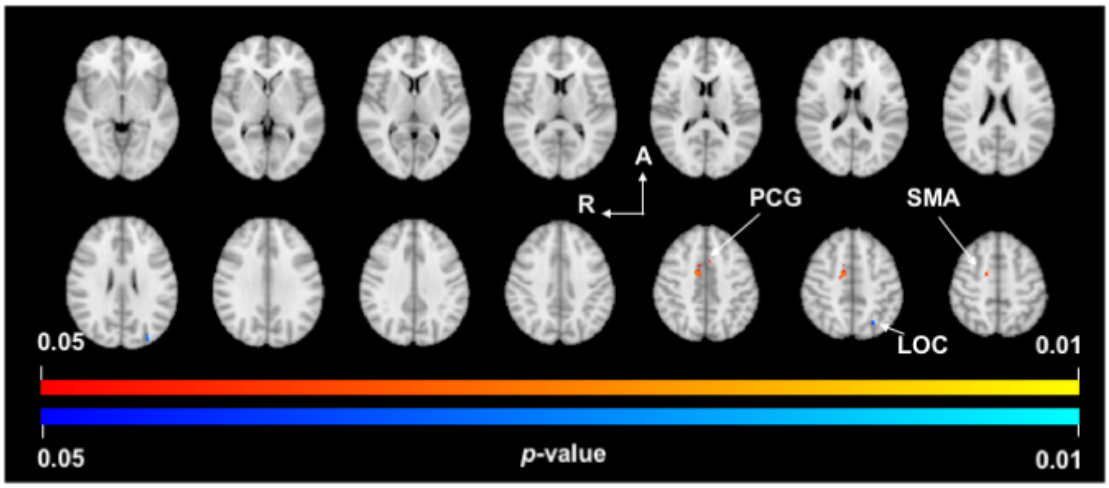

Figure 4.3: VLp/VA thalamus functional connectivity. *p*-value images showing neuroanatomical regions with significant between-group changes in functional connectivity with the VLp/VA thalamus in PD subjects compared to Controls. **Key:** Warm colours (yellow-orange) represent areas of increased functional connectivity in PD and cool colours (light-dark blue) represent areas of decreased functional connectivity in PD. Spacing between each slice in the z-direction is 4.2mm beginning at z = -3.18 in the top left slice (MNI T1 2mm image). R, right; A, anterior; PCG, paracingulate gyrus; SMA, supplementary motor area; LOC, lateral occipital cortex.

Table 4.2. Regions showing functional connectivity differences with the VLp/VA thalamus in PD.

FC Cluster	Peak	Brain Regions	Voxels	MNI x	MNI y	MNI z
Increased	1	R Supplementary motor area (BA6)	64	12	-2	42
	2	L Paracingulate gyrus (BA32)	11	-4	10	42
	3	R Supplementary motor area (BA6)	10	10	6	44

Decreased	4	L Lateral occipital cortex (BA19)	18	-30	-86	24
	5	L Lateral occipital cortex (BA19)	10	-26	-66	46
	6	L Lateral occipital cortex (BA19)	3	-26	-68	56

Brain regions and associated coordinates represent significant peaks within each cluster ($p < 0.05$). Abbreviations: FC, functional connectivity; L, left hemisphere; R, right hemisphere; BA, Brodmann area; MNI, coordinates for location of peak voxels in Montreal Neurological Institute 152 T1 2mm space. Labelling of brain regions based on the Harvard-Oxford Cortical/Subcortical Atlases.

4.4.3. Functional connectivity of the MD/A thalamus in PD

Analysis of the MD/A thalamus in PD found significant clusters of increased FC with the left anterior cingulate (BA24) and left putamen (Fig 4.4, Table 4.3). These clusters extended across the following brain regions: the bilateral anterior (BA24) and paracingulate gyri (BA32), left caudate nucleus, left putamen, left globus pallidus, bilateral dorsolateral prefrontal cortex (BA9) and bilateral anterior prefrontal cortex (BA8). Analysis of the VLp/VA thalamus also found a significant cluster of decreased FC with the left lateral occipital cortex (BA19).

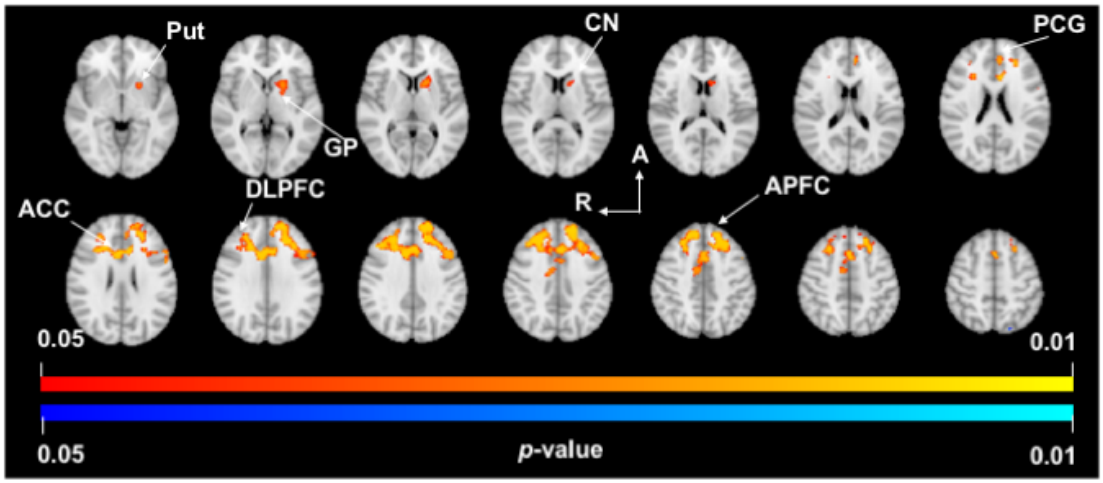

Figure 4.4: MD/A thalamus functional connectivity. *p*-value images showing neuroanatomical regions with significant between-group changes in functional connectivity of the MD/A thalamus in PD subjects compared to Controls. Warm colors (yellow-orange) represent areas of increased functional connectivity in PD.

Spacing between each slice in the z-direction is 4mm beginning at z = -2.3 in the top left slice (MNI T1 2mm image). R, right; A, anterior; Put, putamen; GP, globus pallidus; CN, caudate nucleus; PCG, paracingulate gyrus; ACC, anterior cingulate cortex; DLPFC, dorsolateral prefrontal cortex; APFC, anterior prefrontal cortex.

Table 4.3. Regions showing functional connectivity differences with the MD/A thalamus in PD.

FC Cluster	Peak	Brain Regions	Voxels	MNI x	MNI y	MNI z
Increased	7	L anterior cingulate (BA24)	4319	-8	18	22
	8	L putamen (BA49)	268	-20	10	-4
Decreased	9	L lateral occipital cortex (BA19)	10	-18	-78	52

Brain regions and associated coordinates represent significant peaks within each cluster ($p < 0.05$). Abbreviations: FC, functional connectivity; L, left hemisphere; R, right hemisphere; BA, Brodmann area; MNI, coordinates for location of peak voxels in Montreal Neurological Institute 152 T1 2mm space; Labelling of brain regions are based on the Harvard-Oxford Cortical/Subcortical Atlases.

4.4.4. Correlation between functional connectivity and clinical data

In PD patients we observed a positive correlation between LED and mean FC of the right supplementary motor area (peak 3; r = 0.46, $p = 0.01$) and a negative correlation with the left lateral occipital cortex (peak 4; r = -0.41, $p = 0.04$). We also observed a positive correlation between disease duration and mean FC of the right supplementary motor area (peak 1; r = 0.41, $p = 0.03$; peak 3; r = 0.57, $p = 0.01$). We also observed a positive correlation between TUG scores and mean FC of the left paracingulate gyrus (peak 2; r = 0.43, $p = 0.02$) and lateral occipital cortex (peak 6; r = 0.43, $p = 0.02$; peak 9; r = 0.37, $p = 0.047$). None of these results survived correction for multiple comparisons.

4.4.5. Morphology of the thalamus in PD

Comparisons of thalamic volumes found no difference between the PD group and Controls (Table 4.4).

Table 4.4: Estimated mean volumes of right and left thalamus and pairwise comparison.

Structure	Control	PD	Mean difference	*p*-value
Right thalamus volume (mm^3)	5774.13	5927.45	-153.32	0.25
Left thalamus volume (mm^3)	5594.47	5749.24	-154.78	0.18

Estimated volumes of the right and left thalamus after adjusting for age, eTIV and sex. *p*-value presented has been adjusted for family-wise error rate using a Bonferroni correction.

4.4.6. Surface based shape analysis

Shape analysis found no localized areas of shape change to the surface of the right or left thalamus in the PD group compared to Controls, after correcting for false-discovery rate (Fig 4.5).

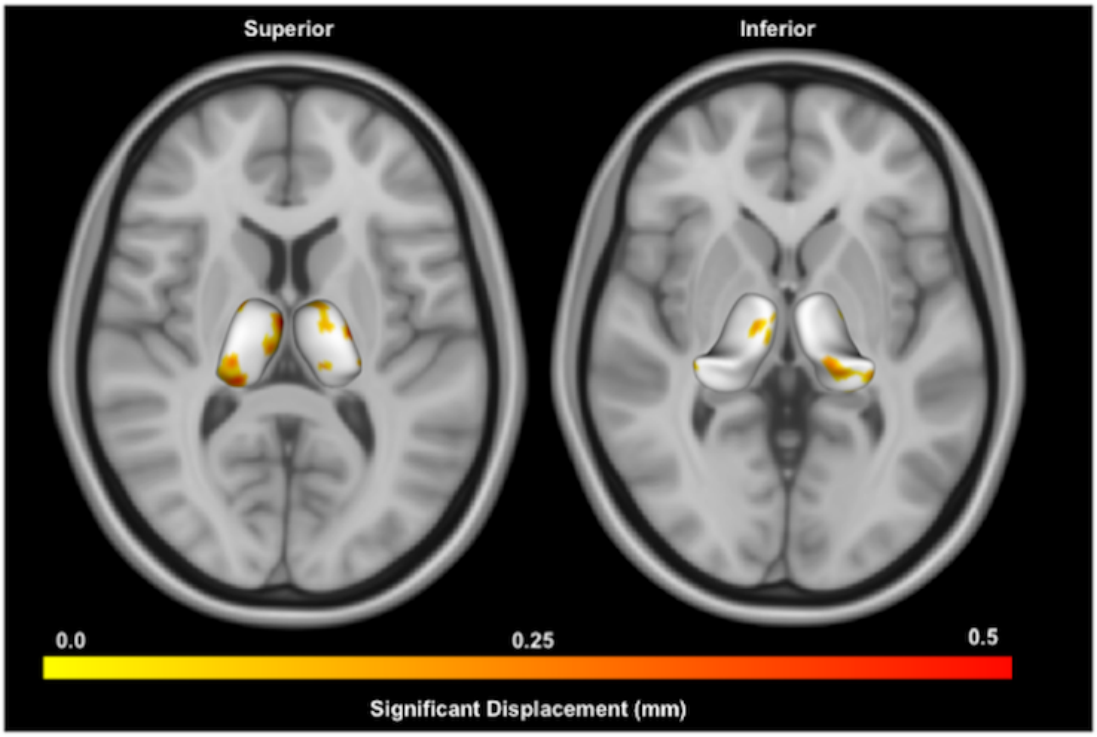

Figure 4.5: Shape analysis of thalamus in PD compared to Controls. Displayed are superior and inferior views of bilateral thalami overlaid on axial MNI T1 0.5mm images. Warmer colors indicate regions of greater inflation in the PD group compared to Controls using point-wise significance tests ($p < 0.05$, uncorrected). No regions were significant after false-discovery rate correction.

4.4.7. Correlations between thalamic volumes and clinical symptoms in PD

We found no significant relationships between volumes of the right or left thalamus and clinical function in the PD or Control groups.

4.5. Discussion

4.5.1. Findings

The results of this study demonstrate that PD patients on medication have increased FC within motor, dorsolateral and anterior cingulate basal ganglia-thalamocortical circuits. Our data support the findings of a recent meta-analysis showing that PD patients have increased FC of basal ganglia-thalamocortical circuity (Ji et al., 2018). and extend these findings by showing for the first time how important functional subterritories of the thalamus are impacted in PD. These changes in functional connectivity were found despite any evidence of morphological alterations to the structure, or any evidence of a relationship between thalamic morphology and clinical dysfunction.

Our findings of increased FC between the VLp/VA thalamus and the supplementary motor area may be indicative of changes within one segment of the classic ‘motor’ basal ganglia-thalamocortical circuit (Alexander et al., 1986). In this model, the motor

circuit originates at the supplementary motor area, receiving input from the primary and the premotor cortices. These areas connect with the nuclei of the basal ganglia, which project back to the ventral anterior and ventral lateral nuclei of the thalamus, closing the loop by reconnecting with the site of origin in motor cortical areas (Alexander et al., 1986). Increased FC between the putamen and the supplementary motor area has been demonstrated previously (Yu et al., 2013) while other research using graph theoretical analyses has demonstrated increased functional connectivity within the sensorimotor network in PD (Göttlich et al., 2013). Evidence suggests that increased FC of sensorimotor networks is likely related to dopaminergic medication usage (Esposito et al., 2013) potentially facilitating increases in FC, which is a mechanism that will be discussed momentarily.

Our research also demonstrates significant and far more widespread increases in FC in PD between the MD/A thalamus and the anterior and dorsolateral prefrontal cortices, potentially indicating a disease related change to the 'dorsolateral prefrontal' basal ganglia-thalamocortical circuit (Alexander et al., 1986). This circuit originates in Brodmann areas 9 and 10 on the lateral surface of the anterior frontal lobe, and after traversing the basal ganglia, connects directly with our intended seed-ROIs at the anterior and mediodorsal nuclei of the thalamus. From there, the circuit projects back to the anterior and dorsolateral prefrontal cortices to form a closed loop (Alexander et al., 1986). Our findings of increased FC between the MD/A thalamus and the dorsolateral prefrontal cortex may represent functional compensatory mechanisms due to the significant cognitive dysfunction common in PD. The dorsolateral prefrontal cortex helps to execute tasks that contribute to cognitive functioning, including working memory, decision-making and action control, achieved through a

top-down modulation of behaviour in concert with diverse cortical and subcortical structures (Caspers et al., 2017). Research has shown that FC is significantly increased *across* the prefrontal cortex in PD subjects on medication, as the brain potentially recruits new anatomical areas to aid in the performance of cognitive tasks. It is argued that changes in FC may indicate a functional compensation to help restore cognitive processes in PD (Caspers et al., 2017). Interestingly, we also found significant increases in FC between the MD/A thalamus and the anterior cingulate cortex in PD subjects, indicating a disease related change to the 'anterior cingulate' basal ganglia-thalamocortical circuit. In this circuit, the anterior cingulate cortex links with the ventral basal ganglia structures, outputs to the ventral anterior nuclei of the thalamus, and links back with the anterior cingulate cortex (Alexander et al., 1986). Our findings of increased FC with the anterior as well as paracingulate gyri fit with the concept of increased FC due to compensatory mechanisms, as this region of the brain interacts with the lateral prefrontal cortex to mediate performance in tasks linked to cognitive processes (Fornito et al., 2004). Research has shown that a common response to neurological disruption is the *hyper*-connectivity of brain circuits, which may reflect a protective mechanism in the brain to maintain normal functioning (Hillary et al., 2015). Such a mechanism has been proposed in PD previously (Gorges et al., 2015, Helmich et al., 2010), as well as in mild cognitive impairment and Alzheimer disease (Mevel et al., 2011, Sheline and Raichle, 2013), and taken together, our results provide support for this model.

There are nonetheless inconsistencies with similar FC research that require consideration. Our data contrast with work demonstrating no significant FC changes between the thalamus and widescale brain networks in subjects on medication (Bell et

al., 2015). A possible explanation for this inconsistency may relate to how FC changes across different disease stages. When compared to the current work, the study in question focused on PD subjects with both a longer disease duration as well as a higher average Hoehn and Yahr stage (Bell et al., 2015). This is important because research has shown that FC in PD may undergo periods of both *hyper*-connectivity and *hypo*-connectivity as the disease progresses (Gorges et al., 2015). Potential FC changes across the course of PD thus make difficult to compare studies with subjects at different disease stages.

Our data also indicate that PD is associated with increases in FC between the MD/A thalamus and the left dorsal caudate nuclei, anterior putamen and globus pallidus. Strong evidence suggests that the output of the basal ganglia, mainly the globus pallidus interna, is hyperactive in PD (Duval et al., 2016) and our results of increased FC with this area suggest that increased activity may be accompanied by increased FC. Increased FC between the caudate nuclei and the thalamus has been shown in a PD cohort on medication (Müller-Oehring et al., 2015), however two studies have demonstrated conflicting results (Agosta et al., 2014b, Owens-Walton et al., 2018). A crucial difference separating these studies relates to patient inclusion. One of these studies focused on early PD patients with a mean disease duration of 1.7 years (Agosta et al., 2014b), which differs markedly from the current study where the average disease duration is 5.16 years. The present study also excluded PD subjects with dementia, fundamentally distinguishing it from our previous work (Owens-Walton et al., 2018). This is crucial as PD dementia is associated with decreases in FC compared to subjects without the diagnosis (Ponsen et al., 2013). Our findings of increased FC between the MD/A thalamus and the anterior putamen are supported by

similar research in this field (Helmich et al., 2010). This research demonstrated that increased inter-regional coupling of the anterior putamen, the region anterior to the anterior commissure, follow the specific spatial pattern of dopamine depletion in PD (Kish et al., 1988). This research suggests that PD patients may undergo a shift in cortico-striatal connections from the neuro-chemically more affected posterior putamen toward the relatively spared anterior putamen. Our results support this finding, suggesting that the anterior putamen may undergo increased FC with the MD/A thalamus, further supporting the model that the pathophysiology of PD may involve compensatory alterations in the FC of key nuclei within basal ganglia-thalamocortical circuits.

While conceiving of FC changes in terms of segregated basal ganglia-thalamocortical circuits is attractive, this inference is theoretical. It is therefore helpful to consider the results of other imaging techniques to substantiate our findings. Graph-based eigenvector centrality mapping research (which informs on the number and quality of node connections within networks) has shown that this metric is increased in the thalamus in PD (Guan et al., 2017). Interestingly, we also found a significant (though small) cluster of reduced FC of both the VLp/VA and MD/A thalamus with the lateral occipital cortex in PD patients, supporting previous work which found reductions in FC between nuclei of the extended basal-ganglia (including the thalamus) and this area of the brain (Guan et al., 2017). The findings from ^{18}F-flurodeoxyglucose PET imaging has indicated that PD is associated with increased pallidothalamic activity (Eckert et al., 2007), which supports our findings. However, this research also demonstrated that regions of the dorsolateral prefrontal cortex and the supplementary

and premotor areas show reductions in metabolic activity in PD, contrasting with our results (Eckert et al., 2007).

We found no significant correlation between FC of our seed-ROI in the thalamus and measures of clinical function, disease duration or antiparkinsonian medication use. This supports previous meta-analytic research which indicates that FC within a basal-ganglia networks does not correlate with clinical indices of disease severity (Szewczyk-Krolikowski et al., 2014), arguing instead that altered FC reflects a constitutional alteration of the networks under consideration. Our results are also bolstered by meta-analytic findings which indicate that increased FC of the thalamus were unaffected by medication status (Ji et al., 2018).

The morphological data from our study are consistent with previous reports indicating that PD is not associated with atrophy of the thalamus (Lee et al., 2014, Mak et al., 2014, Mckeown et al., 2008, Menke et al., 2014, Messina et al., 2011, Nemmi et al., 2015, Tinaz et al., 2011). We also found no significant localized surface shape changes in the PD group, supporting a number of studies (Lee et al., 2014, Menke et al., 2014, Messina et al., 2011). After investigating between-group morphological differences we investigated potential relationships between volumes of the thalamus and measures of clinical function. These analyses revealed no significant findings, supporting previous research (Lee et al., 2014, Mak et al., 2014, Tinaz et al., 2011). These results make intuitive sense, as we found no significant volumetric or localized shape changes in the PD cohort, suggesting there was no discernible relationship between atrophy of the thalamus and the PD disease process.

4.5.2. Strengths and limitations

Possible limitations of the current work warrant further attention. The first is our small sample size. While this is an important factor that negatively impacts the power of our study, our sample size was the result of choosing a highly stringent head motion exclusion criteria, which we believe is a strength of our work. A second possible limitation is the use of atlas-based seed-ROI segmentation, defined by the structural connectivity of thalamic nuclei (Behrens et al., 2003). Future work may benefit from a data-driven parcellation scheme as it may better capture functional boundaries of seed-ROIs. A final limitation is the influence of dopaminergic medication on the functional connectivity of brain networks, which has shown to be impacted in PD participants on this type of medication of medication (Bell et al., 2015). Despite these considerations we believe our data make important statements about the role of the thalamus within basal ganglia-thalamocortical circuits in PD.

4.5.3. Conclusions

We found increases in functional connectivity between the VLp/VA thalamus and the supplementary motor area and paracingulate gyrus, and also between the MD/A thalamus and basal ganglia nuclei, anterior and paracingulate cingulate gyri, anterior and also dorsolateral prefrontal cortical regions. Significant increases in functional connectivity were found despite any observable volumetric or localized shape alterations to the thalamus. The results of this study indicate that functional connectivity changes occur in PD, which likely result from disease-related system level dysfunction of the thalamus as a network hub within basal ganglia-thalamocortical circuits.

5. Project three: Cognitive impairment

Project one and two looked at subcortical input and output structures of basal ganglia-thalamocortical circuits, the striatum and thalamus. Project one looked at morphology of these structures by classifying all of the PD patients as one cohort, then looking at disease progression using years since diagnosis to define early and late PD, and finally PD-dementia to represent the most advanced disease stage. Project two excluded participants with PD-related dementia, and did not break the PD cohort into disease progression groups. Both of these projects did not take into account levels of cognitive impairment beneath the level of dementia. This is an important consideration as there is evidence that structural changes to the brain increase relative to level of cognitive impairment, which can be found in participants diagnosed with only *mild* cognitive impairment (Melzer et al., 2012).

Regarding analyses of functional connectivity of structures, there was also opportunity to build on Projects one as this work investigated the caudate and putamen as whole structures. Research has shown that different regions of the striatum are connected to varied regions of the cortex (Draganski et al., 2008) and mediate different types of functioning based on this connectivity profile (Haber, 2003). Accordingly, Project three divides the PD cohort into subgroups based on levels of cognitive impairment and investigates the functional connectivity of subregions of the caudate nucleus, putamen and thalamus that have putative connectivity with prefrontal regions of the brain, areas involved in cognitive function. This chapter is based on a manuscript under revision, however certain elements have been changed to streamline the project with this thesis.

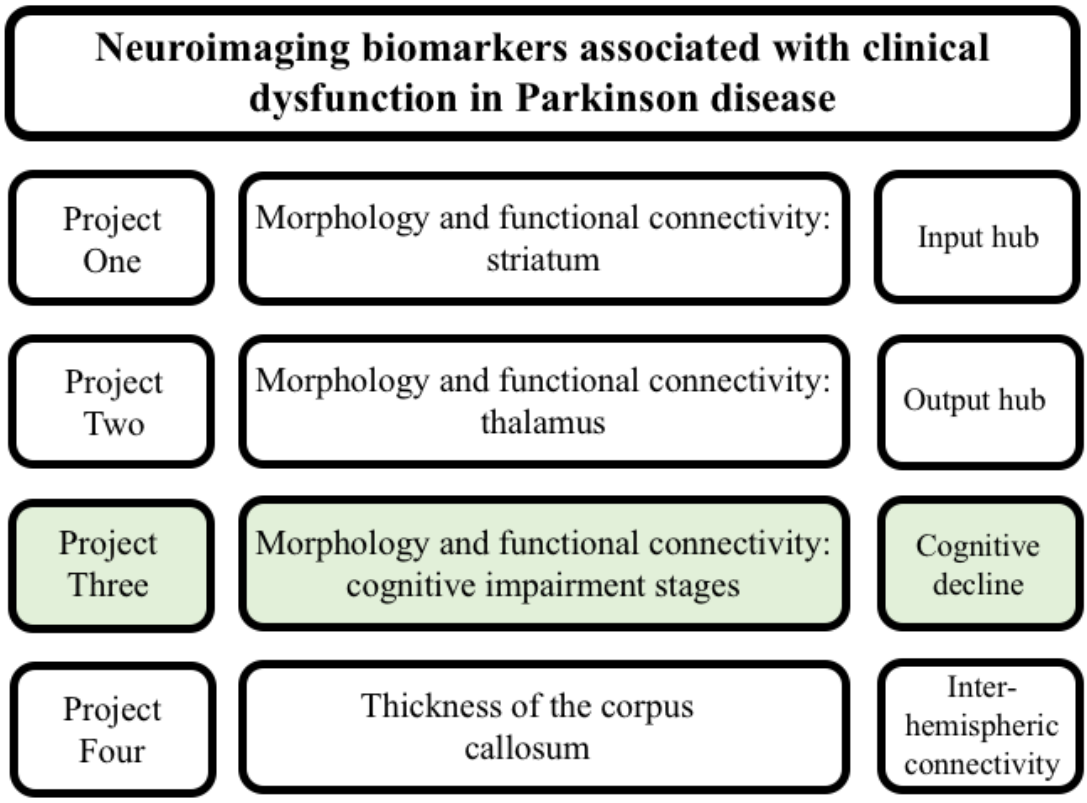

Figure 5.1: Project three. The current project focusses on the caudate nucleus, putamen and thalamus as key hubs within basal ganglia-thalamocortical circuitry, investigating morphology and functional connectivity based on levels of cognitive impairment.

Title:

Neuroimaging biomarkers differentiate Parkinson disease with and without cognitive impairment and dementia

Author names:

Conor Owens-Walton[1]*, David Jakabek[2], Brian D. Power[3,4], Mark Walterfang[5,6], Sara Hall[7,8], Danielle van Westen[9,10,¶], Jeffrey C.L. Looi[1,5,¶], Marnie Shaw[11,¶] and Oskar Hansson[7,8,¶].

Affiliations:

[1] Research Centre for the Neurosciences of Ageing, Academic Unit of Psychiatry and Addiction Medicine, School of Clinical Medicine, Medical School, Australian National University, Canberra, Australia
[2] Graduate School of Medicine, University of Wollongong, Wollongong, Australia.
[3] School of Medicine, The University of Notre Dame, Fremantle, Australia
[4] Clinical Research Centre, North Metropolitan Health Service – Mental Health, Perth, Australia
[5] Neuropsychiatry Unit, Royal Melbourne Hospital, Melbourne Neuropsychiatry Centre, University of Melbourne and Melbourne Health, Melbourne, Australia
[6] Florey Institute of Neurosciences and Mental Health, University of Melbourne, Melbourne, Australia
[7] Memory Clinic, Skåne University Hospital, Malmö, Sweden
[8] Department of Clinical Sciences, Lund University, Malmö, Sweden
[9] Centre for Medical Imaging and Physiology, Skåne University Hospital, Lund, Sweden
[10] Diagnostic Radiology, Department of Clinical Sciences, Lund University, Lund, Sweden
[11] College of Engineering and Computer Science, The Australian National University, Canberra, Australia
¶ Denotes co-senior authors
* Corresponding author: conor.owens-walton@anu.edu.au. Address: Building 4, The Canberra Hospital, Hospital Rd, Garran, ACT, 2605.

Author contributions:

CO-W contributed to project design, organisation and execution, selected the statistical approach, performed the volumetric and functional connectivity analyses and prepared the manuscript and subsequent drafts (> 80% of total work). BDP contributed to project design, provided supervision for CO-W and revised drafts of the manuscript. DJ performed the SPHARM-PDM analysis and contributed to drafts of the manuscript. MW contributed to project design, provided crucial computational infrastructure and contributed to drafts of the manuscript. DvW and SH contributed to project design, organised the clinical/imaging aspects of the study and contributed to drafts of the manuscript. JCLL contributed to project design, acted as supervisor for CO-W and contributed to drafts of the manuscript. MS acted as supervisor for CO-W, helped with functional connectivity analyses and contributed to drafts of the

manuscript. OH contributed to project design, organised the clinical/imaging aspects of the study, provided CO-W with supervision and contributed to drafts of the manuscript.

5.1. Abstract

Cognitive impairment in PD places a high burden on patients and is likely a precursor to PD -related dementia. The pathophysiology of cognitive impairment in PD is complex, and involves networks in the brain that are distinct from those that underlie the motor symptoms of the disorder. Studying the functional connectivity and morphology of subcortical hubs within basal ganglia-thalamocortical circuits may uncover neuroimaging biomarkers of cognitive dysfunction in PD. We first investigated the size and shape of the caudate, putamen and thalamus and how these morphological characteristics differ between groups. We then used an atlas-based seed region-of-interest approach to investigate resting-state functional connectivity of important subdivisions of the caudate nucleus, putamen and thalamus, between Controls (n = 33), cognitively unimpaired PD participants (n = 33), PD participants with mild cognitive impairment (MCI) (n = 22) and PD participants with dementia (n = 17). Extensive volumetric and surface-based deflation was found in PD participants with dementia. The results of pairwise comparisons indicate that cognitively unimpaired PD participants, compared to Controls, display increased functional connectivity of the dorsal caudate, anterior putamen and mediodorsal thalamic subdivisions with areas across the frontal lobe, as well as reduced functional connectivity of the dorsal caudate with posterior cortical and cerebellar regions. Compared to cognitively unimpaired participants, PD participants with MCI demonstrated reduced functional connectivity of the mediodorsal thalamus with

midline nodes within the executive-control network. Compared to participants with MCI, participants with dementia demonstrated reduced functional connectivity of the mediodorsal thalamus with the posterior cingulate cortex, a key node within the default-mode network. Our research demonstrates how functional connectivity of the caudate, putamen and thalamus are implicated in the pathophysiology of cognitive impairment and dementia in PD, with MCI and dementia in PD associated with a breakdown in functional connectivity of the mediodorsal thalamus with para- and posterior cingulate regions of the brain, respectively.

5.2. Introduction

PD is the second most common neurodegenerative disorder in the world, affecting 2-3% of the population over the age of 65 (Poewe et al., 2017). Traditionally categorized as a disorder of movement, it is now widely recognised that patients experience significant neuropsychiatric symptoms relating to executive, memory, attentional and visual disturbances (Litvan et al., 2012). Recent recognition of the high prevalence and substantial impact of cognitive impairment in PD has drawn research attention to PD-related MCI (Goldman et al., 2018) which is associated with a significantly higher likelihood of developing dementia (Broeders et al., 2013).

The neural processes that distinguish PD patients with cognitive impairment from those without it are poorly understood (Williams-Gray et al., 2007). The pathological hallmark of PD is the presence of α-synuclein-immunopositive Lewy bodies and neurites (Obeso et al., 2000) resulting in a loss of dopaminergic neurons in the substantia nigra pars compacta, and subsequent depletion of dopamine at the striatum (caudate nucleus and putamen) (Kish et al., 1988). While nigrostriatal dopamine loss

is a core feature of PD, evidence suggests that pathology within the thalamus also contributes to the abnormal neural activity associated with the disorder (Halliday, 2009). The combined neural activity in these nodes within basal ganglia-thalamocortical circuits results in brain network abnormalities being key aspects of PD pathophysiology (Strafella, 2013).

To understand the functioning of brain networks it is necessary to study both the constituent neuronal elements of networks, as well as their interconnections (Sporns et al., 2005). Investigating neuronal elements can be done by quantifying disease-related effects on the morphology of 'hubs' (Looi et al., 2014) while interconnections can be investigated via resting-state functional connectivity analyses (Damoiseaux et al., 2006). Due to the importance of the caudate nucleus, putamen and the thalamus to the abnormal neural activity associated with PD, coupled with the fact that these structures are considered important hubs in brain networks (Hwang et al., 2017, Looi and Walterfang, 2013), an analysis of the morphology and functional connectivity of these structures may yield neuroimaging biomarkers of brain network abnormalities in PD that relate to cognitive dysfunction.

Data on the morphological changes to the caudate, putamen and thalamus in PD participants without dementia is also varied. Research groups have demonstrated both the presence (Garg et al., 2015, Mckeown et al., 2008) and absence (Menke et al., 2014, Messina et al., 2011) of morphological changes to the thalamus, while others have shown either the presence (Pitcher et al., 2012, Sterling et al., 2013) or absence (Menke et al., 2014, Owens-Walton et al., 2018) of morphological changes to the caudate or putamen. Studies suggest that PD with dementia is associated with atrophic

changes to the caudate nucleus, putamen and thalamus (Owens-Walton et al., 2018, Summerfield et al., 2005), however the presence and extent of such changes in PD-MCI is uncertain (Chen et al., 2016, Melzer et al., 2012). As this demonstrates, there is a significant variability in the field of neuroimaging biomarkers in PD, with reviews of structural and functional studies revealing few clear patterns (Khan et al., 2018). This may be due to the fact that research studies often to not consider the presence of MCI within PD cohorts, instead considering non-demented PD cohorts as a single experimental group. This project seeks to address this area of concern by using MCI as an important clinical staging milestone.

Research in this field has yielded important information about how functional connectivity of widescale intrinsic connectivity networks is impacted in PD relative to cognitive status, however the specific role played by important hubs within basal ganglia-thalamocortical circuitry is yet to be fully elucidated. Studies have found cognitively unimpaired PD is associated with both increases (Gorges et al., 2015) and decreases (Bell et al., 2015) in functional connectivity of basal ganglia-thalamocortical circuitry, while PD participants with MCI have been shown to display decreases in functional connectivity (Amboni et al., 2015, Gorges et al., 2015). Gorges et al. (2015) suggest that PD may involve a transient process from the *hyper*- to the *hypo*-connected state which is linked to cognitive decline. Using a well-defined clinical cohort, and a targeted rs-fMRI functional connectivity approach, the current study aims to better understand how functional connectivity and morphology of the caudate nucleus, putamen and thalamus are impacted in PD, and how these factors may vary between cognitively unimpaired PD patients, PD-MCI and PD patients with dementia.

A common response to neurological disruption is *hype*r-connectivity of brain circuits, and it is suggested that such a response reflects compensatory mechanisms in the brain to maintain normal levels of neuronal functioning (Hillary et al., 2015). This mechanism has been used to explain increases in functional connectivity of structures within basal ganglia-thalamocortical circuits in PD (Gorges et al., 2015, Helmich et al., 2010) and also in disorders such as MCI and Alzheimer's disease (Mevel et al., 2011, Sheline and Raichle, 2013). Hillary et al. (2015) argue that *hyper*-connectivity relies on the availability of sufficient neuronal resources, however these resources can be diminished via the loss of grey matter as diseases processes advance, thus depleting and ultimately exhausting any capacity that might underpin a compensatory response. When this neuronal resource loss reaches a hypothetical 'critical threshold,' increased functional connectivity is no longer a viable response to situational demand, and subsequent reductions in functional connectivity ensue. While the presence and extent of grey matter loss in cognitively unimpaired PD is questionable, PD-MCI and PDD more consistently display grey matter atrophy (Chen et al., 2016, Melzer et al., 2012). Accordingly, we hypothesised that cognitively unimpaired participants with PD would have sufficient neural resources to support functional compensation, and display increased functional connectivity, concomitant with no volumetric or surface-based shape alterations to the caudate, putamen and thalamus. However, we anticipated the presence of morphological alterations in PD-MCI, representing a 'critical threshold,' where functional connectivity begins to decrease along with reductions in morphology, evidenced by reduced volumes and surface deflation when compared to cognitively unimpaired PD participants, and controls. Finally, we hypothesised that PDD participants would demonstrate significant and profound

reductions in volumes and surface shape, along with significant decreases in functional connectivity of the caudate nuclei, putamina and thalami compared to all experimental groups (Figure 5.2).

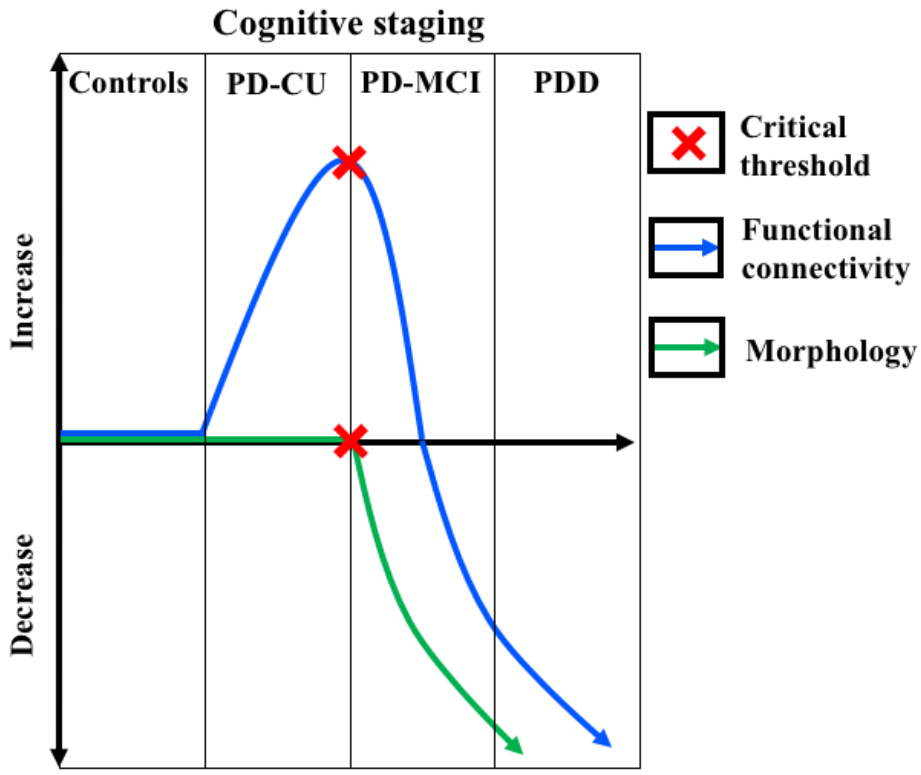

Figure 5.2: Hypothetical 'critical threshold' framework. This figure demonstrates onset of a 'critical threshold,' indicated by red crosses, after which point functional connectivity and morphology (volume and surface shape) changes can be found (Hillary et al., 2015). **Abbreviations:** PD-CU, cognitively unimpaired PD participants; PD-MCI, PD participants with mild cognitive impairment; PDD, PD participants with dementia.

5.3. Methods

5.3.1. Participants

Participants in this study were from the Swedish BioFinder study (www.biofinder.se) and gave informed written consent. All elements of the research were performed in accordance with the World Medical Association's Declaration of Helsinki and ethical

approval was obtained through the Ethical Review Board of Lund, Sweden, and the Human Research Ethics Committee at the Australian National University, Canberra, Australia.

5.3.2. Parkinson disease cognitive impairment subgroups

Diagnosis of probable PD was made by a neurologist using the National Institute of Neurological and Stroke Diagnostic Criteria (Gelb et al., 1999). The total PD cohort was subdivided into three cognitive impairment disease groups. The first group comprises cognitively unimpaired PD patients (PD-CU; n = 33). The second group comprises PD patients with MCI (PD-MCI; n = 22), based on the Movement Disorder Society Task force guidelines (Litvan et al., 2012). This criterion is met when patients score at least 1 standard deviation below the normative mean in at least two cognitive tests, including executive function, attention, visuospatial, memory and language domains. The third subgroup consists of PD participants with dementia (PDD; n = 17) diagnosed using the Clinical Diagnostic Criteria for Dementia Associated with PD (Emre et al., 2007). A healthy control group (Controls) was included for comparative purposes (n = 26). Exclusion criteria for this study included refusing MRI, the presence of significant alcohol or substance misuse and/or a significant systematic illness or organ failure. All participants underwent a cognitive and neurological examination by a medical doctor with extensive experience with movement disorders, while PD participants remained on their usual medication regimes. Clinical functioning of participants was quantified using the Hoehn and Yahr staging, assessing the progression of the disorder; the Unified Parkinson's Disease Rating Scale Part-III test (UPDRS-III), assessing the motor signs of PD (Fahn and Elton, 1987); the Mini Mental State Examination (MMSE), assessing cognitive mental state

(Folstein et al., 1975); the Animal Fluency and Letter S Fluency tests, assessing verbal fluency and executive function (Tombaugh et al., 1999) and the A Quick Test of cognitive speed assessing perceptual and cognitive speed (Palmqvist et al., 2010).

5.3.3. MRI acquisition

Structural MRI data was obtained on a 3T scanner (Trio, Siemens Magnetom, Erlangen, Germany) with a 20-channel head-coil. High resolution T_1-weighted three-dimensional anatomical brain images were acquired using a magnetisation-prepared rapid acquisition technique with gradient-echo sequence (repetition time = 7 ms; echo time = 3 ms; flip angle = 90 degrees; voxel size = isotropic $1mm^3$). Image matrix size was 356 voxels in the coronal and sagittal planes and 176 voxels in the axial plane. Functional MRI data consists of 256 T_2*-weighted echo planar imaging volumes (repetition time = 1850 ms; echo time 30 ms; flip angle = 90 degrees; matrix 64 × 64; voxel size 3 × 3 × 3.75 mm^3) for each participant. Matrix size was 64 voxels in the coronal and sagittal planes and 36 voxels in the axial plane. Participants were instructed to lie still with their eyes closed, not to fall asleep and not to think of anything in particular during the scan, which lasted for approximately 8 minutes.

5.3.4. Preprocessing of T_1 structural MRI data

Preprocessing of T_1-weighted structural data was performed using the FSL software package (FSL, Oxford, UK; version 5.0.10) (Jenkinson et al., 2012). Images underwent brain extraction using the FSL-BET tool (Smith, 2002) which were then processed using FSL-FAST, segmenting the T_1 structural MRI into brain tissue types whilst correcting for image intensity fluctuations caused by inhomogeneities in the radio frequency field (Zhang et al., 2001).

5.3.5. Volumetrics: Statistical analyses

Volumes of the caudate, putamen and thalamus were estimated using the segmentation and registration tool FSL-FIRST (Patenaude et al., 2011). This uses a model-based approach to segment subcortical structures producing output meshes and volumetric data. Investigating differences between experimental groups was performed with SPSS 22.0 (IBM Corporation, Somers, New York, USA) utilising two-tailed multivariate analysis of covariance models controlling for intracranial volume (ICV) (derived from FSL-FAST) and age. Multivariate partial eta squared values (η^2) are used to report effect sizes (Cohen, 1992).

5.3.6. SPHARM-PDM surface shape: Statistical analyses

Volumetric analyses can investigate overall size differences between groups, however they cannot highlight where atrophy/hypertrophy takes place. Accordingly, we used spherical harmonic parametrization three-dimensional point distribution model (SPHARM-PDM) to investigate localised surface changes to the segmentations of the caudate, putamen and thalamus between experimental groups (Styner et al., 2006) described in Methodology section 2.3.2. Segmentations were preprocessed to ensure a spherical topology, then described by spherical harmonic functions and sampled onto surfaces of 1002 points. Surfaces were then aligned using a rigid-body Procrustes alignment to a mean template created from a group sample. Comparisons between groups were performed using multivariate analysis of covariance models with a Hotelling statistic in R (version 3.2.1, R Development Core Team, 2014). All analyses included covariates of ICV, age and sex. SPHARM-PDM produces mean displacement maps which show the magnitude of surface displacement (deflation or

inflation in mm) between corresponding points on the mean surface of one experimental group compared to another. Significant surface changes are indicated by regions with a *p*-value < 0.05, corrected for multiple comparisons with a FDR bound *q* of 5% (Genovese et al., 2002). Results are presented as a composite map of each structure with inflation/deflation only displayed in regions that are significant after FDR correction.

5.3.7. Preprocessing of resting-state fMRI data

Preprocessing of resting-state functional images was performed using FSL-FEAT (v6.0). Steps included deletion of first 6 volumes, motion correction using FSL-MCFLIRT (Jenkinson et al., 2002) and removal of non-brain tissue using FSL-BET (Smith, 2002). Registration of participant's functional images to high resolution T_1-weighted structural images used a boundary-based registration (Greve and Fischl, 2009) within FSL-FLIRT linear registration tool (Jenkinson et al., 2002, Jenkinson and Smith, 2001). Registration of functional images to MNI 152 T_1 $2mm^3$ standard space was performed with FSL-FLIRT with 12 degrees of freedom, further refined using FSL-FNIRT nonlinear registration (Andersson et al., 2007a, Andersson et al., 2007b) with a warp resolution of 10mm and a resampling resolution of 4mm.

Data denoising was then performed with FSL-MELODIC (v3.15) independent component analysis (ICA) (Beckmann and Smith, 2004) to identify any potential influence of head motion, scanner and cerebrospinal fluid artefacts. FSL-FIX (v1.06) (Salimi-Khorshidi et al., 2014) was then used to remove components classified as 'noise' and also correct for motion confounds. This approach masks non-brain voxels, performs a voxel-wise demeaning of the data, followed by normalisation of the voxel-

wise variance. Data were whitened and projected onto a 53-dimensional subspace as estimated by a Laplace approximation of the Bayesian evidence of the model order using a principal component analysis. Observations were decomposed into sets of vectors describing the variation of signal across both the temporal (time-courses) and spatial (maps) domains, optimising for non-gaussian spatial source distributions using a fixed-point iteration technique (Hyvarinen, 1999). We then trained a classifier for our particular dataset by first using the 'Standard.RData trained-weights' classifier over a sample of ICA maps for 10 Controls and 10 PD subjects, with the classifier categorising maps as either 'signal' or 'noise'. We checked each classification against validated guidelines, choosing the conservative approach to component reclassification as outlined in that work (Griffanti et al., 2014). Following this, the FIX classifier was re-trained using this new data and run over the ICA datasets for all subjects, regressing out noise components while also cleaning up motion confounds (24 regressors: 6 motion parameters, 6 first derivatives and the squares of these 12 regressors). This process creates a de-noised filtered functional file which is used at the individual level GLM stage. Spatial smoothing was then performed (full width half maximum Guassian kernel = 5mm) followed by a multiplicative mean intensity normalisation and a high-pass temporal filtering Gaussian-weighted least-squares straight line fitting with sigma = 50.0s (Woolrich et al., 2001).

Three nuisance-variable masks were created for each participant, intended to encompass the white matter, ventricle and whole-brain regions (including both grey and white matter territory). These were produced from participants T_1-structural images using the recon-all command from FreeSurfer (Fischl, 2012). These masks were converted to functional space using FSL-FEAT registration warp files, where

they were then thresholded to only include voxels with a greater than 70% chance of inclusion. Masks were then eroded using the fslmaths tool to reduce partial volume effects. Average timeseries data were then extracted from these masks to be regressed from the data at the individual-level GLM stage.

To reduce potential spurious effects of head motion we used the FSL Motion Outliers tool to identify timepoints in fMRI data that were potentially corrupted by large motion. This step was performed as research has indicated that traditional linear regression methods cannot fully resolve head motion-related signal changes (Power et al., 2012). We chose to identify outliers based on a DVARS metric which indexes the rate of change of BOLD signal across the entire brain at each frame of data (Smyser et al., 2011), with 'D', referring to the temporal derivative of timecourses, and 'VARS' referring to the variance over all voxels of the root mean realignment estimates. We identified timepoints for outliers on this metric as timepoints with a score outside the 75th percentile plus 1.5 multiplied by the interquartile range, which were then removed from the data at the individual GLM stage.

5.3.8. Resting-state fMRI: Seed-based region-of-interest approach

To investigate how the caudate, putamen and thalamus are impacted in PD groups with varying levels of cognitive impairment, we used an atlas-based method to subdivide the structures into functionally relevant regions-of-interest (ROI). We performed this step using the Oxford Thalamic Connectivity Atlas (Behrens et al., 2003) and the Oxford-GSK-Imanova Connectivity Atlas (Tziortzi et al., 2014) within FSLEyes. Regions of the dorsal and central caudate nucleus and the anterior putamen have the highest probability of connectivity with the anterior and dorsolateral

prefrontal cortices in the brain (BA9, 9/46 and 10) and are said to be involved in cognitive processes, including perception, memory, reasoning and judgement (Haber, 2003). The mediodorsal and anterior thalamic nuclei have the highest probability of connectivity to the dorsolateral and prefrontal cortices (Behrens et al., 2003) and these thalamic nuclear regions are said to be involved in limbic, episodic memory and cognitive functions (Power and Looi, 2015). For ease of reference, we will refer to these three seed-ROIs as the 'dorsal caudate', 'anterior putamen' and 'mediodorsal thalamus' respectively. These three bilateral standard space MNI 152 $2mm^3$ seed-ROI masks were thresholded to only include voxels that had a greater than 50% chance of inclusion (Figure 5.3A). Masks were then registered to T_1-weighted structural space where we used them to 'cookie-cut' ROIs from the FSL-FIRST segmentation masks. These seed-ROIs were then converted to subject-specific functional MRI space where we performed a final erosion to avoid partial volume effects (Caballero-Gaudes and Reynolds, 2017). Mean activation data from within the three seed-ROIs at each timepoint was used as explanatory variables for subsequent statistical analyses.

Before investigating the differences in functional connectivity between groups we conducted three one-sample *t*-tests on all of the Control participants to look at the functional connectivity of our seed-ROIs with the rest of the brain. This step indicates the areas of highest functional connectivity with our seed-ROIs and provides a backdrop on which to interpret our results (Figure 5.3B).

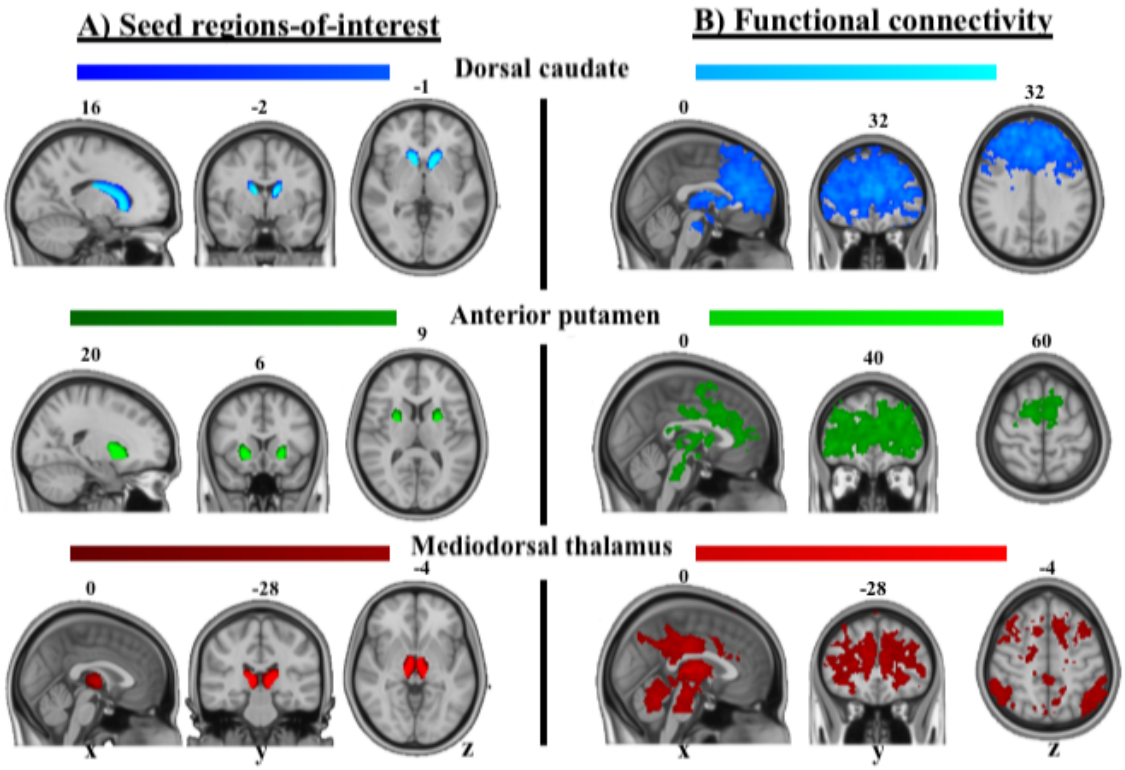

Figure 5.3: Seed regions-of-interest and one-sample *t*-tests demonstrating putative functional connectivity pathways in Controls. A) Subject specific seed regions-of-interest masks were converted to MNI 152 T_1 standard space and combined to produce this image. Lighter areas of each colour are indicative of a greater proportion of voxels in that area being included in the relevant mask. B) Z-statistic (Gaussianised) images from Control participant's individual-level general linear model statistic image, thresholded non-parametrically using clusters determined by $Z > 3.1$ and a (corrected) cluster significance of $p < 0.05$ (Worsley, 2001).

5.3.9. Resting-state fMRI: Statistical analyses

Three individual-level functional connectivity analyses were performed for each participant using a general linear model (GLM) in a mass univariate voxelwise whole-brain analysis (Woolrich et al., 2004). This GLM approach measures the correlation between activity within each of the three seed-ROIs and the rest of the brain. We used a FILM pre-whitening correction, shifted the model with a temporal derivative to account for slice timing effects and variations in the hemodynamic response function,

removed volumes potentially corrupted by large motion and regressed out average signal from within white matter, ventricle and whole-brain masks.

The following higher-level analyses of functional connectivity differences were conducted: PD-CU compared to Controls (section 5.4.4.1); PD-MCI compared to PD-CU (section 5.4.4.2); PDD compared to PD-CU (section 5.4.4.3) and PDD compared to PD-MCI (section 5.4.4.4). These analyses were performed using FSL-FLAME in a mixed-effects design (Woolrich et al., 2004). Age and gender data were included as covariates. When investigating functional connectivity between the PD-CU, PD-MCI and PDD groups we also included levodopa-equivalent daily dosage (LEDD) data as a covariate. Z-statistic (Gaussianised) images from participants individual-level GLM statistical maps were thresholded non-parametrically using clusters determined by $Z > 3.1$ and a (corrected) cluster significance of $p < 0.05$ (Worsley, 2001).

5.3.10. Correlation between functional connectivity and clinical variables

After comparing functional connectivity between groups, we performed a series of post-hoc partial correlation analyses to investigate the relationship between functional connectivity and clinical variables. To do this we investigated functional connectivity at the neuroanatomical sites of significant between group differences, stipulated by the MNI coordinates listed in Tables 5.2, 5.3 and 5.4. In total there were 21 significant clusters found. To sample functional connectivity around these locations, 5mm spheres were placed at the MNI coordinates for each cluster, with the average parameter estimate for each statistic image extracted for each participant. The parameter estimate is an indication of the strength and directionality of the correlation between activity in that brain region and the activity in the seed-ROI. This variable

was then correlated with measures of clinical function within each group. For locations of significant difference when comparing PD-CU and Controls we performed this correlation in PD participants. For locations of significant difference when comparing PD-CU and PD-MCI we performed this correlation for participants in both groups. For locations of significant difference when comparing PD-MCI and PDD, we performed this correlation for participants in both groups.

5.4. Results

5.4.1. Participant characteristics

The characteristics of participants are displayed in Table 5.1. A chi-square test for independence found no significant difference in sex between the groups [χ^2 (3, n = 98) = 0.89, p = 0.86]. One-way analyses of variance found no significant difference in age [F (3, 94) = 2.169, p = 0.10], ICV [F (3, 94) = 0.323, p = 0.81], years of education [F (3, 79) = 1.255, p = 0.30] or average DVARS [F (3, 94) = 2.460, p = 0.07] between groups (Table 5.1). As expected, measures of clinical function were significantly different between disease groups.

Table 5.1: Participant characteristics

Item	Controls	PD-CU	PD-MCI	PDD	*p*-value
Number of participants	26	33	22	17	-
Female/Male	12/14	15/18	12/10	7/10	0.86
Average age in years	69.59 ± 6.17	69.25 ± 6.31	70.53 ± 5.38	73.70 ± 6.68	0.10
ICV (cm^3)	1456.00 ± 135.93	1491.68 ± 139.08	1471.06 ± 132.13	1481.80 ± 168.95	0.81
Years of education	12.73 ± 3.41	11.34 ± 5.36	9.66 ± 6.81	11.50 ± 4.52	0.30
DVARS	11.97 ± 3.21	14.96 ± 3.87	17.46 ± 12.71	15.62 ± 6.39	0.07
Years since diagnosis	-	6.30 ± 5.24	5.54 ± 3.56	11.88 ± 5.48	-

LEDD	-	639.60 ± 485.23	610.73 ± 262.11	1010.72 ± 625.53	-
H&Y	-	1.742 ± 0.73	2.00 ± 0.72	2.853 ± 0.77	-
UPDRS-III	2.35 ± 2.84	12.61 ± 9.55	14.27 ± 9.07	33.00 ± 10.21	<0.01*
MMSE	28.69 ± 1.16	28.76 ± 1.00	27.41 ± 1.65	22.88 ± 3.77	<0.01*
AF	23.88 ± 6.71	23.88 ± 5.71	18.86 ± 6.24	11.81 ± 4.18	<0.01*
LSF	19.00 ± 5.93	15.90 ± 5.26	12.5 ± 5.61	9.31 ± 4.24	<0.01*
AQT	59.08 ± 14.41	63.12 ± 11.308	78.38 ± 28.01	132.93 ± 73.26	<0.01*

Key: Participant data presented as mean ± standard deviation. All data corrected to two decimal places. *, significant difference in means between groups compared using one-way anova. **Abbreviations:** ICV, total intracranial volume; DVARS, average image intensity of each frame *n* in relation to *n*+1; LEDD, levodopa-equivalent daily dosage (mg); H&Y, Hoehn and Yahr Scale; UPDRS-III, Unified Parkinson's Disease Rating Scale, part-III; MMSE, Mini Mental-state Examination; AF, Animal Fluency test; LSF, Letter S Fluency test; AQT, A Quick Test of Cognitive Speed.

5.4.2. Volumetric analyses

Pairwise comparisons of volumes revealed the following significant differences between experimental groups (Table 5.2 and 5.3): the left caudate was significantly reduced in PDD compared to PD-CU (p = 0.009) and Controls ($p < 0.001$) with a large effect size ($\eta^2 = 0.177$) (Figure 5.4A). The right caudate was significantly reduced in PDD compared to PD-CU ($p = 0.021$) and Controls ($p = 0.001$) also with a large effect size ($\eta^2 = 0.143$) (Figure 5.4A). The left putamen was significantly reduced in PDD compared to PD-CU ($p = 0.005$) and Controls ($p < 0.001$) with a large effect size ($\eta^2 = 0.193$) (Figure 5.4B). The right putamen was significantly reduced in PDD compared to Controls ($p = 0.016$) with a medium effect size ($\eta^2 = 0.107$) (Figure 5.4B). The left thalamus was significantly reduced in PDD compared to PD-CU ($p = 0.011$) and Controls ($p = 0.037$) with a medium effect size ($\eta^2 = 0.108$) (Figure 5.4C). The right thalamus was significantly reduced in PDD compared to PD-CU (p = 0.002) with a medium effect size ($\eta^2 = 0.136$) (Figure 5.4C).

Table 5.2: Estimated volumes of caudate, putamen and thalamus

	Controls (mm^3)	PD-CU (mm^3)	PD-MCI (mm^3)	PDD (mm^3)
Left caudate	3450.32 ± 1681.03	3312.09 ± 1762.59	3241.73 ± 1702.63	2964.86 ± 1690.14
Right caudate	3549.40 ± 1581.95	3449.54 ± 1625.13	3372.14 ± 1572.23	3139.56 ± 1515.45
Left putamen	4720.97 ± 410.388	4541.24 ± 533.439	4396.80 ± 547.57	4065.27 ± 589.74
Right putamen	4637.26 ± 494.10	4511.64 ± 563.04	4362.30 ± 582.08	4199.70 ± 455.31
Left thalamus	7312.49 ± 2181.14	7360.32 ± 2285.64	7231.95 ± 2287.58	6814.29 ± 2159.28
Right thalamus	7117.68 ± 1986.33	7273.23 ± 2198.56	7061.30 ± 2116.92	6746.37 ± 2091.38

Key: Volumetric data presented as mean ± standard deviation. All data corrected to two decimal places.

Table 5.3: Pairwise comparisons of ROI volumes

Structure	Group 1	Group 2	Difference [1-2] (mm^3)	*p*-value*	η^2
Left caudate	PD-CU	PD-MCI	70.35	1.000	0.177
		PDD	347.22	0.009*	
		Controls	-138.24	0.797	
	PD-MCI	PDD	276.87	0.098	
		Controls	-208.59	0.243	
	PDD	Controls	-485.46	<0.001*	
Right caudate	PD-CU	PD-MCI	77.40	1.000	0.143
		PDD	309.98	0.021*	
		Controls	-99.86	1.000	
	PD-MCI	PDD	232.58	0.221	
		Controls	-177.27	0.432	
	PDD	Controls	-409.84	0.001*	
Left putamen	PD-CU	PD-MCI	144.44	1.000	0.193
		PDD	475.96	0.005*	
		Controls	-179.73	0.794	
	PD-MCI	PDD	331.52	0.159	
		Controls	-324.17	0.088	
	PDD	Controls	-655.69	<0.001*	
Right putamen	PD-CU	PD-MCI	149.35	1.000	0.107
		PDD	311.94	0.146	
		Controls	-215.62	1.000	
	PD-MCI	PDD	162.59	1.000	
		Controls	-274.97	0.210	
	PDD	Controls	-437.55	0.016*	
Left thalamus	PD-CU	PD-MCI	128.37	1.000	0.108
		PDD	546.02	0.011*	
		Controls	47.83	1.000	
	PD-MCI	PDD	417.66	0.143	
		Controls	-80.54	1.000	
	PDD	Controls	-498.20	0.037*	

Right thalamus	PD-CU	PD-MCI	211.94	0.561	0.136
		PDD	526.87	0.002*	
		Controls	155.55	1.000	
	PD-MCI	PDD	314.92	0.216	
		Controls	-56.39	1.000	
	PDD	Controls	-371.32	0.071	

Key: Covariates appearing in the model are evaluated at the following values: Age = 70.4008; ICV = 147.59; *, *p*-values < 0.05 (adjusted for multiple-comparisons using the Bonferroni method).

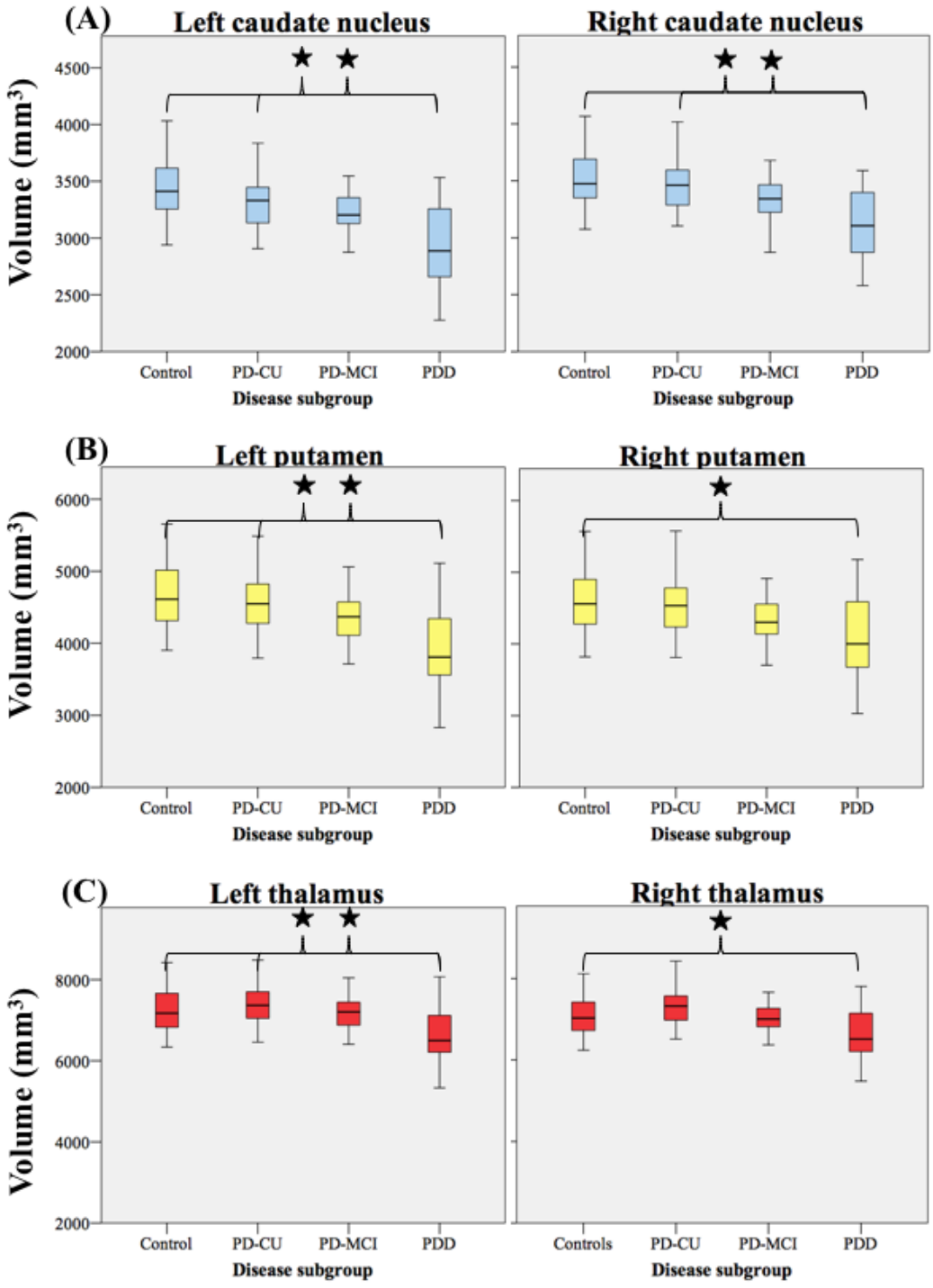

Figure 5.4: Pairwise comparison of volumes between PD subgroups and Controls. (A) Caudate (B) putamen and (C) thalamus. Volumes presented are estimated marginal mean values for each experimental group derived from MANCOVA models controlling for age and ICV. **Abbreviations:** *, indicates a pairwise comparison with a significant *p*-value < 0.05 confidence interval correction: Bonferroni. PD-CU, cognitively unimpaired PD participants; PD-MCI, PD participants with mild cognitive impairment; PDD, PD participants with dementia.

5.4.3. SPHARM-PDM shape analyses

SPHARM-PDM shape analysis of the caudate, putamen and thalamus found widespread deflation to the surface of these structures in PDD compared to PD-CU participants. Surface deflation can be observed at the bilateral rostral as well as dorsomedial surfaces areas of the caudate (Figure 5.5). Widespread deflation was also found on the surface of the left putamen, at the anterior, dorsal and posterior regions. Significant and widespread deflation was found across the medial surface of the bilateral thalami, potentially corresponding to surface regions of the anterior and mediodorsal thalamic nuclei. Surface deflation was also found across the posterior-ventral surfaces of the thalami, potentially corresponding to the pulvinar as well as medial and lateral geniculate bodies. No FDR-corrected significant shape changes were found when comparing PD-CU to PD-MCI or PD-MCI to PDD.

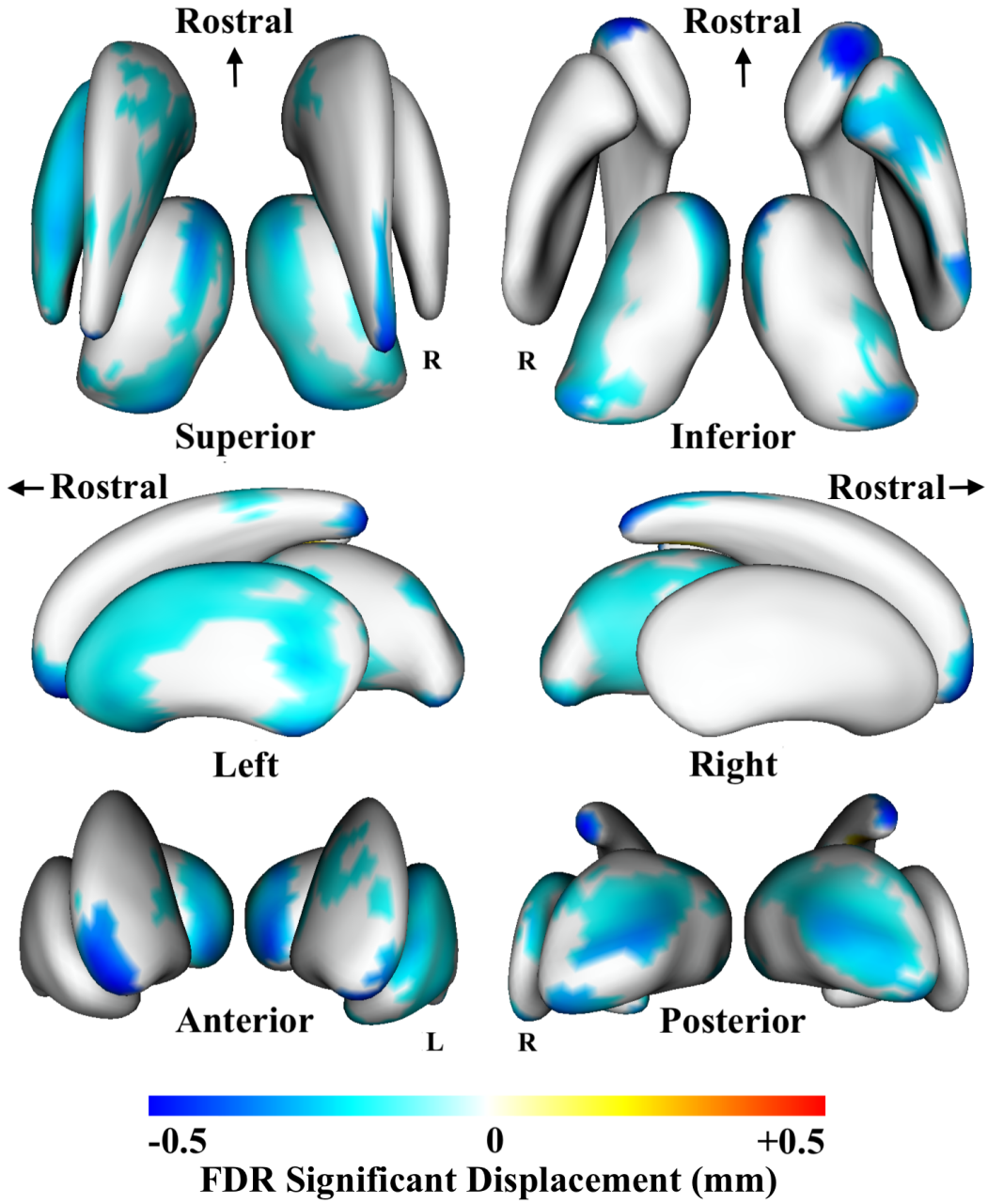

Figure 5.5: SPHARM-PDM shape analysis of the caudate nucleus, putamen and thalamus in PDD compared to PD-CU. Neuroanatomical surface areas of FDR-corrected mean difference displacement maps. Displacement colour scale corresponds to the millimetres of inflation/deflation of the surface in that region in mm; warmer colours correspond to surface inflation in PDD while cooler colours correspond to surface deflation in PDD. The bilateral thalami sit medially, the caudate nuclei rostrally and the putamen are the most lateral of the three structures. **Abbreviations:** R, right hemisphere; FDR, false-discovery rate; Left, looking at the structures from the left side of the brain; L, left hemisphere; Right, looking at the structures from the right side of the brain; R, right hemisphere.

5.4.4. Resting-state seed-based functional connectivity analyses

5.4.4.1. PD-CU compared to Controls

Dorsal caudate: Analysis of the dorsal caudate in PD-CU compared to Controls found clusters of increased functional connectivity with the right superior frontal gyrus (BA8), left frontal pole (BA10) and right middle frontal gyrus (BA8) (Figure 5.6A, Table 5.4). These clusters extended to include local maxima at the left postcentral gyrus (BA3), left precentral gyrus (BA6), left superior frontal gyrus (BA6), left paracingulate gyrus (BA32), right frontal pole (BA10), left anterior cingulate (BA24) and the left middle frontal gyrus (BA8) (Figure 5.6A; Appendix Table 7). We found clusters of decreased functional connectivity at the right lateral occipital cortex (BA19), left cerebellar crus I, left angular gyrus (BA39) and left cerebellar lobule VI (Figure 5.6A; Table 5.4). These clusters extended to include local maxima at the left supramarginal gyrus (BA39) and left cerebellar vermis VI (Figure 5.6A; Appendix Table 7).

Anterior putamen: Analysis of the anterior putamen in PD-CU compared to Controls found clusters of increased functional connectivity at the bilateral middle frontal gyri (BA8, 9), left frontal pole (BA10), bilateral postcentral gyri (BA2, 3), left paracingulate gyrus (BA32) and right inferior frontal gyrus (BA44) (Figure 5.6B; Table 5.4). These clusters extended to include local maxima at the bilateral anterior cingulate cortex (BA24), right frontal pole (BA10), left superior frontal gyrus (BA9), bilateral precentral gyri (BA4, 6) and bilateral central operculum (BA42) (Figure 5.6B; Appendix Table 8). We also found clusters of decreased functional connectivity at the left lateral occipital cortex (BA7) and right precuneus (BA7) (Figure 5.6B;

Table 5.4). These clusters extended to include a local maxima at the left precuneus (Figure 5.6B; Appendix Table 8).

Mediodorsal thalamus: Analysis of the mediodorsal thalamus in PD-CU compared to Controls found clusters of increased functional connectivity at the left postcentral gyrus (BA1) and the right middle frontal gyrus (BA8) (Figure 5.6C; Table 5.4). These clusters extended to include local maxima at the left postcentral gyrus (BA3) and the left precentral gyrus (BA4, 6) (Figure 5.6C; Appendix Table 9). No significant clusters of decreased functional connectivity were found for the mediodorsal thalamus.

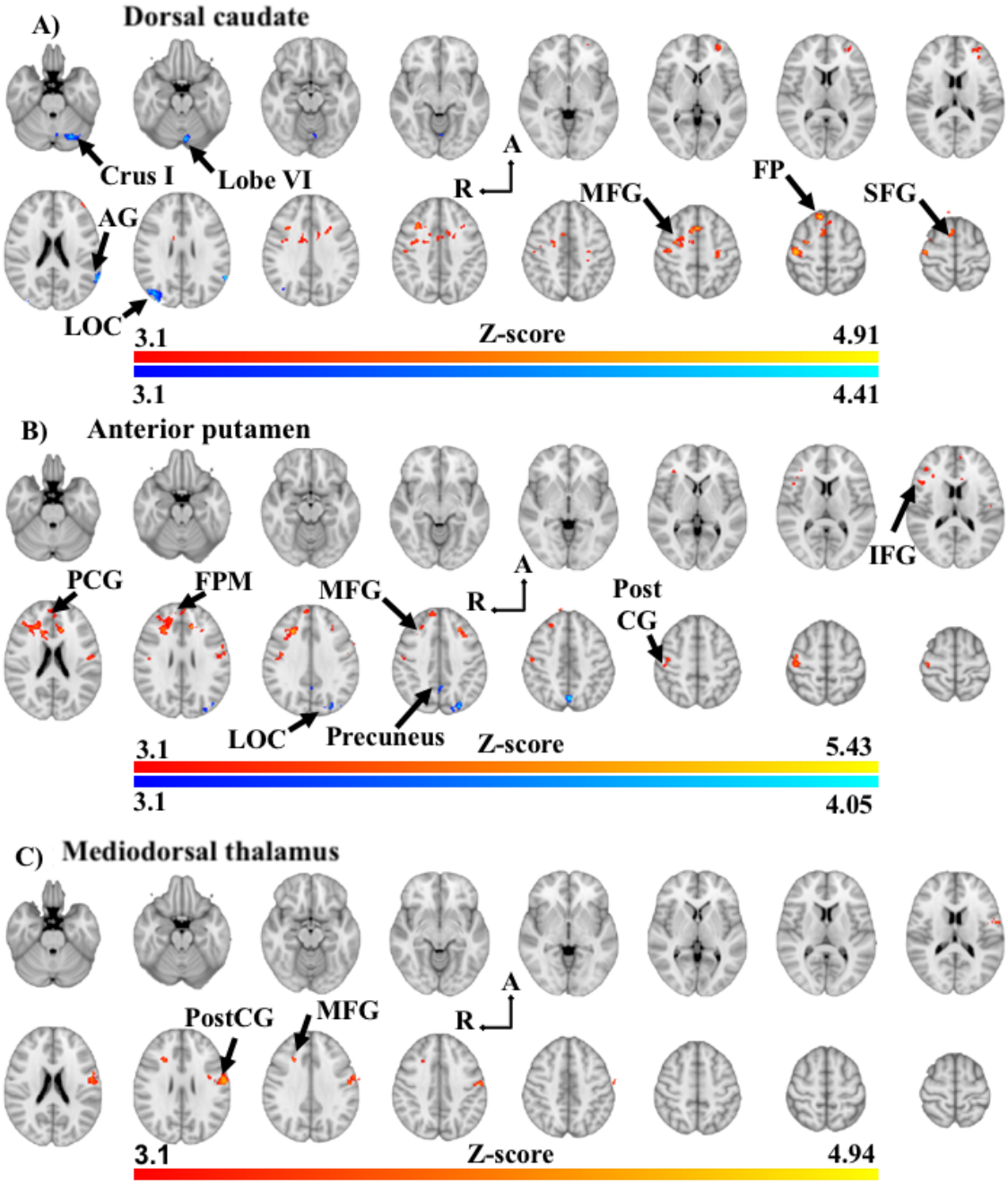

Figure 5.6: Significant between-group differences in functional connectivity in PD-CU compared to Controls. Dorsal caudate (A), anterior putamen (B) and mediodorsal thalamus (C). Z-score statistic (Gaussianised) images thresholded non-parametrically using clusters determined by $Z > 3.1$ and a corrected cluster significance of $p < 0.05$, overlaid on MNI 152 T1 1mm standard axial brain image (Z = -26mm ascending to 64mm; 6mm interslice distance). Warm colours represent increased in functional connectivity in PD-CU, while shades of blue represent decreased functional connectivity in PD-CU. **Abbreviations:** Crus I, Crus I of cerebellum; Lobe VI, posterior cerebellar lobule VI; AG, angular gyrus; LOC, lateral occipital gyrus; A, anterior; R, right hemisphere; MFG, middle frontal gyrus; FP, frontal pole; SFG, superior frontal gyrus; PCG, paracingulate gyrus; FPM, frontal pole (medial); PostCG, postcentral gyrus.

Table 5.4: Functional connectivity differences in PD-CU compared to Controls

Seed region	#	Brain region	Direction	Z	MNI x	MNI y	MNI z
Dorsal caudate	1	R superior frontal gyrus (BA8)	⇑	4.86	10	32	58
	2	L frontal pole (BA10)	⇑	3.81	-28	56	2
	3	R middle frontal gyrus (BA8)	⇑	4.39	34	16	38
	4	R lateral occipital cortex (BA19)	⇓	4.22	40	-76	28
	5	L cerebellar crus I	⇓	4.18	-24	-72	-26
	6	L angular gyrus (BA39)	⇓	4.36	-60	-54	28
	7	L cerebellar lobule VI	⇓	4.16	-6	-76	-20
Anterior putamen	8	R middle frontal gyrus (BA8)	⇑	5.43	26	26	32
	9	L frontal pole (BA10)	⇑	3.93	-2	56	20
	10	R postcentral gyrus (BA3)	⇑	4.24	44	-22	58
	11	L postcentral gyrus (BA2)	⇑	4.08	-54	-12	26
	12	L paracingulate gyrus (BA32)	⇑	4.85	-12	32	28
	13	R postcentral gyrus (BA3)	⇑	4.4	52	-16	44
	14	L middle frontal gyrus (BA9)	⇑	4.42	-28	28	40
	15	R inferior frontal gyrus (BA44)	⇑	3.79	48	29	18
	16	L lateral occipital cortex (BA19)	⇓	4.05	-26	-82	40
	17	R precuneus (BA7)	⇓	4.1	6	-62	42
Mediodorsal thalamus	18	L postcentral gyrus (BA1)	⇑	4.94	-58	-10	26
	19	R middle frontal gyrus (BA8)	⇑	3.97	24	24	32

Key: Coordinates of peak Z-score voxel location for areas of significant functional connectivity differences in PD-CU compared to Controls (family-wise error corrected $p < 0.05$).
Abbreviations: #, number of significant cluster; ⇓, decrease in functional connectivity; ⇑, increase in functional connectivity; L, left hemisphere; R, right hemisphere; BA, Brodmann Area; Z, maximum *Z*-value for cluster; MNI, coordinates for location of maximum *Z*-value, in the Montreal Neurological Institute T_1-standard space.

5.4.4.2 PD-MCI compared to PD-CU

Mediodorsal thalamus: Analysis of the mediodorsal thalamus in PD-MCI compared to PD-CU found one significant cluster of decreased functional connectivity at the right paracingulate gyrus (BA32) (Figure 5.7; Table 5.5). This cluster extended to include local maxima at the medial frontal gyrus (BA9) and right frontal pole (BA8) (Figure 5.7; Appendix Table 10). No significant clusters of increased functional connectivity were found. There were no significant functional connectivity differences to the dorsal caudate or anterior putamen when comparing PD-MCI and PD-CU.

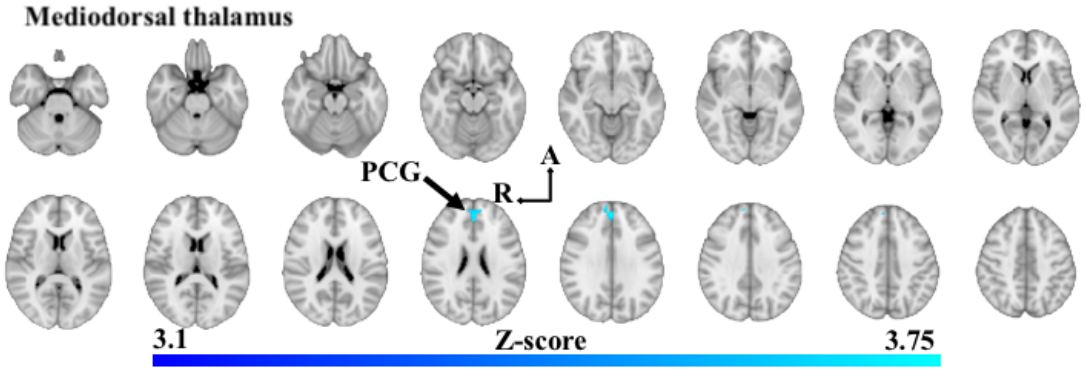

Figure 5.7: Significant between-group differences in functional connectivity of the mediodorsal thalamus in PD-MCI compared to PD-CU. Z-score statistic (Gaussianised) images thresholded non-parametrically using clusters determined by Z > 3.1 and a corrected cluster significance of $p < 0.05$, overlaid on MNI 152 T_1 1mm axial standard brain image (Z = -30.5mm ascending to 45.5mm; 5mm interslice distance). Shades of blue show areas of decreased in functional connectivity in PD-MCI. **Abbreviations:** A, anterior; R, right hemisphere; PCG, paracingulate gyrus.

Table 5.5: Functional connectivity differences in PD-MCI compared to PD-CU

					MNI		
Seed region	**#**	**Brain region**	**Direction**	**Z**	**x**	**y**	**z**
Dorsal caudate		-	-	-	-	-	-
Anterior putamen		-	-	-	-	-	-
Mediodorsal thalamus	20	R paracingulate gyrus (BA32)	⇓	3.92	2	46	30

Key: Coordinates of peak Z-score voxel location for areas of significant functional connectivity differences in PD-MCI compared to PD-CU (family-wise error corrected $p < 0.05$). **Abbreviations:** #, number of significant cluster; FC, functional connectivity; ⇓, decrease in functional connectivity; ⇔, no significant functional connectivity changes; R, right hemisphere; BA, Brodmann Area; Z, maximum *Z*-value for cluster; MNI, coordinates for location of maximum *Z*-value, defined in the Montreal Neurological Institute T1 standard space.

5.4.4.3. PDD compared to PD-CU

There were no significant functional connectivity differences to the dorsal caudate, anterior putamen or mediodorsal thalamus when comparing PD-CU to PDD participants.

5.4.4.4 PDD compared to PD-MCI

Mediodorsal thalamus: Analysis of the mediodorsal thalamus in PDD compared to PD-MCI found one cluster of decreased functional connectivity at the right posterior cingulate cortex (PCC) (BA23) (Figure 5.8; Table 5.6; Appendix Table 11). There were no significant functional connectivity differences of the dorsal caudate or anterior putamen when comparing PDD with PD-MCI.

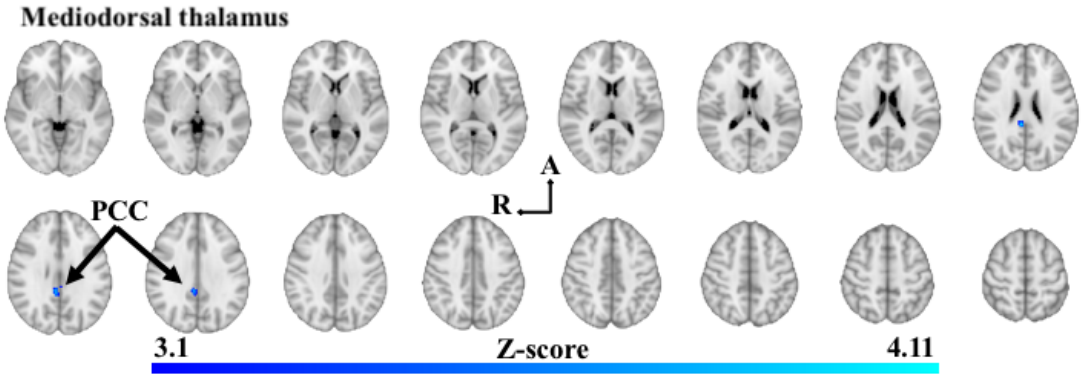

Figure 5.8: Significant between-group differences in functional connectivity of the mediodorsal thalamus in PDD compared to PD-MCI. Z-score statistic (Gaussianised) images thresholded non-parametrically using clusters determined by Z > 3.1 and a corrected cluster significance of $p < 0.05$, overlaid on MNI 152 T1 1mm axial standard brain image (Z = -3mm ascending to 57mm; 4mm interslice distance). Shades of blue show areas of decreased in functional connectivity in PDD. **Abbreviations:** PCC, Posterior cingulate cortex; R, right hemisphere; A, anterior.

Table 5.6: Functional connectivity differences in PDD compared to PD-MCI

					MNI		
Seed region	**#**	**Brain region**	**Direction**	**Z**	**x**	**y**	**z**
Dorsal caudate	-	-	-	-	-	-	-
Anterior putamen	-	-	-	-	-	-	-
Mediodorsal thalamus	21	R posterior cingulate cortex (BA23)	⇓	4.07	6	-38	26

Key: Coordinates of peak Z-score voxel location for areas of significant functional connectivity differences in PDD compared to PD-MCI (family-wise error corrected $p < 0.05$). **Abbreviations:** #, number of significant cluster; FC, functional connectivity; ⇓, decrease in functional connectivity; ⇔, no significant functional connectivity changes; R, right hemisphere; BA, Brodmann Area; *p*, corrected *p*-value; Z, maximum *Z*-value for cluster; MNI,

coordinates for location of maximum *Z*-value, defined in the Montreal Neurological Institute T_1 standard space.

5.4.5. Correlation between functional connectivity and clinical variables

When looking at the possible influences of clinical variables on the differences in functional connectivity in the PD-CU group compared to Controls, we looked at the correlation between average parameter estimate at the locations of clusters 1-7 within dorsal caudate statistic images, the average parameter estimate at the locations of clusters 8-17 within anterior putamen statistic images, and the average parameter estimate at the locations of clusters 18-19 within mediodorsal thalamus statistic images.

When investigating functional connectivity with the dorsal caudate, we found PD-CU participants showed a negative correlation between average parameter estimate at the right middle frontal gyrus and MMSE scores (cluster #3, $\beta = -0.420$, $p = 0.015$). When investigating functional connectivity with the anterior putamen, PD-CU participants also showed a negative correlation between average parameter estimate at the right middle frontal gyrus (cluster #8, $\beta = -0.354$, $p = 0.043$), left paracingulate (cluster #12, $\beta = -0.513$, $p = 0.002$), left middle frontal gyrus (cluster #14, $\beta = -0.445$, $p = 0.009$) and MMSE scores. PD-CU participants also showed a positive correlation between average parameter estimate at the right postcentral gyrus (cluster #13, $\beta = 0.505$, $p = 0.006$) and right inferior frontal gyrus (cluster #15, $\beta = 0.521$, $p = 0.004$) with LEDD levels. PD-CU participants also showed a negative correlation between average parameter estimate at the left lateral occipital cortex (cluster #16, $\beta = -0.471$, $p = 0.012$) and LEDD levels. Finally, when investigating functional connectivity with the mediodorsal thalamus, PD-CU participants showed a negative correlation between

average parameter estimate at the left postcentral gyrus (cluster #18, β = -0.348, p = 0.047) and disease duration (Appendix Table 12).

When looking at the possible influences of clinical variables on the differences in functional connectivity between the PD-CU and PD-MCI groups, we looked at the correlation between average parameter estimate at cluster #20 within the mediodorsal thalamus statistic images. PD-CU participants demonstrated a negative correlation between average parameter estimate at the paracingulate gyrus and LEDD scores (cluster #20, β = -0.486, p = 0.025) and a positive correlation with UPDRS-III scores (cluster #20, β = 0.424, p = 0.049) (Appendix Table 13).

When looking at the possible influences of clinical variables on the differences in functional connectivity between PD-MCI and PDD groups, we looked at the correlation between average parameter estimate at cluster #21 within mediodorsal thalamus statistic images. PD-MCI participants demonstrated a positive correlation between average parameter estimate at the posterior cingulate and disease duration (cluster #21, β = 0.522, p = 0.013) (Appendix Table 14).

While these results were all significant at the standard $p < 0.05$ level, after correcting the p-value using the Bonferroni method, none of these results remained significant (p-value required to reach significance, < 0.000272, based on performing 184 regression analyses).

5.5. Discussion

5.5.1. Findings

This study investigates the pattern of caudate nucleus, putamen and thalamus functional connectivity and morphology alterations associated with cognitive impairment and dementia in PD. Our study contributes new knowledge by showing how important functional subdivisions of these structures are impacted across cognitive disease stages. Our results indicate that PD-CU participants display increased functional connectivity of the dorsal caudate, anterior putamen and mediodorsal thalamus with neuroanatomical areas across the frontal lobe, as well as reduced functional connectivity of the dorsal caudate with posterior cortical and cerebellar regions, compared to Controls. PD-MCI participants demonstrated reduced functional connectivity of the mediodorsal thalamus with midline structures within the executive control network while PDD participants demonstrated reduced functional connectivity of the mediodorsal thalamus with the posterior cingulate cortex, a key node within the default mode network. Significant volumetric and surface based changes to the caudate nucleus, putamen and thalamus were found exclusively in our PDD cohort, suggesting that functional connectivity changes in PD-CU and PD-MCI take place independently of observable morphological alterations.

Our research found no evidence of morphological alterations to the caudate, putamen or thalamus in PD-CU participants compared to Controls, supporting the findings from a number of studies (Lee et al., 2014, Mak et al., 2014, Mckeown et al., 2008, Menke et al., 2014, Messina et al., 2011, Nemmi et al., 2015, Tinaz et al., 2011). We also found no evidence of atrophy to the caudate, putamen or thalamus in PD-MCI

compared to Controls, supporting work by Amboni et al. (2015). Our data indicate that PDD participants have reduced caudate volumes (bilaterally) in PDD compared to PD-CU and Controls. Left putamen and left thalamus volumes were reduced in PDD compared to PD-CU and Controls, while the right putamen and right thalamus was reduced in PDD compared to Controls and PD-CU, respectively. These results support studies showing reduced caudate, putamen and thalamic grey matter changes in PD participants with dementia compared to controls (Burton et al., 2004, Melzer et al., 2012, Summerfield et al., 2005). Shape analysis of these structures found widespread surface contraction in PDD compared to PD-CU, fine-tuning these volumetric results. Regarding the caudate, surface contraction was found primarily at the rostral and dorsomedial surfaces, areas with putative connectivity to the executive regions of the frontal lobe as well as the rostral motor regions (Tziortzi et al., 2014). Surface contraction was also found at the anterior, dorsal and posterior putamen surface regions areas with putative connectivity to the executive regions of the frontal lobe as well as caudal motor regions (Tziortzi et al., 2014). Widespread surface contraction was found primarily across the medial surface of the bilateral thalami, corresponding to surface regions of the anterior and mediodorsal thalamic nuclei with putative structural connections to the dorsolateral and prefrontal cortices (Behrens et al., 2003) as well as posterior cingulate, precuneus and hippocampal brain regions (Cunningham et al., 2017). No significant surface changes were found when comparing the other experimental groups. Our findings support the work of Mak et al. (2014) who found no significant difference between PD-MCI and cognitively unimpaired PD participants using a vertex-wise shape analysis method. Our morphological data on PD-CU participants are also consistent with previous studies which indicate that PD is not associated with localised surface based alterations (Lee

et al., 2014, Menke et al., 2014, Messina et al., 2011) however they contrast with the results of two groups who found localised surface contraction in PD (Garg et al., 2015, Mckeown et al., 2008). Methodological inconsistencies between studies, including disease duration and symptom profiles, may be a significant factor behind these differences.

Our findings of increased functional connectivity between the dorsal caudate, anterior putamen and mediodorsal thalamus with the pre- and postcentral gyri support a recent meta-analysis indicating that PD is associated with increased functional connectivity of these brain regions (Ji et al., 2018). After weighing the relative contributions of seed-ROIs, Ji et al. (2018) were able to demonstrate that seeds placed within the caudate, putamen and thalamus contributed most to this result. More specifically, our finding supports work by Gorges et al. (2015) who found increases in functional connectivity between a basal ganglia-thalamic network and areas of the prefrontal cortex and anterior/paracingulate gyri. These researchers argue that such *hyper*-connectivity in cognitively unimpaired PD participants may be representative of the recruitment of additional resources in the brain to maintain cognitive performance (Gorges et al., 2015). Our results support our hypotheses, and may signal how resources can be recruited to maintain 'normal' cognitive functioning. These increases in functional connectivity may be indicative of compensatory changes taking place within the executive control network (ECN). This network is comprised of dorsal and ventrolateral prefrontal, frontoinsular, lateral parietal, middle prefrontal cortices, anterior and paracingulate gyri, as well as subcortical sites at the mediodorsal and anterior thalamic nuclei and the dorsal caudate (Beckmann et al., 2005, Seeley et al., 2007). The ECN has been validated on a large scale and has shown that activity

within this network corresponds strongly with several paradigms of cognition in task-based functional connectivity analyses (Smith et al., 2009).

Our data also indicate that PD-CU is associated with a reduction in functional connectivity between the dorsal caudate and the cerebellum. This result supports the findings of Hacker et al. (2012) who demonstrated decreases in functional connectivity between the caudate nucleus and an 'extended brainstem' region encompassing the cerebellum. These findings are significant because loss of functional connectivity between the caudate and the cerebellum may serve as a viable candidate for PD related gait difficulties, postural instability and freezing, which can be linked to dysfunction in cerebellar circuitry (Hacker et al., 2012). Our data also indicate that PD-CU participants have decreased functional connectivity between the dorsal caudate/anterior putamen and the precuneus and angular gyrus. This finding supports the work of Amboni et al. (2015) who found decreases in functional connectivity between nodes in the default mode network (DMN), including lateral and medial parietal regions.

While our results support a number of previous research findings, they contrast with similar work, necessitating explication. Bell et al. (2015) demonstrated no significant differences in functional connectivity of the anterior striatum in a PD cohort (when placed on medication) compared to Control participants. They also found no differences in functional connectivity of seed-ROIs in the thalamus with intrinsic connectivity networks. Similarly, our data contrast with the work of Agosta et al. (2014b) who found decreased functional connectivity between the caudate and putamen and brain regions across the frontal lobe, as well as *hypo*-connectivity of the

thalamus with insular cortices. There are a number of methodological considerations that may explain these discrepancies. The work of Bell and colleagues (2015) involved a younger PD cohort to the current study, which brings into question the impact of age related changes in functional connectivity (Fair et al., 2008), while the work of Agosta et al. (2014b) focussed on a PD cohort with unilateral disease presentation, studying functional connectivity of the 'more affected' and 'less affected' hemispheres. This approach increases the specificity of their analysis, however it makes comparisons with the present data difficult as we averaged functional connectivity signals from seeds within both hemispheres.

PD-MCI participants showed decreased functional connectivity of the mediodorsal thalamus with the paracingulate gyrus, medial frontal gyrus and frontal pole compared to PD-CU participants. These findings support the work of Gorges et al. (2015) who showed that PD-MCI is associated with lower functional connectivity between a basal ganglia-thalamic intrinsic connectivity network and the anterior/paracingulate gyri compared to a cognitively unimpaired PD cohort. Decreased functional connectivity between the mediodorsal thalamus and medial prefrontal brain regions provides further evidence for the important link between midline nodes within the ECN and cognitive function. As outlined, structures within this intrinsic connectivity network are related to cognitive function (Beckmann et al., 2005, Seeley et al., 2007), as they work together to provide bias signals to other areas of the brain to implement and maintain cognitive control processes (Miller and Cohen, 2001). While we have demonstrated increased functional connectivity of nodes within this network in cognitively unimpaired PD participants, here we demonstrate that PD-MCI subjects have a reduced functional connectivity between

the mediodorsal thalamus and paracingulate cortices. While traditionally thought to be subserve affective functions, the cingulate has emerged as an important structure associated with higher cognitive processes, and has been shown to be particularly vulnerable to disease processes where executive control is impaired (Carter et al., 2000). Seeley et al. (2007) demonstrated that stronger functional connectivity between nodes of the ECN correlated positively with superior executive task performance of participants. If the corollary holds true, this would indicate that poorer cognitive performance, as our PD-MCI participants demonstrate, would be associated with reduced functional connectivity within this network, which our results show.

PDD participants showed decreased functional connectivity of the mediodorsal thalamus with the PCC compared to PD-MCI participants, directly supporting recent graph theoretical research (Zhan et al., 2018). Decreases in functional connectivity between these regions is significant due to the crucial role played by the PCC in cognitive functioning as well as the role of the mediodorsal thalamus and PCC within the DMN. The functional role played by the PCC involves elements of memory consolidation, attention and the control required to balance internally and externally focussed thoughts (Leech and Sharp, 2014). The PCC is known to be crucial to the symptomology associated Alzheimer disease (Buckner et al., 2009, Greicius et al., 2004, Mevel et al., 2011) and atrophy of the PCC has been demonstrated in PD participants with dementia (Melzer et al., 2012). The PCC has important structural and functional connectivity with the thalamus (Cunningham et al., 2017) and Greicius et al. (2003) suggested that the structure may play an important role balancing the interaction between brain regions in the prefrontal cortex that are involved cognitive processes and posterior nodes within the DMN. These researchers suggested that the

thalamus is uniquely positioned to act as an intermediary structure in the brain that balances the interaction between these regions due to its extensive cortico-cortical connectivity (Greicius et al., 2003). Our research supports this idea, highlighting how the functional connectivity between the mediodorsal thalamus and the PCC is impacted in PD participants with dementia.

We found a number of interesting correlations between functional connectivity and clinical variables, however it is important to reiterate that these findings did not meet the highly conservative criteria for significance after controlling for multiple comparisons ($p < 0.00027$). Firstly, we found evidence that PD-CU participants with lower MMSE scores had increased functional connectivity of the dorsal caudate with the right middle frontal gyrus. We also found evidence that PD-CU participants with lower MMSE scores had increased functional connectivity of the anterior putamen with the right middle frontal, left paracingulate and left middle frontal gyri. These results are interesting as they suggest that PD-CU patients with lower global cognitive scores had increased functional connectivity with prefrontal regions of the brain, supporting our hypothesis that increases in functional connectivity may be evidence of a compensatory response to alleviate the impact of PD pathophysiology. We also found evidence that PD-CU participants with higher LEDD had increased functional connectivity of the anterior putamen with right postcentral and right inferior frontal gyri. These results support research which has demonstrated that dopaminergic medication can increase functional connectivity between the striatum and ventrolateral prefrontal cortices, while it can be associated with a decrease in functional connectivity with posterior cortical regions (Kelly et al., 2009).

Our findings provide partial support for our model regarding the relationship between functional connectivity and morphology across PD cognitive disease states. PD-CU participants showed no observable morphological changes compared to Controls, however they displayed significant increases in functional connectivity with prefrontal regions of the brain. At a number of sites in the brain, increased functional connectivity was associated with lower global cognitive scores. Taken together, these results may be evidence of compensatory mechanisms whereby the brain recruits additional neuronal resources to maintain normal cognitive function, due to impact of disease-related pathology. We hypothesised that neuronal resources that support this functional compensation would be diminished in PD-MCI and PDD, evidenced by morphological alterations to the caudate nucleus, putamen and thalamus with consequent reductions in functional connectivity. Whilst we found that PD-MCI participants showed reductions in functional connectivity compared to PD-CU participants, this was despite any observable morphological differences between the groups, which runs counter to our hypotheses. Supporting our hypothetical model, PDD participants displayed significant reductions in both surface morphology and seed-based functional connectivity.

5.5.2. Limitations

This research was performed in a cross-sectional manner, assuming a sequential temporal relationship between PD-CU, PD-MCI and PDD groupings, though we acknowledge that the progression of cognitive impairment from one stage to the next is not necessarily linear. Future research should follow a longitudinal design to better study how functional connectivity and morphology of basal ganglia-thalamocortical circuits are related to cognitive impairment in PD. This would have the added benefit

of reducing the influence of the significant disease heterogeneity in PD which has been shown to have a significant impact on the reproducibility of results in this field of research (Badea et al., 2017). Drawing conclusions about functional connectivity may also be limited by the influence of dopaminergic medication, which has been shown to be related to changes in functional connectivity in placebo-controlled healthy participants (Kelly et al., 2009) and also in research participants with PD (Bell et al., 2015).

5.5.3. Conclusion

This study demonstrated how the functional connectivity of subcortical hubs within basal ganglia-thalamocortical circuits are implicated in PD between cognitive disease stages. Functional connectivity changes are found in PD-CU participants, who display no morphological changes, while PD-MCI participants and PDD participants both display decreases in functional connectivity of the mediodorsal thalamus with the anterior and posterior cingulate cortices respectively. Our research highlights the importance of the caudate, putamen and thalamus as core structures within key intrinsic connectivity networks in the brain, and indicates that a breakdown in functional connectivity of the mediodorsal thalamus is tied to mild cognitive impairment and dementia in PD.

6. Project four: Corpus callosum

This thesis has investigated subcortical structures of the caudate nucleus, putamen and thalamus and how their morphology and functional connectivity are impacted in PD. Each project focussed on a structure within basal ganglia-thalamocortical networks, with Project three investigating these variables from the vantage point of levels of cognitive impairment. For a more complete view of the neural circuit underpinnings associated with clinical dysfunction in PD, it is helpful to look orthogonally from the basal ganglia-thalamocortical circuit, which can be performed by analysing the structure of the corpus callosum. An analysis of the corpus callosum is warranted due to the important role played by the structure in facilitating interhemispheric neuronal activity. The structure is known to connect widescale networks, and demonstrates topographic connectivity between homologous cortical regions. This provides an opportunity to investigate thickness of the corpus callosum as a possible measure of cortical thickness, which could have potential as a biomarker in clinical contexts. Research for this chapter is based on a draft manuscript currently being prepared for publication.

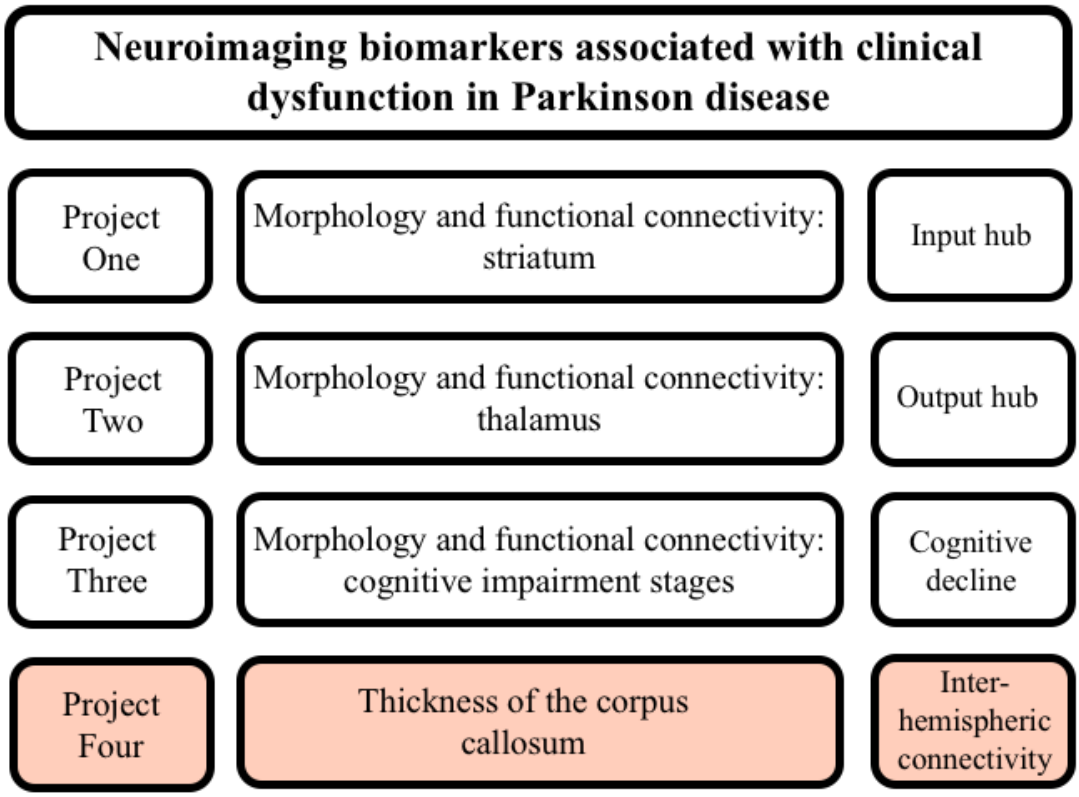

Figure 6.1: Project four. The current project focusses on the corpus callosum as the major white matter tract, or 'spoke', connecting the two cerebral hemispheres, crucial to a range of higher-order processes in the brain. Thickness of the structure was thus investigated relative to levels of cognitive impairment, clinical function and cortical thicknesses.

Title:

Corpus callosum morphometry and cognitive impairment in Parkinson disease

Authors:

Conor Owens-Walton[1]*, Chris Adamson[2], Mark Walterfang[3,4], Sara Hall[5,6], Danielle van Westen[7,8,¶], Jeffrey C.L. Looi[1,¶], Marnie Shaw[9,¶] and Oskar Hansson[5,6,¶]

Affiliations:

[1] Research Centre for the Neurosciences of Ageing, Academic Unit of Psychiatry and Addiction Medicine, School of Clinical Medicine, Medical School, Australian National University, Canberra, Australia
[2] Developmental Imaging, Murdoch Children's Research Institute, Parkville Victoria, Australia.

[3] Neuropsychiatry Unit, Royal Melbourne Hospital, Melbourne Neuropsychiatry Centre, University of Melbourne and Melbourne Health, Melbourne, Australia
[4] Florey Institute of Neurosciences and Mental Health, University of Melbourne, Melbourne, Australia
[5] Memory Clinic, Skåne University Hospital, Malmö, Sweden
[6] Department of Clinical Sciences, Lund University, Malmö, Sweden
[7] Centre for Medical Imaging and Physiology, Skåne University Hospital, Lund, Sweden
[8] Diagnostic Radiology, Department of Clinical Sciences, Lund University, Lund, Sweden
[9] College of Engineering and Computer Science, The Australian National University, Canberra, Australia
¶ Denotes co-senior authors
* Corresponding author: conor.owens-walton@anu.edu.au. Address: Building 4, The Canberra Hospital, Hospital Rd, Garran, ACT, 2605.

Author contributions:

CO-W contributed to project design, selected the statistical approach, performed the statistical analyses and prepared the manuscript (> 70% of total work). CA developed the main software used in this project, and executed the software pipeline. MW acted as supervisor for C-OW, contributed to project design and provided technical support regarding the interpretation of the data. DvW and SH contributed to project design and organised the clinical/imaging aspects of the study. JCLL contributed to project design and acted as supervisor for CO-W. MS acted as supervisor for CO-W, helped with statistical analyses, contributed to drafts of the manuscript and is a co-senior author. OH organised the clinical/imaging aspects of the study.

6.1. Abstract

People diagnosed with Parkinson disease (PD) can experience significant neuropsychiatric symptoms, including cognitive impairment and dementia, the neuroanatomical substrates of which are still not fully understood. The corpus callosum is the largest white matter tract in the brain, crucial to interhemispheric information transfer and thus critical to effective cognitive functioning. Symptoms

associated with cognitive impairment and dementia may relate to structural changes to the callosum via primary white matter pathology or as a secondary outcome due to cortical degeneration. The objective of this project was thus to investigate the thickness of the callosum and cortex in patients with PD with varying levels of cognitive impairment, and study how these two neuroimaging metrics are related. This project investigated the thickness of the callosum in the midsagittal plane using a semi-automated pipeline in cognitively unimpaired PD participants (n = 35), PD participants with mild cognitive impairment (n = 22), PD participants with dementia (n = 17) and a healthy control group (n = 27). Pairwise comparisons of midsagittal callosal thicknesses found thinning of the structure in PD-related dementia compared to PD-related mild cognitive impairment and cognitively unimpaired PD participants. Regression analyses investigating relationships between callosal thickness and cortical thickness found thickness of the left medial orbitofrontal cortex to be positively correlated with thickness of the anterior callosum in PD-related mild cognitive impairment, with all other analyses yielding non-significant results. Regression analyses investigating potential relationships between callosal thickness and clinical variables produced no significant results. This study suggests that a mid-sagittal thickness model can uncover changes to the corpus callosum in PD-related dementia, however it has a limited usefulness in early disease stages, or as a potential biomarker of cortical thickness or clinical function.

6.2. Introduction

Parkinson disease (PD) is the second most common neurodegenerative disease in the world, directly affecting 2-3% of the population over the age of 65 (Poewe et al., 2017). Longitudinal research has indicated that around 80% of PD patients develop

dementia across the disease course (Hely et al., 2005) which has significant impact on patients and caregivers. Mild cognitive impairment (MCI) in PD has emerged as an important clinical diagnosis and research focus, as it may represent an intermediate stage in the progression of the disease from cognitively unimpaired PD to PD-related dementia (Litvan et al., 2012). PD-related MCI identifies patients with impairment primarily affecting attention, working memory, executive function, language and visuospatial function (Litvan et al., 2012). While significant attention has been paid to grey matter changes associated with cognitive impairment, white matter damage may be an important pathological substrate of cognitive impairment, which may precede grey matter changes (Rektor et al., 2018). All domains of cognitive function require the integration of distributed neural activity via white matter connections (Van Den Heuvel and Sporns, 2013) and the corpus callosum is crucial in facilitating the interhemispheric processes associated with cognitive function (Doron and Gazzaniga, 2008). The callosum is the largest white matter structure in the brain, comprising over one hundred million topographically arranged neurons (Schmahmann and Pandya, 2009). Given that the majority of interhemispheric fibres from cortical regions traverse the callosum, the structure is seen as attractive target for research as regional cortical brain changes may be reflected in regional changes to the morphology of the callosum (Walterfang and Velakoulis, 2014). Information on the relationship between the structure of the callosum and clinical function can also be investigated, as it has been argued that the integrity and density of the callosal axons reflects the functional capacity of the brain regions they connect (Aboitiz et al., 1992).

The callosum is an attractive candidate for structural brain imaging analysis due to its bright intensity and clear contrast on sagittal magnetic resonance imaging (MRI),

facilitating segmentation from surrounding tissue types. Accordingly, numerous schemes have been proposed to describe the morphology of the structure, including areal subdivision (Witelson, 1989), cortical endpoint (Hofer and Frahm, 2006), boundary tangent (Joshi et al., 2013) and cross-sectional thickness models (Adamson et al., 2011, Walterfang et al., 2009). Using a manual segmentation approach, early studies demonstrated no significant differences in the area of the total callosum, or in evenly spaced subdivisions of the structure, in PD or PD-dementia cohorts compared to controls (Wiltshire et al., 2005). More recent 3-dimensional volumetric analyses using semi-automated methods found no difference in total volume of the callosum in PD compared to controls, however analyses of callosal subdivisions found significant thinning in PD, driven by changes in PD-dementia participants (Goldman et al., 2017). Goldman et al. (2017) were also able to demonstrate that changes in volumes of the callosum correlated with measures of clinical function (Goldman et al., 2017). Contrasting with this work, Lenka et al. (2017) utilised a volumetric approach and found no differences in total callosal volumes, or callosal subdivisions, in PD compared to controls, while Vasconcellos et al. (2018) found thinning of callosal subdivisions in PD, however they present no data on differences in callosal thickness between groups of PD patients based on levels of cognitive impairment. Our work attempts to advance this field of research by investigating the structure of the corpus callosum using a semi-automated computational tool that that models callosal morphology with thickness ‘streamlines’ placed at 100 points along the length of the structure at the mid-sagittal plane. Such a fine-grained approach may uncover greater detail about how the regional structure of the callosum is impacted in PD early in the disease course, when putative morphological alterations may be harder to detect with traditional volumetric approaches. This approach may also yield important

information on how the structure of the callosum informs on changes to the cerebral cortex, and measures of clinical function, opening up avenues for clinical translation tools.

It was thus hypothesised that PD participants would demonstrate reduced thickness of the corpus callosum and cortex compared to controls. Research has shown that greater thickness of the callosum is linked to measures of general cognitive ability (Luders et al., 2007) and as there are increased structural changes to both grey and white matter structures in the brain with increasing levels of cognitive impairment, we hypothesised that changes in thickness of the corpus callosum would be more pronounced in MCI participants compared to cognitively unimpaired PD, and controls, while PD participants with dementia would have significant and widespread reductions in callosal thickness compared to PD with MCI and cognitively unimpaired PD participants. Due to the structural connectivity between the corpus callosum and cortex, it was also hypothesised that the thickness of the corpus callosum would correlate with thickness at particular cortical regions, highlighting a potential usefulness for corpus callosal thickness as a proxy measure of cortical degeneration in PD. This final hypothesis would be useful as the quantification of corpus callosal thickness has a potential for clinical translation and can be measured on an MRI scan, whereas quantifying changes to the cerebral cortex requires full processing of a scan which takes between 20 and 30 hours per individual (Gronenschild et al., 2012).

6.3. Methods

6.3.1. Participants

Participants in this research (n = 101) were from the Swedish BioFinder study (www.biofinder.se) and gave informed written consent. This research was performed in accordance with the World Medical Association's Declaration of Helsinki and ethical approval was obtained through the Ethical Review Board of Lund, Sweden, and the Human Research Ethics Committee at the Australian National University, Canberra, Australia.

6.3.2. PD disease groups: cognitive impairment

Diagnosis of PD was made by a neurologist using the National Institute of Neurological and Stroke Diagnostic Criteria (Gelb et al., 1999). PD participants were divided into three cognitive impairment disease groups, the first group comprising cognitively unimpaired PD patients (PD-CU; n = 35); the second group comprising PD patients with MCI (PD-MCI; n = 22), with the diagnosis based on the Movement Disorder Society Task force guidelines (Litvan et al., 2012). This criterion is met when patients score at least 1 standard deviation below the normative mean in at least two cognitive tests, including executive function, attention, visuospatial, memory and language domains. The third subgroup consisted of PD participants with comorbid dementia (PDD; n = 17) (Emre et al., 2007). A healthy control group (Controls) was included for comparative purposes (n = 27). Exclusion criteria for this study included presence of a developmental disability, alcohol or substance abuse, poor knowledge of the Swedish language or the presence of a metabolic disorder. All participants underwent a cognitive and neurological examination by a medical doctor with extensive experience with movement disorders, while PD patients remained on their

usual medication regimes. Clinical functioning of participants was quantified using the Hoehn and Yahr staging, assessing the progression of the disorder, the Unified Parkinson's Disease Rating Scale Part-III test (UPDRS-III), assessing the motor signs of PD (Fahn and Elton, 1987); the Mini Mental State Examination (MMSE), assessing cognitive mental state (Folstein et al., 1975); the A Quick Test of Cognitive Speed (AQT) assessing perceptual and cognitive speed (Jacobson et al., 2004) and the 'Letter S Fluency' (LSF) and 'Animal Fluency' (AF) tests, assessing the verbal fluency aspect of executive function (Tombaugh et al., 1999).

6.3.3. MRI acquisition

MRI data was obtained on a 3T scanner (Trio, Siemens Magnetom, Erlangen, Germany) with a 20-channel head-coil. High resolution T_1-weighted three-dimensional anatomical brain images were acquired using a magnetization-prepared rapid acquisition technique with gradient-echo sequence (repetition time = 7 ms; echo time = 3 ms; flip angle = 90 degrees; voxel size = isotropic $1mm^3$). Image matrix size was 356 voxels in the coronal and sagittal planes and 176 voxels in the axial plane.

6.3.4. Morphometry of the corpus callosum

Morphometry of the corpus callosum was estimated using a semi-automated pipeline (https://github.com/chrisadamsonmcri/CCSegThickness), explained in detail in previously published works (Adamson et al., 2014, Adamson et al., 2011). Generally speaking, the pipeline involves the identification of the mid-sagittal plane in subjects T_1-MRI data (Figure 6.2 A), followed by template guided segmentation of the corpus callosum, topological error fixing and the removal of pericallosal blood vessels (Adamson et al., 2014). After the structure has been segmented, thickness profile

generation is performed using the following steps: the callosum is split into left (posterior) and right (anterior) halves with an endpoint selected at the bottom-right and -left extrema. A midline equipotential contour is produced between these endpoints, as a solution to Laplace's equation, maximising the length of the midline contour of the callosum, subdividing the outside boundary contour of the structure into superior and inferior contours. Streamlines are then generated at evenly spaced intervals along the centre contour, which are non-overlapping nominally parallel lines intersecting the superior and inferior contours orthogonally along an anterior-posterior trajectory (Figure 6.2B). 100 streamlines per subject were created for this study, modelled as callosal thickness during statistical analyses (Figure 6.2C). The first and last ten streamlines are removed during statistical analyses as the meaning of the MSP-thickness profile at the genu and splenium is still not yet fully characterised.

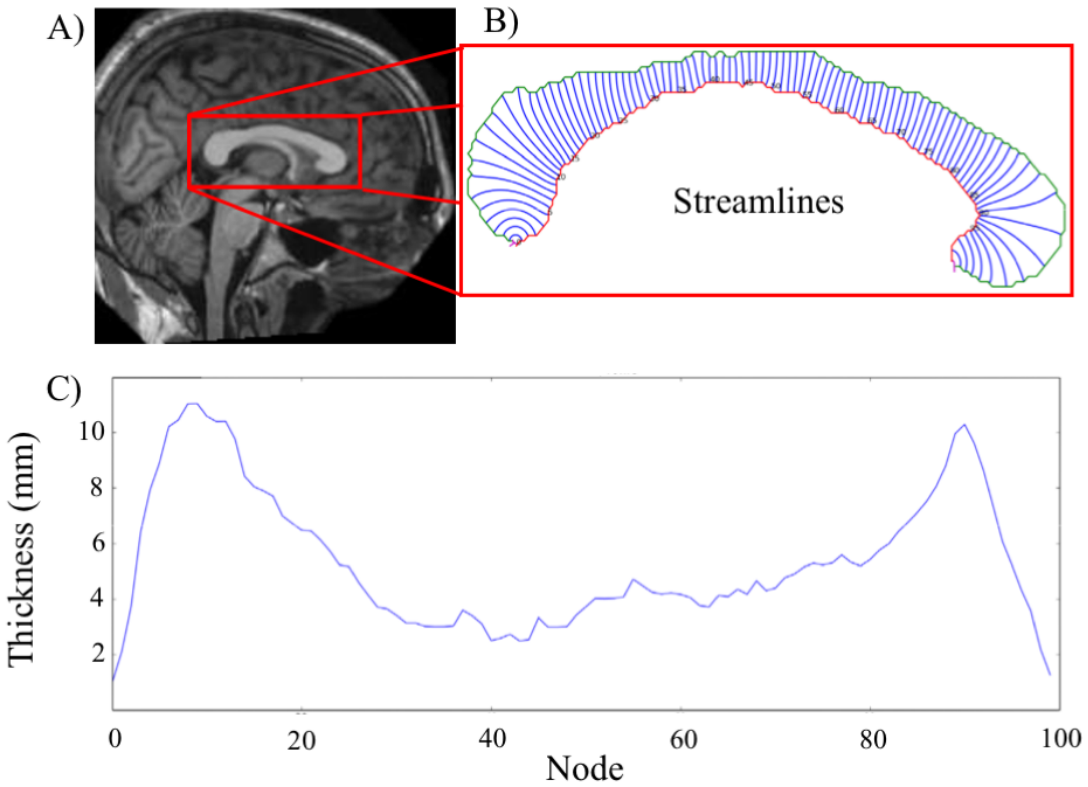

Figure 6.2: Generation of mid-sagittal thickness streamlines. A) Shows a mid-

sagittal callosal segmentation in an example subject; B) shows the non-overlapping cross-sectional contour lengths (streamlines) numbered from 0 at the intersection of the inferior and superior contours of the corpus callosum, moving anteriorly to node 100 at the most rostral end of the corpus callosum; C) shows the lengths (thickness) of each streamline at the 100 nodes.

6.3.5. Cortical grey matter thickness analysis

Cortical reconstruction and segmentation of grey matter was performed with the FreeSurfer image analysis suite (version 6.00). Technical details of these procedures are described in published works (Dale et al., 1999, Fischl and Dale, 2000). Briefly, processing includes motion correction and averaging (Reuter et al., 2010) of multiple volumetric T_1-weighted images, removal of non-brain tissue using a deformation procedure (Segonne et al., 2004), automated Talairach transformation, intensity normalization (Sled et al., 1998), tessellation of the grey matter-white matter boundary, automated topology correction (Fischl et al., 2001, Segonne et al., 2007), surface deformation along intensity gradients to optimally define cortical surface borders, registration to a spherical atlas using individual cortical folding patterns to align cortical anatomy between participants (Fischl et al., 1999), and finally, the parcellation of the cerebral cortex into units with respect to gyral and sulcal structure based on the Desikan-Killiany atlas (Desikan et al., 2006, Fischl et al., 2004).

6.3.6. Statistical analyses

Statistical analyses were performed using IBM SPSS Statistics for Macintosh, (Version 22.0). Multiple regression analyses were performed with scripts utilising the following Python packages: Pandas, Matplotlib, Numpy, Statsmodels and Seaborn.

6.3.6.1. Group differences in corpus callosum thickness

To investigate group differences in the morphometry of the corpus callosum at the 80 streamlines, we performed a series of multivariate analyses of covariance. Group membership was the fixed factor, with average callosal thickness for each group at each streamline serving as the dependent variable. Estimated total intracranial volume (eTIV), sex and age were entered as confounding variables. We controlled the false-discovery rate (FDR) using the Benjamini-Hochberg procedure with a q = 5%.

6.3.6.2. Group differences in cortical thickness

Average cortical thicknesses for the 31 ROIs (per hemisphere) for each participant were used as dependent variables in a multivariate analysis of covariance, with experimental group as the fixed factor, and age and eTIV as confounding variables. We controlled the FDR using the Benjamini-Hochberg procedure with a q = 5%.

6.3.6.3. Correlations between corpus callosal and cortical thickness

To investigate the relationship between thickness of the callosum and cortical thickness at the 62 cortical ROIs, we ran a series of multiple regressions for each experimental group. These analyses controlled for age and eTIV, producing beta correlation coefficients indicating the magnitude and directionality of the relationship for each group and p-value n x m matries, where n = the number of callosal thickness measurements (n = 80) and m = the number of cortical thickness measurements (m = 62), FDR corrected using the Benjamini-Hochberg procedure with a q = 5%. The Python scripts used for these analyses are available online in a Github repository (https://github.com/ConorOW/corpus_callosum/blob/master/CC_CT_correlations.py).

6.3.6.4. Correlations between corpus callosal thickness and clinical function

To investigate the relationship between thickness of the callosum and measures of clinical function, we ran a series of multiple regressions for each experimental group. These analyses controlled for age and eTIV, producing beta correlation coefficients indicating the directionality of the relationship for each group and *p*-value n x m matries, where n = the number of callosal thickness measurements (n = 80) and m = the number of clinical function metrics (m = 6), FDR corrected q = 5%. The script used for these analyses are available online in a Github repository (https://github.com/ConorOW/corpus_callosum/blob/master/CC_function_correlations.py).

6.4. Results

6.4.1. Participant characteristics

Participant characteristics in this research are displayed in Table 6.1. A Chi-square test for independence found no significant difference in sex between the groups [$\chi^2(3, n = 98) = 0.828$, $p = 0.843$]. One-way analyses of variance found no significant difference in age [$F(3, 97) = 2.166$, $p = 0.097$], years of education [$F(3, 82) = 1.159$, $p = 0.331$] or eTIV [$F(3, 97) = 0.036$, $p = 0.991$] between experimental groups (Table 6.1). There was a significant difference in disease duration between the PD cohorts [$F(2, 71) = 10.299$, $p = <0.001$], with post-hoc analyses of variance showing that the PDD cohort had a significantly longer duration than the PD and PD-MCI cohorts. As expected, there were significant differences in UPDRS-III [$F(3,97) = 47.96$, $p < 0.001$], MMSE [$F(3,97) = 4.049$, $p < 0.001$], AF [$F(3,96) = 17.28$, $p <0.001$], LSF

[F(3,94) = 11.37, $p < 0.001$] and AQT [F(3,94) = 18.59, $p < 0.001$] scores between experimental groups.

Table 6.1: Participant characteristics

Item	Controls	PD	PD-MCI	PDD	*p*-value
Number of participants	27	35	22	17	-
Female /Male	12/15	17/18	12/10	7/10	0.843
Average age in years	69.47 (6.09)	69.45 (6.18)	70.53 (5.38)	73.70 (6.67)	0.097
eTIV (cm^3)	1572.64 (157.37)	1584.91 (192.19)	1570.74 (179.15)	1580.79 (222.55)	0.991
Years of education	12.54 (3.47)	11.68 (5.35)	9.66 (6.807)	11.5 (4.52)	0.331
Years since diagnosis	-	6.17 (5.14)	5.45 (3.56)	11.88 (5.48)	-
H&Y	-	1.73 (0.72)	2 (0.72)	2.85 (0.77)	-
UPDRS-III	2.26 (2.28)	12.37 (9.54)	14.28 (9.07)	33 (10.21)	<0.001*
MMSE	28.56 (1.34)	28.83 (1.01)	27.41 (1.65)	22.88 (3.77)	<0.001*
AF	23.56 (6.26)	23.57 (5.79)	18.86 (6.24)	11.81 (4.18)	<0.001*
LSF	18.56 (6.26)	16.15 (5.33)	12.5 (5.62)	9.31 (4.24)	<0.001*
AQT	60.41 (15.73)	63.37 (11.49)	78.32 (28.01)	132.93 (73.26)	<0.001*

Key: Participant data presented as mean (standard deviation). All data corrected to two decimal places. **Abbreviations:** eTIV, estimated total intracranial volume; H&Y, Hoehn and Yahr Scale; UPDRS-III, Unified Parkinson's Disease Rating Scale part-III; MMSE, Mini Mental-state Examination; AF, Animal Fluency Test; LSF, Letter S Fluency Test; AQT, A Quick Test of Cognitive Speed.

6.4.2 Corpus callosal thickness: pairwise analyses

Estimated thicknesses of callosal streamlines are presented in Figure 6.3.

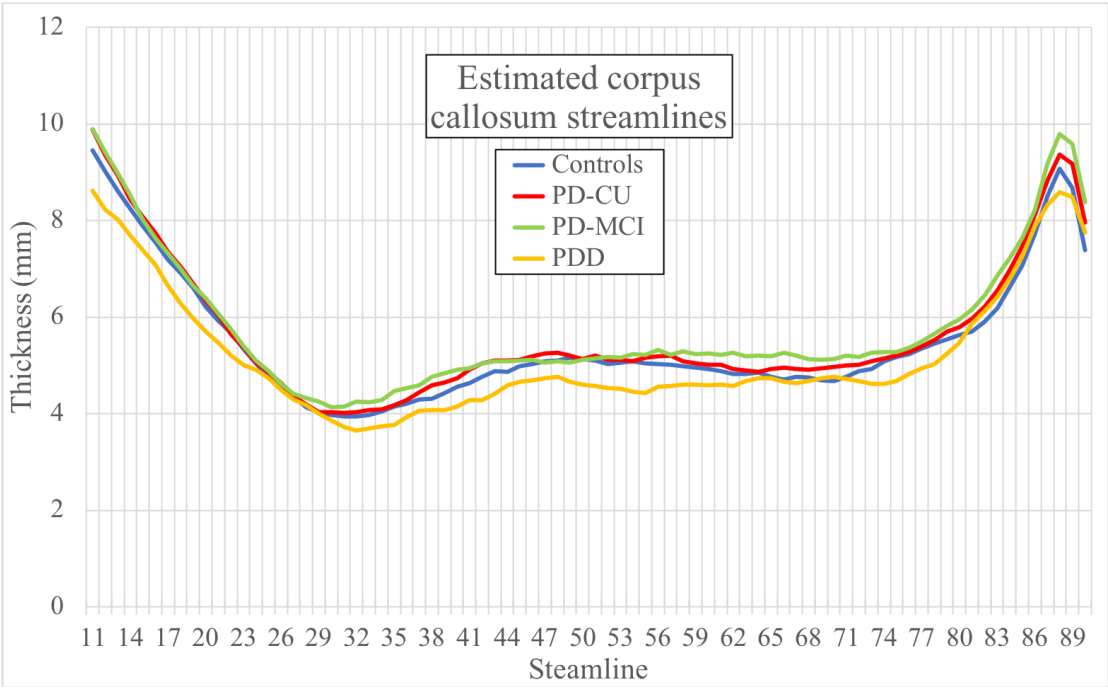

Figure 6.3: Estimated corpus callosum streamlines for all experimental groups. Streamline data represents the estimated averages for each group after controlling for head size and age. **Abbreviations:** PD-CU, cognitively unimpaired PD participants; PD-MCI, PD participants with mild cognitive impairment; PDD, PD participants with dementia.

6.4.2.1. Controls and PD-CU

We found no significant differences in callosal thickness when comparing Controls and PD participants (Figure 6.4).

6.4.2.2. Controls and PD-MCI

We found no significant differences in callosal thickness when comparing Controls and PD-MCI participants (Figure 6.4).

6.4.2.3. Controls and PDD

Although this comparison is of less scientific interest, for full transparency we compared Controls and PDD groups and found no significant differences in callosal thickness when comparing Controls and PDD participants (Figure 6.4)

6.4.2.4. PD and PD-MCI

We found no differences in callosal thickness when comparing PD to PD-MCI participants (Figure 6.4).

6.4.2.5. PD and PDD

When comparing PD-CU and PDD participants, we found PDD subjects demonstrated reduced thickness at streamlines 42 (p = 0.023), 51 (p = 0.049) and 55 (p = 0.032) (Figure 6.4).

6.4.2.6. PD-MCI and PDD

When comparing PD-MCI and PDD subjects, we found PDD subjects demonstrated reduced thickness at thickness at streamlines 42 (p = 0.039), 54 (p = 0.037), 55 (p = 0.029) and 56 (p = 0.049) (Figure 6.4)

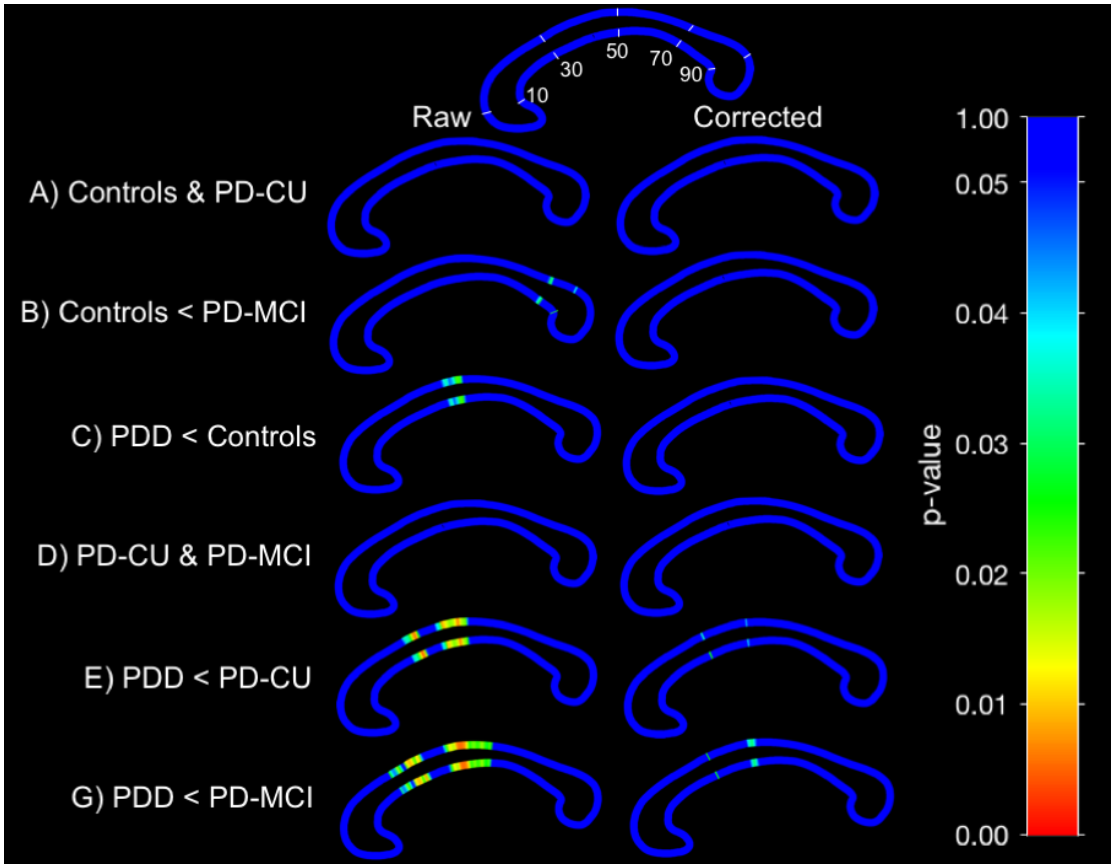

Figure 6.4. Group differences in midsagittal plane corpus callosum thickness. Areas of the corpus callosum where the thickness is reduced in one group compared to the other. Significant *p*-values (< 0.05) appear in light blue, becoming warmer in colour with lower values. Raw *p*-values are presented in the left column, with *p*-values corrected for multiple comparisons using the Bonferroni method presented on the right. Positioning of streamlines are guided by the image at the top. The genu of the corpus callosum points to the right of the image, while the splenium faces left. **Abbreviations:** PD-CU, cognitively unimpaired PD participants; PD-MCI, PD participants with mild cognitive impairment; PDD, PD participants with dementia.

6.4.3. Cortical thickness profiles: pairwise analyses

6.4.3.1. Controls and PD

When comparing Controls and PD-CU groups, after controlling for multiple comparisons, we found no significant differences in thickness at any cortical region of interest (Appendix Table 15).

6.4.3.2. Controls and PD-MCI

When comparing Controls and PD-MCI groups, after controlling for multiple comparisons, we found no significant differences in thickness at any cortical region of interest (Appendix Table 16).

6.4.3.3. Controls and PDD

When comparing Controls and PDD groups, after contolling for multiple comparisons, we found that PDD subjects had significantly reduced cortical thickness at the left lateral orbitofrontal cortex ($p = 0.028$), left entorhinal cortex ($p = 0.002$), left fusiform gyrus ($p < 0.001$), left superior temporal gyrus ($p = 0.014$), left middle temporal gyrus ($p = 0.044$), left inferior temporal gyrus ($p = 0.005$), left insula cortex ($p = 0.023$), right lateral orbitofrontal cortex ($p = 0.001$), right pars triangularis ($p = 0.034$), right fusiform gyrus ($p < 0.001$), right middle temporal gyrus ($p = 0.009$), right inferior temporal gyrus ($p < 0.001$), right supramarginal cortex ($p = 0.011$) and the right inferior parietal cortex ($p = 0.014$) (Appendix Table 17)

6.4.3.4. PD and PD-MCI

When comparing PD-CU and PD-MCI groups, after controlling for multiple comparisons, we found no significant differences in thickness at any cortical region of interest (Appendix Table 18).

6.4.3.5. PD and PDD

When comparing PD-CU and PDD groups, we found that PDD subjects had reduced cortical thickness at the left fusiform gyrus (p = 0.005), left superior temporal gyrus (p = 0.0056), left middle temporal gyrus (p = 0.035), left insula (p = 0.044), right lateral orbitofrontal cortex (p = 0.015), right pars triangularis (p = 0.004), right rostral middle frontal cortex (p = 0.006), right fusiform gyrus (p = 0.001), right middle temporal cortex (p = 0.008) and right inferior temporal cortex (p = 0.001) (Appendix Table 19).

6.4.3.6. PD-MCI and PDD

When comparing PD-MCI and PDD groups, we found that PDD subjects had reduced cortical thickness at the left fusiform gyrus (p = 0.003), left superior temporal gyrus (p = 0.003), left transverse temporal gyrus (p = 0.026), left inferior temporal gyrus (p = 0.029), right lateral orbitofrontal cortex (p = 0.01), right fusiform gyrus (p = 0.004), right parahippocampal gyrus (p = 0.047), right middle temporal gyrus (p = 0.048) and right inferior temporal gyrus (p = 0.006) (Appendix Table 20).

6.4.4. Correlation between thickness of the corpus callosum and cortex

When correlating callosal and cortical thicknesses within each experimental group, we found that the thickness of the left medial orbitofrontal cortex, after controlling for

multiple comparisons, was significantly positively correlated with thickness of the corpus callosum at streamlines 78, 79 and 80 in the PD-MCI group (Figure 6.5). All other correlations were non-significant.

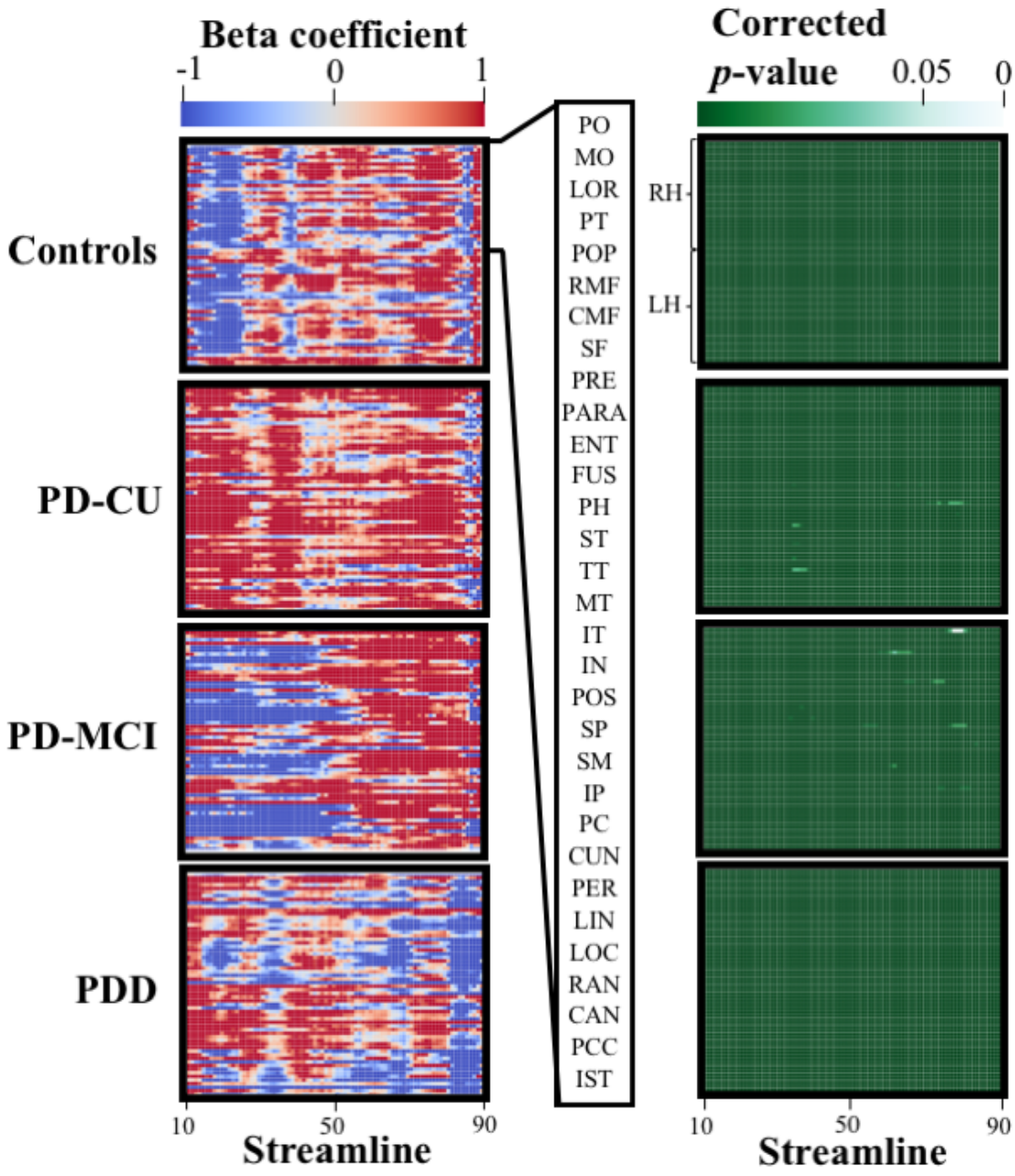

Figure 6.5. Correlation between callosal thickness and cortical thickness. Beta correlation coefficients show the directionality of the relationship between callosal and cortical thicknesses. Corrected *p*-values show the significance for each of these

corresponding analyses. Only three relationships remained significant after FDR correction for testing, which can be seen in a small white region of the PD-MCI group at streamlines 78, 79 and 80. **Abbreviations:** PO, pars orbitalis; MO, medial orbitofrontal cortex; LOR, lateral orbitofrontal cortex; PT, pars triangularis; POP, pars opercularis; RMF, rostral middle frontal cortex; CMF, caudal middle frontal cortex; SF, superior frontal cortex; PRE, precentral cortex; PARA, paracentral cortex; ENT, entorhinal cortex; FUS, fusiform gyrus; PH, parahippocampal gyrus; ST, superior temporal cortex; TT, transverse temporal cortex; MT, medial temporal cortex; IT, inferior temporal cortex; IN, insula; POS, postcentral cortex; SP, superior parietal cortex; SM, supramarginal cortex; IP, inferior parietal cortex; PC, precuneus; CUN, cuneus; PER, pericalcarine cortex; LIN, lingual cortex; LOC, lateral occipital cortex; RAN, rostral anterior cingulate; CAN, caudal anterior cingulate cortex; PCC, posterior cingulate cortex; IST, isthmus cingulate cortex;

6.4.5. Correlation between thickness of the corpus callosum and clinical variables

We found no significant correlations between thickness of the corpus callosum and clinical variables in any of the PD subgroups or Controls.

6.5. Discussion

6.5.1. Findings

This study uses an advanced mid-sagittal corpus callosal morphology technique to investigate changes to the thickness of the structure in Parkinson disease patients with varying levels of cognitive impairment. This was followed by an analysis of the thickness of cortical regions of interest across these disease subgroups, and an

investigation of the usefulness of callosal thickness as a predictor of cortical thicknesses and clinical variables.

This study demonstrated no significant differences in thickness of callosal streamlines in PD-CU subjects compared to Controls, supporting early 2-dimensional area-based findings (Wiltshire et al., 2005) as well as a recent 3-dimensional volumetric study (Lenka et al., 2017). Two studies showed volumes of callosal subdivisions are reduced in a total PD cohort comprising participants with and without cognitive impairment and also dementia (Goldman et al., 2017, Vasconcellos et al., 2018). Analyses between PD-disease subgroups in Goldman et al. (2017) indicate that their finding is likely due to significant changes in the PD participants diagnosed with dementia, and the results of the current study supports this finding. PDD participants in our study demonstrated reduced callosal thickness compared to PD-CU and PD-MCI, predominantly around central and mid-posterior callosal regions. The work of Goldman et al. (2017) also found no differences in callosal volumes in a PD cohort with MCI compared to cognitively unimpaired PD participants, or a control group, supporting our findings. In this context, our study builds on previous research findings and indicates that the morphology of the corpus callosum is impacted in advanced PD stages, and that PD patients with mild or no cognitive impairment have observable structural alterations to the callosum.

Considering possible pathophysiological mechanisms that may be responsible for structural changes observed in the callosum in PD dementia, it has been suggested that changes may be due to ‘Wallerian degeneration’ whereby atrophy of connected cortical regions is passed down neuronal axons causing a loss of synapses and

subsequent neurodegeneration of the structure (Coleman and Freeman, 2010). A second pathophysiological mechanism that may contribute to thinning of the corpus callosum in PD related dementia relates to the effects of primary white matter pathology. This has been hypothesised to drive atrophic callosal changes in Alzheimer disease (Di Paola et al., 2010) and diffusion weighted imaging research has demonstrated that microstructural white matter integrity is reduced in PD, and that these changes increase with levels of cognitive dysfunction (Agosta et al., 2014a, Bledsoe et al., 2018, Melzer et al., 2013).

To investigate whether changes in the thickness of the corpus callosum are reflective of changes to connected cortical regions, this study investigated associations between these two metrics. Such an investigation was performed due to there being evidence that there are partially overlapping genetic loci involved in the thickness of both structures (Gozzo et al., 1979), while in people with corpus callosum agenesis, there are fewer cortical neurons in areas which are expected to receive input from the callosum (Abreu-Villaca et al., 2002). While we found a small relationship between left medial orbitofrontal cortical thickness and streamlines in the anterior corpus callosum in PD-MCI participants, the overwhelming majority of correlational analyses between thickness of the callosum and thickness of the cortex showed no significant relationships. Due to this lack of a clear relationship between callosal and cortical thickness, our chosen method of modelling callosal thickness via mid-sagittal non-overlapping streamlines is unable to be used as a proxy measure of changes to the cerebral cortex.

Cortical thickness changes were not the primary focus of this study, and have been documented both cross-sectionally (Mak et al., 2015, Melzer et al., 2012, Pereira et al., 2014, Segura et al., 2014, Tinaz et al., 2011, Wilson et al., 2019, Zarei et al., 2013) and longitudinally (Hanganu and Monchi, 2016, Ibarretxe-Bilbao et al., 2012, Mak et al., 2015), however they are worth mentioning at this stage as they can shed light on other results in this study. The present work found a lack of significant differences in cortical thickness between our PD-CU group and Controls, which is consistent with a number of previous studies (Ibarretxe-Bilbao et al., 2012, Melzer et al., 2012, Zarei et al., 2013). However, a number of works have demonstrated reduced cortical thickness in cognitively unimpaired groups compared to control subjects (Pereira et al., 2014, Segura et al., 2014, Tinaz et al., 2011, Wilson et al., 2019). Changes in PD cohorts with MCI are more common (Mak et al., 2015, Melzer et al., 2012), and our demonstration of reductions in cortical thickness in frontal and temporal cortices in PDD broadly support findings in the literature, with extensive grey matter changes commonly found in frontal, temporal and also parietal cortices (Burton et al., 2004, Zarei et al., 2013). While there are a number of similarities between the present work and previous studies, both in terms of changes to the corpus callosum and the cortex, there are also inconsistencies. Factors that may account for these discordant findings include variable disease staging and symptom profiles of PD cohorts, as well as variable methods used to assess structural brain changes, and the statistical methods used to analyse the results.

6.5.2. Limitations

Morphological analysis of brain structures can be performed with a number of shape descriptors, and thickness is just one way to sample this concept. The current work

models thickness of the callosum via the use of nominally-parallel non-overlapping thickness streamlines which are evenly placed along the midline of the structure, connecting orthogonally with the superior and inferior callosal edges. This method was developed to better model thickness of the structure without having to use a volumetric approach, which can be a difficult concept to reconcile given that lateral boundaries of the structure are hard to model in 3-dimensions due to a lack of clear anatomical boundaries (Walterfang and Velakoulis, 2014). While our chosen method samples thickness at very fine-grained level of detail, the approach may miss morphological alterations to the callosum that take place at other points along the sagittal plane. A second possible limitation involves the incompatibility of our chosen method for analysing the genu and splenium of the callosum. As shown in Figure 6.2B, streamlines generated in these regions run in a curvilinear fashion, to maintain orthogonal connecting points with the superior and inferior boundaries of the structure. This makes the interpretation of their lengths difficult, which is important for the current work when we consider the callosal genu, as fibres from this region give rise to the white matter tract of the forceps minor that connects frontal cortices and is crucial to prefrontal cortical functioning (Goldstein and Mesfin, 2019).

6.5.3. Conclusion

This study demonstrates thinning of the callosum in PD participants with dementia compared to cognitively unimpaired PD participants and those with mild cognitive impairment. PD participants with dementia also demonstrated significant thinning of the cortex, primarily across the frontal and temporal lobes. Thickness of the corpus callosum was only correlated with thickness of the cortex in one very small region, while callosal thickness was also not significantly correlated with measures of clinical

function, limiting the applicability of this metric as a proxy for changes in these domains. The findings of this study suggest that the mid-sagittal thickness technique is able to detect the expected structural changes to the callosum in the advanced disease stage of PD-related dementia, however it is limited in usefulness when investigating PD participants with mild or no cognitive impairment.

7. General discussion

This thesis presents a search for neuroimaging biomarkers associated with clinical dysfunction in PD, focussing on the caudate nuclei, putamina, thalami, corpus callosum and cortex.

This work was motivated by the fact that significant uncertainty still exists around the underlying pathophysiological mechanisms of the disorder and its clinical manifestations. The development of novel therapeutic interventions for neurodegenerative disorders requires a complete understanding of the *in vivo* neurobiology associated with each disorder, and accordingly the neural circuit basis of clinical dysfunction (Looi et al., 2014). A neural circuit-based framework was used as a number of the clinical features of the disorder are linked structural brain changes, while others are arise due to aberrant brain activity between brain regions (Mcgregor and Nelson, 2019). This General Discussion will now present a brief summary of the findings of each research project, followed by a consideration of the main neuroimaging changes found in this thesis, functional changes in early disease stages followed by structural changes in later disease stages. This chapter will then examine the main methodological considerations that warrant attention, limitations of the projects and possible future directions that may stem from this thesis. This chapter

will finish with concluding remarks about what this thesis has demonstrated about neuroimaging biomarkers associated with clinical dysfunction in PD.

7.1. Brief Summary of Findings

Project one of this thesis investigated the morphology and functional connectivity of caudate nucleus and putamen, and how morphological changes relate to clinical dysfunction in PD. This project demonstrated that volumes of the caudate nuclei and putamina are reduced in PD, with subgroup analyses revealing that this result is driven by significant atrophy in participants with PD-related dementia. PD participants demonstrated a significant correlation between caudate nuclei volumes and measures of general cognitive impairment and speed, while putamina volumes were correlated with general motor function. No significant surface-based shape changes were found in PD compared to Controls. Increased functional connectivity was found between the caudate nucleus and the anterior cingulate, medial prefrontal and superior frontal gyri, compared to Controls. Decreased functional connectivity was found between the caudate nucleus and the brainstem, thalamus, parahippocampal gyrus and precuneus. The PD group also showed decreased connectivity of the putamen with the cerebellum, inferior and superior parietal lobules.

Project two investigated the morphology and functional connectivity of the important subdivisions of the thalamus, and how morphological changes relate to clinical dysfunction. This project found no evidence of significant volumetric or surface-based changes to the thalamus in PD compared to Controls. Further, thalamic volumes were not correlated with measures of clinical function. Despite this, PD

participants demonstrated significant increases in functional connectivity between the VLp/VA thalamic nuclei and the supplementary motor area, and between the MD/A thalamus and widespread regions across anterior and dorsolateral prefrontal cortices, nuclei of the basal ganglia and anterior cingulate regions.

Project three investigated the morphology and functional connectivity of the caudate nucleus, putamen and thalamus, but focussed on how these factors are impacted in PD relative to levels of cognitive impairment. This project demonstrated significant volumetric changes to the caudate nucleus, putamen and thalamus in PDD compared to PD-CU and Controls. Surface-based shape analyses of these structures found widespread surface deflation at the bilateral rostral as well as dorsomedial surface areas of the caudate. Deflation was found at the anterior, dorsal and posterior surface regions of the putamen, and significant and widespread deflation was found across the medial surface of the bilateral thalami. Significant increases in functional connectivity were found between the dorsal caudate nucleus, anterior putamen and mediodorsal thalamic subdivisions with areas across the frontal lobe, as well as reduced functional connectivity of the dorsal caudate with posterior parietal/lateral occipital and cerebellar regions. Compared to cognitively unimpaired participants, PD participants with MCI demonstrated reduced functional connectivity of the mediodorsal thalamus with midline nodes within the executive-control network. Compared to participants with MCI, participants with dementia demonstrated reduced functional connectivity of the mediodorsal thalamus with the posterior cingulate cortex, a key area within the default-mode network. While not meeting highly conservative multiple comparison-corrected *p*-values, this project found evidence that PD participants with lower general cognitive scores on the MMSE had increased functional connectivity of the

caudate nucleus with the middle frontal gyrus, and between the anterior putamen and the middle frontal and paracingulate gyri. Project Three also demonstrated that PD participants on higher levodopa-equivalent daily dosages had increased functional connectivity of the anterior putamen with right postcentral and inferior frontal gyri.

Project four investigated possible morphological alterations to the corpus callosum and cerebral cortex in PD participants relative to levels of cognitive impairment. This project also investigated how thickness of the corpus callosum related to the thickness of the cerebral cortex and levels of clinical function. This project demonstrated widespread thinning of the corpus callosum in PD-related dementia compared to PD-MCI and PD-CU participants. This was coupled with significant thinning of frontal, temporal and parietal cortices in PDD. Cognitively unimpaired and PD participants with MCI demonstrated minimal changes in corpus callosal and cortical thicknesses. When correlating the corpus callosal and cortical thicknesses, we found very little evidence of a relationship between these metrics, or between the corpus callosal thickness and clinical function, limiting the scope for corpus callosal thickness to be used as a proxy measure of cortical changes in PD.

The four projects presented in this thesis were focussed on uncovering neuroimaging biomarkers associated clinical dysfunction in PD from individual vantage points. However, a number of consistent scientific and methodological concepts developed, warranting further discussion.

7.2. What neuroimaging biomarkers may reveal about the mechanisms underlying clinical dysfunction in Parkinson disease

As outlined in section 1.9. of the Introduction, this thesis employed a network-based framework to investigate structural and functional changes to brain 'hubs' and 'spokes' and how these changes are related to clinical dysfunction in PD. Using functional MRI, this thesis demonstrates that changes to brain 'spokes' are more pronounced in early disease stages, evidenced by both increases and decreases in connectivity of the caudate, putamen and thalamus, despite no significant morphological alterations to these structures. Alterations in functional connectivity may be indicative of adaptive or maladaptive changes in the brain in response to disease pathology. Using structural MRI, this thesis demonstrates that changes to the brain 'hubs', including the caudate, putamen, thalamus, corpus callosum and also cortex in PD are more pronounced at advanced disease stages. Structural changes may be due to transneuronal neurodegeneration or the consequences of Lewy pathology, both of which may spread via brain networks. This thesis will now unpack these two concepts to reveal more about possible pathophysiological mechanisms associated with clinical dysfunction in PD.

7.2.1. Functional changes to brain networks in early disease stages

This thesis showed that PD patients demonstrate *decreased* functional connectivity of striatal and thalamic nuclei with cingulate, lateral occipital and cerebellar brain regions. This *hypo*-connectivity associated with PD may be evidence of a 'connectional diaschisis' which is a maladaptive brain mechanism associated with neural injury. Diaschisis was first defined by von Monakow as a temporary interruption of function in a particular brain region distal to an injured site in the brain

(Von Monakow, 1969). Originally thought to be a transient deafferentation of excitatory input most often tied to damage to brain regions following stroke (Fornito et al., 2015), the concept has been extended to include alterations in functional networks in the brain. This connectional diaschisis, whereby *activity* changes can be found in areas of the brain distal to the site of pathological insult (Carrera and Tononi, 2014), can occur even if anatomical connectivity between damaged and undamaged brain regions remains intact (Van Meer et al., 2010). Results from this thesis suggest that such a connectional diaschisis may be useful in understanding network-based changes associated with clinical dysfunction in PD patients early in the disease. Such a model would suggest that loss of cells in the substantia nigra pars compacta causes changes in neural dynamics to the connected nuclei of the striatum, which has flow-on consequences for brain regions distal to the substantia nigra.

Hypo-connectivity of the striatum was found alongside *increases* in functional connectivity of both the striatum and thalamus with prefrontal regions of the brain. This may be evidence of a maladaptive process called 'dedifferentiation,' whereby typically specialised and segregated brain circuits undergo a non-specific recruitment of new brain areas (Rajah and D'esposito, 2005). Reconfiguration of networks in this way has been demonstrated experimentally, whereby PD patients shift toward a more integrated brain network topology, which is then reversed with the administration of dopaminergic medication (Shine et al., 2019). However, this increased integration of brain networks was inversely correlated with the symptoms of the disorder, suggesting that increased integration of networks may represent a potential compensatory mechanism. Compensatory mechanisms may also be tied to the h*yper*-connectivity of brain circuits, shown to be a common response to neurological

disruption (Hillary et al., 2015). Such an adaptive change associated with neurological insult may represent an attempt to maintain homeostasis and performance after neural injury (Marder and Goaillard, 2006).

As suggested in Projects one, two and three of this thesis, increases in functional connectivity of brain regions found in PD may be evidence of a compensatory mechanism whereby the brain attempts to preserve function following pathological insult (O'shea et al., 2007). Project three of this thesis presented evidence that the degree of cognitive impairment was inversely correlated with the strength of functional connectivity of the striatum with prefrontal regions in the brain, a concept that is supported by research showing that greater compensatory recruitment of brain areas is correlated with the extent and severity of neural damage (Bestmann et al., 2010). However, persistent *hyper*-activation of brain regions may place neurons under high metabolic duress, making them susceptible to degeneration with progression of the disease. Such a process has been suggested to occur across the disease course in Alzheimer (Sheline and Raichle, 2013) and Huntington disease (Poudel et al., 2014) and our research, as well as work from Gorges et al. (2015) suggests a similar course may be involved in PD.

Hyper-connectivity of brain regions as an adaptive response to pathology also relies on neuronal degeneracy and reserve. Neuronal degeneracy is the capacity of elements of a system to perform the same function (Tononi et al., 1999), meaning that elements of a brain network can make overlapping contributions. Such a capacity affords brain networks with the ability to adapt, while also making them more resistant to damage (Tononi et al., 1999). The loss of dopaminergic input to the striatum in PD may result

in basal ganglia-thalamocortical circuits using inherent degeneracy to alleviate the impact of this pathological insult. Functional compensation of brain networks using degeneracy in this way also require sufficient brain tissue that can facilitate this response. While it was hypothesised in Project three that the stage at which such a compensatory response would no longer viable, due to a loss of neural reserve, would be when patients demonstrated MCI, experimental support for this model could not be found. However it is clear that at advanced disease stages, significant losses of brain tissue in subcortical, corpus callosal and cortical brain regions is demonstrated, likely limiting any potential adaptive compensatory response due to the widespread loss of neuronal reserve. This thesis will now discuss some of the possible mechanisms that might be involved in the significant structural changes that were observed in PD patients with dementia.

7.2.2. Structural changes to brain networks in advanced disease stages

This thesis presents evidence of widespread structural changes to the brain in PD patients with dementia. Changes to the white matter of the corpus callosum were discussed in Project four, and will not be expanded upon here. The likely mechanisms that underlie structural changes to the grey matter of brain networks in PD dementia may be due to the consequences of abnormal patterns of neural activity causing transsynaptic neurodegeneration or to a 'prion-like' spread of α-synuclein causing neurodegeneration.

Transneuronal neurodegeneration is a process whereby altered regulation of synaptic connections, due to synaptic depression or aberrant network synchronisation, interferes with the regulation of synapses (Palop and Mucke, 2010). Based on the

Hebbian notion regarding synaptic efficiency relying on the interaction between pre- and post-synaptic activity (Hebb, 2005), it is suggested that as activity can strengthen synaptic connections, so to does mismatched firing weaken these synapses resulting in neurodegeneration (Palop and Mucke, 2010). Such an activity-dependent neurodegeneration may proceed in the anterograde (damage to one neuron causes degeneration of the connected postsynaptic target) or retrograde direction (presynaptic neuron is damaged due to a lack of trophic support from postsynaptic target) (Cowan, 1970).

Structural brain changes in PD may also be due to the *propagation* of misfolded α-synuclein, moving from cell-to-cell, causing a spread of neurodegeneration, in what is termed the 'prion-hypothesis'. The build-up of aggregated proteins is a common denominator in most neurodegenerative disorders (Brundin et al., 2010), and evidence for the prion-hypothesis spread of these misfolded proteins in PD is extensive (Brundin and Melki, 2017). However, important questions still remain unanswered, such as how certain cell types in the brain are resistant to the spread of misfolded α-synuclein while others are not (Surmeier et al., 2017). It has been suggested that highly connected hub structures such as the striatum and thalamus are vulnerable to neurodegeneration in this way as they form crucial nodes of functional networks, inherently vulnerable to this process in neurodegenerative diseases (Seeley et al., 2009). Activity dependent transneuronal neurodegeneration and the prion-hypothesis are not mutually exclusive however, and it is possible that these two pathophysiological mechanisms represent elements of the same cycle (Palop and Mucke, 2010).

7.3. Methodological considerations, limitations and future directions

The research in this thesis contains a number of important methodological characteristics that require more extensive discussion beyond what was provided in the preceding project chapters. These include the use of patients on medication, the cross-sectional nature of the study, the significant PD-symptomatic heterogeneity and the use of cluster-based thresholding. Future directions that may address these potential limitations are also suggested.

7.3.1. Dopaminergic medication

PD participants in the current thesis remained on their usual medication during the clinical assessment and MRI acquisition phases, which has some important scientific implications. In particular, this factor needs to be taken into account when considering functional connectivity results. Research has shown that dopaminergic medication can restore decreased functional connectivity (Bell et al., 2015), produce increases in functional connectivity (Esposito et al., 2013), or as mentioned previously, influence the functional integration between brain networks (Shine et al., 2019). While these results suggest a clear relationship between functional connectivity changes and dopaminergic medication, a meta regression analysis performed by Ji et al. (2018) found that the main finding of their work, increased functional connectivity of structures of the basal ganglia with post central gyri in PD, was not significantly affected by medication data. Project three of this thesis attempted to address the issue by controlling for LEDD when comparing functional connectivity between PD cohorts using linear regression. While using such an approach is common and found to be generally reliable in this field of research (Tomlinson et al., 2010), future investigations may benefit from being longitudinal in nature, incorporating a more

sophisticated approach that could take into account not only the particular LEDD of the participant on the day of clinical assessment or image acquisition, but the full complexity of the clinical medication regime that may change over time.

Longitudinal research would also better characterise the progression of the disease. This thesis attempts to quantify disease progression in terms of years since diagnosis (Project one) and levels of cognitive impairment (Project three and four). While these two progression schemes are common in research, we cannot assume a linear progression of clinical dysfunction and disease processes according to these metrics. While there is strong evidence that PD-MCI does represent an intermediate cognitive disease stage between cognitively unimpaired PD and PDD (Litvan et al., 2012), a longitudinal approach would more accurately characterise the disease progression of participants. This would have the added benefit of more accurately characterising the significant clinical heterogeneity associated with PD.

7.3.2. Disease heterogeneity

A second important methodological consideration relates to disease heterogeneity in PD patients. Clinical features of the disorder can vary significantly between individuals, which has significant therapeutic and research implications (Greenland et al., 2019). This is such an important issue in PD, suggestions have been put forward arguing that the disorder be classified as a collection of distinct disease entities (Weiner, 2008) while other groups argue that PD is a clear disorder only with varying pathological kinetics (Barker and Williams-Gray, 2016).

Nonetheless, clinical and research observations have resulted in a clear subtyping of two distinct groups based on motor features of the disorder: a 'tremor-dominant' and a 'postural instability/gait disturbance' group (Jankovic et al., 1990). Patients with a tremor-dominant form of the disorder are more likely to have a mild disease phenotype and are slow to develop postural and gait disturbances. Conversely, those who present with predominant rigidity and bradykinesia are more likely to report impairments in mobility and postural stability, and are more likely to progress to advanced disease stages faster (Williams-Gray et al., 2013). However, while these two disease subtype profiles have clinical and research support, there is a significant overlap between these two motor phenotypes with the majority of patients experiencing some combination of features (Greenland et al., 2019). Alongside this motor subtyping, clinical and research evidence also suggests PD subtypes based on the type of cognitive impairment, that show links to these motor subtypes.

Parsing the heterogeneous nature of cognitive impairment into ontologically meaningful groups has led to a theory of the 'dual-syndrome hypothesis.' This hypothesis suggests two broad syndromes based on type of cognitive impairment, linked to a tremor-dominant or postural instability/gait disturbance subtypes (Kehagia et al., 2013). The first group identifies a cohort of non-demented tremor-dominant PD patients with cognitive impairment who demonstrate deficits on tests of planning, working memory and executive function. These deficits are linked to fronto-striatal dysfunction, and the majority of their symptoms are amenable to dopaminergic medication. The second cohort is linked to the postural instability/gait disturbance subtype and generally identifies patients with pronounced deficits in visuospatial function and semantic fluency. These deficits are linked to posterior cortical and

temporal lobe function, the symptoms respond poorly to dopaminergic medication (cholinergic treatment shows more efficacy) and these patients can exhibit a more rapid cognitive decline to dementia (Kehagia et al., 2013). However, as with the tremor-dominant and postural instability/gait motor distinction, there is significant overlap between these syndromes, both in terms of clinical features and responsiveness to medication. Future research in this field may benefit from an increased specificity to any cognitive impairment diagnosis, which can group participants based on the types of dysfunction observed.

7.3.3. Statistical approach to functional connectivity analyses

As outlined in the Methodology 2.5.1.2 section of this thesis, there are a number of ways that functional MRI data can be analysed for statistical significance. The two main approaches used are parametric cluster-based and non-parametric permutation-based thresholding. This thesis implemented both alternatives, however evidence is emerging that non-parametric permutation-based methods are more effective in minimising false-positive rates and they have a higher test-retest reliability/replicability (Chen et al., 2018).

Cluster-based thresholding of statistic images in functional MRI makes use of the spatial neighbourhood information to assign probability values to clusters of voxels. Such an approach makes a number of assumptions about the data, and if violated, serve as limitations to this method. The first is the selection of an initial cluster-forming threshold, which is set as a threshold above which values within a statistic image can be considered significant. Researchers in this field often select an arbitrary value, use the default option available in analysis software, or choose a value that is

commonly used in previously published articles. This is important as the choice of the cluster-forming threshold value has significant implications to the results of the research (Woo et al., 2014).

Cluster-based thresholding also relies on data within the statistic image being normally distributed (Gaussian) and also can be impacted by the amount of spatial smoothing used on the data. Spatial smoothing (see Methodology 2.5.2) is a value that, similar to the cluster-forming threshold, is often arbitrarily selected (Smith and Nichols, 2009). When making inferences about significant results found using this method, cluster-based thresholding also only allows researchers to infer anatomical information based on significant regions that are within a cluster, but it is unable to provide high neuroanatomical specificity. If a significant cluster of functional connectivity is found that crosses neuroanatomical boundaries, cluster-based approaches are unable to accurately infer whether the significant result is driven by changes in one area to the next. Non-parametric permutation based approaches have been developed to address these issues, and the threshold-free cluster enhancement method in particular has shown significant promise as it does not require the selection of an arbitrary cluster-forming threshold value and can be applied to data that is non-Gaussian (Smith and Nichols, 2009).

The threshold-free cluster enhancement method with permutation testing uses the raw statistic image and creates an output that indicates how much cluster-like local support exists for each voxel within the image. This value is the sum of ‘scores’ or all ‘supporting sections’ that exist underneath it, with the score being the height of the cluster multiplied by its spatial extent (Smith and Nichols, 2009). This new value

represents a weighted sum of the local cluster signal, able to detect both diffuse low-amplitude brain activation in statistic images as well as sharp focal-activation.

The 'permutation' element of the method works by adjusting the uncorrected *p*-values by permuting the participants in the study such that they do not correspond to their original group labels. Under the assumption that the null hypothesis is true (i.e. there is no difference in statistic images between the groups) the results would not change regardless of how participants were characterised. Each new permutation of the group labelling is run and the result varies as a result of the noise in the data. Once a sufficiently large number of permutations are run, values for each run are combined into an empirical null distribution at each voxel, which can then be compared with the original unpermuted statistic image and a *p*-value can be produced (Jenkinson and Chappell, 2018). Future research should consider the use of non-parametric approaches such as the threshold-free cluster enhancement method with permutation testing, which may partially address the significant replicability issues that cluster-based approaches have caused in the field of functional neuroimaging (Eklund et al., 2016).

7.4. Conclusion

This thesis demonstrates that PD is associated with significant morphological changes to structures in the brain in PD participants with dementia, that may be linked to transneuronal neurodegeneration or the spread of misfolded α-synuclein. Decreases in functional connectivity of striatal nuclei was found in PD participants, which may be evidence of maladaptive connectional diaschisis or dedifferentiation of brain networks. PD participants also demonstrated increased functional connectivity of

striatal and thalamic nuclei, potentially evidence of increased integration or an adaptive functional compensation of basal ganglia-thalamocortical brain networks.

In conclusion, this thesis argues that alterations to the functional connectivity of basal ganglia-thalamocortical circuits may precede morphological alterations to the structures, which become impacted later in the disease course. These changes potentially represent structural and functional neuroimaging biomarkers associated with clinical dysfunction in Parkinson disease, revealing important insights about adaptive and maladaptive brain changes associated with the disorder.

8. Appendices

Appendix 1: Tracing reliability of manual ROI segmentation

Reliability of the manual segmentation of the bilateral caudate nucleus, putamen method and thalamus was quantified by the calculation of an *inter*-rater reliability coefficient, measuring the tracer's agreement with an expert tracer and an *intra*-rater reliability coefficient, measuring the consistency of the rater over time. The inter-rater coefficient is the final correlation metric obtained after an extensive training period using an MRI example dataset of 20 ROIs of interest, re-traced in a blinded fashion until a satisfactory standard was reached. The intra-rater coefficient was obtained by re-tracing every ~10^{th} participant's MRI scan during the manual segmentation process, with obtained volumes at the first attempt correlated against the volumes obtained at the second attempt. The tracer for this task was COW, while the experienced rater for the inter-rater comparator group was FAW. Both the inter- and intra-rater reliability coefficient values relate to the conservative 'absolute agreement' definition. For the caudate nucleus and putamen, inter-rater reliability was r = 0.89 and r = 0.83, respectively), while the intra-rater reliability (as an intra-class) coefficient was r = 0.98 for both structures. For the thalamus, the inter-rater reliability was 0.908 while the intra-rater score was r = 0.879 (Shrout and Fleiss, 1979).

Appendix Table 1: Correlations between striatal volumes and clinical function - PD subgroups

Group	Nuclei	Clinical measure	R^2 change	β	*p* value
Early PD	BPV	UPDRS-III	0.114	0.475	0.056
Late PDD			0.132	0.436	0.060
PDD			0.030	0.239	0.464
Early PD	RPV		0.129	0.484	0.042
Late PDD			0.122	0.441	0.072
PDD			0.092	0.478	0.187
Early PD	LPV		0.061	0.331	0.168
Late PDD			0.097	0.347	0.113

PDD			0.006	0.095	0.743
Early PD	BCV	MMSE	0.176	0.457	0.036
Late PDD			0.028	-0.214	0.477
PDD			0.202	0.670	0.191
Early PD	RCV		0.128	0.399	0.078
Late PDD			0.011	0.520	0.657
PDD			0.130	0.520	0.308
Early PD	LCV		0.216	0.494	0.019
Late PDD			0.047	-0.292	0.352
PDD			0.236	0.716	0.151
Early PD	BCV	AQT	0.189	0.473	0.012
Late PDD			0.016	0.163	0.602
PDD			0.409	0.952	0.035
Early PD	RCV		0.133	0.407	0.040
Late PDD			0.047	0.264	0.366
PDD			0.338	0.839	0.075
Early PD	LCV		0.234	0.525	0.004
Late PDD			0.002	0.058	0.860
PDD			0.421	0.955	0.030

Abbreviations: β, standardised beta values; BCV, bilateral caudate nucleus volume; RCV, right caudate nucleus volume; LCV, left caudate nucleus volume; BPV, bilateral putamen volume; RPV, right putamen volume; LPV, left putamen volume; UPDRS-III, Unified Parkinson's Disease Rating Scale part III; TUG, Timed Up and Go; AF, Animal Fluency; LSF, Letter S Fluency; MMSE, Mini Mental-State Examination; AQT, A Quick Test of Cognitive Speed; ** significant at the Bonferroni corrected $p < 0.0018$; data correct to 3 decimal places.

Appendix Table 2: Pairwise ANOVA results comparing PD disease subgroups on demographic variables.

Group 1	Group 2	Variable	Difference (Group 1 - Group 2)	*p*-value
Control	Early PD	Age	0.057	1.00
	Late PD		-0.517	0.992
	PDD		-3.962	0.19
Early PD	Late PD		-0.575	0.987
	PDD		-4.029	0.15
Late PD	PDD		-3.445	0.332
Control	Early PD	UPDRS-III	3.655	0.052
	Late PD		-0.071	1.00
	PDD		1.229	0.899
Early PD	Late PD		-3.726	0.064
	PDD		-2.426	0.504
Late PD	PDD		1.300	0.892
Control	Early PD	AF	8.775*	<0.001
	Late PD		14.154*	<0.001
	PDD		30.091*	<0.001
Early PD	Late PD		5.379	0.081
	PDD		21.316*	<0.001
Late PD	PDD		15.938*	<0.001
Control	Early PD	MMSE	1.767	0.075
	Late PD		1.059	0.539
	PDD		3.023*	0.019
Early PD	Late PD		-0.707	0.785
	PDD		1.256	0.583

Late PD	PDD		1.964	0.24
Control	Early PD	Education	1.430	0.816
	Late PD		2.885	0.382
	PDD		11.951*	<0.001
Early PD	Late PD		1.455	0.83
	PDD		10.521*	<0.001
Late PD	PDD		9.067*	<0.001
Control	Early PD	TUG	5.939*	<0.001
	Late PD		2.15	0.532
	PDD		9.267*	<0.001
Early PD	Late PD		-3.789	0.066
	PDD		3.327	0.196
Late PD	PDD		7.117*	0.001
Control	Early PD	LSF	0.48	0.781
	Late PD		0.465	0.841
	PDD		5.505*	<0.001
Early PD	Late PD		-0.015	1.00
	PDD		5.025*	<0.001
Late PD	PDD		5.040*	<0.001
Control	Early PD	AQT	11.711	0.179
	Late PD		7.741	0.613
	PDD		56.385*	<0.001
Early PD	Late PD		-3.97	0.911
	PDD		44.674*	<0.001
Late PD	PDD		48.643*	<0.001

Key: This table demonstrates the pairwise comparison of demographic data between PD disease subgroups and Controls showing the significant differences. *, indicates differences between groups that have a p-value of < 0.05.

Appendix Table 3: Correlations between thalami volumes and clinical measures - PD and Controls

Structure	Group	Clinical measure	β	*p*-value
Right thalamus	Controls	Animal Fluency	-0.008	0.973
	PD		0.257	0.058
Left thalamus	Controls		-0.048	0.839
	PD		0.247	0.069
Right thalamus	Controls	Letter S Fluency	-0.236	0.317
	PD		0.086	0.542
Left thalamus	Controls		-0.11	0.646
	PD		-0.056	0.688
Right thalamus	Controls	MMSE	-0.143	0.547
	PD		0.274	0.043*
Left thalamus	Controls		-0.205	0.387
	PD		0.225	0.099
Right thalamus	Controls	AQT	0.164	0.489
	PD		0.260	0.060
Left thalamus	Controls		-0.113	0.635
	PD		0.086	0.543
Right thalamus	Controls	UPDRS-III	-0.053	0.809
	PD		0.264	0.029*
Left thalamus	Controls		0.269	0.215

	PD		0.316	0.009*
Right thalamus	Controls	TUG	-0.212	0.33
	PD		0.079	0.543
Left thalamus	Controls		0.041	0.851
	PD		0.190	0.143

Abbreviations: UPDRS-III, Unified Parkinson's Disease Rating Scale part III; MMSE, Mini Mental-State Examination; β, standardized beta coefficient indicating effect size.

Appendix Table 4: Correlations between thalami volumes and clinical measures - PD subgroups

Structure	Group	Clinical measure	β	*p*-value
Right thalamus	Early PD	Animal Fluency	0.295	0.172
	Late PD		0.027	0.921
	PDD		-0.327	0.429
Left thalamus	Early PD		0.311	0.149
	Late PD		0.248	0.355
	PDD		-0.407	0.317
Right thalamus	Early PD	Letter S Fluency	0.385	0.070
	Late PD		-0.105	0.721
	PDD		-0.685	0.061
Left thalamus	Early PD		0.264	0.224
	Late PD		-0.194	0.506
	PDD		-0.387	0.343
Right thalamus	Early PD	MMSE	0.275	0.204
	Late PD		0.445	0.084
	PDD		0.135	0.750
Left thalamus	Early PD		0.229	0.293
	Late PD		0.143	0.596
	PDD		0.353	0.391
Right thalamus	Early PD	AQT	0.129	0.557
	Late PD		0.372	0.156
	PDD		-0.254	0.627
Left thalamus	Early PD		0.117	0.595
	Late PD		0.212	0.430
	PDD		0.194	0.713
Right thalamus	Early PD	UPDRS-III	0.122	0.520
	Late PD		0.296	0.218
	PDD		0.170	0.580
Left thalamus	Early PD		-0.149	0.432
	Late PD		0.664	0.002*
	PDD		-0.102	0.74
Right thalamus	Early PD	TUG	0.313	0.098
	Late PD		0.296	0.219
	PDD		-0.050	0.915
Left thalamus	Early PD		-1.60	0.408
	Late PD		0.662	0.002*
	PDD		0.396	0.379

Key: Family-wise error rate correction using the Bonferroni method stipulate a $p < 0.0014$ required for significance (after running 36 analyses). **Abbreviations:** UPDRS-III, Unified Parkinson's Disease Rating Scale part III; MMSE, Mini Mental-State Examination; β, standardized beta coefficient indicating effect size;

Appendix Table 5: Local maxima of significant differences in functional connectivity of dorsal caudate in PD-CU compared to Controls

			MNI Coordinate		
FC	**Brain Region**	**Z**	**x**	**y**	**z**
⇑	R superior frontal gyrus (BA8)	4.86	10	32	58
	R postcentral gyrus (BA3)	4.56	44	-18	58
	R precentral gyrus (BA6)	4.43	32	-4	54
	R superior frontal gyrus (BA6)	4.4	2	14	54
	R precentral gyrus (BA6)	4.35	46	-18	66
	R paracingulate gyrus (BA32)	4.32	8	12	50
	L frontal pole (BA10)	3.81	-28	56	2
	L frontal pole (BA10)	3.8	-36	54	18
	L frontal pole (BA10)	3.73	-32	40	18
	L frontal pole (BA10)	3.72	-40	50	20
	L frontal pole (BA10)	3.56	-30	52	18
	L frontal pole (BA10)	3.53	-44	46	20
	R middle frontal gyrus (BA8)	4.39	34	16	38
	R middle frontal gyrus (BA8)	3.37	20	18	40
⇓	R lateral occipital cortex (BA19)	4.22	40	-76	28
	R lateral occipital cortex (BA19)	3.95	46	-74	28
	R lateral occipital cortex (BA19)	3.9	36	-86	26
	R lateral occipital cortex (BA19)	3.8	28	-88	30
	R lateral occipital cortex (BA19)	3.22	32	-72	30
	L cerebellar crus I	4.18	-24	-72	-26
	L cerebellar crus I	3.74	-38	-70	-28
	L cerebellar crus I	3.5	-34	-76	-28
	L angular gyrus (BA39)	4.36	-60	-54	28
	L angular gyrus (BA39)	4.23	-62	-56	24
	L angular gyrus (BA39)	4.01	-60	-60	20
	L supramarginal gyrus (BA40)	4.01	-62	-50	20
	L cerebellar lobule VI	4.16	-6	-76	-20
	L cerebellar vermis VI	3.69	-2	-70	-10
	L cerebellar vermis VI	3.54	-2	-76	-30
	L cerebellar vermis VI	3.39	-4	-70	-26

Key: Brain regions and associated coordinates represent areas of significant functional connectivity differences with the dorsal caudate in PD-CU participants compared to Controls (family-wise error corrected $p < 0.05$). **Abbreviations:** FC, functional connectivity; ⇓, decrease in functional connectivity; ⇑, increase in functional connectivity; n/a, coordinates fall outside brain tissue space; L, left hemisphere; R, right hemisphere; BA, Brodmann Area; Z, maximum *Z*-value for cluster; MNI, coordinates for location of maximum *Z*-value, in the Montreal Neurological Institute T_1 standard space.

Appendix Table 6: Local maxima of significant differences in functional connectivity of the anterior putamen in PD-CU compared to Controls

			MNI Coordinate		
FC	**Region**	**Z**	**x**	**y**	**z**

⇑	R middle frontal gyrus (BA8)	5.43	26	26	32
	R middle frontal gyrus (BA8)	4.33	24	34	44
	R anterior cingulate cortex (BA24)	4.14	12	24	20
	R middle frontal gyrus (BA9)	4.06	32	30	20
	L frontal pole (medial) (BA10)	3.93	-2	56	20
	R frontal pole (BA10)	3.91	8	54	32
	R frontal pole (BA10)	3.83	10	50	40
	L superior frontal gyrus (BA9)	3.56	-2	56	30
	L paracingulate gyrus (BA32)	3.51	-2	46	22
	R postcentral gyrus (BA3)	4.24	44	-22	58
	R precentral gyrus (BA4)	4.23	44	-12	56
	R precentral gyrus (BA4)	4.1	40	-20	60
	R precentral gyrus (BA4)	4.03	42	-8	60
	R precentral gyrus (BA4)	3.83	42	-14	52
	R postcentral gyrus (BA3)	3.83	46	-24	52
	L postcentral gyrus (BA2)	4.08	-54	-12	26
	L precentral gyrus (BA6)	3.78	-56	2	28
	L postcentral gyrus (BA2)	3.73	-56	-10	20
	L precentral gyrus (BA6)	3.58	-60	-4	28
	L central operculum (BA42)	3.54	-50	-16	18
	L precentral gyrus (BA6)	3.37	-50	-6	30
	L paracingulate gyrus (BA32)	4.85	-12	32	28
	L anterior cingulate gyrus (BA24)	4.56	-12	28	22
	L paracingulate gyrus (BA32)	3.67	-4	36	20
	L anterior cingulate gyrus (BA24)	3.49	-6	32	22
	R postcentral gyrus (BA3)	4.4	52	-16	44
	R precentral gyrus (BA4)	4.08	42	-8	34
	R postcentral gyrus (BA3)	3.58	46	-12	32
	R postcentral gyrus (BA3)	3.48	50	-14	36
	L middle frontal gyrus (BA9)	4.42	-28	28	40
	L middle frontal gyrus (BA8)	3.81	-32	22	40
	L middle frontal gyrus (BA8)	3.71	-30	28	30
	R inferior frontal gyrus (BA44)	3.79	48	20	18
	R inferior frontal gyrus (BA44)	3.76	46	16	14
	R inferior frontal gyrus (BA44)	3.67	48	16	10
	R central operculum (BA42)	3.65	40	20	8
	R inferior frontal gyrus (BA44)	3.46	54	22	12
⇓	L lateral occipital cortex (BA19)	4.05	-26	-82	40
	L lateral occipital cortex (BA19)	3.79	-28	-76	40
	L lateral occipital cortex (BA19)	3.76	-34	-88	32
	L lateral occipital cortex (BA19)	3.73	-42	-80	32
	L lateral occipital cortex (BA19)	3.72	-18	-84	38
	L lateral occipital cortex (BA19)	3.69	-28	-82	34
	R precuneus (BA7)	4.1	6	-62	42
	Precuneus (BA7)	4.08	0	-68	46
	L precuneus (BA7)	3.56	-2	-54	38

Key: Brain regions and associated coordinates represent areas of significant functional connectivity changes with the anterior putamen in PD-CU participants compared to Controls (family-wise error corrected $p < 0.05$). **Abbreviations:** FC, functional connectivity; ⇓, decrease in functional connectivity; ⇑, increase in functional connectivity; n/a, coordinates fall outside brain tissue space; L, left hemisphere; R, right hemisphere; BA, Brodmann Area; *p*, corrected *p*-value; Z, maximum *Z*-value for cluster; MNI, coordinates for location of maximum *Z*-value, in the Montreal Neurological Institute T_1 standard space.

Appendix Table 7: Local maxima of significant differences in functional connectivity of the mediodorsal thalamus in PD-CU participants compared to Controls

FC	Region	Z	MNI Coordinate		
			x	y	z
⇑	**L postcentral gyrus (BA1)**	**4.94**	**-58**	**-10**	**26**
	L precentral gyrus (BA6)	4.45	-60	-2	32
	L postcentral gyrus (BA3)	4.37	-58	-12	42
	L precentral gyrus (BA6)	4.09	-56	4	20
	L precentral gyrus (BA4)	4.01	-54	-12	40
	L postcentral gyrus (BA3)	3.95	-54	-12	32
	R middle frontal gyrus (BA8)	**3.97**	**24**	**24**	**32**
	R middle frontal gyrus (BA8)	3.63	24	20	38

Key: Brain regions and associated coordinates represent areas of significant functional connectivity changes with the mediodorsal thalamus in PD-CU participants compared to Controls (family-wise error corrected $p < 0.05$). **Abbreviations:** FC, functional connectivity; ⇑, increase in functional connectivity; n/a, coordinates fall outside brain tissue space; L, left hemisphere; R, right hemisphere; BA, Brodmann Area; *p*, corrected *p*-value; Z, maximum *Z*-value for cluster; MNI, coordinates for location of maximum *Z*-value, in the Montreal Neurological Institute T_1 standard space.

Appendix Table 8: Local maxima of significant differences in functional connectivity of the mediodorsal thalamus in PD-MCI participants compared to PD-CU

FC	Region	Z	MNI Coordinate		
			x	y	z
⇓	**R paracingulate gyrus (BA32)**	**3.92**	**2**	**46**	**30**
	Paracingulate gyrus (BA32)	3.76	0	42	24
	Medial frontal gyrus (BA9)	3.75	0	46	24
	R frontal pole (BA8)	3.67	8	48	38
	R frontal pole (BA8)	3.63	10	52	36
	R frontal pole (BA8)	3.52	10	52	32

Key: Brain regions and associated coordinates represent areas of significant functional connectivity changes with the mediodorsal thalamus in PD-MCI participants compared to Controls (family-wise error corrected $p < 0.05$). **Abbreviations:** FC, functional connectivity; ⇓, decrease in functional connectivity; L, left hemisphere; R, right hemisphere; BA, Brodmann Area; Z, maximum *Z*-value for cluster; MNI, coordinates for location of maximum *Z*-value, in the Montreal Neurological Institute T_1 standard space.

Appendix Table 9: Local maxima of significant differences in functional connectivity of the mediodorsal thalamus in PDD participants compared to PD-MCI

FC	Region	Z	MNI Coordinate		
			x	y	z
⇓	**R posterior cingulate cortex (BA23)**	**4.07**	**6**	**-38**	**26**
	R posterior cingulate cortex (BA23)	3.97	4	-42	30
	Posterior cingulate cortex (BA23)	3.93	0	-34	26

Key: Brain regions and associated coordinates represent areas of significant functional connectivity changes with the mediodorsal thalamus in PDD participants compared to PD-MCI participants (family-wise error corrected $p < 0.05$). **Abbreviations:** FC, functional connectivity; ⇓, decrease in functional connectivity; n/a, coordinates fall outside brain tissue space; L, left hemisphere; R, right hemisphere; BA, Brodmann Area; *p*, corrected *p*-value; Z,

maximum *Z*-value for cluster; MNI, coordinates for location of maximum *Z*-value, in the Montreal Neurological Institute T_1 standard space.

Appendix Table 10: Correlations between average parameter estimate clinical variables - PD participants compared to Controls

Cluster	Result	LEDD	UPDRS	AF	LSF	MMSE	AQT	DD
#1	⇑ in PD	0.243	0.055	0.048	0.017	-0.157	-0.028	0.241
		(0.213)	(0.76)	(0.789)	(0.928)	(0.382)	(0.876)	(0.177)
#2	⇑ in PD	-0.041	0.08	0.189	0.121	-0.306	0.16	-0.02
		(0.834)	(0.658)	(0.293)	(0.518)	(0.083)	(0.374)	(0.913)
#3	⇑ in PD	0.358	-0.073	0.044	0.057	**-.420***	0.278	0.34
		(0.062)	(0.688)	(0.806)	(0.761)	**(0.015)**	(0.118)	(0.053)
#4	⇓ in PD	-0.14	0.017	-0.331	-0.211	0.246	-0.245	-0.108
		(0.476)	(0.925)	(0.06)	(0.255)	(0.168)	(0.17)	(0.548)
#5	⇓ in PD	-0.264	0.091	0.044	-0.274	0.284	-0.131	-0.271
		(0.175)	(0.616)	(0.808)	(0.136)	(0.109)	(0.468)	(0.126)
#6	⇓ in PD	-0.334	0.316	0.166	-0.076	0.165	0.024	-0.284
		(0.082)	(0.073)	(0.357)	(0.685)	(0.359)	(0.897)	(0.109)
#7	⇓ in PD	-0.14	-0.01	-0.209	-0.208	0.302	-0.191	-0.084
		(0.476)	(0.957)	(0.244)	(0.262)	(0.087)	(0.286)	(0.641)
#8	⇑ in PD	0.327	-0.046	-0.044	0.207	**-.354***	0.206	0.222
		(0.09)	(0.801)	(0.809)	(0.263)	**(0.043)**	(0.251)	(0.214)
#9	⇑ in PD	0.144	-0.196	0.258	0.33	-0.319	0.033	0.008
		(0.464)	(0.274)	(0.147)	(0.07)	(0.07)	(0.856)	(0.964)
#10	⇑ in PD	0.073	0.015	-0.095	-0.106	-0.272	0.033	0.147
		(0.712)	(0.935)	(0.599)	(0.57)	(0.126)	(0.857)	(0.415)
#11	⇑ in PD	0.106	0.193	-0.193	-0.192	-0.001	0.029	0.075
		(0.593)	(0.281)	(0.282)	(0.302)	(0.994)	(0.875)	(0.679)
#12	⇑ in PD	0.139	0.024	0.044	0.171	**-.513***	0.059	0.086
		(0.481)	(0.893)	(0.806)	(0.358)	**(0.002)**	(0.743)	(0.635)
#13	⇑ in PD	**.505***	-0.245	-0.197	0.073	-0.325	-0.074	0.324
		(0.006)	(0.17)	(0.272)	(0.697)	(0.065)	(0.682)	(0.066)
#14	⇑ in PD	0.17	-0.076	0.04	0.193	**-.445***	0.091	0.222
		(0.386)	(0.676)	(0.823)	(0.298)	**(0.009)**	(0.614)	(0.214)
#15	⇑ in PD	**.521***	-0.191	-0.115	0.185	-0.197	0.177	0.321
		(0.004)	(0.287)	(0.526)	(0.319)	(0.273)	(0.325)	(0.069)
#16	⇓ in PD	**-.471***	-0.043	0.045	-0.077	0.233	-0.148	-0.295
		(0.012)	(0.812)	(0.803)	(0.682)	(0.192)	(0.411)	(0.095)
#17	⇓ in PD	-0.1	0.009	0.102	0.043	-0.063	-0.131	0.096
		(0.613)	(0.961)	(0.573)	(0.818)	(0.728)	(0.467)	(0.593)
#18	⇑ in PD	-0.074	0.039	-0.224	-0.251	0.26	0.081	**-.348**
		(0.71)	(0.831)	(0.21)	(0.174)	(0.144)	(0.653)	**(0.047)**
#19	⇑ in PD	0.109	-0.097	-0.017	0.24	0.11	0.136	0.201
		(0.581)	(0.592)	(0.924)	(0.193)	(0.541)	(0.452)	(0.261)

Key: Beta correlation coefficients showing direction of correlation between average parameter estimate at each cluster location and measures of clinical function, with associated *p*-value shown in brackets. Correlations are performed within each PD disease group that had a significant difference in FC at that location. **Abbreviations:** ⇓, decrease in functional connectivity; ⇑, increase in functional connectivity; LEDD, levodopa-equivalent daily dosage; UPDRS, Unified Parkinson Disease Rating Scale Part-III; AF, Animal Fluency test; LSF, Letter S Fluency Test; MMSE, Mini Mental State Examination; AQT, A Quick Test of Cognitive Speed; DD, disease duration.

Appendix Table 11: Correlations between average parameter estimate clinical variables - PD compared to PD-MCI

Cluster	Result	LEDD	UPDRS	AF	LSF	MMSE	AQT	DD
#20	⇑ in PD	**-.486***	**.424***	0.13	0.293	-0.386	-0.105	-0.352
		(0.025)	**(0.049)**	(0.565)	(0.185)	(0.076)	(0.642)	(0.108)
#20	⇓ in PD-MCI	-0.259	-0.034	0.197	0.061	0.001	0.098	-0.269
		(0.183)	(0.85)	(0.271)	(0.744)	(0.995)	(0.588)	(0.13)

Key: Beta correlation coefficients showing direction of correlation between average parameter estimate at each cluster location and measures of clinical function, with associated *p*-value shown in brackets. Correlations are performed within each PD disease group that had a significant difference in FC at that location. Clusters are repeated as the significant difference in FC found at cluster #20 could be due to increases in PD or decreases in PD-MCI.
Abbreviations: ⇓, decrease in functional connectivity; ⇑, increase in functional connectivity; LEDD, levodopa-equivalent daily dosage; UPDRS, Unified Parkinson Disease Rating Scale Part-III; AF, Animal Fluency test; LSF, Letter S Fluency Test; MMSE, Mini Mental State Examination; AQT, A Quick Test of Cognitive Speed; DD, disease duration.

Appendix Table 12: Correlations between average parameter estimate clinical variables - PD-MCI compared to PDD

Cluster	Result	LEDD	UPDRS	AF	LSF	MMSE	AQT	DD
#21	⇑ in PD-MCI	0.367	-0.279	-0.396	-0.099	0.238	-0.009	**.522***
		(0.102)	(0.209)	(0.068)	(0.662)	(0.287)	(0.969)	**(0.013)**
#21	⇓ in PDD	0.391	-0.04	0.045	0.271	0.268	0.283	0.235
		(0.135)	(0.88)	(0.868)	(0.311)	(0.299)	(0.327)	(0.365)

Key: Beta correlation coefficients showing direction of correlation between average parameter estimate at each cluster location and measures of clinical function, with associated *p*-value shown in brackets. Correlations are performed within each PD disease group that had a significant difference in FC at that location. Clusters are repeated as the significant difference in FC found at cluster #21 could be due to increases in PD-MCI or decreases in PDD.
Abbreviations: ⇓, decrease in functional connectivity; ⇑, increase in functional connectivity; LEDD, levodopa-equivalent daily dosage; UPDRS, Unified Parkinson Disease Rating Scale Part-III; AF, Animal Fluency test; LSF, Letter S Fluency Test; MMSE, Mini Mental State Examination; AQT, A Quick Test of Cognitive Speed; DD, disease duration.

Appendix Table 13: Estimated corpus callosal streamline thicknesses and corresponding corrected *p*-values for pairwise comparisons - Controls and PD-CU

Node	Controls (mm)	PD-CU (mm)	*p*-value	Node	Controls (mm)	PD-CU (mm)	*p*-value
11	9.451	9.883	1	**51**	5.099	5.198	1
12	9.009	9.35	1	**52**	5.026	5.116	1
13	8.607	8.924	1	**53**	5.06	5.111	1
14	8.244	8.448	1	**54**	5.09	5.091	1
15	7.879	8.071	1	**55**	5.042	5.159	1
16	7.552	7.731	1	**56**	5.033	5.184	1
17	7.184	7.345	1	**57**	5.008	5.202	1
18	6.896	7.036	1	**58**	4.978	5.09	1
19	6.611	6.704	1	**59**	4.954	5.042	1
20	6.219	6.342	1	**60**	4.92	5.012	1
21	5.925	6.033	1	**61**	4.875	5.015	1

22	5.67	5.647	1	**62**	4.82	4.922	1
23	5.351	5.381	1	**63**	4.823	4.897	1
24	5.049	5.058	1	**64**	4.855	4.872	1
25	4.752	4.855	1	**65**	4.769	4.928	1
26	4.544	4.631	1	**66**	4.708	4.958	1
27	4.356	4.373	1	**67**	4.761	4.928	1
28	4.132	4.186	1	**68**	4.752	4.905	1
29	4.031	4.038	1	**69**	4.69	4.946	1
30	3.968	4.031	1	**70**	4.683	4.972	1
31	3.949	4.017	1	**71**	4.769	5	1
32	3.944	4.038	1	**72**	4.885	5.014	1
33	3.975	4.076	1	**73**	4.921	5.087	1
34	4.04	4.096	1	**74**	5.082	5.145	1
35	4.154	4.182	1	**75**	5.179	5.202	1
36	4.214	4.278	1	**76**	5.226	5.275	1
37	4.297	4.447	1	**77**	5.343	5.389	1
38	4.314	4.588	1	**78**	5.449	5.52	1
39	4.429	4.654	1	**79**	5.539	5.695	1
40	4.562	4.729	1	**80**	5.633	5.79	1
41	4.632	4.915	1	**81**	5.696	5.97	1
42	4.762	5.04	1	**82**	5.909	6.219	1
43	4.885	5.108	1	**83**	6.181	6.558	1
44	4.868	5.098	1	**84**	6.605	6.968	1
45	4.977	5.12	1	**85**	7.067	7.462	1
46	5.033	5.195	1	**86**	7.72	8.113	1
47	5.084	5.247	1	**87**	8.512	8.844	1
48	5.095	5.259	1	**88**	9.066	9.36	1
49	5.164	5.206	1	**89**	8.67	9.174	1
50	5.127	5.135	1	**90**	7.393	7.954	0.831

Key: Estimated corpus callosal streamlines and associated pairwise comparison *p*-values, adjusted using the Bonferroni method. Covariates in the model are evaluated at the following values: age = 70.407, eTIV = 1577849.18 mm^3.

Appendix Table 14: Estimated corpus callosal streamline thicknesses and corresponding corrected *p*-values for pairwise comparisons - Controls and PD-MCI

Node	Controls (mm)	PD-MCI (mm)	*p*-value	Node	Controls (mm)	PD-MCI (mm)	*p*-value
11	9.451	9.891	1	**51**	5.099	5.141	1
12	9.009	9.413	1	**52**	5.026	5.181	1
13	8.607	8.975	1	**53**	5.06	5.166	1
14	8.244	8.523	1	**54**	5.09	5.236	1
15	7.879	8.023	1	**55**	5.042	5.223	1
16	7.552	7.642	1	**56**	5.033	5.314	1
17	7.184	7.319	1	**57**	5.008	5.221	1
18	6.896	6.99	1	**58**	4.978	5.293	1
19	6.611	6.655	1	**59**	4.954	5.227	1
20	6.219	6.393	1	**60**	4.92	5.252	1
21	5.925	6.067	1	**61**	4.875	5.219	0.947
22	5.67	5.748	1	**62**	4.82	5.258	0.508
23	5.351	5.408	1	**63**	4.823	5.185	1
24	5.049	5.101	1	**64**	4.855	5.207	1
25	4.752	4.876	1	**65**	4.769	5.187	0.774
26	4.544	4.616	1	**66**	4.708	5.26	0.274

27	4.356	4.408	1	**67**	4.761	5.206	0.694
28	4.132	4.322	1	**68**	4.752	5.131	1
29	4.031	4.258	1	**69**	4.69	5.109	0.996
30	3.968	4.135	1	**70**	4.683	5.125	0.759
31	3.949	4.154	1	**71**	4.769	5.197	0.822
32	3.944	4.245	1	**72**	4.885	5.177	1
33	3.975	4.23	1	**73**	4.921	5.259	1
34	4.04	4.288	1	**74**	5.082	5.279	1
35	4.154	4.471	1	**75**	5.179	5.271	1
36	4.214	4.535	1	**76**	5.226	5.364	1
37	4.297	4.585	1	**77**	5.343	5.494	1
38	4.314	4.761	0.418	**78**	5.449	5.651	1
39	4.429	4.843	0.624	**79**	5.539	5.814	1
40	4.562	4.912	1	**80**	5.633	5.951	1
41	4.632	4.933	1	**81**	5.696	6.158	0.92
42	4.762	5.048	1	**82**	5.909	6.455	0.477
43	4.885	5.084	1	**83**	6.181	6.855	0.18
44	4.868	5.081	1	**84**	6.605	7.214	0.443
45	4.977	5.108	1	**85**	7.067	7.63	0.698
46	5.033	5.109	1	**86**	7.72	8.226	1
47	5.084	5.061	1	**87**	8.512	9.186	0.877
48	5.095	5.082	1	**88**	9.066	9.795	1
49	5.164	5.058	1	**89**	8.67	9.579	0.546
50	5.127	5.113	1	**90**	7.393	8.387	0.122

Key: Estimated corpus callosal streamlines and associated pairwise comparison *p*-values, adjusted using the Bonferroni method. Covariates in the model are evaluated at the following values: age = 70.407, eTIV = 1577849.18 mm^3.

Appendix Table 15: Estimated corpus callosal streamline thicknesses and corresponding corrected *p*-values for pairwise comparisons - Controls and PDD

Node	Controls (mm)	PDD (mm)	*p*-value	Node	Controls (mm)	PDD (mm)	*p*-value
11	9.451	8.613	1	**51**	5.099	4.569	0.189
12	9.009	8.224	1	**52**	5.026	4.529	0.274
13	8.607	8.013	1	**53**	5.06	4.509	0.234
14	8.244	7.698	1	**54**	5.09	4.463	0.128
15	7.879	7.388	1	**55**	5.042	4.43	0.144
16	7.552	7.086	1	**56**	5.033	4.557	0.5
17	7.184	6.646	1	**57**	5.008	4.568	0.689
18	6.896	6.271	1	**58**	4.978	4.606	1
19	6.611	5.984	1	**59**	4.954	4.598	1
20	6.219	5.702	1	**60**	4.92	4.584	1
21	5.925	5.467	1	**61**	4.875	4.599	1
22	5.67	5.204	1	**62**	4.82	4.577	1
23	5.351	5.014	1	**63**	4.823	4.676	1
24	5.049	4.907	1	**64**	4.855	4.731	1
25	4.752	4.74	1	**65**	4.769	4.734	1
26	4.544	4.479	1	**66**	4.708	4.665	1
27	4.356	4.29	1	**67**	4.761	4.627	1
28	4.132	4.171	1	**68**	4.752	4.67	1
29	4.031	4.007	1	**69**	4.69	4.734	1
30	3.968	3.861	1	**70**	4.683	4.759	1
31	3.949	3.725	1	**71**	4.769	4.715	1

32	3.944	3.649	1	**72**	4.885	4.675	1
33	3.975	3.696	1	**73**	4.921	4.618	1
34	4.04	3.734	1	**74**	5.082	4.622	0.951
35	4.154	3.765	0.991	**75**	5.179	4.683	0.845
36	4.214	3.925	1	**76**	5.226	4.824	1
37	4.297	4.065	1	**77**	5.343	4.946	1
38	4.314	4.078	1	**78**	5.449	5.032	1
39	4.429	4.079	1	**79**	5.539	5.243	1
40	4.562	4.153	0.879	**80**	5.633	5.465	1
41	4.632	4.286	1	**81**	5.696	5.864	1
42	4.762	4.286	0.461	**82**	5.909	6.127	1
43	4.885	4.417	0.587	**83**	6.181	6.424	1
44	4.868	4.591	1	**84**	6.605	6.782	1
45	4.977	4.662	1	**85**	7.067	7.249	1
46	5.033	4.695	1	**86**	7.72	7.891	1
47	5.084	4.735	1	**87**	8.512	8.32	1
48	5.095	4.769	1	**88**	9.066	8.584	1
49	5.164	4.658	0.433	**89**	8.67	8.49	1
50	5.127	4.607	0.277	**90**	7.393	7.747	1

Key: Estimated corpus callosal streamlines and associated pairwise comparison *p*-values, adjusted using the Bonferroni method. Covariates in the model are evaluated at the following values: age = 70.407, eTIV = 1577849.18 mm^3.

Appendix Table 16: Estimated corpus callosal streamline thicknesses and corresponding corrected *p*-values for pairwise comparisons - PD-CU and PDD

Node	PD-CU (mm)	PDD (mm)	*p*-value	Node	PD-CU (mm)	PDD (mm)	*p*-value
11	9.883	8.613	0.305	**51**	5.198	4.569	0.049*
12	9.35	8.224	0.442	**52**	5.116	4.529	0.085
13	8.924	8.013	0.784	**53**	5.111	4.509	0.114
14	8.448	7.698	1	**54**	5.091	4.463	0.097
15	8.071	7.388	1	**55**	5.159	4.43	0.032*
16	7.731	7.086	1	**56**	5.184	4.557	0.108
17	7.345	6.646	1	**57**	5.202	4.568	0.112
18	7.036	6.271	0.778	**58**	5.09	4.606	0.443
19	6.704	5.984	0.808	**59**	5.042	4.598	0.512
20	6.342	5.702	0.921	**60**	5.012	4.584	0.583
21	6.033	5.467	1	**61**	5.015	4.599	0.643
22	5.647	5.204	1	**62**	4.922	4.577	1
23	5.381	5.014	1	**63**	4.897	4.676	1
24	5.058	4.907	1	**64**	4.872	4.731	1
25	4.855	4.74	1	**65**	4.928	4.734	1
26	4.631	4.479	1	**66**	4.958	4.665	1
27	4.373	4.29	1	**67**	4.928	4.627	1
28	4.186	4.171	1	**68**	4.905	4.67	1
29	4.038	4.007	1	**69**	4.946	4.734	1
30	4.031	3.861	1	**70**	4.972	4.759	1
31	4.017	3.725	1	**71**	5	4.715	1
32	4.038	3.649	0.677	**72**	5.014	4.675	1
33	4.076	3.696	0.719	**73**	5.087	4.618	0.762
34	4.096	3.734	0.913	**74**	5.145	4.622	0.57
35	4.182	3.765	0.724	**75**	5.202	4.683	0.647
36	4.278	3.925	1	**76**	5.275	4.824	1

37	4.447	4.065	0.873	**77**	5.389	4.946	1
38	4.588	4.078	0.302	**78**	5.52	5.032	0.788
39	4.654	4.079	0.202	**79**	5.695	5.243	0.904
40	4.729	4.153	0.202	**80**	5.79	5.465	1
41	4.915	4.286	0.11	**81**	5.97	5.864	1
42	5.04	4.286	0.023*	**82**	6.219	6.127	1
43	5.108	4.417	0.069	**83**	6.558	6.424	1
44	5.098	4.591	0.354	**84**	6.968	6.782	1
45	5.12	4.662	0.538	**85**	7.462	7.249	1
46	5.195	4.695	0.422	**86**	8.113	7.891	1
47	5.247	4.735	0.411	**87**	8.844	8.32	1
48	5.259	4.769	0.46	**88**	9.36	8.584	1
49	5.206	4.658	0.255	**89**	9.174	8.49	1
50	5.135	4.607	0.208	**90**	7.954	7.747	1

Key: Estimated corpus callosal streamlines and associated pairwise comparison *p*-values, adjusted using the Bonferroni method. Covariates in the model are evaluated at the following values: age = 70.407, eTIV = 1577849.18 mm^3. *, significant difference at the $p < 0.05$ level.

Appendix Table 17: Estimated corpus callosal streamline thicknesses and corresponding corrected *p*-values for pairwise comparisons: PD-MCI and PDD

Node	PD-MCI (mm)	PDD (mm)	*p*-value	Node	PD-MCI (mm)	PDD (mm)	*p*-value
11	9.891	8.613	0.405	**51**	5.141	4.569	0.146
12	9.413	8.224	0.475	**52**	5.181	4.529	0.069
13	8.975	8.013	0.828	**53**	5.166	4.509	0.105
14	8.523	7.698	1	**54**	5.236	4.463	0.037*
15	8.023	7.388	1	**55**	5.223	4.43	0.029*
16	7.642	7.086	1	**56**	5.314	4.557	0.049*
17	7.319	6.646	1	**57**	5.221	4.568	0.146
18	6.99	6.271	1	**58**	5.293	4.606	0.115
19	6.655	5.984	1	**59**	5.227	4.598	0.147
20	6.393	5.702	0.913	**60**	5.252	4.584	0.102
21	6.067	5.467	1	**61**	5.219	4.599	0.159
22	5.748	5.204	1	**62**	5.258	4.577	0.115
23	5.408	5.014	1	**63**	5.185	4.676	0.541
24	5.101	4.907	1	**64**	5.207	4.731	0.765
25	4.876	4.74	1	**65**	5.187	4.734	0.886
26	4.616	4.479	1	**66**	5.26	4.665	0.348
27	4.408	4.29	1	**67**	5.206	4.627	0.432
28	4.322	4.171	1	**68**	5.131	4.67	0.932
29	4.258	4.007	1	**69**	5.109	4.734	1
30	4.135	3.861	1	**70**	5.125	4.759	1
31	4.154	3.725	0.785	**71**	5.197	4.715	0.849
32	4.245	3.649	0.149	**72**	5.177	4.675	0.77
33	4.23	3.696	0.26	**73**	5.259	4.618	0.321
34	4.288	3.734	0.257	**74**	5.279	4.622	0.311
35	4.471	3.765	0.094	**75**	5.271	4.683	0.544
36	4.535	3.925	0.181	**76**	5.364	4.824	0.806
37	4.585	4.065	0.397	**77**	5.494	4.946	0.738
38	4.761	4.078	0.092	**78**	5.651	5.032	0.458
39	4.843	4.079	0.055	**79**	5.814	5.243	0.556
40	4.912	4.153	0.059	**80**	5.951	5.465	0.994
41	4.933	4.286	0.145	**81**	6.158	5.864	1

42	5.048	4.286	0.039*	**82**	6.455	6.127	1
43	5.084	4.417	0.137	**83**	6.855	6.424	1
44	5.081	4.591	0.535	**84**	7.214	6.782	1
45	5.108	4.662	0.744	**85**	7.63	7.249	1
46	5.109	4.695	0.974	**86**	8.226	7.891	1
47	5.061	4.735	1	**87**	9.186	8.32	0.606
48	5.082	4.769	1	**88**	9.795	8.584	0.369
49	5.058	4.658	0.999	**89**	9.579	8.49	0.451
50	5.113	4.607	0.356	**90**	8.387	7.747	1

Key: Estimated corpus callosal streamlines and associated pairwise comparison *p*-values, adjusted using the Bonferroni method. Covariates in the model are evaluated at the following values: age = 70.407, eTIV = 1577849.18 mm^3. *, significant difference at the $p < 0.05$ level.

Appendix Table 18: Cortical thicknesses and corresponding corrected *p*-values for pairwise comparisons: Controls and PD-CU

		Hemisphere					
		Left			**Right**		
Lobe	**Cortical region**	**Ctrls (mm)**	**PD-CU (mm)**	***p*-value**	**Ctrls (mm)**	**PD-CU (mm)**	***p*-value**
Frontal	Pars orbitalis	2.571	2.518	1	2.629	2.605	1
	Medial orbitofrontal	2.356	2.335	1	2.384	2.394	1
	Lateral orbitofrontal	2.626	2.598	1	2.646	2.603	1
	Pars triangularis	2.358	2.338	1	2.366	2.389	1
	Pars opercularis	2.497	2.451	1	2.474	2.453	1
	Rostral middle frontal	2.4	2.427	1	2.375	2.399	1
	Caudal middle frontal	2.523	2.481	1	2.497	2.465	1
	Superior frontal	2.621	2.618	1	2.58	2.603	1
	Precentral	2.549	2.517	1	2.508	2.475	1
	Paracentral	2.385	2.392	1	2.354	2.353	1
Temporal	Entorhinal	3.298	3.217	1	3.42	3.317	1
	Fusiform	2.688	2.636	1	2.754	2.677	0.332
	Parahippocampal	2.767	2.706	1	2.685	2.648	1
	Superior temporal	2.732	2.738	1	2.785	2.765	1
	Transverse temporal	2.297	2.248	1	2.314	2.271	1
	Middle temporal	2.744	2.718	1	2.819	2.814	1
	Inferior temporal	2.868	2.827	1	2.892	2.851	1
	Insula	2.959	2.937	1	2.947	2.898	1
Parietal	Postcentral	2.104	2.092	1	2.055	2.073	1
	Superior parietal	2.227	2.211	1	2.184	2.205	1
	Supramarginal	2.489	2.432	0.948	2.49	2.451	1
	Inferior parietal	2.462	2.416	1	2.482	2.441	1
	Precuneus	2.335	2.315	1	2.336	2.308	1
	Cuneus	1.889	1.863	1	1.883	1.869	1
	Pericalcarine	1.547	1.561	1	1.551	1.584	1
	Lingual thickness	1.982	1.93	0.641	2.002	1.977	1
	Lateral occipital	2.275	2.241	1	2.326	2.25	0.146
Cingulate	Rostral anterior	2.696	2.679	1	2.79	2.758	1
	Caudal anterior	2.638	2.617	1	2.497	2.49	1
	Posterior	2.355	2.376	1	2.414	2.388	1
	Isthmus	2.329	2.263	1	2.362	2.29	1

Key: Cortical thicknesses estimated using a multivariate analysis of covariance model, with covariates evaluated at the following values: age = 70.407, eTIV = 1577849.18 mm^3. *p*-values were adjusted using the Bonferroni method. Ctrls, Controls.

Appendix Table 19: Cortical thicknesses and corresponding corrected *p*-values for pairwise comparisons: Controls and PD-MCI

		Hemisphere					
		Left			Right		
Lobe	Cortical region	Ctrls (mm)	PD-MCI (mm)	*p*-value	Ctrls (mm)	PD-MCI (mm)	*p*-value
Frontal	Pars orbitalis	2.571	2.498	1	2.629	2.568	1
	Medial orbitofrontal	2.356	2.303	1	2.384	2.403	1
	Lateral orbitofrontal	2.626	2.591	1	2.646	2.614	1
	Pars triangularis	2.358	2.299	0.925	2.366	2.295	0.56
	Pars opercularis	2.497	2.436	1	2.474	2.427	1
	Rostral middle frontal	2.4	2.399	1	2.375	2.373	1
	Caudal middle frontal	2.523	2.512	1	2.497	2.464	1
	Superior frontal	2.621	2.612	1	2.58	2.61	1
	Precentral	2.549	2.52	1	2.508	2.436	1
	Paracentral	2.385	2.367	1	2.354	2.374	1
Temporal	Entorhinal	3.298	3.154	0.733	3.42	3.272	0.768
	Fusiform	2.688	2.657	1	2.754	2.666	0.304
	Parahippocampal	2.767	2.697	1	2.685	2.707	1
	Superior temporal	2.732	2.761	1	2.785	2.795	1
	Transverse temporal	2.297	2.395	1	2.314	2.341	1
	Middle temporal	2.744	2.736	1	2.819	2.797	1
	Inferior temporal	2.868	2.848	1	2.892	2.838	1
	Insula	2.959	2.928	1	2.947	2.888	1
Parietal	Postcentral	2.104	2.139	1	2.055	2.068	1
	Superior parietal	2.227	2.257	1	2.184	2.206	1
	Supramarginal	2.489	2.465	1	2.49	2.429	0.926
	Inferior parietal	2.462	2.448	1	2.482	2.448	1
	Precuneus	2.335	2.318	1	2.336	2.305	1
	Cuneus	1.889	1.911	1	1.883	1.884	1
	Pericalcarine	1.547	1.577	1	1.551	1.571	1
	Lingual thickness	1.982	1.941	1	2.002	1.971	1
	Lateral occipital	2.275	2.257	1	2.326	2.304	1
Cingulate	Rostral anterior	2.696	2.711	1	2.79	2.784	1
	Caudal anterior	2.638	2.591	1	2.497	2.446	1
	Posterior	2.355	2.339	1	2.414	2.415	1
	Isthmus	2.329	2.311	1	2.362	2.308	1

Key: Cortical thicknesses estimated using a multivariate analysis of covariance model, with covariates evaluated at the following values: age = 70.407, eTIV = 1577849.18 mm^3. *p*-values were adjusted using the Bonferroni method. Ctrls, Controls.

Appendix Table 20: Cortical thicknesses and corresponding corrected *p*-values for pairwise comparisons: Controls and PDD

		Hemisphere					
		Left			Right		
Lobe	Cortical region	Ctrls (mm)	PDD (mm)	*p*-value	Ctrls (mm)	PDD (mm)	*p*-value
Frontal	Pars orbitalis	2.571	2.492	1	2.629	2.507	0.212
	Medial orbitofrontal	2.356	2.24	0.164	2.384	2.293	0.566
	Lateral orbitofrontal	2.626	2.507	0.028*	2.646	2.464	0.001*

	Pars triangularis	2.358	2.32	1	2.366	2.235	0.034*
	Pars opercularis	2.497	2.405	0.526	2.474	2.367	0.196
	Rostral middle frontal	2.4	2.336	0.815	2.375	2.276	0.061
	Caudal middle frontal	2.523	2.45	0.961	2.497	2.411	0.602
	Superior frontal	2.621	2.544	0.67	2.58	2.495	0.388
	Precentral	2.549	2.412	0.095	2.508	2.402	0.48
	Paracentral	2.385	2.319	1	2.354	2.304	1
Temporal	Entorhinal	3.298	2.913	0.002*	3.42	3.142	0.063
	Fusiform	2.688	2.459	<0.001*	2.754	2.487	<0.001*
	Parahippocampal	2.767	2.541	0.169	2.685	2.474	0.077
	Superior temporal	2.732	2.568	0.014*	2.785	2.662	0.118
	Transverse temporal	2.297	2.148	0.439	2.314	2.213	1
	Middle temporal	2.744	2.606	0.044*	2.819	2.671	0.009*
	Inferior temporal	2.868	2.684	0.005*	2.892	2.659	<0.001*
	Insula	2.959	2.77	0.023*	2.947	2.81	0.184
Parietal	Postcentral	2.104	2.087	1	2.055	2.034	1
	Superior parietal	2.227	2.173	1	2.184	2.119	1
	Supramarginal	2.489	2.372	0.132	2.49	2.341	0.011*
	Inferior parietal	2.462	2.371	0.317	2.482	2.332	0.014*
	Precuneus	2.335	2.216	0.163	2.336	2.262	0.741
	Cuneus	1.889	1.889	1	1.883	1.89	1
	Pericalcarine	1.547	1.601	1	1.551	1.561	1
	Lingual thickness	1.982	1.928	1	2.002	1.966	1
	Lateral occipital	2.275	2.201	0.43	2.326	2.266	0.897
Cingulate	Rostral anterior	2.696	2.688	1	2.79	2.751	1
	Caudal anterior	2.638	2.546	0.742	2.497	2.459	1
	Posterior	2.355	2.358	1	2.414	2.36	1
	Isthmus	2.329	2.292	1	2.362	2.323	1

Key: Cortical thicknesses estimated using a multivariate analysis of covariance model, with covariates evaluated at the following values: age = 70.407, eTIV = 1577849.18 mm^3. *p*-values were adjusted using the Bonferroni method. Ctrls, Controls; *, significant difference at the $p < 0.05$ level.

Appendix Table 21: Cortical thicknesses and corresponding corrected *p*-values for pairwise comparisons: PD-CU and PD-MCI

		Hemisphere					
		Left			**Right**		
Lobe	**Cortical region**	**PD-CU (mm)**	**PD-MCI (mm)**	***p*-value**	**PD-CU (mm)**	**PD-MCI (mm)**	***p*-value**
Frontal	Pars orbitalis	2.518	2.498	1	2.605	2.568	1
	Medial orbitofrontal	2.335	2.303	1	2.394	2.403	1
	Lateral orbitofrontal	2.598	2.591	1	2.603	2.614	1
	Pars triangularis	2.338	2.299	1	2.389	2.295	0.118
	Pars opercularis	2.451	2.436	1	2.453	2.427	1
	Rostral middle frontal	2.427	2.399	1	2.399	2.373	1
	Caudal middle frontal	2.481	2.512	1	2.465	2.464	1
	Superior frontal	2.618	2.612	1	2.603	2.61	1
	Precentral	2.517	2.52	1	2.475	2.436	1
	Paracentral	2.392	2.367	1	2.353	2.374	1
Temporal	Entorhinal	3.217	3.154	1	3.317	3.272	1
	Fusiform	2.636	2.657	1	2.677	2.666	1
	Parahippocampal	2.706	2.697	1	2.648	2.707	1
	Superior temporal	2.738	2.761	1	2.765	2.795	1

	Transverse temporal	2.248	2.395	0.234	2.271	2.341	1
	Middle temporal	2.718	2.736	1	2.814	2.797	1
	Inferior temporal	2.827	2.848	1	2.851	2.838	1
	Insula	2.937	2.928	1	2.898	2.888	1
Parietal	Postcentral	2.092	2.139	1	2.073	2.068	1
	Superior parietal	2.211	2.257	1	2.205	2.206	1
	Supramarginal	2.432	2.465	1	2.451	2.429	1
	Inferior parietal	2.416	2.448	1	2.441	2.448	1
	Precuneus	2.315	2.318	1	2.308	2.305	1
	Cuneus	1.863	1.911	1	1.869	1.884	1
	Pericalcarine	1.561	1.577	1	1.584	1.571	1
	Lingual thickness	1.93	1.941	1	1.977	1.971	1
	Lateral occipital	2.241	2.257	1	2.25	2.304	0.777
Cingulate	Rostral anterior	2.679	2.711	1	2.758	2.784	1
	Caudal anterior	2.617	2.591	1	2.49	2.446	1
	Posterior	2.376	2.339	1	2.388	2.415	1
	Isthmus	2.263	2.311	1	2.29	2.308	1

Key: Cortical thicknesses estimated using a multivariate analysis of covariance model, with covariates evaluated at the following values: age = 70.407, eTIV = 1577849.18 mm^3. *p*-values were adjusted using the Bonferroni method.

Appendix Table 22: Cortical thicknesses and corresponding corrected *p*-values for pairwise comparisons: PD-CU and PDD

		Hemisphere					
		Left			**Right**		
Lobe	**Cortical region**	**PD-CU (mm)**	**PDD (mm)**	***p*-value**	**PD-CU (mm)**	**PDD (mm)**	***p*-value**
Frontal	Pars orbitalis	2.518	2.492	1	2.605	2.507	0.468
	Medial orbitofrontal	2.335	2.24	0.352	2.394	2.293	0.306
	Lateral orbitofrontal	2.598	2.507	0.136	2.603	2.464	0.015*
	Pars triangularis	2.338	2.32	1	2.389	2.235	0.004*
	Pars opercularis	2.451	2.405	1	2.453	2.367	0.42
	Rostral middle frontal	2.427	2.336	0.176	2.399	2.276	0.006*
	Caudal middle frontal	2.481	2.45	1	2.465	2.411	1
	Superior frontal	2.618	2.544	0.665	2.603	2.495	0.086
	Precentral	2.517	2.412	0.316	2.475	2.402	1
	Paracentral	2.392	2.319	1	2.353	2.304	1
Temporal	Entorhinal	3.217	2.913	0.014	3.317	3.142	0.54
	Fusiform	2.636	2.459	0.005*	2.677	2.487	0.001*
	Parahippocampal	2.706	2.541	0.552	2.648	2.474	0.189
	Superior temporal	2.738	2.568	0.006*	2.765	2.662	0.236
	Transverse temporal	2.248	2.148	1	2.271	2.213	1
	Middle temporal	2.718	2.606	0.132	2.814	2.671	0.008*
	Inferior temporal	2.827	2.684	0.035*	2.851	2.659	0.001*
	Insula	2.937	2.77	0.044*	2.898	2.81	0.858
Parietal	Postcentral	2.092	2.087	1	2.073	2.034	1
	Superior parietal	2.211	2.173	1	2.205	2.119	0.447
	Supramarginal	2.432	2.372	1	2.451	2.341	0.09
	Inferior parietal	2.416	2.371	1	2.441	2.332	0.116
	Precuneus	2.315	2.216	0.317	2.308	2.262	1
	Cuneus	1.863	1.889	1	1.869	1.89	1
	Pericalcarine	1.561	1.601	1	1.584	1.561	1
	Lingual thickness	1.93	1.928	1	1.977	1.966	1

	Lateral occipital	2.241	2.201	1	2.25	2.266	1
Cingulate	Rostral anterior	2.679	2.688	1	2.758	2.751	1
	Caudal anterior	2.617	2.546	1	2.49	2.459	1
	Posterior	2.376	2.358	1	2.388	2.36	1
	Isthmus	2.263	2.292	1	2.29	2.323	1

Key: Cortical thicknesses estimated using a multivariate analysis of covariance model, with covariates evaluated at the following values: age = 70.407, eTIV = 1577849.18 mm^3. *p*-values were adjusted using the Bonferroni method. *, significant difference at the $p < 0.05$ level.

Appendix Table 23: Cortical thicknesses and corresponding corrected *p*-values for pairwise comparisons: PD-MCI and PDD

		Hemisphere					
		Left			**Right**		
Lobe	**Cortical region**	**PD-MCI**	**PDD**	***p*-value**	**PD-MCI**	**PDD**	***p*-value**
Frontal	Pars orbitalis	2.498	2.492	1	2.568	2.507	1
	Medial orbitofrontal	2.303	2.24	1	2.403	2.293	0.289
	Lateral orbitofrontal	2.591	2.507	0.305	2.614	2.464	0.014*
	Pars triangularis	2.299	2.32	1	2.295	2.235	1
	Pars opercularis	2.436	2.405	1	2.427	2.367	1
	Rostral middle frontal	2.399	2.336	0.951	2.373	2.276	0.085
	Caudal middle frontal	2.512	2.45	1	2.464	2.411	1
	Superior frontal	2.612	2.544	1	2.61	2.495	0.091
	Precentral	2.52	2.412	0.382	2.436	2.402	1
	Paracentral	2.367	2.319	1	2.374	2.304	1
Temporal	Entorhinal	3.154	2.913	0.14	3.272	3.142	1
	Fusiform	2.657	2.459	0.003*	2.666	2.487	0.004*
	Parahippocampal	2.697	2.541	0.831	2.707	2.474	0.047*
	Superior temporal	2.761	2.568	0.003*	2.795	2.662	0.088
	Transverse temporal	2.395	2.148	0.026*	2.341	2.213	0.983
	Middle temporal	2.736	2.606	0.085	2.797	2.671	0.048*
	Inferior temporal	2.848	2.684	0.021*	2.838	2.659	0.006*
	Insula	2.928	2.77	0.107	2.888	2.81	1
Parietal	Postcentral	2.139	2.087	1	2.068	2.034	1
	Superior parietal	2.257	2.173	0.523	2.206	2.119	0.568
	Supramarginal	2.465	2.372	0.456	2.429	2.341	0.406
	Inferior parietal	2.448	2.371	0.669	2.448	2.332	0.127
	Precuneus	2.318	2.216	0.381	2.305	2.262	1
	Cuneus	1.911	1.889	1	1.884	1.89	1
	Pericalcarine	1.577	1.601	1	1.571	1.561	1
	Lingual thickness	1.941	1.928	1	1.971	1.966	1
	Lateral occipital	2.257	2.201	1	2.304	2.266	1
Cingulate	Rostral anterior	2.711	2.688	1	2.784	2.751	1
	Caudal anterior	2.591	2.546	1	2.446	2.459	1
	Posterior	2.339	2.358	1	2.415	2.36	1
	Isthmus	2.311	2.292	1	2.308	2.323	1

Key: Cortical thicknesses estimated using a multivariate analysis of covariance model, with covariates evaluated at the following values: age = 70.407, eTIV = 1577849.18 mm^3. *p*-values were adjusted using the Bonferroni method. *, significant difference at the $p < 0.05$ level.

9. References

Aarsland, D., Brønnick, K., Larsen, J., Tysnes, O. & Alves, G. 2009. Cognitive impairment in incident, untreated Parkinson disease: the Norwegian ParkWest study. *Neurology,* 72**,** 1121-1126.

Aarsland, D., Creese, B., Politis, M., Chaudhuri, K. R., Weintraub, D. & Ballard, C. 2017. Cognitive decline in Parkinson disease. *Nature Reviews Neurology,* 13**,** 217.

Aboitiz, F., Scheibel, A. B., Fisher, R. S. & Zaidel, E. 1992. Fiber composition of the human corpus callosum. *Brain Res,* 598**,** 143-53.

Abreu-Villaca, Y., Silva, W. C., Manhaes, A. C. & Schmidt, S. L. 2002. The effect of corpus callosum agenesis on neocortical thickness and neuronal density of BALB/cCF mice. *Brain Res Bull,* 58**,** 411-6.

Adamson, C. L., Beare, R., Walterfang, M. & Seal, M. 2014. Software pipeline for midsagittal corpus callosum thickness profile processing. *Neuroinformatics,* 12**,** 595-614.

Adamson, C. L., Wood, A. G., Chen, J., Barton, S., Reutens, D. C., Pantelis, C., Velakoulis, D. & Walterfang, M. 2011. Thickness profile generation for the corpus callosum using Laplace's equation. *Hum Brain Mapp,* 32**,** 2131-40.

Agosta, F., Canu, E., Stefanova, E., Sarro, L., Tomic, A., Spica, V., Comi, G., Kostic, V. S. & Filippi, M. 2014a. Mild cognitive impairment in Parkinson's disease is associated with a distributed pattern of brain white matter damage. *Hum Brain Mapp,* 35**,** 1921-9.

Agosta, F., Caso, F., Stankovic, I., Inuggi, A., Petrovic, I., Svetel, M., Kostic, V. S. & Filippi, M. 2014b. Cortico-striatal-thalamic network functional connectivity in hemiparkinsonism. *Neurobiology of Aging,* 35**,** 2592-2602.

Albin, R. L., Young, A. B. & Penney, J. B. 1989. The functional anatomy of basal ganglia disorders. *Trends in neurosciences,* 12**,** 366-375.

Alexander, G. E., Delong, M. R. & Strick, P. L. 1986. Parallel organization of functionally segregated circuits linking basal ganglia and cortex. *Annual review of neuroscience,* 9**,** 357-381.

Almeida, O. P., Burton, E. J., Mckeith, I., Gholkar, A., Burn, D. & O'brien, J. T. 2003. MRI study of caudate nucleus volume in Parkinson's disease with and without dementia with Lewy bodies and Alzheimer's disease. *Dementia and geriatric cognitive disorders,* 16**,** 57-63.

Alvarez, L., Macias, R., Lopez, G., Alvarez, E., Pavon, N., Rodriguez-Oroz, M., Juncos, J., Maragoto, C., Guridi, J. & Litvan, I. 2005. Bilateral subthalamotomy in Parkinson's disease: initial and long-term response. *Brain,* 128**,** 570-583.

Amboni, M., Tessitore, A., Esposito, F., Santangelo, G., Picillo, M., Vitale, C., Giordano, A., Erro, R., De Micco, R. & Corbo, D. 2015. Resting-state functional connectivity associated with mild cognitive impairment in Parkinson's disease. *Journal of neurology,* 262**,** 425-434.

Andersson, J. L. R., Jenkinson, M. & Smith, S. M. 2007a. Non-linear optimisation. *FMRIB technical report TR07JA1*.

Andersson, J. L. R., Jenkinson, M. & Smith, S. M. 2007b. Non-linear optimisation, aka spatial normalisation. *FMRIB technical report TR07JA2*.

Apostolova, L. G., Beyer, M., Green, A. E., Hwang, K. S., Morra, J. H., Chou, Y. Y., Avedissian, C., Aarsland, D., Janvin, C. C. & Larsen, J. P. 2010. Hippocampal, caudate, and ventricular changes in Parkinson's disease with and without dementia. *Movement Disorders,* 25**,** 687-695.

Apostolova, L. G., Dinov, I. D., Dutton, R. A., Hayashi, K. M., Toga, A. W., Cummings, J. L. & Thompson, P. M. 2006. 3D comparison of hippocampal atrophy in amnestic mild cognitive impairment and Alzheimer's disease. *Brain,* 129**,** 2867-73.

Ardekani, B. A., Bachman, A. H., Figarsky, K. & Sidtis, J. J. 2014. Corpus callosum shape changes in early Alzheimer's disease: an MRI study using the OASIS brain database. *Brain structure & function,* 219**,** 343-352.

Atkinson-Clement, C., Pinto, S., Eusebio, A. & Coulon, O. 2017. Diffusion tensor imaging in Parkinson's disease: Review and meta-analysis. *Neuroimage Clin,* 16**,** 98-110.

Aylward, E. H., Li, Q., Stine, O. C., Ranen, N., Sherr, M., Barta, P. E., Bylsma, F. W., Pearlson, G. D. & Ross, C. A. 1997. Longitudinal change in basal ganglia volume in patients with Huntington's disease. *Neurology,* 48**,** 394-9.

Aziz, T. Z., Peggs, D., Sambrook, M. & Crossman, A. 1991. Lesion of the subthalamic nucleus for the alleviation of 1-methyl-4-phenyl-1, 2, 3, 6-tetrahydropyridine (MPTP)-induced parkinsonism in the primate. *Movement disorders: official journal of the Movement Disorder Society,* 6**,** 288-292.

Badea, L., Onu, M., Wu, T., Roceanu, A. & Bajenaru, O. 2017. Exploring the reproducibility of functional connectivity alterations in Parkinson's disease. *PLoS ONE,* 12**,** e0188196.

Baliyan, V., Das, C. J., Sharma, R. & Gupta, A. K. 2016. Diffusion weighted imaging: Technique and applications. *World journal of radiology,* 8**,** 785-798.

Bandettini, P. A., Jesmanowicz, A., Wong, E. C. & Hyde, J. S. 1993. Processing strategies for time-course data sets in functional MRI of the human brain. *Magnetic resonance in medicine,* 30**,** 161-173.

Barker, R. A. & Williams-Gray, C. H. 2016. Review: The spectrum of clinical features seen with alpha synuclein pathology. *Neuropathol Appl Neurobiol,* 42**,** 6-19.

Basser, P. J. & Pierpaoli, C. 1996. Microstructural and physiological features of tissues elucidated by quantitative-diffusion-tensor MRI. *Journal of magnetic resonance, Series B,* 111**,** 209-219.

Beckmann, C. F., Deluca, M., Devlin, J. T. & Smith, S. M. 2005. Investigations into resting-state connectivity using independent component analysis. *Philos Trans R Soc Lond B Biol Sci,* 360**,** 1001-13.

Beckmann, C. F. & Smith, S. M. 2004. Probabilistic independent component analysis for functional magnetic resonance imaging. *IEEE Trans Med Imaging,* 23**,** 137-52.

Behrens, T. E., Johansen-Berg, H., Woolrich, M. W., Smith, S. M., Wheeler-Kingshott, C. A., Boulby, P. A., Barker, G. J., Sillery, E. L., Sheehan, K., Ciccarelli, O., Thompson, A. J., Brady, J. M. & Matthews, P. M. 2003. Non-invasive mapping of connections between human thalamus and cortex using diffusion imaging. *Nature Neuroscience,* 6**,** 750-7.

Bell, P. T., Gilat, M., O'callaghan, C., Copland, D. A., Frank, M. J., Lewis, S. J. G. & Shine, J. M. 2015. Dopaminergic basis for impairments in functional connectivity across subdivisions of the striatum in Parkinson's disease. *Human Brain Mapping,* 36**,** 1278-1291.

Bergman, H., Wichmann, T. & Delong, M. R. 1990. Reversal of experimental parkinsonism by lesions of the subthalamic nucleus. *Science,* 249**,** 1436-1438.

Bestmann, S., Swayne, O., Blankenburg, F., Ruff, C. C., Teo, J., Weiskopf, N., Driver, J., Rothwell, J. C. & Ward, N. S. 2010. The role of contralesional dorsal premotor cortex after stroke as studied with concurrent TMS-fMRI. *Journal of Neuroscience,* 30**,** 11926-11937.

Bianciardi, M., Fukunaga, M., Van Gelderen, P., Horovitz, S. G., De Zwart, J. A., Shmueli, K. & Duyn, J. H. 2009. Sources of functional magnetic resonance imaging signal fluctuations in the human brain at rest: a 7 T study. *Magnetic Resonance Imaging,* 27**,** 1019-1029.

Birn, R. M., Murphy, K. & Bandettini, P. A. 2008. The effect of respiration variations on independent component analysis results of resting state functional connectivity. *Human Brain Mapping,* 29**,** 740-50.

Biswal, B., Yetkin, F. Z., Haughton, V. M. & Hyde, J. S. 1995. Functional connectivity in the motor cortex of resting human brain using echo-planar MRI. *Magn Reson Med,* 34**,** 537-41.

Blazejewska, A. I., Schwarz, S. T., Pitiot, A., Stephenson, M. C., Lowe, J., Bajaj, N., Bowtell, R. W., Auer, D. P. & Gowland, P. A. 2013. Visualization of nigrosome 1 and its loss in PD: pathoanatomical correlation and in vivo 7 T MRI. *Neurology,* 81**,** 534-40.

Bledsoe, I. O., Stebbins, G. T., Merkitch, D. & Goldman, J. G. 2018. White matter abnormalities in the corpus callosum with cognitive impairment in Parkinson disease. *Neurology,* 91**,** e2244-e2255.

Bohnen, N. I. & Albin, R. L. 2009. Cholinergic denervation occurs early in Parkinson disease. AAN Enterprises.

Bolam, J. P. & Pissadaki, E. K. 2012. Living on the edge with too many mouths to feed: why dopamine neurons die. *Movement Disorders,* 27**,** 1478-1483.

Bookstein, F. L. 1997. Shape and the Information in Medical Images: A Decade of the Morphometric Synthesis. *Computer Vision and Image Understanding,* 66**,** 97-118.

Bouwmans, A. E., Vlaar, A. M., Mess, W. H., Kessels, A. & Weber, W. E. 2013. Specificity and sensitivity of transcranial sonography of the substantia nigra in the diagnosis of Parkinson's disease: prospective cohort study in 196 patients. *BMJ open,* 3**,** e002613.

Braak, H. & Del Tredici, K. 2008. Cortico-basal ganglia-cortical circuitry in Parkinson's disease reconsidered. *Experimental neurology,* 212**,** 226-229.

Braak, H., Del Tredici, K., Rüb, U., De Vos, R. A., Jansen Steur, E. N. & Braak, E. 2003. Staging of brain pathology related to sporadic Parkinson's disease. *Neurobiology of Aging,* 24**,** 197-211.

Brechbühler, C., Gerig, G. & Kübler, O. 1995. Parametrization of Closed Surfaces for 3-D Shape Description. *Computer Vision and Image Understanding,* 61**,** 154-170.

Broeders, M., De Bie, R., Velseboer, D. C., Speelman, J. D., Muslimovic, D. & Schmand, B. 2013. Evolution of mild cognitive impairment in Parkinson disease. *Neurology,* 81**,** 346-352.

Brundin, P. & Melki, R. 2017. Prying into the prion hypothesis for Parkinson's disease. *Journal of Neuroscience,* 37**,** 9808-9818.

Brundin, P., Melki, R. & Kopito, R. 2010. Prion-like transmission of protein aggregates in neurodegenerative diseases. *Nature reviews Molecular cell biology,* 11**,** 301.

Buckner, R. L., Sepulcre, J., Talukdar, T., Krienen, F. M., Liu, H., Hedden, T., Andrews-Hanna, J. R., Sperling, R. A. & Johnson, K. A. 2009. Cortical hubs revealed by intrinsic functional connectivity: mapping, assessment of stability, and relation to Alzheimer's disease. *Journal of Neuroscience,* 29**,** 1860-1873.

Bullmore, E. & Sporns, O. 2009. Complex brain networks: graph theoretical analysis of structural and functional systems. *Nature reviews neuroscience,* 10**,** 186.

Burton, E. J., Mckeith, I. G., Burn, D. J., Williams, E. D. & O'brien, J. T. 2004. *Cerebral atrophy in Parkinson's disease with and without dementia: a comparison with Alzheimer's disease, dementia with Lewy bodies and controls*.

Caballero-Gaudes, C. & Reynolds, R. C. 2017. Methods for cleaning the BOLD fMRI signal. *Neuroimage,* 154**,** 128-149.

Caligiore, D., Helmich, R. C., Hallett, M., Moustafa, A. A., Timmermann, L., Toni, I. & Baldassarre, G. 2016. Parkinson's disease as a system-level disorder. *npj Parkinson's Disease,* 2**,** 16025.

Carrera, E. & Tononi, G. 2014. Diaschisis: past, present, future. *Brain,* 137**,** 2408-22.

Caspers, J., Mathys, C., Hoffstaedter, F., Südmeyer, M., Cieslik, E. C., Rubbert, C., Hartmann, C. J., Eickhoff, C. R., Reetz, K., Grefkes, C., Michely, J., Turowski, B., Schnitzler, A. & Eickhoff, S. B. 2017. Differential Functional Connectivity Alterations of Two Subdivisions within the Right dlPFC in Parkinson's Disease. *Frontiers in Human Neuroscience,* 11**,** 288.

Chang, D., Nalls, M. A., Hallgrímsdóttir, I. B., Hunkapiller, J., Van Der Brug, M., Cai, F., International Parkinson's Disease Genomics, C., Andme Research, T., Kerchner, G. A., Ayalon, G., Bingol, B., Sheng, M., Hinds, D., Behrens, T. W., Singleton, A. B., Bhangale, T. R. & Graham, R. R. 2017. A meta-analysis of genome-wide association studies identifies 17 new Parkinson's disease risk loci. *Nature genetics,* 49**,** 1511-1516.

Chen, F. X., Kang, D. Z., Chen, F. Y., Liu, Y., Wu, G., Li, X., Yu, L. H., Lin, Y. X. & Lin, Z. Y. 2016. Gray matter atrophy associated with mild cognitive impairment in Parkinson's disease. *Neuroscience Letters,* 617**,** 160-5.

Chen, X., Lu, B. & Yan, C. G. 2018. Reproducibility of R-fMRI metrics on the impact of different strategies for multiple comparison correction and sample sizes. *Human brain mapping,* 39**,** 300-318.

Chiang, M. C., Dutton, R. A., Hayashi, K. M., Lopez, O. L., Aizenstein, H. J., Toga, A. W., Becker, J. T. & Thompson, P. M. 2007. 3D pattern of brain atrophy in HIV/AIDS visualized using tensor-based morphometry. *Neuroimage,* 34**,** 44-60.

Cohen, J. 1992. Statistical power analysis. *Current directions in psychological science,* 1**,** 98-101.

Coleman, M. P. & Freeman, M. R. 2010. Wallerian degeneration, wld(s), and nmnat. *Annual review of neuroscience,* 33**,** 245-267.

Compta, Y., Parkkinen, L., O'sullivan, S. S., Vandrovcova, J., Holton, J. L., Collins, C., Lashley, T., Kallis, C., Williams, D. R. & De Silva, R. 2011. Lewy-and Alzheimer-type pathologies in Parkinson's disease dementia: which is more important? *Brain,* 134**,** 1493-1505.

Connolly, B. S. & Lang, A. E. 2014. Pharmacological treatment of Parkinson disease: a review. *Jama,* 311**,** 1670-1683.

Cootes, T. F., Taylor, C. J., Cooper, D. H. & Graham, J. 1995. Active Shape Models-Their Training and Application. *Computer Vision and Image Understanding,* 61**,** 38-59.

Cowan, W. 1970. Anterograde and retrograde transneuronal degeneration in the central and peripheral nervous system. *Contemporary research methods in neuroanatomy.* Springer.

Cox, R. W. 1996. AFNI: software for analysis and visualization of functional magnetic resonance neuroimages. *Comput Biomed Res,* 29**,** 162-73.

Cronin-Golomb, A. & Braun, A. E. 1997. Visuospatial dysfunction and problem solving in Parkinson's disease. *Neuropsychology,* 11**,** 44.

Crossley, N. A., Mechelli, A., Scott, J., Carletti, F., Fox, P. T., Mcguire, P. & Bullmore, E. T. 2014. The hubs of the human connectome are generally implicated in the anatomy of brain disorders. *Brain,* 137**,** 2382-95.

Cunningham, S. I., Tomasi, D. & Volkow, N. D. 2017. Structural and functional connectivity of the precuneus and thalamus to the default mode network. *Hum Brain Mapp,* 38**,** 938-956.

Dale, A. M., Fischl, B. & Sereno, M. I. 1999. Cortical surface-based analysis. I. Segmentation and surface reconstruction. *Neuroimage,* 9**,** 179-94.

Damoiseaux, J. S., Rombouts, S. a. R. B., Barkhof, F., Scheltens, P., Stam, C. J., Smith, S. M. & Beckmann, C. F. 2006. Consistent resting-state networks across healthy subjects. *Proceedings of the National Academy of Sciences of the United States of America,* 103**,** 13848-13853.

Delong, M. & Wichmann, T. 2009. Update on models of basal ganglia function and dysfunction. *Parkinsonism & Related Disorders,* 15**,** S237-S240.

Delong, M. R. 1990. Primate models of movement disorders of basal ganglia origin. *Trends in neurosciences,* 13**,** 281-285.

Delong, M. R. & Georgopoulos, A. P. 1981. Motor functions of the basal ganglia. *Handbook of physiology,* 2**,** 1017-61.

Desikan, R. S., Segonne, F., Fischl, B., Quinn, B. T., Dickerson, B. C., Blacker, D., Buckner, R. L., Dale, A. M., Maguire, R. P., Hyman, B. T., Albert, M. S. & Killiany, R. J. 2006. An automated labeling system for subdividing the human cerebral cortex on MRI scans into gyral based regions of interest. *Neuroimage,* 31**,** 968-80.

Di Paola, M., Luders, E., Cherubini, A., Sanchez-Castaneda, C., Thompson, P. M., Toga, A. W., Caltagirone, C., Orobello, S., Elifani, F., Squitieri, F. & Sabatini, U. 2012. Multimodal MRI Analysis of the Corpus Callosum Reveals White Matter Differences in Presymptomatic and Early Huntington's Disease. *Cerebral Cortex,* 22**,** 2858-2866.

Di Paola, M., Luders, E., Di Iulio, F., Cherubini, A., Passafiume, D., Thompson, P. M., Caltagirone, C., Toga, A. W. & Spalletta, G. 2010. Callosal atrophy in mild cognitive impairment and Alzheimer's disease: different effects in different stages. *Neuroimage,* 49**,** 141-9.

Dias, V., Junn, E. & Mouradian, M. M. 2013. The role of oxidative stress in Parkinson's disease. *Journal of Parkinson's disease,* 3**,** 461-491.

Dickerson, B. C., Bakkour, A., Salat, D. H., Feczko, E., Pacheco, J., Greve, D. N., Grodstein, F., Wright, C. I., Blacker, D. & Rosas, H. D. 2008. The cortical signature of Alzheimer's disease: regionally specific cortical thinning relates to symptom severity in very mild to mild AD dementia and is detectable in asymptomatic amyloid-positive individuals. *Cerebral cortex,* 19**,** 497-510.

Dickson, D. W., Braak, H., Duda, J. E., Duyckaerts, C., Gasser, T., Halliday, G. M., Hardy, J., Leverenz, J. B., Del Tredici, K. & Wszolek, Z. K. 2009. Neuropathological assessment of Parkinson's disease: refining the diagnostic criteria. *The Lancet Neurology,* 8**,** 1150-1157.

Dissanayaka, N. N., Sellbach, A., Matheson, S., O'sullivan, J. D., Silburn, P. A., Byrne, G. J., Marsh, R. & Mellick, G. D. 2010. Anxiety disorders in Parkinson's disease: prevalence and risk factors. *Movement Disorders,* 25**,** 838-845.

Doron, K. W. & Gazzaniga, M. S. 2008. Neuroimaging techniques offer new perspectives on callosal transfer and interhemispheric communication. *Cortex,* 44**,** 1023-9.

Dorsey, E. R., Elbaz, A., Nichols, E., Abd-Allah, F., Abdelalim, A., Adsuar, J. C., Ansha, M. G., Brayne, C., Choi, J.-Y. J., Collado-Mateo, D., Dahodwala, N., Do, H. P., Edessa, D., Endres, M., Fereshtehnejad, S.-M., Foreman, K. J., Gankpe, F. G., Gupta, R., Hankey, G. J., Hay, S. I., Hegazy, M. I., Hibstu, D. T., Kasaeian, A., Khader, Y., Khalil, I., Khang, Y.-H., Kim, Y. J., Kokubo, Y., Logroscino, G., Massano, J., Mohamed Ibrahim, N., Mohammed, M. A., Mohammadi, A., Moradi-Lakeh, M., Naghavi, M., Nguyen, B. T., Nirayo, Y. L., Ogbo, F. A., Owolabi, M. O., Pereira, D. M., Postma, M. J., Qorbani, M., Rahman, M. A., Roba, K. T., Safari, H., Safiri, S., Satpathy, M., Sawhney, M., Shafieesabet, A., Shiferaw, M. S., Smith, M., Szoeke, C. E. I., Tabarés-Seisdedos, R., Truong, N. T., Ukwaja, K. N., Venketasubramanian, N., Villafaina, S., Weldegwergs, K. G., Westerman, R., Wijeratne, T., Winkler, A. S., Xuan, B. T., Yonemoto, N., Feigin, V. L., Vos, T. & Murray, C. J. L. 2018. Global, regional, and national burden of Parkinson's disease, 1990-2016: a systematic analysis for the Global Burden of Disease Study 2016. *The Lancet Neurology,* 17**,** 939-953.

Draganski, B., Kherif, F., Klöppel, S., Cook, P. A., Alexander, D. C., Parker, G. J., Deichmann, R., Ashburner, J. & Frackowiak, R. S. 2008. Evidence for segregated and integrative connectivity patterns in the human basal ganglia. *The Journal of Neuroscience,* 28**,** 7143-7152.

Du, A.-T., Schuff, N., Kramer, J. H., Rosen, H. J., Gorno-Tempini, M. L., Rankin, K., Miller, B. L. & Weiner, M. W. 2007. Different regional patterns of cortical thinning in Alzheimer's disease and frontotemporal dementia. *Brain,* 130**,** 1159-1166.

Dujardin, K., Degreef, J. F., Rogelet, P., Defebvre, L. & Destee, A. 1999. Impairment of the supervisory attentional system in early untreated patients with Parkinson’s disease. *Journal of neurology,* 246**,** 783-788.

Duval, C., Daneault, J.-F., Hutchison, W. D. & Sadikot, A. F. 2016. A brain network model explaining tremor in Parkinson's disease. *Neurobiology of Disease,* 85**,** 49-59.

Duvernoy, H. M. 2012. *The human brain: surface, three-dimensional sectional anatomy with MRI, and blood supply*, Springer Science & Business Media.

Eckert, T., Tang, C. & Eidelberg, D. 2007. Assessment of the progression of Parkinson's disease: a metabolic network approach. *Lancet Neurol,* 6**,** 926-32.

Eklund, A., Nichols, T. E. & Knutsson, H. 2016. Cluster failure: Why fMRI inferences for spatial extent have inflated false-positive rates. *Proceedings of the National Academy of Sciences,* 113**,** 7900-7905.

Emre, M. 2014. Dementia in Parkinson's Disease. *Neurobiology of Aging,* 35**,** 716.

Emre, M., Aarsland, D., Brown, R., Burn, D. J., Duyckaerts, C., Mizuno, Y., Broe, G. A., Cummings, J., Dickson, D. W., Gauthier, S., Goldman, J., Goetz, C., Korczyn, A., Lees, A., Levy, R., Litvan, I., Mckeith, I., Olanow, W., Poewe, W., Quinn, N., Sampaio, C., Tolosa, E. & Dubois, B. 2007. Clinical diagnostic

criteria for dementia associated with Parkinson's disease. *Movment Disorders,* 22**,** 1689-707; quiz 1837.

Esposito, F., Tessitore, A., Giordano, A., De Micco, R., Paccone, A., Conforti, R., Pignataro, G., Annunziato, L. & Tedeschi, G. 2013. Rhythm-specific modulation of the sensorimotor network in drug-naïve patients with Parkinson's disease by levodopa. *Brain,* 136**,** 710-725.

Fahn, S. & Elton, R. (eds.) 1987. *Members of the UPDRS development committee: The unified Parkison disease rating scale,* Florham Park, NJ.: Macmillan Health Care Information.

Fair, D. A., Cohen, A. L., Dosenbach, N. U., Church, J. A., Miezin, F. M., Barch, D. M., Raichle, M. E., Petersen, S. E. & Schlaggar, B. L. 2008. The maturing architecture of the brain's default network. *Proceedings of the National Academy of Sciences,* 105**,** 4028-4032.

Fénelon, G., Soulas, T., Zenasni, F. & De Langavant, L. C. 2010. The changing face of Parkinson's disease-associated psychosis: a cross-sectional study based on the new NINDS-NIMH criteria. *Movement Disorders,* 25**,** 763-766.

Fine, J., Duff, J., Chen, R., Hutchison, W., Lozano, A. M. & Lang, A. E. 2000. Long-term follow-up of unilateral pallidotomy in advanced Parkinson's disease. *New England Journal of Medicine,* 342**,** 1708-1714.

Fischl, B. 2012. FreeSurfer. *Neuroimage,* 62**,** 774-781.

Fischl, B. & Dale, A. M. 2000. Measuring the thickness of the human cerebral cortex from magnetic resonance images. *Proceedings of the National Academy of Sciences,* 97**,** 11050-5.

Fischl, B., Liu, A. & Dale, A. M. 2001. Automated manifold surgery: constructing geometrically accurate and topologically correct models of the human cerebral cortex. *IEEE Trans Med Imaging,* 20**,** 70-80.

Fischl, B., Salat, D. H., Van Der Kouwe, A. J., Makris, N., Segonne, F., Quinn, B. T. & Dale, A. M. 2004. Sequence-independent segmentation of magnetic resonance images. *Neuroimage,* 23 Suppl 1**,** S69-84.

Fischl, B., Sereno, M. I., Tootell, R. B. H. & Dale, A. M. 1999. High-resolution intersubject averaging and a coordinate system for the cortical surface. *Human Brain Mapping,* 8**,** 272-284.

Folstein, M. F., Folstein, S. E. & Mchugh, P. R. 1975. "Mini-mental state": a practical method for grading the cognitive state of patients for the clinician. *Journal of psychiatric research,* 12**,** 189-198.

Foltynie, T., Brayne, C. E., Robbins, T. W. & Barker, R. A. 2004. The cognitive ability of an incident cohort of Parkinson's patients in the UK. The CamPaIGN study. *Brain,* 127**,** 550-560.

Fornito, A., Yucel, M., Wood, S., Stuart, G. W., Buchanan, J. A., Proffitt, T., Anderson, V., Velakoulis, D. & Pantelis, C. 2004. Individual differences in anterior cingulate/paracingulate morphology are related to executive functions in healthy males. *Cereb Cortex,* 14**,** 424-31.

Fornito, A., Zalesky, A. & Breakspear, M. 2015. The connectomics of brain disorders. *Nat Rev Neurosci,* 16**,** 159-72.

Fox, M. D. & Raichle, M. E. 2007. Spontaneous fluctuations in brain activity observed with functional magnetic resonance imaging. *Nat Rev Neurosci,* 8**,** 700-11.

Frank, M. J. 2005. Dynamic dopamine modulation in the basal ganglia: a neurocomputational account of cognitive deficits in medicated and nonmedicated Parkinsonism. *J Cogn Neurosci,* 17**,** 51-72.

Friston, K. J., Frith, C. D., Liddle, P. F. & Frackowiak, R. S. 1993. Functional connectivity: the principal-component analysis of large (PET) data sets. *J Cereb Blood Flow Metab,* 13**,** 5-14.

Friston, K. J., Holmes, A. P., Worsley, K. J., Poline, J. P., Frith, C. D. & Frackowiak, R. S. 1994. Statistical parametric maps in functional imaging: a general linear approach. *Human brain mapping,* 2**,** 189-210.

Gao, H.-M., Kotzbauer, P. T., Uryu, K., Leight, S., Trojanowski, J. Q. & Lee, V. M.-Y. 2008. Neuroinflammation and oxidation/nitration of α-synuclein linked to dopaminergic neurodegeneration. *Journal of Neuroscience,* 28**,** 7687-7698.

Gao, L.-L. & Wu, T. 2016. The study of brain functional connectivity in Parkinson's disease. *Translational neurodegeneration,* 5**,** 18-18.

Garg, A., Appel-Cresswell, S., Popuri, K., Mckeown, M. J. & Beg, M. F. 2015. Morphological alterations in the caudate, putamen, pallidum, and thalamus in Parkinson's disease. *Frontiers in Neuroscience,* 9.

Geevarghese, R., Lumsden, D. E., Hulse, N., Samuel, M. & Ashkan, K. 2014. Subcortical Structure Volumes and Correlation to Clinical Variables in Parkinson's Disease. *Journal of Neuroimaging*.

Gelb, D. J., Oliver, E. & Gilman, S. 1999. Diagnostic criteria for Parkinson disease. *Archives of neurology,* 56**,** 33-39.

Geng, D.-Y., Li, Y.-X. & Zee, C.-S. 2006. Magnetic resonance imaging-based volumetric analysis of basal ganglia nuclei and substantia nigra in patients with Parkinson's disease. *Neurosurgery,* 58**,** 256-262.

Genovese, C. R., Lazar, N. A. & Nichols, T. 2002. Thresholding of statistical maps in functional neuroimaging using the false discovery rate. *Neuroimage,* 15**,** 870-878.

Gerig, G., Styner, M., Shenton, M. E. & Lieberman, J. A. Shape versus size: Improved understanding of the morphology of brain structures. Medical Image Computing and Computer-Assisted Intervention–MICCAI 2001, 2001. Springer, 24-32.

Goldman, J. G., Bledsoe, I. O., Merkitch, D., Dinh, V., Bernard, B. & Stebbins, G. T. 2017. Corpus callosal atrophy and associations with cognitive impairment in Parkinson disease. *Neurology,* 88**,** 1265-1272.

Goldman, J. G., Holden, S. K., Litvan, I., Mckeith, I., Stebbins, G. T. & Taylor, J. P. 2018. Evolution of diagnostic criteria and assessments for Parkinson's disease mild cognitive impairment. *Movement Disorders,* 33**,** 503-510.

Goldstein, A. & Mesfin, F. B. 2019. Neuroanatomy, Corpus Callosum. *StatPearls.* Treasure Island (FL): StatPearls Publishing

StatPearls Publishing LLC.

Gomperts, S. N. 2016. Lewy Body Dementias: Dementia With Lewy Bodies and Parkinson Disease Dementia. *Continuum (Minneapolis, Minn.),* 22**,** 435-463.

Gorges, M., Muller, H. P., Lule, D., Pinkhardt, E. H., Ludolph, A. C. & Kassubek, J. 2015. To rise and to fall: functional connectivity in cognitively normal and cognitively impaired patients with Parkinson's disease. *Neurobiology of Aging,* 36**,** 1727-1735.

Göttlich, M., Münte, T. F., Heldmann, M., Kasten, M., Hagenah, J. & Krämer, U. M. 2013. Altered Resting State Brain Networks in Parkinson's Disease. *PLOS ONE,* 8**,** e77336.

Gozzo, S., Renzi, P. & D'udine 1979. Morphological differences in cerebral cortex and corpus callosum are genetically determined in two different strains of mice. *Int J Neurosci,* 9**,** 91-6.

Gray, R., Ives, N., Rick, C., Patel, S., Gray, A., Jenkinson, C., Mcintosh, E., Wheatley, K., Williams, A. & Clarke, C. 2014. PD Med Collaborative Group. Long-term effectiveness of dopamine agonists and monoamine oxidase B inhibitors compared with levodopa as initial treatment for Parkinson's disease (PD MED): a large, open-label, pragmatic randomised trial. *Lancet,* 384**,** 1196-1205.

Greenland, J. C., Williams-Gray, C. H. & Barker, R. A. 2019. The clinical heterogeneity of Parkinson's disease and its therapeutic implications. *European Journal of Neuroscience,* 49**,** 328-338.

Greicius, M. D., Krasnow, B., Reiss, A. L. & Menon, V. 2003. Functional connectivity in the resting brain: a network analysis of the default mode hypothesis. *Proc Natl Acad Sci U S A,* 100**,** 253-8.

Greicius, M. D., Srivastava, G., Reiss, A. L. & Menon, V. 2004. Default-mode network activity distinguishes Alzheimer's disease from healthy aging: Evidence from functional MRI. *Proceedings of the National Academy of Sciences of the United States of America,* 101**,** 4637-4642.

Greve, D. N. & Fischl, B. 2009. Accurate and robust brain image alignment using boundary-based registration. *Neuroimage,* 48**,** 63-72.

Griffanti, L., Salimi-Khorshidi, G., Beckmann, C. F., Auerbach, E. J., Douaud, G., Sexton, C. E., Zsoldos, E., Ebmeier, K. P., Filippini, N., Mackay, C. E., Moeller, S., Xu, J., Yacoub, E., Baselli, G., Ugurbil, K., Miller, K. L. & Smith, S. M. 2014. ICA-based artefact removal and accelerated fMRI acquisition for improved resting state network imaging. *Neuroimage,* 95**,** 232-47.

Gronenschild, E. H. B. M., Habets, P., Jacobs, H. I. L., Mengelers, R., Rozendaal, N., Van Os, J. & Marcelis, M. 2012. The Effects of FreeSurfer Version, Workstation Type, and Macintosh Operating System Version on Anatomical Volume and Cortical Thickness Measurements. *PLOS ONE,* 7**,** e38234.

Guan, X., Zeng, Q., Guo, T., Wang, J., Xuan, M., Gu, Q., Wang, T., Huang, P., Xu, X. & Zhang, M. 2017. Disrupted Functional Connectivity of Basal Ganglia across Tremor-Dominant and Akinetic/Rigid-Dominant Parkinson's Disease. *Front Aging Neurosci,* 9**,** 360.

Guenette, J. P., Stern, R. A., Tripodis, Y., Chua, A. S., Schultz, V., Sydnor, V. J., Somes, N., Karmacharya, S., Lepage, C., Wrobel, P., Alosco, M. L., Martin, B. M., Chaisson, C. E., Coleman, M. J., Lin, A. P., Pasternak, O., Makris, N., Shenton, M. E. & Koerte, I. K. 2018. Automated versus manual segmentation of brain region volumes in former football players. *NeuroImage: Clinical,* 18**,** 888-896.

Haber, S. N. 2003. The primate basal ganglia: parallel and integrative networks. *Journal of chemical neuroanatomy,* 26**,** 317-330.

Haber, S. N. & Calzavara, R. 2009. The cortico-basal ganglia integrative network: the role of the thalamus. *Brain research bulletin,* 78**,** 69-74.

Hacker, C. D., Perlmutter, J. S., Criswell, S. R., Ances, B. M. & Snyder, A. Z. 2012. Resting state functional connectivity of the striatum in Parkinson's disease. *Brain,* 135**,** 3699-3711.

Hall, S., Ohrfelt, A., Constantinescu, R., Andreasson, U., Surova, Y., Bostrom, F., Nilsson, C., Hakan, W., Decraemer, H., Nagga, K., Minthon, L., Londos, E., Vanmechelen, E., Holmberg, B., Zetterberg, H., Blennow, K. & Hansson, O. 2012. Accuracy of a panel of 5 cerebrospinal fluid biomarkers in the

differential diagnosis of patients with dementia and/or parkinsonian disorders. *Arch Neurol,* 69**,** 1445-52.

Halliday, G., Hely, M., Reid, W. & Morris, J. 2008. The progression of pathology in longitudinally followed patients with Parkinson's disease. *Acta Neuropathologica,* 115**,** 409-15.

Halliday, G. M. 2009. Thalamic changes in Parkinson's disease. *Parkinsonism & Related Disorders,* 15, Supplement 3**,** S152-S155.

Halliday, G. M., Leverenz, J. B., Schneider, J. S. & Adler, C. H. 2014. The neurobiological basis of cognitive impairment in Parkinson's disease. *Movement Disorders,* 29**,** 634-650.

Hanganu, A. & Monchi, O. 2016. Structural neuroimaging markers of cognitive decline in Parkinson's disease. *Parkinson's Disease,* 2016.

He, H. & Liu, T. T. 2012. A geometric view of global signal confounds in resting-state functional MRI. *Neuroimage,* 59**,** 2339-48.

He, R., Yan, X., Guo, J., Xu, Q., Tang, B. & Sun, Q. 2018. Recent advances in biomarkers for Parkinson's disease. *Frontiers in aging neuroscience,* 10**,** 305.

Hebb, D. O. 2005. *The organization of behavior: A neuropsychological theory*, Psychology Press.

Helmich, R. C., Derikx, L. C., Bakker, M., Scheeringa, R., Bloem, B. R. & Toni, I. 2010. Spatial remapping of cortico-striatal connectivity in Parkinson's disease. *Cerebral cortex,* 20**,** 1175-1186.

Helmich, R. C., Vaillancourt, D. E. & Brooks, D. J. 2018. The Future of Brain Imaging in Parkinson's Disease. *Journal of Parkinson's disease,* 8**,** S47-S51.

Hely, M. A., Morris, J. G., Reid, W. G. & Trafficante, R. 2005. Sydney Multicenter Study of Parkinson's disease: non-L-dopa-responsive problems dominate at 15 years. *Mov Disord,* 20**,** 190-9.

Henchcliffe, C. & Beal, M. F. 2008. Mitochondrial biology and oxidative stress in Parkinson disease pathogenesis. *Nature clinical practice Neurology,* 4**,** 600-609.

Hillary, F. G., Roman, C. A., Venkatesan, U., Rajtmajer, S. M., Bajo, R. & Castellanos, N. D. 2015. Hyperconnectivity is a fundamental response to neurological disruption. *Neuropsychology,* 29**,** 59-75.

Hirsch, L., Jette, N., Frolkis, A., Steeves, T. & Pringsheim, T. 2016. The Incidence of Parkinson's Disease: A Systematic Review and Meta-Analysis. *Neuroepidemiology,* 46**,** 292-300.

Hoenen, C., Gustin, A., Birck, C., Kirchmeyer, M., Beaume, N., Felten, P., Grandbarbe, L., Heuschling, P. & Heurtaux, T. 2016. Alpha-Synuclein Proteins Promote Pro-Inflammatory Cascades in Microglia: Stronger Effects of the A53T Mutant. *PLOS ONE,* 11**,** e0162717.

Hofer, S. & Frahm, J. 2006. Topography of the human corpus callosum revisited—comprehensive fiber tractography using diffusion tensor magnetic resonance imaging. *Neuroimage,* 32**,** 989-994.

Hopes, L., Grolez, G., Moreau, C., Lopes, R., Ryckewaert, G., Carrière, N., Auger, F., Laloux, C., Petrault, M., Devedjian, J.-C., Bordet, R., Defebvre, L., Jissendi, P., Delmaire, C. & Devos, D. 2016. Magnetic Resonance Imaging Features of the Nigrostriatal System: Biomarkers of Parkinson's Disease Stages? *PLoS ONE,* 11**,** e0147947.

Hughes, A. J., Daniel, S. E., Kilford, L. & Lees, A. J. 1992. Accuracy of clinical diagnosis of idiopathic Parkinson's disease: a clinico-pathological study of 100 cases. *Journal of Neurology, Neurosurgery and Psychiatry,* 55**,** 181-184.

Hurtig, H., Trojanowski, J., Galvin, J., Ewbank, D., Schmidt, M., Lee, V.-Y., Clark, C., Glosser, G., Stern, M. & Gollomp, S. 2000. Alpha-synuclein cortical Lewy bodies correlate with dementia in Parkinson's disease. *Neurology,* 54**,** 1916-1921.

Hwang, K., Bertolero, M. A., Liu, W. B. & D'esposito, M. 2017. The human thalamus is an integrative hub for functional brain networks. *Journal of Neuroscience,* 37**,** 5594-5607.

Hwang, O. 2013. Role of oxidative stress in Parkinson's disease. *Exp Neurobiol,* 22**,** 11-7.

Hyvarinen, A. 1999. Fast and robust fixed-point algorithms for independent component analysis. *IEEE transactions on Neural Networks,* 10**,** 626-634.

Ibarretxe-Bilbao, N., Junque, C., Segura, B., Baggio, H. C., Marti, M. J., Valldeoriola, F., Bargallo, N. & Tolosa, E. 2012. Progression of cortical thinning in early Parkinson's disease. *Movement Disorders,* 27**,** 1746-1753.

Jacobson, J. M., Nielsen, N. P., Minthon, L., Warkentin, S. & Wiig, E. H. 2004. Multiple rapid automatic naming measures of cognition: normal performance and effects of aging. *Percept Mot Skills,* 98**,** 739-53.

Jankovic, J. 2008. Parkinson's disease: clinical features and diagnosis. *Journal of neurology, neurosurgery & psychiatry,* 79**,** 368-376.

Jankovic, J., Mcdermott, M., Carter, J., Gauthier, S., Goetz, C., Golbe, L., Huber, S., Koller, W., Olanow, C. & Shoulson, I. 1990. Variable expression of Parkinson's disease: A base-line analysis of the DAT ATOP cohort. *Neurology,* 40**,** 1529-1529.

Janvin, C. C., Larsen, J. P., Aarsland, D. & Hugdahl, K. 2006. Subtypes of mild cognitive impairment in Parkinson's disease: progression to dementia. *Movement disorders: official journal of the Movement Disorder Society,* 21**,** 1343-1349.

Jenkinson, M., Bannister, P., Brady, M. & Smith, S. 2002. Improved optimization for the robust and accurate linear registration and motion correction of brain images. *Neuroimage,* 17**,** 825-41.

Jenkinson, M., Beckmann, C. F., Behrens, T. E. J., Woolrich, M. W. & Smith, S. M. 2012. FSL. *Neuroimage,* 62**,** 782-790.

Jenkinson, M. & Chappell, M. (eds.) 2018. *Introduction to Neuroimaging Analysis,* Oxford, UK: Oxford University Press.

Jenkinson, M. & Smith, S. 2001. A global optimisation method for robust affine registration of brain images. *Medical image analysis,* 5**,** 143-156.

Ji, G.-J., Hu, P., Liu, T.-T., Li, Y., Chen, X., Zhu, C., Tian, Y., Chen, X. & Wang, K. 2018. Functional Connectivity of the Corticobasal Ganglia–Thalamocortical Network in Parkinson Disease: A Systematic Review and Meta-Analysis with Cross-Validation. *Radiology,* 287**,** 172183.

Jones, E. G. 2012. *The thalamus*, Springer Science & Business Media.

Joshi, S. H., Narr, K. L., Philips, O. R., Nuechterlein, K. H., Asarnow, R. F., Toga, A. W. & Woods, R. P. 2013. Statistical shape analysis of the corpus callosum in Schizophrenia. *Neuroimage,* 64**,** 547-59.

Kandel, E. R., Schwartz, J. H. & Jessell, T. M. 2000. *Principles of neural science*, McGraw-Hill New York.

Kehagia, A. A., Barker, R. A. & Robbins, T. W. 2010. Neuropsychological and clinical heterogeneity of cognitive impairment and dementia in patients with Parkinson's disease. *Lancet Neurol,* 9**,** 1200-1213.

Kehagia, A. A., Barker, R. A. & Robbins, T. W. 2013. Cognitive impairment in Parkinson's disease: the dual syndrome hypothesis. *Neurodegener Dis,* 11**,** 79-92.

Kelly, C., De Zubicaray, G., Di Martino, A., Copland, D. A., Reiss, P. T., Klein, D. F., Castellanos, F. X., Milham, M. P. & Mcmahon, K. 2009. l-Dopa Modulates Functional Connectivity in Striatal Cognitive and Motor Networks: A Double-Blind Placebo-Controlled Study. *The Journal of Neuroscience,* 29**,** 7364-7378.

Khan, A. R., Hiebert, N. M., Vo, A., Wang, B. T., Owen, A. M., Seergobin, K. N. & Macdonald, P. A. 2018. Biomarkers of Parkinson's disease: Striatal sub-regional structural morphometry and diffusion MRI. *Neuroimage: Clinical*.

Kim, C. & Lee, S. J. 2008. Controlling the mass action of alpha-synuclein in Parkinson's disease. *J Neurochem,* 107**,** 303-16.

Kish, S. J., Shannak, K. & Hornykiewicz, O. 1988. Uneven pattern of dopamine loss in the striatum of patients with idiopathic Parkinson's disease. Pathophysiologic and clinical implications. *New England Journal of Medicine,* 318**,** 876-80.

Kulisevsky, J. 2000. Role of dopamine in learning and memory: implications for the treatment of cognitive dysfunction in patients with Parkinson's disease. *Drugs Aging,* 16**,** 365-79.

Lande, R. 1979. Quantitative genetic analysis of multivariate evolution, applied to brain: body size allometry. *Evolution,* 33**,** 402-416.

Lee, H. M., Kwon, K.-Y., Kim, M.-J., Jang, J.-W., Suh, S.-I., Koh, S.-B. & Kim, J. H. 2014. Subcortical grey matter changes in untreated, early stage Parkinson's disease without dementia. *Parkinsonism & related disorders,* 20**,** 622-626.

Lee, S., Kim, S., Tae, W., Lee, S., Choi, J., Koh, S. & Kwon, D. 2011. Regional volume analysis of the Parkinson disease brain in early disease stage: gray matter, white matter, striatum, and thalamus. *American Journal of Neuroradiology,* 32**,** 682-687.

Leech, R. & Sharp, D. J. 2014. The role of the posterior cingulate cortex in cognition and disease. *Brain,* 137**,** 12-32.

Lenka, A., Pasha, S. A., Mangalore, S., George, L., Jhunjhunwala, K. R., Bagepally, B. S., Naduthota, R. M., Saini, J., Yadav, R. & Pal, P. K. 2017. Role of Corpus Callosum Volumetry in Differentiating the Subtypes of Progressive Supranuclear Palsy and Early Parkinson's Disease. *Movement Disorders Clinical Practice,* 4**,** 552-558.

Lewis, M. M., Du, G., Lee, E. Y., Nasralah, Z., Sterlin, N. W., Zhang, L., Wagner, D., Kong, L., Troster, A. I., Styner, M., Eslinger, P. J., Mailman, R. B. & Huang, X. 2016. The pattern of gray matter atrophy in Parkinson's disease differs in cortical and subcortical regions. *J Neurol,* 263**,** 68-75.

Lewis, S. J., Cools, R., Robbins, T. W., Dove, A., Barker, R. A. & Owen, A. M. 2003. Using executive heterogeneity to explore the nature of working memory deficits in Parkinson's disease. *Neuropsychologia,* 41**,** 645-654.

Lill, C. M. 2016. Genetics of Parkinson's disease. *Molecular and Cellular Probes,* 30**,** 386-396.

Litvan, I., Goldman, J. G., Troster, A. I., Schmand, B. A., Weintraub, D., Petersen, R. C., Mollenhauer, B., Adler, C. H., Marder, K., Williams-Gray, C. H., Aarsland, D., Kulisevsky, J., Rodriguez-Oroz, M. C., Burn, D. J., Barker, R. A. & Emre, M. 2012. Diagnostic criteria for mild cognitive impairment in

Parkinson's disease: Movement Disorder Society Task Force guidelines. *Movment Disorders,* 27**,** 349-56.

Logothetis, N. K. 2008. What we can do and what we cannot do with fMRI. *Nature,* 453**,** 869-78.

Logothetis, N. K., Pauls, J., Augath, M., Trinath, T. & Oeltermann, A. 2001. Neurophysiological investigation of the basis of the fMRI signal. *Nature,* 412**,** 150-7.

Looi, J. C., Svensson, L., Lindberg, O., Zandbelt, B. B., Ostberg, P., Orndahl, E. & Wahlund, L. O. 2009. Putaminal volume in frontotemporal lobar degeneration and Alzheimer disease: differential volumes in dementia subtypes and controls. *AJNR Am J Neuroradiol,* 30**,** 1552-60.

Looi, J. C. & Walterfang, M. 2013. Striatal morphology as a biomarker in neurodegenerative disease. *Molecular Psychiatry,* 18**,** 417-24.

Looi, J. C., Walterfang, M., Nilsson, C., Power, B. D., Van Westen, D., Velakoulis, D., Wahlund, L. O. & Thompson, P. M. 2014. The subcortical connectome: Hubs, spokes and the space between - a vision for further research in neurodegenerative disease. *Australian and New Zealand Journal of Psychiatry*.

Looi, J. C. L., Lindberg, O., Liberg, B., Tatham, V., Kumar, R., Maller, J., Millard, E., Sachdev, P., Högberg, G. & Pagani, M. 2008. Volumetrics of the caudate nucleus: reliability and validity of a new manual tracing protocol. *Psychiatry Research: Neuroimaging,* 163**,** 279-288.

Luders, E., Narr, K. L., Bilder, R. M., Thompson, P. M., Szeszko, P. R., Hamilton, L. & Toga, A. W. 2007. Positive correlations between corpus callosum thickness and intelligence. *Neuroimage,* 37**,** 1457-64.

Maguire, E. A., Gadian, D. G., Johnsrude, I. S., Good, C. D., Ashburner, J., Frackowiak, R. S. J. & Frith, C. D. 2000. Navigation-related structural change in the hippocampi of taxi drivers. *Proceedings of the National Academy of Sciences,* 97**,** 4398-4403.

Mak, E., Bergsland, N., Dwyer, M. G., Zivadinov, R. & Kandiah, N. 2014. Subcortical atrophy is associated with cognitive impairment in mild Parkinson disease: a combined investigation of volumetric changes, cortical thickness, and vertex-based shape analysis. *American Journal of Neuroradiology,* 35**,** 2257-64.

Mak, E., Su, L., Williams, G. B., Firbank, M. J., Lawson, R. A., Yarnall, A. J., Duncan, G. W., Owen, A. M., Khoo, T. K. & Brooks, D. J. 2015. Baseline and longitudinal grey matter changes in newly diagnosed Parkinson's disease: ICICLE-PD study. *Brain,* 138**,** 2974-2986.

Marder, E. & Goaillard, J. M. 2006. Variability, compensation and homeostasis in neuron and network function. *Nat Rev Neurosci,* 7**,** 563-74.

Martinez-Ramirez, D., Almeida, L., Giugni, J. C., Ahmed, B., Higuchi, M.-A., Little, C. S., Chapman, J. P., Mignacca, C., Wagle Shukla, A., Hess, C. W., Hegland, K. W. & Okun, M. S. 2015. Rate of aspiration pneumonia in hospitalized Parkinson's disease patients: a cross-sectional study. *BMC neurology,* 15**,** 104-104.

Mcdonald, J. H. 2014. *Handbook of Biological Statistics,* Baltimore, Maryland, Sparky House Publishing.

Mcgregor, M. M. & Nelson, A. B. 2019. Circuit Mechanisms of Parkinson's Disease. *Neuron,* 101**,** 1042-1056.

Mckeown, M. J., Uthama, A., Abugharbieh, R., Palmer, S., Lewis, M. & Huang, X. 2008. Shape (but not volume) changes in the thalami in Parkinson disease. *BMC neurology,* 8**,** 8.

Mega, M. S. & Cummings, J. L. 1994. Frontal-subcortical circuits and neuropsychiatric disorders. *J Neuropsychiatry Clin Neurosci,* 6**,** 358-70.

Meijer, F. J., Bloem, B. R., Mahlknecht, P., Seppi, K. & Goraj, B. 2013. Update on diffusion MRI in Parkinson's disease and atypical parkinsonism. *Journal of the neurological sciences,* 332**,** 21-29.

Melzer, T. R., Watts, R., Macaskill, M. R., Pitcher, T. L., Livingston, L., Keenan, R. J., Dalrymple-Alford, J. C. & Anderson, T. J. 2012. Grey matter atrophy in cognitively impaired Parkinson's disease. *Journal of Neurology, Neurosurgery and Psychiatry,* 83**,** 188.

Melzer, T. R., Watts, R., Macaskill, M. R., Pitcher, T. L., Livingston, L., Keenan, R. J., Dalrymple-Alford, J. C. & Anderson, T. J. 2013. White matter microstructure deteriorates across cognitive stages in Parkinson disease. *Neurology,* 80**,** 1841-1849.

Menke, R. A., Szewczyk-Krolikowski, K., Jbabdi, S., Jenkinson, M., Talbot, K., Mackay, C. E. & Hu, M. 2014. Comprehensive morphometry of subcortical grey matter structures in early-stage Parkinson's disease. *Human brain mapping,* 35**,** 1681-1690.

Messina, D., Cerasa, A., Condino, F., Arabia, G., Novellino, F., Nicoletti, G., Salsone, M., Morelli, M., Lanza, P. L. & Quattrone, A. 2011. Patterns of brain atrophy in Parkinson's disease, progressive supranuclear palsy and multiple system atrophy. *Parkinsonism & related disorders,* 17**,** 172-176.

Mesulam, M. M. 1990. Large-scale neurocognitive networks and distributed processing for attention, language, and memory. *Ann Neurol,* 28**,** 597-613.

Mevel, K., Chetelat, G., Eustache, F. & Desgranges, B. 2011. The default mode network in healthy aging and Alzheimer's disease. *International journal of Alzheimer's disease,* 2011**,** 535816.

Miller, E. K. & Cohen, J. D. 2001. An integrative theory of prefrontal cortex function. *Annu Rev Neurosci,* 24**,** 167-202.

Mishra, V. R., Sreenivasan, K. R., Yang, Z., Zhuang, X., Cordes, D., Mari, Z., Litvan, I., Fernandez, H. H., Eidelberg, D. & Ritter, A. 2019. Unique white matter structural connectivity in early-stage, drug-naive Parkinson disease. *Neurology*.

Mitchell, T. N., Free, S. L., Merschhemke, M., Lemieux, L., Sisodiya, S. M. & Shorvon, S. D. 2003. Reliable callosal measurement: population normative data confirm sex-related differences. *American Journal of Neuroradiology,* 24**,** 410-418.

Moehle, M. S. & West, A. B. 2015. M1 and M2 immune activation in Parkinson's disease: foe and ally? *Neuroscience,* 302**,** 59-73.

Morel, A. 2007. *Stereotactic atlas of the human thalamus and basal ganglia*, CRC Press.

Morey, R. A., Petty, C. M., Xu, Y., Hayes, J. P., Wagner, H. R., Lewis, D. V., Labar, K. S., Styner, M. & Mccarthy, G. 2009. A comparison of automated segmentation and manual tracing for quantifying hippocampal and amygdala volumes. *Neuroimage,* 45**,** 855-866.

Mosley, P. E., Paliwal, S., Robinson, K., Coyne, T., Silburn, P., Tittgemeyer, M., Stephan, K. E., Breakspear, M. & Perry, A. 2019. The structural connectivity

of discrete networks underlies impulsivity and gambling in Parkinson's disease. *Brain,* 142**,** 3917-3935.

Moustafa, A. A. & Poletti, M. 2013. Neural and behavioral substrates of subtypes of Parkinson's disease. *Frontiers in systems neuroscience,* 7**,** 117.

Müller-Oehring, E. M., Sullivan, E. V., Pfefferbaum, A., Huang, N. C., Poston, K. L., Bronte-Stewart, H. M. & Schulte, T. 2015. Task-rest modulation of basal ganglia connectivity in mild to moderate Parkinson's disease. *Brain Imaging Behav,* 9**,** 619-38.

Murphy, K., Birn, R. M. & Bandettini, P. A. 2013. Resting-state fMRI confounds and cleanup. *Neuroimage,* 80**,** 349-359.

Nemmi, F., Sabatini, U., Rascol, O. & Peran, P. 2015. Parkinson's disease and local atrophy in subcortical nuclei: insight from shape analysis. *Neurobiology of Aging,* 36**,** 424-33.

Nichols, T. E. & Holmes, A. P. 2002. Nonparametric permutation tests for functional neuroimaging: a primer with examples. *Hum Brain Mapp,* 15**,** 1-25.

O'shea, J., Johansen-Berg, H., Trief, D., Göbel, S. & Rushworth, M. F. 2007. Functionally specific reorganization in human premotor cortex. *Neuron,* 54**,** 479-490.

Obeso, J. A., Rodriguez-Oroz, M. C., Rodriguez, M., Lanciego, J. L., Artieda, J., Gonzalo, N. & Olanow, C. W. 2000. Pathophysiology of the basal ganglia in Parkinson's disease. *Trends in neurosciences,* 23**,** S8-S19.

Obeso, J. A., Rodríguez-Oroz, M. C., Benitez-Temino, B., Blesa, F. J., Guridi, J., Marin, C. & Rodriguez, M. 2008. Functional organization of the basal ganglia: therapeutic implications for Parkinson's disease. *Movement Disorders,* 23**,** S548-S559.

Owens-Walton, C., Jakabek, D., Li, X., Wilkes, F. A., Walterfang, M., Velakoulis, D., Van Westen, D., Looi, J. C. L. & Hansson, O. 2018. Striatal changes in Parkinson disease: An investigation of morphology, functional connectivity and their relationship to clinical symptoms. *Psychiatry Research: Neuroimaging,* 275**,** 5-13.

Pagano, G., Ferrara, N., Brooks, D. J. & Pavese, N. 2016. Age at onset and Parkinson disease phenotype. *Neurology,* 86**,** 1400-1407.

Pallant, J. 2013. *SPSS survival manual*, McGraw-Hill International.

Palmqvist, S., Minthon, L., Wattmo, C., Londos, E. & Hansson, O. 2010. A Quick Test of cognitive speed is sensitive in detecting early treatment response in Alzheimer's disease. *Alzheimers Res Ther,* 2**,** 29.

Palop, J. J. & Mucke, L. 2010. Synaptic depression and aberrant excitatory network activity in Alzheimer's disease: two faces of the same coin? *Neuromolecular medicine,* 12**,** 48-55.

Parkinson, J. 1817. *An essay on the shaking palsy*, Printed by Whittingham and Rowland for Sherwood, Neely, and Jones.

Patenaude, B., Smith, S. M., Kennedy, D. N. & Jenkinson, M. 2011. A Bayesian model of shape and appearance for subcortical brain segmentation. *Neuroimage,* 56**,** 907-922.

Pavese, N., Rivero-Bosch, M., Lewis, S. J., Whone, A. L. & Brooks, D. J. 2011. Progression of monoaminergic dysfunction in Parkinson's disease: a longitudinal 18F-dopa PET study. *Neuroimage,* 56**,** 1463-1468.

Pedrosa Carrasco, A. J., Timmermann, L. & Pedrosa, D. J. 2018. Management of constipation in patients with Parkinson's disease. *NPJ Parkinson's disease,* 4**,** 6-6.

Pereira, J. B., Ibarretxe-Bilbao, N., Marti, M. J., Compta, Y., Junque, C., Bargallo, N. & Tolosa, E. 2012. Assessment of cortical degeneration in patients with Parkinson's disease by voxel-based morphometry, cortical folding, and cortical thickness. *Hum Brain Mapp,* 33**,** 2521-34.

Pereira, J. B., Svenningsson, P., Weintraub, D., Brønnick, K., Lebedev, A., Westman, E. & Aarsland, D. 2014. Initial cognitive decline is associated with cortical thinning in early Parkinson disease. *Neurology,* 82**,** 2017-2025.

Pitcher, T. L., Melzer, T. R., Macaskill, M. R., Graham, C. F., Livingston, L., Keenan, R. J., Watts, R., Dalrymple-Alford, J. C. & Anderson, T. J. 2012. Reduced striatal volumes in Parkinson's disease: a magnetic resonance imaging study. *Translational Neurodegeneration,* 1**,** 68-76.

Podsiadlo, D. & Richardson, S. 1991. The timed "Up & Go": a test of basic functional mobility for frail elderly persons. *J Am Geriatr Soc,* 39**,** 142-8.

Poewe, W. 2009. Clinical measures of progression in Parkinson's disease. *Movement Disorders,* 24 Suppl 2**,** S671-6.

Poewe, W., Seppi, K., Tanner, C. M., Halliday, G. M., Brundin, P., Volkmann, J., Schrag, A.-E. & Lang, A. E. 2017. Parkinson disease. *Nature Reviews Disease Primers,* 3**,** 17013.

Poline, J.-B., Worsley, K. J., Evans, A. C. & Friston, K. J. 1997. Combining spatial extent and peak intensity to test for activations in functional imaging. *Neuroimage,* 5**,** 83-96.

Politis, M. 2014. Neuroimaging in Parkinson disease: from research setting to clinical practice. *Nature Reviews Neurology,* 10**,** 708-722.

Ponsen, M. M., Stam, C. J., Bosboom, J. L. W., Berendse, H. W. & Hillebrand, A. 2013. A three dimensional anatomical view of oscillatory resting-state activity and functional connectivity in Parkinson's disease related dementia: An MEG study using atlas-based beamforming. *Neuroimage: Clinical,* 2**,** 95-102.

Pontone, G. M., Williams, J. R., Anderson, K. E., Chase, G., Goldstein, S. A., Grill, S., Hirsch, E. S., Lehmann, S., Little, J. T. & Margolis, R. L. 2009. Prevalence of anxiety disorders and anxiety subtypes in patients with Parkinson's disease. *Movement disorders: official journal of the Movement Disorder Society,* 24**,** 1333-1338.

Postuma, R. B. & Berg, D. 2019. Prodromal Parkinson's Disease: The Decade Past, the Decade to Come. *Mov Disord,* 34**,** 665-675.

Postuma, R. B., Berg, D., Stern, M., Poewe, W., Olanow, C. W., Oertel, W., Obeso, J., Marek, K., Litvan, I. & Lang, A. E. 2015. MDS clinical diagnostic criteria for Parkinson's disease. *Movement Disorders,* 30**,** 1591-1601.

Poudel, G. R., Egan, G. F., Churchyard, A., Chua, P., Stout, J. C. & Georgiou-Karistianis, N. 2014. Abnormal synchrony of resting state networks in premanifest and symptomatic Huntington disease: the IMAGE-HD study. *Journal of psychiatry & neuroscience: JPN,* 39**,** 87.

Power, B. D. & Looi, J. C. 2014. The thalamus as a putative biomarker in neuropsychiatry. *Neurosciences,* 2**,** 6.

Power, B. D. & Looi, J. C. 2015. The thalamus as a putative biomarker in neurodegenerative disorders. *Australian and New Zealand Journal of Psychiatry***,** 0004867415585857.

Power, B. D., Wilkes, F. A., Hunter-Dickson, M., Van Westen, D., Santillo, A. F., Walterfang, M., Nilsson, C., Velakoulis, D. & Looi, J. C. 2015. Validation of a protocol for manual segmentation of the thalamus on magnetic resonance imaging scans. *Psychiatry Research: Neuroimaging,* 232**,** 98-105.

Power, J. D., Barnes, K. A., Snyder, A. Z., Schlaggar, B. L. & Petersen, S. E. 2012. Spurious but systematic correlations in functional connectivity MRI networks arise from subject motion. *Neuroimage,* 59**,** 2142-54.

Pringsheim, T., Jette, N., Frolkis, A. & Steeves, T. D. 2014. The prevalence of Parkinson's disease: A systematic review and meta-analysis. *Movement disorders,* 29**,** 1583-1590.

Przedborski, S. 2017. The two-century journey of Parkinson disease research. *Nat Rev Neurosci,* 18**,** 251-259.

Rajah, M. N. & D'esposito, M. 2005. Region-specific changes in prefrontal function with age: a review of PET and fMRI studies on working and episodic memory. *Brain,* 128**,** 1964-83.

Rakic, P. 1988. Specification of cerebral cortical areas. *Science,* 241**,** 170-176.

Ray, N. J. & Strafella, A. P. 2012. The neurobiology and neural circuitry of cognitive changes in Parkinson's disease revealed by functional neuroimaging. *Movement disorders : official journal of the Movement Disorder Society,* 27**,** 1484-1492.

Rektor, I., Svátková, A., Vojtíšek, L., Zikmundova, I., Vaníček, J., Király, A. & Szabó, N. 2018. White matter alterations in Parkinson's disease with normal cognition precede grey matter atrophy. *PloS one,* 13**,** e0187939.

Reuter, M., Rosas, H. D. & Fischl, B. 2010. Highly accurate inverse consistent registration: a robust approach. *Neuroimage,* 53**,** 1181-96.

Rinne, J. O., Portin, R., Ruottinen, H., Nurmi, E., Bergman, J., Haaparanta, M. & Solin, O. 2000. Cognitive impairment and the brain dopaminergic system in Parkinson disease:[18F] fluorodopa positron emission tomographic study. *Archives of neurology,* 57**,** 470-475.

Rocha, E. M., De Miranda, B. & Sanders, L. H. 2018. Alpha-synuclein: Pathology, mitochondrial dysfunction and neuroinflammation in Parkinson's disease. *Neurobiology of Disease,* 109**,** 249-257.

Salimi-Khorshidi, G., Douaud, G., Beckmann, C. F., Glasser, M. F., Griffanti, L. & Smith, S. M. 2014. Automatic denoising of functional MRI data: combining independent component analysis and hierarchical fusion of classifiers. *Neuroimage,* 90**,** 449-468.

Schapira, A. H. V. 2007. Mitochondrial dysfunction in Parkinson's disease. *Cell Death & Differentiation,* 14**,** 1261-1266.

Schapira, A. H. V., Chaudhuri, K. R. & Jenner, P. 2017. Non-motor features of Parkinson disease. *Nat Rev Neurosci,* 18**,** 435-450.

Schmahmann, J. & Pandya, D. 2009. *Fiber pathways of the brain*, OUP USA.

Schneider, J. S., Pioli, E. Y., Jianzhong, Y., Li, Q. & Bezard, E. 2013. Levodopa improves motor deficits but can further disrupt cognition in a macaque Parkinson model. *Mov Disord,* 28**,** 663-7.

Schuster, C., Kasper, E., Dyrba, M., Machts, J., Bittner, D., Kaufmann, J., Mitchell, A. J., Benecke, R., Teipel, S. & Vielhaber, S. 2014. Cortical thinning and its relation to cognition in amyotrophic lateral sclerosis. *Neurobiology of aging,* 35**,** 240-246.

Seeley, W. W., Crawford, R. K., Zhou, J., Miller, B. L. & Greicius, M. D. 2009. Neurodegenerative diseases target large-scale human brain networks. *Neuron,* 62**,** 42-52.

Seeley, W. W., Menon, V., Schatzberg, A. F., Keller, J., Glover, G. H., Kenna, H., Reiss, A. L. & Greicius, M. D. 2007. Dissociable intrinsic connectivity

networks for salience processing and executive control. *J Neurosci,* 27**,** 2349-56.

Segonne, F., Dale, A. M., Busa, E., Glessner, M., Salat, D., Hahn, H. K. & Fischl, B. 2004. A hybrid approach to the skull stripping problem in MRI. *Neuroimage,* 22**,** 1060-75.

Segonne, F., Pacheco, J. & Fischl, B. 2007. Geometrically accurate topology-correction of cortical surfaces using nonseparating loops. *IEEE Trans Med Imaging,* 26**,** 518-29.

Segura, B., Baggio, H. C., Marti, M. J., Valldeoriola, F., Compta, Y., Garcia-Diaz, A. I., Vendrell, P., Bargallo, N., Tolosa, E. & Junque, C. 2014. Cortical thinning associated with mild cognitive impairment in Parkinson's disease. *Mov Disord,* 29**,** 1495-503.

Sheline, Y. I. & Raichle, M. E. 2013. Resting state functional connectivity in preclinical Alzheimer's disease. *Biological Psychiatry,* 74**,** 340-7.

Shen, H. H. 2015. Core Concept: Resting-state connectivity. *Proceedings of the National Academy of Sciences,* 112**,** 14115-14116.

Shine, J. M., Bell, P. T., Matar, E., Poldrack, R. A., Lewis, S. J., Halliday, G. M. & O'callaghan, C. 2019. Dopamine depletion alters macroscopic network dynamics in Parkinson's disease. *Brain,* 142**,** 1024-1034.

Shrout, P. E. & Fleiss, J. L. 1979. Intraclass correlations: uses in assessing rater reliability. *Psychological bulletin,* 86**,** 420.

Simuni, T., Uribe, L., Cho, H. R., Caspell-Garcia, C., Coffey, C. S., Siderowf, A., Trojanowski, J. Q., Shaw, L. M., Seibyl, J. & Singleton, A. 2020. Clinical and dopamine transporter imaging characteristics of non-manifest LRRK2 and GBA mutation carriers in the Parkinson's Progression Markers Initiative (PPMI): a cross-sectional study. *The Lancet Neurology,* 19**,** 71-80.

Singleton, A. B., Farrer, M. J. & Bonifati, V. 2013. The genetics of Parkinson's disease: progress and therapeutic implications. *Mov Disord,* 28**,** 14-23.

Sled, J. G., Zijdenbos, A. P. & Evans, A. C. 1998. A nonparametric method for automatic correction of intensity nonuniformity in MRI data. *IEEE Trans Med Imaging,* 17**,** 87-97.

Smith, S. M. 2002. Fast robust automated brain extraction. *Human brain mapping,* 17**,** 143-155.

Smith, S. M., Fox, P. T., Miller, K. L., Glahn, D. C., Fox, P. M., Mackay, C. E., Filippini, N., Watkins, K. E., Toro, R., Laird, A. R. & Beckmann, C. F. 2009. Correspondence of the brain's functional architecture during activation and rest. *Proc Natl Acad Sci U S A,* 106**,** 13040-5.

Smith, S. M. & Nichols, T. E. 2009. Threshold-free cluster enhancement: addressing problems of smoothing, threshold dependence and localisation in cluster inference. *Neuroimage,* 44**,** 83-98.

Smyser, C. D., Snyder, A. Z. & Neil, J. J. 2011. Functional connectivity MRI in infants: exploration of the functional organization of the developing brain. *Neuroimage,* 56**,** 1437-52.

Sporns, O., Honey, C. J. & Kötter, R. 2007. Identification and classification of hubs in brain networks. *PloS one,* 2**,** e1049.

Sporns, O., Tononi, G. & Kötter, R. 2005. The Human Connectome: A Structural Description of the Human Brain. *PLoS Comput Biol,* 1.

Starkstein, S. E., Petracca, G., Chemerinski, E., Tesón, A., Sabe, L., Merello, M. & Leiguarda, R. 1998. Depression in classic versus akinetic-rigid Parkinson's

disease. *Movement disorders: official journal of the Movement Disorder Society,* 13**,** 29-33.

Sterling, N. W., Du, G., Lewis, M. M., Dimaio, C., Kong, L., Eslinger, P. J., Styner, M. & Huang, X. 2013. Striatal shape in Parkinson's disease. *Neurobiology of Aging,* 34**,** 2510-2516.

Strafella, A. P. 2013. Anatomical and functional connectivity as a tool to study brain networks in Parkinson's disease. *Movement Disorders,* 28**,** 411-412.

Strafella, A. P., Bohnen, N. I., Pavese, N., Vaillancourt, D. E., Van Eimeren, T., Politis, M., Tessitore, A., Ghadery, C., Lewis, S. & Group, O. B. O. I.-N. S. 2018. Imaging Markers of Progression in Parkinson's Disease. *Movement Disorders Clinical Practice,* 5**,** 586-596.

Styner, M., Oguz, I., Xu, S., Brechbuhler, C., Pantazis, D., Levitt, J. J., Shenton, M. E. & Gerig, G. 2006. Framework for the Statistical Shape Analysis of Brain Structures using SPHARM-PDM. *Insight J***,** 242-250.

Summerfield, C., Junque, C., Tolosa, E., Salgado-Pineda, P., Gomez-Anson, B., Marti, M. J., Pastor, P., Ramirez-Ruiz, B. & Mercader, J. 2005. Structural brain changes in Parkinson disease with dementia: a voxel-based morphometry study. *Arch Neurol,* 62**,** 281-5.

Surmeier, D. J., Obeso, J. A. & Halliday, G. M. 2017. Parkinson's Disease Is Not Simply a Prion Disorder. *J Neurosci,* 37**,** 9799-9807.

Szewczyk-Krolikowski, K., Menke, R. A., Rolinski, M., Duff, E., Salimi-Khorshidi, G., Filippini, N., Zamboni, G., Hu, M. T. & Mackay, C. E. 2014. Functional connectivity in the basal ganglia network differentiates PD patients from controls. *Neurology,* 83**,** 208-214.

Tandberg, E., Larsen, J. P., Aarsland, D. & Cummings, J. L. 1996. The occurrence of depression in Parkinson's disease: a community-based study. *Archives of neurology,* 53**,** 175-179.

Tekin, S. & Cummings, J. L. 2002. Frontal–subcortical neuronal circuits and clinical neuropsychiatry: an update. *Journal of psychosomatic research,* 53**,** 647-654.

Thenganatt, M. A. & Jankovic, J. 2014. Parkinson disease subtypes. *JAMA neurology,* 71**,** 499-504.

Thompson, P. M., Hayashi, K. M., De Zubicaray, G. I., Janke, A. L., Rose, S. E., Semple, J., Hong, M. S., Herman, D. H., Gravano, D., Doddrell, D. M. & Toga, A. W. 2004. Mapping hippocampal and ventricular change in Alzheimer disease. *Neuroimage,* 22**,** 1754-66.

Tinaz, S., Courtney, M. G. & Stern, C. E. 2011. Focal cortical and subcortical atrophy in early Parkinson's disease. *Movement Disorders,* 26**,** 436-441.

Tombaugh, T. N., Kozak, J. & Rees, L. 1999. Normative data stratified by age and education for two measures of verbal fluency: FAS and animal naming. *Archives of Clinical Neuropsychology,* 14**,** 167-177.

Tomlinson, C. L., Stowe, R., Patel, S., Rick, C., Gray, R. & Clarke, C. E. 2010. Systematic review of levodopa dose equivalency reporting in Parkinson's disease. *Mov Disord,* 25**,** 2649-53.

Tononi, G., Sporns, O. & Edelman, G. M. 1999. Measures of degeneracy and redundancy in biological networks. *Proceedings of the National Academy of Sciences,* 96**,** 3257-3262.

Tziortzi, A. C., Haber, S. N., Searle, G. E., Tsoumpas, C., Long, C. J., Shotbolt, P., Douaud, G., Jbabdi, S., Behrens, T. E. J., Rabiner, E. A., Jenkinson, M. & Gunn, R. N. 2014. Connectivity-Based Functional Analysis of Dopamine

Release in the Striatum Using Diffusion-Weighted MRI and Positron Emission Tomography. *Cerebral Cortex,* 24**,** 1165-1177.

Van Den Heuvel, M. P., Mandl, R. C. W., Kahn, R. S. & Hulshoff Pol, H. E. 2009. Functionally linked resting-state networks reflect the underlying structural connectivity architecture of the human brain. *Human Brain Mapping,* 30**,** 3127-3141.

Van Den Heuvel, M. P. & Sporns, O. 2013. Network hubs in the human brain. *Trends in cognitive sciences,* 17**,** 683-696.

Van Meer, M. P., Van Der Marel, K., Wang, K., Otte, W. M., El Bouazati, S., Roeling, T. A., Viergever, M. A., Berkelbach Van Der Sprenkel, J. W. & Dijkhuizen, R. M. 2010. Recovery of sensorimotor function after experimental stroke correlates with restoration of resting-state interhemispheric functional connectivity. *J Neurosci,* 30**,** 3964-72.

Vasconcellos, L. F., Pereira, J. S., Adachi, M., Greca, D., Cruz, M., Malak, A. L. & Charchat-Fichman, H. 2018. Volumetric brain analysis as a predictor of a worse cognitive outcome in Parkinson's disease. *Journal of psychiatric research,* 102**,** 254-260.

Villalba, R. M., Lee, H. & Smith, Y. 2009. Dopaminergic denervation and spine loss in the striatum of MPTP-treated monkeys. *Experimental Neurology,* 215**,** 220-227.

Vita, A., De Peri, L., Silenzi, C. & Dieci, M. 2006. Brain morphology in first-episode schizophrenia: a meta-analysis of quantitative magnetic resonance imaging studies. *Schizophrenia research,* 82**,** 75-88.

Volkmann, J., Daniels, C. & Witt, K. 2010. Neuropsychiatric effects of subthalamic neurostimulation in Parkinson disease. *Nature Reviews Neurology,* 6**,** 487.

Von Monakow, C. 1969. Diaschisis. *Brain and behavior I: mood states and mind***,** 27-36.

Voon, V. & Fox, S. H. 2007. Medication-related impulse control and repetitive behaviors in Parkinson disease. *Archives of Neurology,* 64**,** 1089-1096.

Wager, T. D., Lindquist, M. & Kaplan, L. 2007. Meta-analysis of functional neuroimaging data: current and future directions. *Social cognitive and affective neuroscience,* 2**,** 150-158.

Walterfang, M., Luders, E., Looi, J. C. L., Rajagopalan, P., Velakoulis, D., Thompson, P. M., Lindberg, O., Ostberg, P., Nordin, L. E., Svensson, L. & Wahlund, L.-O. 2014. Shape analysis of the corpus callosum in Alzheimer's disease and frontotemporal lobar degeneration subtypes. *Journal of Alzheimer's disease : JAD,* 40**,** 897-906.

Walterfang, M. & Velakoulis, D. 2014. Callosal morphology in schizophrenia: what can shape tell us about function and illness? *Br J Psychiatry,* 204**,** 9-11.

Walterfang, M., Yucel, M., Barton, S., Reutens, D. C., Wood, A. G., Chen, J., Lorenzetti, V., Velakoulis, D., Pantelis, C. & Allen, N. B. 2009. Corpus callosum size and shape in individuals with current and past depression. *J Affect Disord,* 115**,** 411-20.

Wang, L., Joshi, S. C., Miller, M. I. & Csernansky, J. G. 2001. Statistical analysis of hippocampal asymmetry in schizophrenia. *Neuroimage,* 14**,** 531-45.

Wang, S., Chu, C.-H., Guo, M., Jiang, L., Nie, H., Zhang, W., Wilson, B., Yang, L., Stewart, T. & Hong, J.-S. 2016. Identification of a specific α-synuclein peptide (α-Syn 29-40) capable of eliciting microglial superoxide production to damage dopaminergic neurons. *Journal of neuroinflammation,* 13**,** 158.

Weiner, W. J. 2008. There Is No Parkinson Disease. *JAMA Neurology,* 65**,** 705-708.

Weintraub, D. & Burn, D. J. 2011. Parkinson's disease: the quintessential neuropsychiatric disorder. *Movement Disorders,* 26**,** 1022-1031.

Williams-Gray, C. H., Foltynie, T., Brayne, C. E. G., Robbins, T. W. & Barker, R. A. 2007. Evolution of cognitive dysfunction in an incident Parkinson's disease cohort. *Brain,* 130**,** 1787-1798.

Williams-Gray, C. H., Mason, S. L., Evans, J. R., Foltynie, T., Brayne, C., Robbins, T. W. & Barker, R. A. 2013. The CamPaIGN study of Parkinson's disease: 10-year outlook in an incident population-based cohort. *J Neurol Neurosurg Psychiatry,* 84**,** 1258-64.

Wilson, H., Niccolini, F., Pellicano, C. & Politis, M. 2019. Cortical thinning across Parkinson's disease stages and clinical correlates. *J Neurol Sci,* 398**,** 31-38.

Wiltshire, K., Foster, S., Kaye, J. A., Small, B. J. & Camicioli, R. 2005. Corpus callosum in neurodegenerative diseases: findings in Parkinson's disease. *Dementia and geriatric cognitive disorders,* 20**,** 345-351.

Winkler, A. M., Ridgway, G. R., Webster, M. A., Smith, S. M. & Nichols, T. E. 2014. Permutation inference for the general linear model. *Neuroimage,* 92**,** 381-97.

Witelson, S. F. 1989. Hand and sex differences in the isthmus and genu of the human corpus callosum: a postmortem morphological study. *Brain,* 112**,** 799-835.

Woo, C.-W., Krishnan, A. & Wager, T. D. 2014. Cluster-extent based thresholding in fMRI analyses: pitfalls and recommendations. *Neuroimage,* 91**,** 412-419.

Woolrich, M. W., Behrens, T. E. J., Beckmann, C. F., Jenkinson, M. & Smith, S. M. 2004. Multilevel linear modelling for FMRI group analysis using Bayesian inference. *Neuroimage,* 21**,** 1732-1747.

Woolrich, M. W., Ripley, B. D., Brady, M. & Smith, S. M. 2001. Temporal autocorrelation in univariate linear modeling of FMRI data. *Neuroimage,* 14**,** 1370-1386.

Worsley, K. 2001. Statistical analysis of activation images. *Functional MRI: an introduction to methods,* 14**,** 251-270.

Worsley, K. J. 1995. Estimating the number of peaks in a random field using the Hadwiger characteristic of excursion sets, with applications to medical images. *The Annals of Statistics,* 23**,** 640-669.

Wright, I. C., Mcguire, P. K., Poline, J. B., Travere, J. M., Murray, R. M., Frith, C. D., Frackowiak, R. S. & Friston, K. J. 1995. A voxel-based method for the statistical analysis of gray and white matter density applied to schizophrenia. *Neuroimage,* 2**,** 244-52.

Yu, R., Liu, B., Wang, L., Chen, J. & Liu, X. 2013. Enhanced Functional Connectivity between Putamen and Supplementary Motor Area in Parkinson's Disease Patients. *PLOS ONE,* 8**,** e59717.

Zarei, M., Ibarretxe-Bilbao, N., Compta, Y., Hough, M., Junque, C., Bargallo, N., Tolosa, E. & Martí, M. J. 2013. Cortical thinning is associated with disease stages and dementia in Parkinson9s disease. *J Neurol Neurosurg Psychiatry,* 84**,** 875-882.

Zhan, Z.-W., Lin, L.-Z., Yu, E.-H., Xin, J.-W., Lin, L., Lin, H.-L., Ye, Q.-Y., Chen, X.-C. & Pan, X.-D. 2018. Abnormal resting-state functional connectivity in posterior cingulate cortex of Parkinson's disease with mild cognitive impairment and dementia. *CNS Neuroscience & Therapeutics,* 24**,** 897-905.

Zhang, D. & Raichle, M. E. 2010. Disease and the brain's dark energy. *Nature Reviews Neurology,* 6**,** 15.

Zhang, Y., Brady, M. & Smith, S. 2001. Segmentation of brain MR images through a hidden Markov random field model and the expectation-maximization algorithm. *IEEE Transactions on Medical Imaging,* 20**,** 45-57.

Zhou, J., Gennatas, E. D., Kramer, J. H., Miller, B. L. & Seeley, W. W. 2012. Predicting regional neurodegeneration from the healthy brain functional connectome. *Neuron,* 73**,** 1216-1227.

Zweig, R., Cardillo, J., Cohen, M., Giere, S. & Hedreen, J. 1993. The locus ceruleus and dementia in Parkinson's disease. *Neurology,* 43**,** 986-986.